Novel Optical Materials Based on Molecular Ultrathin Films and Nanocomposites

A Thesis Submitted for the Degree of
DOCTOR OF PHILOSOPHY

by

K. Rajesh

School of Chemistry
University of Hyderabad
Hyderabad 500 046
INDIA

February 2010

Dedicated

To

My Family Members

CONTENTS

Chapter 1 Introduction

Chapter 2 Optical Response Sensitive to the Form of Assembly in a Molecular Material: Ultrathin Film with a Vanishing Electronic Absorption

Chapter 3 Fluorescence Enhancement in Langmuir-Blodgett Films: Role of Amphiphile Structure, Orientation and Assembly

Chapter 4 Polyelectrolyte Templating Strategy for the Fabrication of Hemicyanine LB Films Showing Enhanced and Stable SHG

Chapter 5 Assembly of Gold Nanoparticles on a Molecular Ultrathin Film: Tuning the Surface Plasmon Resonance

Chapter 6 Overview of the Present Work and Future Prospects

Scope

Tailored assembly of molecules poses the basic challenge and fascination in the area of molecular materials. Careful selection of molecules and their assembly through suitable fabrication methods, lead to the realization of a wide array of molecular materials exhibiting different properties and capable of various functions. Among the several methods to assemble molecules in materials, Langmuir-Blodgett technique (LB) is developed as a unique technique because of the versatility it affords in manipulations at the molecular level. The potential applications of ultrathin films formed by the LB method in fundamental sciences and in technological applications have attracted interest for several decades. Immobilization of functional molecules in LB films has found applications in various disciplines. This thesis addresses the fabrication of ultrathin films of different amphiphilic molecules by the LB approach and discusses the effect of molecular organization in these films on their optical responses. The utility of LB films as templates for the assembly of metal nanoparticles is a related area that is explored.

In this chapter we present a brief overview of molecular materials in Sec. 1.1, followed by a discussion of ultrathin films in Sec 1.2. The LB technique is described in detail in Sec 1.3, following a brief historical prespective, the experimental techniques involved and characterization methods for Langmuir and LB films are presented. Potential applications of LB films are noted; specific reference is made to LB film-nanoparticle composites. Concepts relavant to a discussion of optical and nonlinear optical effects in molecular materials is outlined in Sec 1.4 as these form the basis of several studies presented in the thesis. Sec 1.5 provides an outline of the layout of the thesis.

1.1. Molecular Materials

Materials hold a prominent place in defining and shaping our daily lives and culture and civilization at large. Every kind of activity such as food production, transportation and communication, clothing and entertainment etc. is influenced by the type of materials we use. Early humans used materials as they found them in nature, with little or no modifications. With the passage of time they developed primitive techniques to process natural materials to improve their characteristics and enhance the quality of performance. Subsequently it was discovered that properties of a material could be altered by heat treatment and by the addition or incorporation of other substances. Development of such processes made available whole new classes of materials. Alloys and ceramics are fine examples that illustrate the evolution of materials. Around 19th century, organic chemistry started emerging as a definitive field of study and manipulation at the molecular level became possible. Development of polymers was a major milestone. It became possible to design materials to suit specific needs. Today, the demand for new and improved materials is increasing constantly, and regular breakthroughs occur in the introduction of novel materials. Designed materials are probably best illustrated by composites, which allow us to reinforce materials at appropriate places and in desired amounts, optimizing features such as weight and mechanical properties. With the development of new types of materials, and the advent of new technologies, the quality of life has improved enormously.

The latter part of the last century has witnessed the emergence of a new class of materials known as ‘molecular materials’ that are made up of small molecules or molecular ions. They form potential candidates for a variety of applications.[1,2] Molecular materials exhibit weak intermolecular forces; their cohesion is mediated by dipolar, hydrogen bonding and π-π interactions.[3] The molecules involved in the formation of such materials may be purely organic or based on hybrid organic-inorganic combinations. The main advantage of molecular materials over their more classical inorganic counterparts is that their building blocks, the molecules, can be designed and synthesized and modified further if required. The iterative design strategy allows the production of optimal materials with predetermined properties. The uniqueness of molecular materials is that they can be easily disassembled into the constituents (molecules) by dissolving in suitable solvents, melting or sublimation, the molecules retaining largely the characteristics they exhibited in the assembled state. In view of the several common features and common characteristics polymeric materials,[4] nanocomposites[5] and liquid crystals can also be classified as belonging to the general family of molecular materials. Molecular materials are superior candidates for several technological applications. The basis of this could be attributed to their unique electronic structural features such as delocalized π electrons, polarized charge distribution induced by functional groups etc.. The fabrication of molecular materials generally involves two stages: the first one involves the synthesis of the desired building blocks (molecules) from the appropriate precursors (atoms or molecules) and the second is their assembly into the material of interest. The versatility and variety of organic and inorganic synthesis strategies can be exploited in the first step. Methods that can be employed to assemble molecular materials include simple crystallization,[6] host-guest complexation,[7] intercalation,[8] self assembly through layer-by-layer deposition methodology,[9] deposition by Langmuir-Blodgett transfer method,[10] spin casting of polymers and electric field induced poling of dopents[11] and organic molecular beam deposition technique.[12] Molecular materials span various forms, ranging from nanostructures and ultrathin films to glasses and crystals. Development of new materials with desired properties necessarily involves significant inputs from chemists, physicists, biologist and engineers. Such multidisciplinary activities have led to the emergence of a wide array of materials such as conducting, superconducting, magnetic, optical and nonlinear optical materials.[1] Molecular materials displaying many such properties exploited in various applications such as electronics[13]and photonics,[14] spintronics,[15] sensors,[16] and energy storage[8] and conversion.[17] In the following section we present an overview of molecular ultrathin films. This is followed by a detailed discussion of Langmuir-Blodgett films. As optical and nonlinear optical properties of molecular materials are of special interest to us, an introduction to the basic concepts involved is also presented.

1.2. Molecular Ultrathin Films

Organic thin films having thickness of a few nanometers have attracted much attention because of their technological applications in various fields such as sensors, detectors, displays and molecular electronic devices. The power of modern synthetic organic chemistry that allows the synthesis of molecules with nearly any desired structure and functionality, coupled with sophistication available in thin film deposition technology enables the production of electrically, optically and biologically active components on a nanometer scale. Molecular ultrathin films can be deposited on a wide variety of solid substrates using techniques such as vapor deposition, molecular beam epitaxy, layer-by-layer deposition and Langmuir-Blodgett transfer.

1.2.1 *Vapor Deposition*

Vapor deposition refers to any process in which materials in a vapor state are deposited through condensation, chemical reaction to form a solid material. Vapor deposition processes usually take place within a vacuum chamber. This technique is applicable to molecules which are sublimable and stable in the vapor phase. Besides the characteristics of the materials , the important factors that affect the size and morphology of the film/nanostructures are the nature of the substrate, rate of evaporation and the distance between the source and the substrate.[18] There are two broad categories of vapor deposition processes namely physical vapor deposition and chemical vapor deposition.

In physical vapor deposition (PVD) the material to be deposited is converted into vapor by a range of physical means and the vapor is transported across a region of low pressure from its source to the substrate and finally the vapor undergoes condensation on the substrate to form the thin film. The controlled transfer of the materials to the substrate placed at a distance from the source is followed by the film formation and growth on the substrate. PVD is often used to fabricate ultrathin films and nanostructures of organic molecules. Yao *et al.* have reported the growth of crystalline nanowires of small organic molecules with the adsorbent-assisted PVD method.[19] Perpendicular growth of one-dimensional organic nanoneedles of an organic molecule 1-cyano-trans-1,2-bis-(3′,5′-bis-trifluoromethyl-biphenyl)ethylene on a substrate by vapor phase deposition has been reported recently.[20] High density single crystalline organic semiconductor nanowires of porphyrin and phthalocyanine were grown by vapor transport deposition method on a silicon substrate coated with a thin film of silver oxide. Sequential synthesis of these two types of nanowires on the same substrate produced a novel type of open core@shell heterostructure.[21] Thin films of 2-((*Z*)-2-(4-diphenylamino)benzylidene)-1,2-dihydro-1-oxoinden-3-ylidene) malononitrile deposited by PVD technique have been successfully employed in reversible data storage application.[22]

Chemical vapor deposition (CVD) is a process that uses chemical reaction between the reactant gases, and forms a solid phase which is deposited on a substrate. Generally CVD is carried out by exposing the substrate to volatile precursors which react or decompose on the substrate surface to produce the desired deposit. Molecular layer deposition (MLD) is a special type of CVD in which molecular fragments are deposited during the surface reaction. MLD is mainly used for growing organic and hybrid organic-inorganic ultrathin films. Polymeric MLD films of pyromellitic dianhydride and 3,2,4-diaminonitrobenzene or 4,4′-diaminodiphenyl ether were fabricated by the condensation of the reactants on the substrate.[23] George *et al.* utilized *in situ* Fourier transform infrared (FTIR) measurements successfully to demonstrate the growth of nylon 66 polymeric MLD film using adipoyl chloride and 1,6-hexanediamine as the precursors.[24] The growth rate of the nylon 66 MLD films was estimated using *in situ* transmission FTIR measurements on flat KBr substrates with an amine-terminated Al_2O_3. Hybrid organic-inorganic MLD films can be grown by using an inorganic reactant together with an organic one.[25] Thin films of alucone, a hybrid inorganic-organic polymer is fabricated by sequential reaction between trimethylaluminum and ethylene glycol.

Evaporation of organic molecules in ultra high vacuum is often referred to as organic molecular beam deposition (OMBD) or organic molecular beam epitaxy (OMBE).[12] Monolayer control over the growth of organic thin films with extremely high chemical purity and structural precision is possible with this deposition method. In this method, the substance to be deposited is evaporated in a background vacuum ranging from 10^{-7} to 10^{-11} Torr and the evaporant is collimated by passing through a series of orifices. The deposition occurs on a substrate held perpendicular to the beam approximately 10 - 20 cm from the source. Ruben *et al.* have reported temperature induced phase transformations and hierarchical organization of a macrocyclic molecule 4,4′,4″-benzene-1,3,5-triyl-tribenzoic Acid (BTA) on silver (111) surface.[26] Ultrathin films of BTA were prepared by the OMBD method. BTA forms two-dimensional (2D) honeycomb structures at 250 K which transformed into one-dimensional (1D) ribbons and close packed 2D adlayer as the substrate was annealed at different temperatures. 2D supramolecular chiral network was observed recently by Chen *et al.* in ultrathin films of binary molecular system of pentacene and 3,4,9,10-perylenetetracarboxylic dianhydride deposited by OMBD.[27]

1.2.2 *Layer-by-Layer Deposition*

Layer-by-layer (LbL) deposition has emerged as an important method of fabricating ultrathin films of water soluble materials with controlled layer structure and lattice parameters. In general, the LbL deposition is achieved by alternately exposing a substrate to positively and negatively charged polymers or particles to form mono and multilayered structures. Ultrathin films prepared by the LbL method have found applications in various fields include drug delivery systems,[28] battery electrolytes,[29] sensors and membranes. Several reports have appeared in recent times describing the LbL approach to the assembly of polymers with inorganic nanoparticles, providing an opportunity to combine the electronic, optical, and magnetic properties of inorganic nanostructures with the unique physical attributes of macromolecules.[30]

1.2.3 *Langmuir-Blodgett Films*

Langmuir-Blodgett method involves the organization of a monolayer of molecules on a liquid surface, usually water followed by its transfer to a solid support to form ultrathin film with the thickness dependant on the length and orientation of the constituent molecules.[31] As this thesis makes use of this methodology extensively, a detailed discussion is presented in the following section.

1.3. Langmuir and Langmuir-Blodgett Films

Langmuir-Blodgett (LB) films are the earliest examples of supramolecular assembly that facilitates molecular level control over the organization and structure of the resulting films. As such ultrathin films offer several advantages over crystalline materials for various applications; the LB technique has become one of the favorite choices for the fabrication of molecular materials. The LB technique is simple and versatile. It facilitates: (i) organized assembly of molecules at the level of monolayers, (ii) precise control of the thickness of the deposited film, (iii) homogeneous deposition over large areas, (iv) fabrication of multilayer with varying layer composition and, (v) deposition on a wide variety of substrates.

Spreading of oil on water is a phenomenon known for ages and has been a topic of long-standing interest. The effect of these films in calming ripples on the ocean has been exploited traditionally by fishermen and sailors. The scientific origin of Langmuir and Langmuir-Blodgett films may be traced to the report of Benjamin Franklin at the British Royal Society [32] in which he wrote, "*the oil, though not more than a teaspoonful, produced an instant calm over a space several yards square, which spread amazingly and extended itself gradually until it reached the leeside, making all that quarter of the pond, perhaps half an acre, as smooth as a looking glass*". However, the first systematic studies of the spread molecules were made by Agnes Pockels at the end of the 19th century working in her home, using simple home-made apparatus. Publications of Pockels's work in Nature[33] laid the foundation for the basis of LB technique as practiced even today. In 1899 Lord Rayleigh suggested that these films were monolayers and thus afforded direct molecular level measurements. Subsequent work done by Hardy and Devaux showed that only amphiphilic molecules form monolayers whereas simple aliphatic molecules do not.

In the beginning of the 20th century, Irving Langmuir carried out systematic studies on monolayers of amphiphilic molecules at the air-water interface.[34] In 1920, Langmuir presented a paper in the transactions of the Faraday Society where he described the transfer of monolayers on to solid supports.[35] It was Katherine Blodgett working principally with fatty acids, who refined the method of transferring floating monolayers on to solid supports.[36] The technique is now popularly known as Langmuir-Blodgettry. The floating monolayer at the interface is termed as Langmuir film and after transfer it is called Langmuir-Blodgett films.

The current interest in LB films derives inspiration from the pioneering work of Hans Kuhn who used LB methods to control the position and orientation of functional molecules within complex assemblies,[37] an elegant early example of supramolecular assembly. To acknowledge Kuhn's contributions, some authors now call the transferred films of functional molecules, Langmuir-Blodgett-Kuhn (LBK) films.[38]

1.3.1 *The Air-Water Interface*

The interface between a liquid and a gas or between two liquids shows a transition between the composition and properties of the two bulk phases. A surface layer will exist with properties different from those of either bulk phase. The air-water interface (Fig. 1.1) is a case in point. The molecules in a liquid have a certain level of attractive interaction with each other. In the bulk liquid, the molecules are attracted equally in all directions. This attraction force, also known as cohesion, is uniform in all directions. However, the

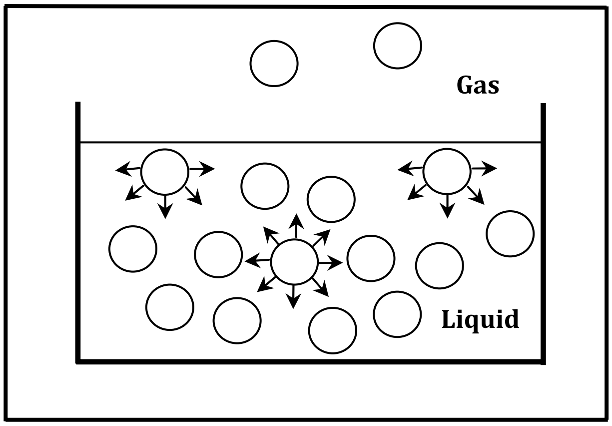

Figure 1.1. *Force experienced by molecules in the bulk liquid and at the liquid/gas interface.*

molecule present at the interface experience imbalance of forces i.e., a net attractive force exists towards the bulk liquid (water in this case) than towards the air or gas phase and hence the interface will try to minimize its area and contract. As a result, more molecules from the surface will diffuse initially in to the bulk, increasing the mean separation between surface molecules. The activation energy for a surface molecule escaping into bulk will increase until it is equal to that of molecules diffusing from the bulk to the interface and a state of equilibrium is achieved. The net effect of this situation is the increase of free energy at the surface. The line force acting on the surface is referred to as the surface tension, γ and is quantified as force/length. Strong intermolecular interactions exist in polar liquids and thus they have high surface tension. Any factors which decrease the strength of the interactions will lower the surface tension. Temperature and contamination of the surface with surfactant molecules generally alter the surface tension of the liquid. The LB method is based on the latter effect. The presence of a thin film on the surface will affect the surface tension. In the LB experiment the term 'surface pressure' is commonly used. The surface pressure π is equal to the reduction in the surface tension of the pure liquid by the presence of the surfactant, i.e.

$$\pi = \gamma_0 - \gamma$$

where γ_0 is the surface tension of the pure liquid and γ is the surface tension in presence of the surfactant.

1.3.2 *Surfactants*

The term 'surfactant' is derived from the word surface active agent. A surface active agent is one which tends to accumulate at a surface or interface and reduce the surface tension when used in very low concentrations. Amphiphilic molecules are typical surfactants; they consist of a hydrophobic and a hydrophilic part. The hydrophobic part in a surfactant is usually a hydrocarbon chain typically about 18 - 20 carbons long but may be fluorocarbon or siloxane chain of appropriate chain length. The hydrophilic group consists of polar functional groups such as COOH, NH_2, OH and CN or ionic groups such as sulfon-

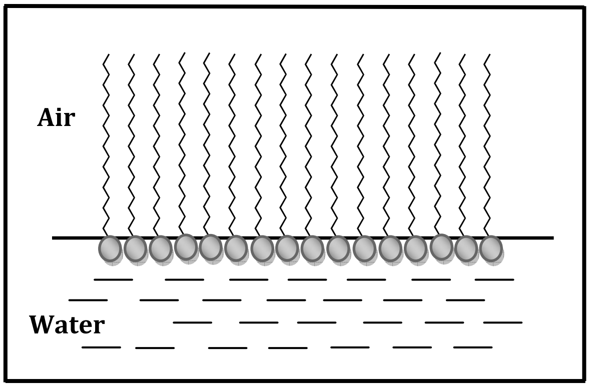

Figure 1.2. *A schematic representation of a monolayer of surfactant molecules at the air-water interface.*

ate, carboxylate or ammonium. The hydrophilic group improves solubility in water while the hydrophobic part reduces it. It is the balance between these two opposing forces that results in the formation of an insoluble monolayer at the air-water interface (Fig. 1.2). Any change in the nature of either the alkyl chain or the polar group can affect the noncovalent intermolecular interaction and the monolayer characteristics. Dispersion interaction between the hydrocarbon chains is normally a dominant force in the close packed two-dimensional structures. Factors such as π interactions may also contribute to lateral binding. Amphiphiles are often synthesized with specific functionalities to achieve desired properties in the LB film. In addition to the structural aspects, the purity of materials is critical for stable and reproducible LB film fabrication.

1.3.3 *LB trough, Compression System and Surface Pressure Monitoring*

LB troughs are usually made with Teflon (PTFE) which provides a strongly hydrophobic environment for the subphase. Teflon is highly stable towards the solvents used for spreading the monolayer and allows cleaning under harsh conditions such as strong acids and bases. Most of the troughs are either rectangular or circular in shape (Fig. 1.3). There are three common types of barriers used to compress the monolayer at the

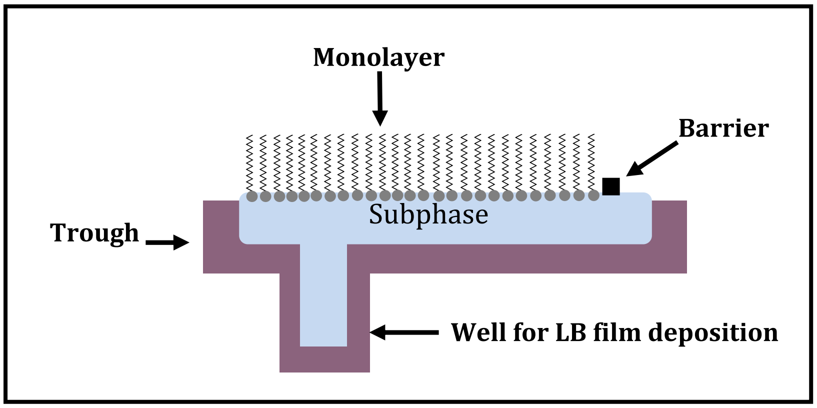

Figure 1.3. *Cross-sectional view of a trough with a single barrier and a well to facilitate LB film deposition* (Figure adapted from Ref. 10b).

surface and they are lateral sliding barrier on the rectangular trough, rotating sliding barrier on the circular trough and a constant perimeter barrier. The trough need not be very deep, as a 'well' can allow the vertical dipping of the substrate for transfer of the floating layer on to it. Two-compartment troughs for alternate layer depositions of two different monolayer materials on to the same substrate are also used in special application. LB experiments are carried out in a clean room environment with controlled temperature as contamination can alter the experimental results adversely. Other basic accessories attached to an LB trough are the pressure sensor and the dipper. The pressure is often measured using a Wilhelmy plate (typically a clean piece of Whatman 1 filter paper) which is hung over the subphase from the sensor unit. The dipper provides for vertical motion of the substrate, controlled by motor. Details of the trough used in this thesis work are given in Appendix A.

The commonly used subphase for LB experiments is water though use of mercury and other liquids such as ethylene glycol and glycerol have also been reported. Purity of the subphase is very important in LB experiments and ultrapure water with a typical resistivity of 18.2 MΩ.cm is used normally. The surface tension of water is 72.8 mN/m at 20^{o}C and any alteration in this value indicates surface contamination.

Surface pressure measurement is carried out by immersing a plate partially in the subphase from a sensitive balance equipped with the trough. The forces acting on the plate are due to gravity and surface tension downwards and buoyancy due to displaced water upwards. The net forces are recorded. For a rectangular plate of dimensions l, w and t (Fig. 1.4) and of material of density ρ_W, immersed to a depth h in a liquid of density ρ_L, the net downward force F is given by

$$F = \rho_w g l w t - \rho_L g h w t + 2\gamma(t+w)\cos\theta$$

(Force = weight – upthrust + surface tension)

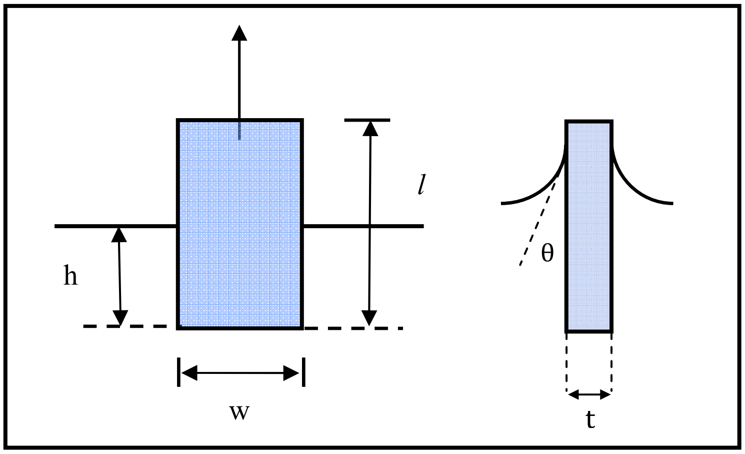

Figure 1.4. *Front and side views of a Wilhelmy plate* (Figure adapted from Ref. 10b).

where γ is the surface tension of the liquid, θ is the contact angle on the solid plate and g is the acceleration due to gravity (10 m/s^2). The usual procedure is to choose a plate that is completely wetted by the liquid so that $\theta = 0$ and to measure the change in F for a stationary plate. The difference in downward force ΔF, experienced by the Wilhelmy plate between immersion in pure water and immersion in surfactant-covered water is given by:

$$\Delta F = 2(\gamma^o - \gamma)(t+w)$$

γ^o being the surface tension of pure, clean water. If the plate is considered to be of negligible thickness compared to its width this can be simplified to:

$$\Delta F/w = 2\pi$$

where π is the difference between the surface tension of pure water and that of surfactant covered water, the surface pressure as defined earlier. The forces acting on the plate are normally measured with a sensitive balance. Some of the precautions needed with the Wilhelmy method are discussed by Middleton *et al.*. [39]

Pressure-area isotherm

The first step in a typical LB experiment is the spreading of a dilute solution of the amphiphile in a volatile solvent usually $CHCl_3$ or hexane, at the air-water interface. The concentration of the solution should not exceed what is required to form monomolecular layer in the available trough area. The solvent used should be of high purity since the contamination of the solvent may affect the film behavior significantly. After the evaporation of the solvent the film is compressed with the help of the mechanical barrier attached to the trough and the variation of the surface pressure with area of the monolayer at constant temperature (pressure-area isotherm) is recorded. Various phase transitions are observed during the monolayer compression which is analogues to the transitions between gases, liquids and solids in 3-dimensional space. These phase changes can be followed by monitoring the pressure-area isotherm (π-A), which is the 2-dimensional equivalent of the familiar pressure-volume isotherm. The different states associated with a monolayer compression are usually called the (i) gaseous phase, (ii) expanded phase and (iii) condensed phase (Fig. 1.5). Before starting the compression, the molecules are far apart on the water surface and practically non-interacting. In this stage the molecules behave like those in two dimensional gas, and can be described by,

$$\pi A = kT$$

where the area, A and surface pressure, π are equivalent to volume ,V and pressure ,P in the
where the area, A and surface pressure, π are equivalent to volume ,V and pressure ,P in the
3-dimensional case. Upon compression, the molecules are forced to come closer. They start

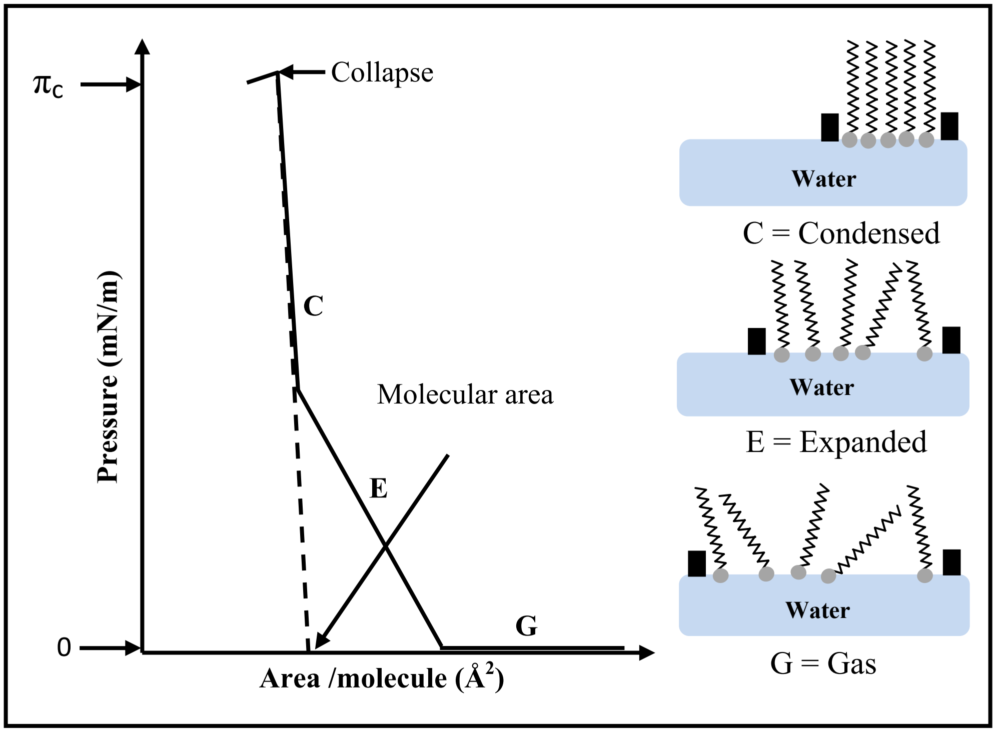

Figure 1.5. S*chematic illustration of a typical pressure-area isotherm and the organization of amphiphiles in different phases.*

interacting with each other in what resembles a liquid state and is generally called the expanded phase. The hydrocarbon chains of the molecules are in a random state at this point, and the polar groups in contact with the subphase. Further compression of the monolayer results in the formation of a condensed phase in which the molecules are organized in a close packed array and like solids they are relatively incompressible. At this stage, molecules form floating monolayer called the ‘Langmuir film’. Extrapolation of the condensed region of the π-A isotherm to the area-axis gives the absolute area/molecule, if the molecule is oriented nearly perpendicular to the plane of the interface, this will be close to the cross-sectional area of the molecule with extended hydrocarbon chain. The surface pressure continues to increase with decreasing surface area until a point is reached where the film cannot sustain any further. The pressure at which the film collapses is known as the collapse pressure (π_c).

In some cases a plateau region or constant pressure region is observed between the expanded and condensed phases. This constant pressure region represents a transition region between the two phases. Various factors including reoriantation of headgroup contribute[40] to the plateau formation. The position of the plateau region is affected by factors like chain length and the temperature. An increase in the temperature or decrease in the chain length will generally increase the surface pressure corresponding to the plateau and *vice versa*.

The π-A is rich in information on the stability of monolayer, reorientation of the molecules, phase transitions, conformational changes *etc*. The behavior of a particular material can vary greatly depending on the experimental conditions such as temperature, time delay between spreading and commencement of compression, pH of the subphase and the speed at which the barriers are closed.[41]

1.3.4 *Langmuir films to Langmuir-Blodgett films*

The term LB film traditionally refres to the monolayer that is transferred onto a solid support from the subphase. The most common choices for the substrate are glass, quartz, silicon, highly oriented pyrolitic graphite (HOPG) and mica . The substrate surface can be made hydrophilic or hydrophobic through suitable treatments. In principle the LB deposition method simply consists of dipping and pulling a solid substrate, oriented vertically, through the coating monolayer while keeping the surface pressure constant at a desired value (Fig. 1.6). Multilayers formed by multiple dipping/stroke of the substrate through the monolayer-air interface are usually of three types, x, y, and z depending on the sequence in which the amphiphiles are attached. In x- type deposition the monolayer transfer will occur only during the down strokes and the molecules in every layer align with their hydrophobic tail towards the substarte. Monolayer transfer occurs during the upstroke in z- type deposition and the molecules are oriented with their hydrophilic head group towards the substrate in the resulting film. The y- type film results when the transfer occurs during both the up and down strokes. Head to head and tail to tail pattern of deposition are observed in this film. The x- and z- type films are noncentrosymmetric and the y- type film is generally centrosymmetric. Even though vertical deposition is the most common method of LB transfer horizontal lifting of Langmuir monolayers onto solid supports, called Langmuir–Schaeffer deposition, is also possible.The extent of film transfer is expressed as the transfer ratio (TR), which is the ratio of the reduction in the monolayer area to the area of the substrate moved through the monolayer. TR should be ideally unity or 100%. Quality

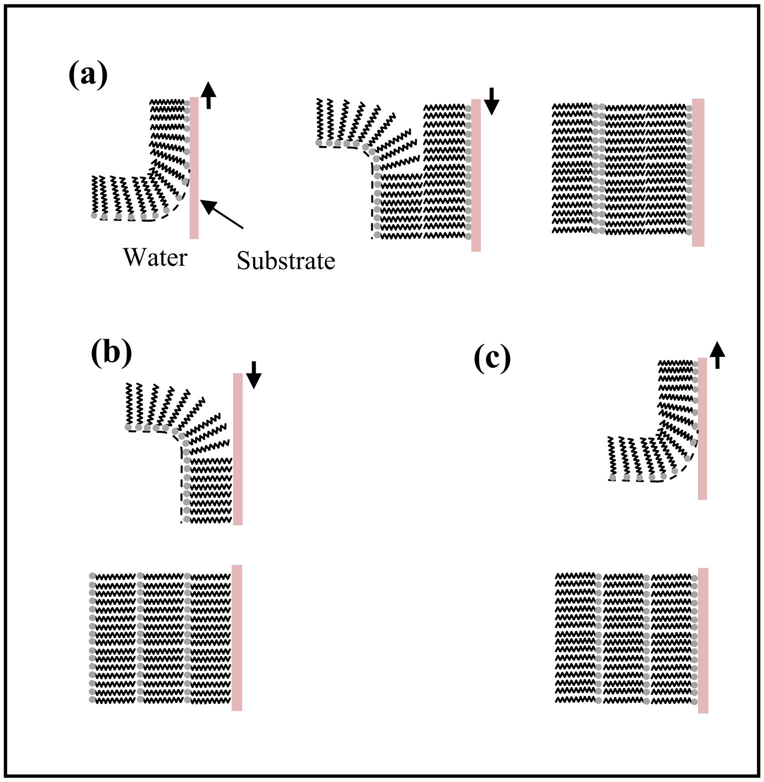

Figure 1.6. *Langmuir-Blodgett film depostion* ***(a)*** y- *type;* ***(b)*** x-*type; (c)* z-*type.*

of the LB film depends on the monolayer stability as well as parameters like the dipping speed and nature of the substrate.

1.3.5 *Characterization of Langmuir and LB films*

Several techniques are available to characterize Langmuir and LB films. The material properties are sensitively dependent on various characteristics of the film such as molecular orientation and packing, thickness, interlayer spacing and interactions, film coverage, surface topology, chemical composition and the content of defects or pinholes. Coupling of two or more complimetary techniques is often essential to derive useful information about the film characteristics.

π-A is the most basic and preliminary characterization of the Langmuir monolayer. Surafce potential or conductance measurements during the compression of the monolayer is also used to study the evolution of the Langmuir film. Spectroscopic[42] and second harmonic generation (SHG)[43] studies on Langmuir films reveals the molecular orientation at the air-water interface. A brief description of some of the commonly used techniques for Langmuir and Langmuir-Blodgett film characterization is given below.

Brewster angle microscopy (BAM) is a powerful technique, for morphological characterization of monolayers at the interface.[44]A brief description of BAM is given in Appendix B. Phase separation in mixtures of pulmonary surfactant and phospholipid films at the air-water interface was demonstrated using BAM.[45]The monolayer evolution during the compression of the molecules at the interface can be monitored by measuring the thickness of the Langmuir film by using quantitative analysis of BAM images. Fluorescence microscopy[46] provides useful information on domain structures. Scanning probe microscopies like scanning tunneling microscopy (STM),[47] atomic force microscopy (AFM)[48] and friction force microscopy (FFM)[49] are ideally suited for surface structure studies and defects in LB films with high resolution. Electron microscopies like transmission electron microscopy (TEM) can also provide a great deal of information on the in-plane structure. Scanning electron microscopy (SEM)[50] can be used to detect defects like microcrystal formation. X-ray scattering techniques like small angle X-ray scattering (SAXS), provide information on the layer structure of the film. Grazing incidence X-ray diffraction (GIXD) is used to determining the arrangement of molecules within a floating monolayer.[51]

Ellipsometric,[52] X-ray[53] and neutron reflectivity[54] methods are often used to measure LB film thickness. To study the chemical structure of the films, standard spectroscopic methods can be used, including FTIR spectroscopy, Raman scattering, and UV-Visible absorption. Polarized absorption spectra contain information on the orientation of the chromophore with respect to the substrate plane and dipping direction. Solid state NMR spectroscopy has been used recently to characterize LB films.[55]The elemental composition can be determined with X-ray photoelectron spectroscopy (XPS).[56] If the molecules have appreciable hyperpolarizability and noncentrosymmetric packing, then LB films can be characterized by their SHG (see sec 1.4.2). Analysis of the SHG signal can be performed to yield an effective second-order susceptibility tensor, $\chi^{(2)}$ for the thin film by comparison with standards such as Y-cut quartz crystal. The $\chi^{(2)}$ together with the knowledge of molecular organization can be used to estimate the molecular hyperpolarizability.[57] Homogeneous growth of LB multilayers in x or z form is usually indicated by a quadratic increase of SHG intensity with the number of layers.

1.3.6 Applications of LB films

LB films have found applications in various areas of science and technology.[58] Kuhn's pioneering studies demonstrated the power of this simple technique in controlling materials fabrication at the molecular level. His work moved away from the established studies on traditional fatty acids and their salts and used the LB technique to control the position and orientation of functional molecules in complex assemblies for optical and energy transfer applications. Several amphiphilic molecules form stable Langmuir and LB films. Common examples are fatty acids,[59] dyes,[60] chromoionophores,[61] porphyrins,[62] fullerenes,[63] polymers,[64]and phospholipids.[65] These systems in the pure state or in mixtures are convenient model systems for various applications. Multilayer LB films of chromoionophores were used as metal ion sensors.[66] Phthalocyanines[67] and dendrimers[68] have been studied as LB films with device applications as the ultimate goal. Molecular conductors and magnets based on LB films of various amphiphiles have been investigated extensively.[38c] Patterned LB films of the phospholipid dipalmitoylphosphatidylcholine was used to organize luminescent nanocrystals and gold nanoclusters; they were used also for selective adsorption of thermally evaporated silver on to the channels in the films.[69] LB films of fullerene derivatives show electrochemical[70] and third order nonlinear optical properties[71] of interest in various fields. Some of the specific applications of LB films are elaborated below.

Sensors

LB films are ideally suited for sensing applications because of their ultrathin nature that is conducive to quick response and short recovery times leading to efficient sensing. In order to function as a sensor, the active element in the LB film has to be designed so that one or more of its properties change markedly and reversibly in response to the appropriate stimulus. By modifying the structure of the molecule and hence the nature of the film it is possible to make the response selective. Phthalocyanine based LB films have been shown to be efficient sensors for gases such as NH_3, NO_2, halogens, hydrazines[72] and organophosphorus vapours.[73] Moriizum *et al.*[74] have described a sensor in which glucose oxidase is immobilized on the head groups of a lipid. LB films are employed in several commercial glucose sensors.[75] Temperature sensing device based on LB films of poly(azo)urethane was demonstrated recently by Alessio *et al.*[76] LB films have been used in a wide variety of gas and ion sensors,[77] biosensors,[78] and molecular recognition[79] applications.

Electronic Applications

Rectification using mono and multilayer LB films is one of the most interesting applications in molecular electronics.[80] LB films of phthalocyanine,[81] cyclo[8]pyrolle[82] and poly(3-hexylthiphene)[83] have been used in the design of field effect transistors (FET).

Molecular conductors based on LB films[38c] of appropriate amphiphiles are also important in the field molecular electronics. Other applications include switching and memory devices, electroluminescent displays[84] and photovoltaic energy conversion and optical data storage systems.[85]

Optical and Nonlinear Optical Applications

Optical and nonlinear optical effects in general and concepts of interest for molecular materials will be discussed in Sec. 1.4. Here we note some of the related applications of LB films. Ultrathin films of molecules that can absorb or emit in the UV or visible range, are of current interest in various technological applications such as optical data storage, optical switching, sensors and light emitting diodes. Optically induced stable birefringence of the film can be used in data storage applications. Cis-trans isomerization of molecules in the film is triggered by irradiation with linearly polarized light and the accompanying molecular reorientation is one mechanism by which birefringence and dichroism are produced.[86] This induced birefringence can be read with a probe beam in the non-resonance absorption region. Mixed LB films of disperse red-19 isophorone polyurethane and cadmium stearate have been demonstrated to be optical storage devices owing to their optically induced birefringence that originates from the cis-trans isomerization of the azobenzene chromophore.[86] Utility of LB films based on polythiophene[87] and thiophene spaced N-alkyl pyridinium malononitrile zwitterionic dyes[88] in similar applications have also been demonstrated. Reversible change in wettability due to optically induced cis-trans isomerization was observed in LB films of a polymer with azobenzene as a pendant group.[89] Optical switches based on bacteriorhodopsin LB films have also been established.[90]

Electroluminescence is the emission of light from a material when an electric field is applied across it. LB films of suitable molecules are ideal candidates for this application because of their ultrathin nature and the high effective fields that can be produced. Very low threshold voltages are required to produce light emission from LB films. For example, in order to achieve a specific light intensity, only 6 V are required for LB films of a certain material as compared to 200 V for an evaporated film of the same material.[91] Monolayer LB films of polyfluorene have been used to create a polymer light emitting diode (PLED).[92] Incorporation of a liquid crystal in LB films of poly(p-phenylene vinylene) derivatives is found to enhance the light emitting properties of the film. Xu *et al*.[93] showed that organized films of poly(3,4-ethylene dioxythiophene) fabricated by the LB technique exhibited improved electroluminescence performance over those fabricated by other techniques. The LED's based on multilayer LB films can be used for the fabrication of flat-panel displays. Application of an array of fluorescent polymer nanosheets fabricated by the LB technique, in luminescence based optical memory, was demonstrated by Matsui *et al.*[94] Potential applications of fluorescent LB films include sensors[95] and probes for film structure[96] and imaging.[97]

As will be discussed in Sec. 1.4.2, a material has to be noncentrosymmetric to exhibit quadratic NLO effects. Several methodologies have been developed for the fabrication of noncentrosymmetric materials. LB method is one of those methods which facilitates the organization of NLO phores in a noncentrosymmetric manner. LB films need to posses high second order nonlinear susceptibility $\chi^{(2)}$, good transparency over the wavelength of interest, and thickness of a few microns, in order to function as SHG based devices like waveguides. NLO active LB films of polymers have been employed successfully in waveguide applications.[98] LB films of pyrazine derivatives[99]alternating with fatty acids have also been used. Strong SHG responses have been observed in a number of LB films of hemicyanine based amphiphiles.[100] The polyelectrolyte templating strategy developed in our laboratory has been found to be effective in stabilizing these LB films against aggregation and hence enhancing their SHG response.[101] Cresswell *et al.* have utilized the second order NLO properties of LB films in electrooptic modulation devices.[102]

1.3.7 *Ultrathin Film-Nanoparticle Composite Materials*

The area of nanotechnology is witnessing an unprecedented boom primarily due to the development of improved nanoparticle synthesis protocols and progress made in the understanding of their fundamental physicochemical properties.[103] One of the factors that will influence significantly the next developments in the area of nanoscience and technology is the facility with which systematic two- and three-dimensional organization of metal and semiconductor nanoparticles can be effected. Self assembly or assisted assembly of nanoparticles is currently of much interest due to the collective properties that arise from coupling of optical or electronic properties of individual nanoparticles. The main challenge in the area of organization of nanoparticles in two- and three- dimensional structures is to develop protocols wherein the size, shape and separation between the nanoparticles can be tailored. Several attempts have been made to organize nanoparticles in two- dimensional structures by a variety of methods that include self assembly of particles during solvent evaporation,[104] immobilization by covalent attachment at the surface of self assembled monolayers[105] or on surface modified polymer,[106] electrophoretic assembly on suitable substrates,[107] LbL deposition,[108] organization at the air-organic solvent interface,[109] and by diffusion into fatty lipid films.[110]

Although several methods have been developed as noted above, the bottom-up assembly of nanoparticles for device fabrication and processing remains a big challenge. An ideal strategy should be cheap, fast, efficient and applicable to a wide range of materials. LB assembly is an efficient and convenient method to assemble a variety of nanostructures on several choices of substrates for different applications. This method is unique in its ability to achieve control over the two-dimensional assembly of nanostructures over a large area, and the fabrication can be controlled by tuning experimental conditions such as compression speed, surface pressure, dipping speed etc. Close packed assembly of nanostructures can be obtained by compressing the floating monolayer of nanoparticles on the subphase and transferring to a solid surface. Tao *et al.* obtained close packed assembly of silver nanocrystals with tunable plasmonic responses using the LB technique.[111] Well aligned stripe patterns of gold nanoparticles with varying orientation, thickness and periodicity at the micrometer scale have been fabricated by the LB method.[112] The assembly strategies reported using the LB technique have exploited (i) the electrostatic attraction between particles in the subphase and a surfactant monolayer,[113] (ii) post deposition treatment of LB films containing precursors of nanoparticles,[114] and (iii) direct spreading of the surfactant capped particles at the air-water interface.[115] Recently Mitsuishi *et al.*[116] demonstrated the immobilization of metal nanoparticles on cationic polymer LB films utilizing electrostatic interaction between the LB film and the nanoparticles. The assembly was achieved by immersing the LB film in solutions of nanoparticles bearing negative surface charges for different time periods. The resulting hybrid nanoassemblies have been used for the fabrication of optoelectric devices.

The assembly of nanoparticles into two- or three-dimensional nanostructures and in the form of thin films has potential applications in X-ray optics,[117] nonlinear optics,[118] microelectronics[119] and optical data storage. Interaction of metal nanoparticles modifies the surface plasmon resonance (SPR)[120] leading to significant changes in the optical extinction; this is of interest in several applications including surface enhanced Raman scattering (SERS)[121] and sensors.[122] It has been found that the presence of assembled nanoparticles in LB films affect the optical responses of the film to a great extent.[123] Recently, Ishifuji *et al.*[124] have reported the effective utilization of the surface plasmons for enhancing second harmonic generation from nonlinear optical polymer nanosheets. In this thesis we describe the assembly of gold nanoparticles on monolayer LB films of a hemicyanine dye and tuning the SPR of gold nanoparticles over a wavelength window.

1.4. Optical and Nonlinear Optical Properties of Molecular Materials

In some respects, molecular materials exhibit fundamentally different electronic and optical properties compared to their inorganic counterparts based on extended atomic or ionic lattices. This arises due to the fact that a variety of noncovalent interactions exist in molecular crystals, most of them relatively weak, and some highly directional. Hydrogen bonds, π-π stacking, van der Waals forces and charge transfer interactions direct the assembly of the molecular building blocks and hence influence the properties of the molecular materials. Several novel electronic and optical attributes have been realized in molecular materials. A brief introduction to optical and nonlinear optical properties of materials is given in the following section with special reference to the case of molecular materials where relevant.

1.4.1 *Linear Optical Properties*

When an electromagnetic radiation interacts with an atom or molecule, it induces oscillating dipoles which follow the frequency of oscillation of the electric field of the incident radiation. A resonance state is established when the frequency of the incident beam matches the natural frequencies of the molecule determined by its energy states. In this situation, radiation is absorbed by the molecule which gets promoted to a higher energy state. The molecule is then said to be in an excited states. The electronic transition generally follows the Frank Condon principle: *an electronic transition is most likely to occur without changes in the positions of the nuclei in the molecular entity and its environment since the electronic transitions are much faster (10^{-15} s) than the nuclear motion (10^{-13} s).* The resulting state is called the Franck–Condon state, and the transition is called a vertical transition. Electronic transitions are governed by selection rules based on symmetry.[125] The strength of an electronic transition is generally expressed in terms of the oscillator strength (f), and is given by[125]

$$f = \frac{8\pi^2 m_e \nu |\mu_{nm}|^2}{3he^2}$$

where m_e is the mass of the electron, ν is the frequency of transition, h is the Planck's constant, e is the charge of electron and μ_{nm} is the transition dipole between the two electronic states n and m involved in the transition defined as:

$$\mu_{nm} = \int \psi_n^* \hat{\mu}_{nm} \psi_m d\tau$$

where ψ_n and ψ_m are the wavefunctions of the two states and $\hat{\mu}_{nm}$ is the dipole moment operator. The oscillator strength for an electronic absorption is directly proportional to the integrated absorption coefficient, A defined as

$$A = \int \varepsilon(\nu) d\nu$$

where $\varepsilon(\nu)$ is the molar absorption coefficient at frequency ν. The absorbance, A (defined as log I_o/I, where I_o is the incident light intensity and I is the transmitted light intensity) of a sample at frequency ν (or wavelength λ), generally follows Beer-Lambert Law.

$$A(\lambda) = \varepsilon(\lambda)cl$$

where $\varepsilon(\lambda)$ is the molar absorption coefficient at wavelength λ, c is the concentration of the absorbing species and l is the absorption path length. Deviations from Beer–Lambert law are indicative of possible aggregate formation at high concentrations or the presence of other species with overlapping absorption.

Assembly or aggregation of dye molecules in solutions and at interfaces (solid/liquid, air/liquid) is of current interest because of their potential impact on technological applications.[126] Intermolecular interactions ranging from strong electrostatic effects to weak van der Waals attractions could be responsible for the molecular aggregation. The type of molecular association (sandwich, head-to-tail) and the size of the aggregates significantly affect the optical properties of the materials. H- and J- are the two main types of aggregates distinguished, based on the nature of intermolecular association, structure of the aggregate and the optical responses. H- aggregates are formed by sandwich type molecular association and their absorption at higher energy leads to a hypsochromic (blue) shift with respect to the monomer absorption. J- aggregates which are less common, and typically with a head-to-tail formation, absorb at lower energy and giving rise to a bathochromic (red) shift compared to the monomer.[127]

Organized assemblies of molecules such as those in crystals and thin films can exhibit linear dichroism i.e. difference in the molar absorption coefficient and hence in the absorbance for light polarized in different planes. Typical experiments measure absorbances for s- and p- polarized light incident at different angles with respect to selected areas of the sample.

A molecule excited by absorption of a photon, can return to the ground state by emission of light (fluorescence); however, many other pathways for de-excitation also exist (Fig. 1.7). Internal conversion is a nonradiative transition between two electronic states of the same spin multiplicity. Fluorescence arises due to emission of photons during the transition from the first excited state (S_1) to the ground state (S_0). Fluorescence generally occurs at a higher wavelength than that of the absorption due to vibrational relaxation. The difference between the maximum of the lowest energy absorption band and the maximum of the fluorescence band is called Stoke shift. Intersystem crossing (ISC) is a non-radiative transition between two isoenergetic vibrational levels belonging to electronic states of different multiplicities. The molecule in the S_1 state can cross to the corresponding triplet excited state (T_1) through ISC and then returning to the ground state ($T_1 \rightarrow S_0$) by emission of radiation; this process is called phosphorescence. Since phosphorescence is forbidden by the spin selection rule, the process is slow and occurs over a long period even after the

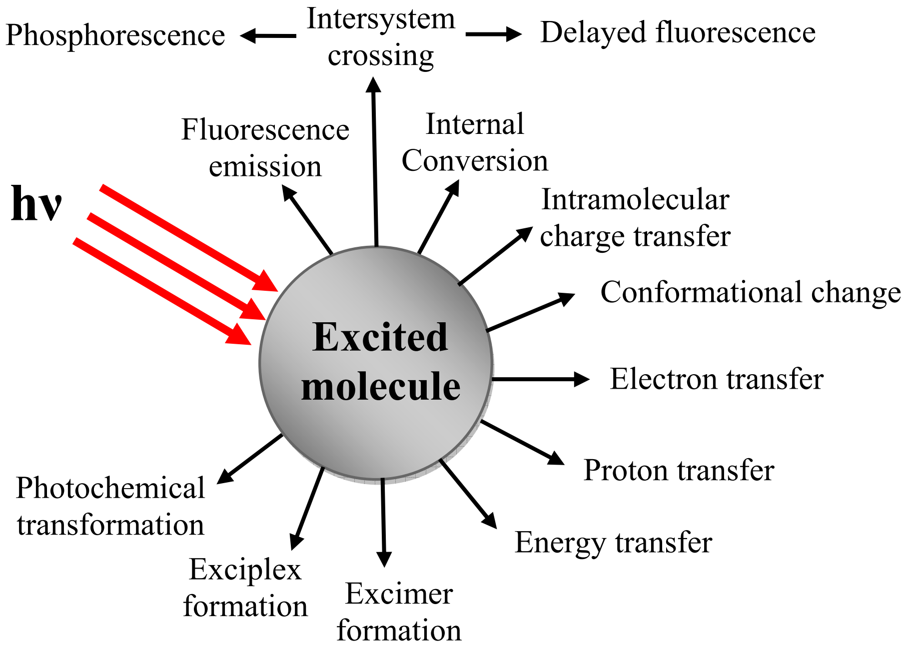

Figure 1.7. *Possible de-excitation pathways of excited molecules* (figure adapted from Ref.125).

exciting radiation is shut off. Intramolecular charge transfer and conformational changes are the other possible ways of de-excitation. The main intermolecular photophysical processes that compete with fluorescence emission are electron transfer, proton transfer, energy transfer, excimer or exciplex formation. Excimers are formed by the collision between an excited molecule and an identical molecule in its ground state. Excimer formation is a diffusion-controlled process. Excimers are observed at higher concentrations of the species when sufficient number of collisions can occur during the excited state lifetime.

The formation of H- aggregates generally quenches the luminescence of the molecules[128] whereas the J- aggregates show strong emission.[129] Fluorescence of most of the dyes get quenched in the condensed phase, e.g., in the solid state due to the so called concentration quenching or self quenching effect. The opposite effect 'aggregation induced emission' has been noticed in several systems and is a topic of active current interest.[130] The size dependent optical properties in molecular nano/micro crystals have been established by Patra *et al*.[131]

Metal nanoparticles can manifest the characteristics of molecules[132] and their organized assembly is reminiscent of the formation of supramolecular architectures, both accompanied by perturbation of the electronic structure and hence the optical responses. The optical properties of metal nanoparticles have long been of interest in physical chemistry, starting with Faraday's investigations of colloidal gold in the 1800s. The origin of the phenomenon of light absorption by the metal nanoparticles was explained by Mie. When a small spherical metallic nanoparticle is irradiated by light, the oscillating electric field causes the conduction electrons to oscillate coherently. This is shown schematically in Figure 1.8. When the electron cloud is displaced relative to the nuclei, a restoring force arises from Coulomb attraction between electrons and nuclei that results in oscillation of the electron cloud relative to the nuclear framework. According to Mie theory,[133] the extinction cross-section for small spherical particles of radius R (where $R << \lambda$, wavelength of light), can be expressed as

$$C_{ext} = \frac{24\pi^2 R^3 \varepsilon_m^{3/2}(\lambda)}{\lambda} \frac{\varepsilon''(\lambda)}{[\varepsilon'(\lambda) + 2\varepsilon_m(\lambda)]^2 + \varepsilon''^2(\lambda)}$$

where, $\varepsilon = \varepsilon'(\lambda) + i\varepsilon''(\lambda)$ is the wavelength dependent, complex dielectric function of the nanoparticle material and ε_m is the dielectric constant of the surrounding medium. The quantity C_{ext} reaches maximum when $\varepsilon' = -2\varepsilon_m$. The collective oscillation of the electrons induced by the electric field of the radiation under this condition is known as surface plasmon resonance (SPR). It is obvious from the Mie equation that the plasmon peak position and intensity depend on the composition, size and shape of nanoparticles, dielectric properties of the surrounding medium and interparticle interactions.[134] SPR in gold, silver and copper nanoparticles occur in the visible range of the electromagnetic spectrum. Coupling of the Plasmon resonances lead to new absorption peaks, often red shifted with respect to those of single particles.

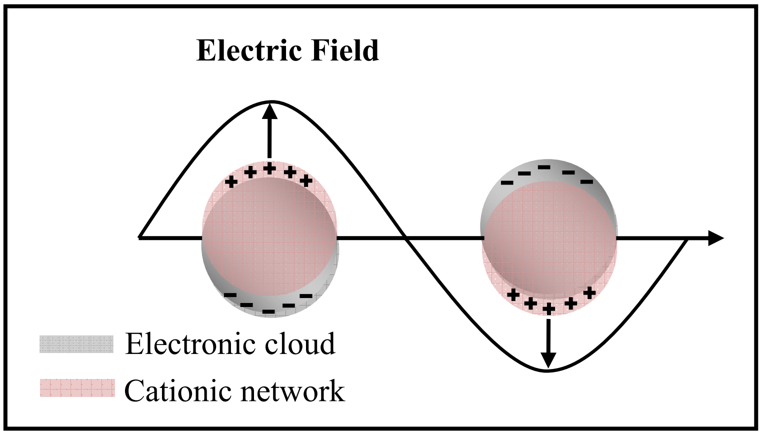

Figure 1.8. *Schematic descriptions of electron cloud displacements in nanoparticles under the effect of an electromagnetic wave.*

1.4.2 *Nonlinear Optical Properties*

When electromagnetic radiation interacts with matter, the associated electronic field induces electric polarization in the matter. If the radiation frequency is in the optical range the polarization is dominantly electronic. The polarization, p(dipole moment per unit volume) induced is related linearly to the field, E by the proportionality constant, $\chi^{(1)}$ the linear electric susceptibility, when the field is low as in the case with ordinary light. At high electric field, as in the case of lasers, the induced polarization has a nonlinear dependence on the field, due to significant contributions from higher order terms[135] (Fig. 1.9). The ith component of the polarization depends on the various electric field components as

$$P_{material} = \chi^{(1)}_{ij}.E_j + \chi^{(2)}_{ijk}.E_j.E_k + \chi^{(3)}_{ijkl}.E_j.E_k.E_l + ...$$

where *i*, *j*, *k* and *l* refer to the coordinate framework of the bulk material. The tensor term $\chi^{(n)}$ represents the electric susceptibility of order n. The polarization at the molecular level, similarly depends on the molecular polarizability, *α* and hyperpolarizabilities, *β*, γ etc as.

$$P_{molecule} = \alpha_{ij}.E_j + \beta_{ijk}.E_j.E_k + \gamma_{ijkl}.E_j.E_k.E_l + ...$$

The phenomenon of frequency doubling or second harmonic generation (SHG) can be visualized as follows. If the applied electric field of frequency ω, is represented as the function sin(ωt), the quadratic terms in the above equation will have a 2ω dependence as seen below.

$$E \propto \sin \omega t$$

$$E^2 \propto \sin^2 \omega t = \frac{1}{2}(1 - \cos 2\omega t)$$

There is an important symmetry constraint for observing SHG or other quadratic (in general any even order) NLO effects. In systems having a centre of symmetry, reversal of the electric field should exactly reverse the polarization *i.e.* P (-E) = -P (E). From equation for the polarization it can be seen that this is possible if and only if all terms with even powers of E becomes zero. In a noncentrosymmetric system, generally P(-E) ≠ -P(E). This implies that quadratic and other even order effects are possible only in noncentrosymmetric systems. This aspect is of critical relevance in the design of molecular materials for quadratic NLO applications.

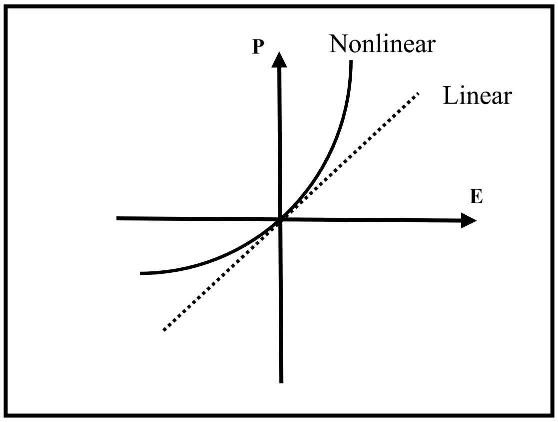

Figure 1.9. *Nonlinear polarization at high electric fields; the linearity at low fields is shown using the dashed line.*

1.5. Layout of the Thesis

In this thesis, we describe the novel molecular ultrathin films we have fabricated using the LB technique and the enhanced optical and nonlinear optical responses that were realized in them through tailored design. Unusual optical properties as well as new applications in the formation of nanocomposites with tunable optical properties are also investigated. In all cases, we have attempted to unravel the correlation of the properties/functions at the supramolecular/materials level with the molecular structure/organization in the ultrathin film. Optimization of fabrication conditions, spectroscopic and microscopic characterizations, evolution of materials attributes and computational modeling form integral parts of the studies. The thesis contains six chapters in all; a brief outline of the content of the following chapters is provided below.

Chapter 2: In this chapter we present our studies of the unique optical properties of LB films of a zwitterionic compound with a 'push-pull' structure, 7,7-bis(octadecylamino)-8,8-dicyanoquinodimethane (BODDQ). This molecule shows similar electronic absorption spectra in the solution as well as the bulk solid state, but a dramatically different one in LB films; the lowest energy absorption is switched off completely in the latter. The lowest energy electronic absorption of solutions of BODDQ occurs at ~ 370 - 420 nm depending on the solvent; an additional absorption peak is seen in the UV region. The lowest energy peak appears at 380 nm in the solid state; the UV peak is also observed. The remarkable disappearance of the lowest energy optical absorption of the molecule in its stable LB films arising without the intervention of complexing partners, chemical or electrochemical changes or the impact of external fields, is a direct consequence of the molecular assembly in the LB film, as the same absorption is starkly visible in the solution as well as the bulk solid states. It is demonstrated further that a metastable form of the LB film exhibiting the normal molecular spectrum can be generated; but its lowest energy absorption decays and vanishes over a period of time. Following a description of the experimental investigations and the characterizations of Langmuir and LB films of BODDQ through π-A isotherms, BAM and AFM, the salient spectroscopic observations are discussed. In an effort to gain insight into the unusual effects revealed by the experiments, we present a model for the molecular assemblies in LB films and based on computational studies, develop a rationale to account for the unusual and unique switching off of the electronic absorption. The phenomenon is attributed to the impact of the strong local electric fields arising due to the highly dipolar neighboring molecules in the assembly.

Chapter 3: This chapter describes our studies on fluorescence emission of LB films of three different amphiphiles based on the same hemicyanine fluorophore possessing different modes of attachment of alkyl chains. We have focused our investigations on the three amphiphiles N-*n*-octadecyl-4-[2-(4-(N,N-dimethylamino)phenyl)ethenyl]pyridinium bromide ($ODEP^+Br^-$), N-methyl-4-[2-(4-(N,N-ethyloctadecylamino)phenyl)ethenyl]-pyridinium iodide ($MEOEP^+I^-$) and N-*n*-octadecyl-4-[2-(4-(N,N-ethyloctadecylamino)phenyl)ethenyl]pyridinium bromide ($OEOEP^+Br^-$). The orientation and organization of the hemicyanine based amphiphiles at the air-water interface and hence in the LB film are found to be dependent on the molecular structure, specifically the mode of attachment of the hydrocarbon chains at the two ends. This in turn alters the optical responses while the chromophore unit remains the same. Investigations of the polarization dependence of the electronic absorption spectra provide insight into the chromophore orientations in the different LB films. Comparison of the fluorescence properties of the monolayer LB films indicates that LB films of $OEOEP^+Br^-$ deposited under specific conditions show 30–50 times enhancement over that of the weakest one based on $ODEP^+Br^-$. In $OEOEP^+Br^-$, the long hydrocarbon chains at both ends of the headgroup bestow a 'tail-head-tail' structure that guides the packing of the fluorophore units and controls the intermolecular interactions, leading to minimization of self-quenching effects and enhancement of fluorescence emission.

Chapter 4: The utility of the 'polyelectrolyte templating' methodology in the fabrication of multilayer LB films of a hemicyanine based amphiphile with stable and enhanced second harmonic generation (SHG) response is presented in this chapter. In this study we explored the impact of different polyelectrolytes (salts of poly(4-styrenesulfonic acid) (PSS), deoxyribonucleic acid (DNA) and carboxymethylcellulose (CMC)) on the mode of formation of multilayer LB films of the hemicyanine amphiphile, $ODEP^+Br^-$ and their SHG responses. π-A isotherms and BAM reveal the impact of the polyelectrolyte complexation on the Langmuir films. Transfer ratios observed during film deposition, supported by electronic absorption spectra and AFM images of the multilayer LB films, suggest that the polyanions influence the deposition sequence leading to significant variations in the SHG. CMC is identified as an optimal template that induces favorable z-type deposition, leading to the formation of stable multilayer films. These films exhibit the expected quadratic increase of SHG with the extent of deposition; significantly the film response is very stable under extended laser irradiation. It is proposed that structural adjustments of the sandwiched polymer layer leads to the observed deposition sequence and film stability. Polyelectrolyte templating is demonstrated to be a simple and effective strategy for the fabrication of multilayer LB film to elicit efficient quadratic nonlinear optical responses. The effect of polyelectrolyte templating on the SHG response of LB films of other hemicyanine derivatives ($MEOEP^+I^-$ and $OEOEP^+Br^-$) are also presented in this chapter.

Chapter 5: We have investigated a very simple technique to utilize LB films to assemble metal nanoparticles in 2-dimensional aggregate structures and thus tune their optical properties. The study presented in this chapter focuses on the exploration of the electrostatic interaction between the LB film of cationic amphiphile ($ODEP^+$) and the negatively charged citrate-stabilized gold nanoparticles. Electron microscopy and spectroscopy studies show that a single step process involving immersion of monolayer LB films of $ODEP^+Br^-$ in aqueous solutions of citrate-stabilized gold nanoparticles for times as short as 10 min initiates adsorption of the nanoparticles on the LB film and that systematic variation of the immersion time up to ~ 6 h can be used to achieve controlled 2-dimensional aggregation of the nanoparticles and smooth tuning of the surface plasmon resonance absorption peak over a wide wavelength range. The gradual aggregation of nanoparticles on the ultrathin film and the control experiments that establish the relevance of the LB film in the present protocol are discussed. AFM imaging is used to construct a model that describes reorganization of the monolayer LB film into multilayer structures facilitating the immobilization of the nanoparticles. Finally we compare the present protocol with procedures developed in earlier studies, and show that the current strategy is very convenient to implement and efficient.

Chapter 6: The final chapter presents a brief overview of the various investigations presented in the thesis and highlights the different methods that we have developed for the fabrication of molecular ultrathin films and their optical attributes. The important inferences are the following: (i) the studies presented in the thesis are illustrative examples of the realization of unique and enhanced optical attributes in molecular ultrathin films through a concerted interplay of molecular structural features and assembly pattern; (ii) the polyelectrolyte templating technique is established as an efficient route to the stabilization of Langmuir monolayers against molecular aggregation and the realization of stable and enhanced SHG responses in multilayer LB films making them more realistic candidates for the fabrication of molecular scale devices; (iii) monolayer LB films of ionic amphiphiles act as convenient platforms to induce 2-dimensional assembly of metal nanoparticles over large area and effect efficient tuning of their optical responses.

The enhanced materials attributes obtained in optical materials based on molecular ultrathin films that we have demonstrated through our studies can be used in several applications. Application of strongly fluorescent ultrathin films developed in the present study in devices such as light emitting diodes and sensors, and the utilization of the stable

SHG response in the polyelectrolyte templated multilayer LB films in the fabrication of waveguides are some of the important avenues for exploration in future. Another aspect to be explored is the extension of the fabrication methodology developed in our study for ultrathin film-nanoparticle composite materials to achieve enhanced nonlinear optical responses and surface enhanced Raman scattering (SERS) applications. Feasibility of employing patterned LB films for organized assembly of metal nanoparticles will be another important target for future studies. Some of these areas for future extensions of the work presented in the thesis are discussed in the last chapter.

References

1. (a) *Organic Molecular Solids*; Jones, W., Ed.; CRC Press: Boca Raton, 1997; (b) Simon, J.; Bassoul, P. *Design of Molecular Materials: Supramolecular Engineering*; Wiley: New York, 2000.
2. (a) Radhakrishnan, T. P. *Resonance* **1998**, *3*, 30. (b) Radhakrishnan, T. P. *Acc. Chem. Res.* **2008**, *41*, 367 and references 1-12 therein.
3. (a) Lehn, J. M. *Angew. Chem. Int. Ed. Engl.* **1988**, *27*, 89. (b) Desiraju, G. R. *Crystal Engineering*: *The Design of Organic Solids*; Elsevier: Amsterdam, 1989.
4. Cowie, J. M. G.; Arrighi, V. *Polymers*: *Chemistry and Physics of Modern Materials*, 3rd ed.; CRC Press: Boca Raton, 2008.
5. Shi, Y.; Fu, Y.; Lu, C.; Hui, L.; Su, Z. *Dyes and Pigments* **2010**, *85*, 66.
6. Hulliger, J. *Angew. Chem. Int. Ed. Engl.* **1994**, *33*, 143.
7. Dalgarno, S. J.; Tucker, S. A.; Bassil, D. B.; Atwood, J. L. *Science* **2005**, *309*, 2037.
8. *New Trends in Intercalation Compounds for Energy Storage*; Julien, C.; Pereira-Ramos, J. P.; Momchilov, A., Eds.; Springer: Berlin, 2002.
9. (a) Ulman, A. *Chem. Rev.* **1996**, *96*, 1533. (b) Zhang, X.; Chen, H.; Zhang, H. *Chem. Commun.* **2007**, 1395.
10. (a) Roberts, G. G. *Langmuir-Blodgett Films* Plenum Press: New York, 1990.
    (b) Petty, M. C. *Langmuir-Blodgett Films: An Introduction*; Cambridge University Press: New York, 1996.
11. *Poled Polymers and their Applications to SHG and EO Devices*; Miyata, S.; Sasabe, H., Eds.; Gordon and Breach Science Publishers: Amsterdam, 1997; Vol. 4.
12. Forrest, S. R. *Chem. Rev.* **1997**, *97*, 1793.
13. (a) Joachim, C.; Gimzewski, J. K.; Aviram, A. *Nature* **2000**, *408*, 541. (b) Nitzan, A.; Ratner, M. A. *Science* **2003**, *300*, 1384.

14. (a) Holten, D.; Bocian, D. F.; Lindsey, J. S. *Acc. Chem. Res.* **2002**, *35*, 57. (b) Mallia, V. A.; Tamaoki, N. *Chem. Soc. Rev.* **2004**, *33*, 76.

15. (a) Rocha, A. R.; García-suárez, V. M.; Bailey, S. W.; Lambert, C. J.; Ferrer, J.; Sanvito, S. *Nat. Mater.* **200**5, *4*, 335. (b) Bogani, L.; Wernsdorfer, W. *Nat. Mater.* **2008**, *7*, 179.
16. (a) Swager, T. M. *Acc. Chem. Res.* **1998**, *31*, 201. (b) Basabe-Desmonts, L.; Reinhoudt, D. N.; Crego-Calama, M. *Chem. Soc. Rev.* **2007**, *36*, 993.
17. (a) Irie, M. *Chem. Rev.* **2000**, *100*, 1685. (b) Pischel, U. *Angew. Chem. Int. Ed.* **2007**, *46*, 4026.
18. (a) Balzar, F.; Rubahn, H. *Adv. Funct. Mater.* **2005**, *15*, 17. (b) Ng, A. M.; Djurišić, A. B.; Tam, K.; Kwok, W.; Chan, W.; Tam, W. Y.; Phillips, D. L.; Cheah, K. *Adv. Funct. Mater.* **2008**, *18*, 566.
19. Zhao, Y. S.; Xiao, D. B.; Yang, W. S.; Peng, A. D.; Yao, J. N. *Chem. Mater.* **2006**, *18*, 2302.
20. Chung, J. W.; An, B.; Kim, J. W.; Kim, J.; Park, S. Y. *Chem. Commun.* **2008**, 2998.
21. Borras, A.; Aguirre, M.; Groening, O.; Cartes, C. L.; Groening, P. *Chem. Mater.* **2008**, *20*, 7371.
22. Shang, Y.; Wen, Y.; Li, S.; Du, S.; He, X.; Cai, Li.; Li, Y.; Yang. L.; Gao, H.; Song, Y. *J. Am. Chem. Soc*. **2007**, *129*, 11674.
23. Yoshimura, T.; Tatsuura, S.; Sotoyama, W. *Appl. Phys. Lett*. **1991**, *59*, 482.
24. Du, Y.; George, S. M. *J. Phys. Chem*. C **2007**, *111*, 8509.
25. Dameron, A. A.; Seghete, D.; Burton, B. B.; Davidson, S. D.; Cavanagh, A. S.; Bertrand, J. A.; George, S. M. *Chem. Mater.* **2008**, *20*, 3315.
26. Ruben, M.; Payer, D.; Landa, A.; Comisso, A.; Gattinoni, C.; Lin, N.; Collin, J. P.; Sauvage, J. P.; De Vita, A.; Kern, K. *J. Am. Chem. Soc.* **2006**, *128*, 15644.

27. Chen, W.; Li, H.; Huang, H.; Fu, Y.; Zhang, H, L.; Ma, J.; Wee, A, T, S. *J. Am. Chem. Soc.* **2008**, *130*, 12285.
28. Wood, K. C.; Boedicker, J. Q.; Lynn, D. M.; Hammond, P. T. *Langmuir* **2005**, *21*, 1603.
29. DeLongchamp, D. M.; Hammond, P. T. *Langmuir* **2004**, *20*, 5403.
30. (a) Murray, C. B.; Kagan, C. R.; Bawendi, M. G. *Annu. Rev. Mater. Sci.* **2000**, *30*, 545. (b) Gangopadhyay, R.; De, A. *Chem. Mater.* **2000**, *12*, 608. (c) Srivastava, S.; Kotov, N. A. *Acc. Chem. Res.* **2008**, *41*, 1831.
31. (a) Gaines, G. J. *Insoluble monolayers at Liquid-Gas Interfaces*; Wiley – Interscience: New York, 1966. (b) Roberts, G. G. *Langmuir-Blodgett Films*; Plenum Press: New York, 1990. (c) Ulman, A. *An Introduction to Ultrathin Organic Films*: *From Langmuir-Blodgett to Self-Assembly*; Academic Press: Boston, 1991.
32. Franklin, B. *Phil. Trans. R. Soc. London*. **1774**, *64*, 445.
33. (a) Pockels, A. *Nature* **1891**, *43*, 437. (b) Pockels, A. *Nature* **1892**, *46*, 418.
34. Langmuir, I. *J. Am. Chem. Soc.* **1917**, *39*, 1848.
35. Langmuir, I. *Trans. Faraday Soc*. **1920**, *15*, 62.
36. Blodgett, K. B. *J. Am. Chem. Soc*. **1934**, *56*, 495.
37. Kuhn, H.; Möbius, D.; Bücher, H. Weissberger, A.; Rossiter, B., (Eds.), *Physical Methods of Chemistry*; Vol. 1 Part **3B** Chapter **7** , Wiley : NY (1972).
38. Advincula, R.; Knoll, W. *Colloids and Surfaces A: Physicochemical and Engineering Aspects* **1997**, *123-124*, 443. (b) Ravindranath, R.; Ajikumar, P.K.; Advincula, R. C.; Knoll, W.; Valiyaveettil, S. *Langmuir* **2006**, *22*, 9002. (c) Talham, R. D. *Chem. Rev*. **2004**, *104*, 5479.
39. Middleton, S. R.; Iwahashi, M.; Pallas, N. R.; Pethica, B. A. *Proc. R. Soc. London*, **1984**, *396*, 143.
40. Pallas, N. R.; Pethica, B. A. *Langmuir* **1985,** *1***,** 509.

41. (a) Ricceri, R.; Dei, L.; Ottaviani, M. F.; Grando, D.; Gabrielli, G. *Langmuir* **1996**, *12*, 5869. (b) Kwok, D. Y.; Tadros, B.; Deol, H.; Vollhardt, D.; Miller, R.; Cabrerizo-Vílchez, M. A.; Newmann, A. W. *Langmuir* **1996**, *12*, 1851. (c) Sharma, S.; Radhakrishnan, T. P. *Thin Solid Films* **2001**, *382*, 246.

42. (a) Ravaine, S.; Pecq, F. L.; Mingotaud, C.; Delhaes, P. *J. Phys. Chem*. **1995**, *99*, 9551. (b) Cornut, I.; Desbat, B.; Turlet, J. M.; Dufourcq, J. *Biophysical Journal* **1996**, *70*, 305.

43. (a) Eisenthal, K. B. *Chem. Rev.* **1996**, *96*, 1343.

44. Volhardt, D. *Adv. Colloid Interface Sci*. **1996**, *64*, 143.

45. Discher, B. M.; Schief, W. R.; Vogel, V.; Hall, S. B. *Biophys. J.* **1990**, *77*, 2051.

46. (a) Chi, L. F.; Johnston, R. R.; Ringsdorf, H. *Langmuir* **1991**, *7*, 2323. (b) Krüger, P.; Schalke, M.; Wang, Z.; Notter, R. H.; Dluhy, R. A.; Lösche, M. *Biophys. J.* **1999**, *77*, 903.

47. Frommer, J. *Angew. Chem. Int. Ed. Engl.* **1992**, *31*, 1298.

48. Schwartz, D. K.; Garnaes, J.; Viswanathan, R.; Zasadzinski, J. A. N. *Science* **1992**, *257*, 508.

49. Yokoyama, S.; Kakimoto, M.; Imai, Y. *Synthetic Metals* **1996**, *81*, 265.

50. Sui, G.; Micic, M.; Huo, Q.; Leblanc, R. M. *Colloid and Surfaces A: Physiochemical and Engineering Aspects* **2000**, *17*, 185.

51. Als-Nielsen, J.; Jacquemain, D.; Kjaer, K.; Leveiller, F.; Lahav, M.; Leiserowitz, L. *Phys. Rep.* **1994**, *246*, 252.

52. (a) Knoll, W.; Rabe, J.; Philpott, M. R.; Swallen, J. D. *Thin Solid Films* **1983**, *99*, 173. (b) Sastry, M. *Bull. Mater. Sci.* **2000**, *23*, 159.

53. Momose, A.; Hirai, Y.; Waki, I.; Imazeki, S.; Tomioka, Y.; Hayakawa, K.; Naito, M. *Thin Solid Films* **1989**, *178*, 519.

54. Wu, J. C.; Lin, L. T.; Jeng, U. S.; Lee, H. Y.; Gutberlet, T. *Physica B: Condensed Matter* **2006**, *385*, 841.

55. Fanucci, G. E.; Bowers, C. R.; Talham, D. R. *J. Am. Chem. Soc.***1999**, *121*, 1088.

56. Byrd, H.; Whipps, S.; Pike, J. K.; Ma, J.; Nagler, S. E.; Talham, D. R. *J. Am. Chem. Soc.* **1994**, *116*, 295.
57. (a) Flueraru, C.; Schrader, S.; Zauls, V.; Dietzel, B.; Motschmann, H. *Opt. Commun.* **2000**, *182*, 457. (b) Era, M.; Tsutsui, T.; Saito, S. *New Developments in Construction and Functions of Organic Thin Films:* Kajiyama, T.; Aizawa, M. (Eds.), Elsevier Science: Amsterdam, 1996, p. 287.
58. (a) Petty, M. C. *Thin Solid Films* **1992**, *210/211*, 417. (b) Roberts, G. G.; Vincett, P. S.; Barlow, W. A. *Phys. Technol*. **1981**, *12*, 69.
59. Peng, J. B.; Barnes, G. T.; Gentle, I. R. *Adv. Colloid Interface. Sci.* **2001**, *91*, 163.
60. (a) Neal, D. B.; Petty, M. C.; Roberts, G. G.; Ahmed, M. M.; Feast, W. J.; Girling, I. R.; Cade, N. A.; Kolinsky, P. V.; Peterson, I. R. *Proc. IEEE Int. Symp. Applications of Ferroelectrics, ISAF '86.* **1986**, 89. (b) Kuhn, H.; Möbius, D.; Bücher, H. *Techniques of Chemistry*, Weissberger, A.; Rossiter, B. W. (Eds.), Wiley: New York, 1972, Vol. 1, Pt. 3B, p 577.
61. Lednev, I. K.; Petty, M. C. *Advanced Materials for Optics and Electronic* **1994**, *4*, 225.
62. (a) Chou, H.; Chen, C. T.; Stork, K. F.; Bohn, P. W.; Suslick, S. K. *J. Phys. Chem.* **1994**, *98*, 383. (b) Facii, P.; Fontana, M. P.; Dalcanale, E.; Costa, M.; Sacchelli, T. *Langmuir* **2000**, *16*, 7726.
63. (a) Nakamura, T.; Tachibana, H.; Yumura, M.; Matsumoto, M.; Azumi, R.; Tanaka, M.; Kawabata, Y. *Langmuir* **1992**, *8*, 4. (b) Hirano, C.; Imae, T.; Fujima, S.; Yanagimoto, Y.; Takaguchi, Y. *Langmuir* **2005**, *21*, 272.
64. Li, X. D.; Aoki, A.; Miyashita, T. *Langmuir* **1996**, *12*, 5444.
65. (a) Bell, G. M.; Combs, L. L.; Dunne, L. J. *Chem. Rev.* **1981**, *81*, 15. (b) Lösche, M. *Lower Dimensional Systems and Molecular Electronics:* Metzer, R. M.; Day, P.; Papavassiliou, G. V. (Eds.), Plenum Press: New York, 1991, Vol. 248, p 491.
66. (a) Lednev, K. I.; Petty, M. C. *J. Phys. Chem.* **1994**, *98*, 9601. (b) Prabhakaran, D.; Yuehong, M.; Nanjo, H.; Matsunaga, H. *Anal. Chem.* **2007**, *79*, 4056.

67. Baker, S. M.; Danzer, J.; Desaire, H.; Credo, G.; Flitton, R. *Langmuir* **1998**, *14*, 5267.
68. Nierengarten, J. F.; Eckert, J. F.; Rio, Y.; Carreon, M. D. P.; Gallani, J. L.; Gullion, D. *J. Am. Chem. Soc.* **2001**, *123*, 9743.
69. Chen, X.; Lenhert, S.; Hirtz, M.; Lu, N.; Fuchs, H.; Chi, L. *Acc. Chem. Res*. **2007**, *40*, 393.
70. Zhu, C.; Xu, Y.; Long, C.; Li, Y.; Fan, L.; Li, Y.; Zhu, D. *Synthetic Metals* **1997**, *86*, 2291.
71. Ma, S.; Lu, X.; Chen, J.; Han, K.; Liu, L.; Huang, Z.; Cai, R.; Wang, G.; Wang, W.; Li, Y. *J. Phys. Chem.* **1996**, *100*, 16629.
72. Grate, J. W.; Pehrsson, S. R.; Barger, W. R. *Langmuir* **1988**, *4*, 1293.
73. Grate, J. W.; Klusty, M.; Barger, W. R.; Snow, A. W. *Anal. Chem.* **1990**, *62*, 1927.
74. Moriizumi, T. *Thin Solid Films* **1988**, *160*¸ 413.
75. (a) Singhal, R.; Takashima, W.; Kaneto, K.; Samanta, S. B.; Annapoorni, S.; Malhotra, B. D. *Sensors and Actuators B* **2002**, *86*, 42.
76. Alessio, P.; Ferreira, D. M.; Job, A. E.; Aroca, R. F.; Riul, A.; Constantino, C. J. L.; Gonzalez, E. R. P. *Langmuir* **2008**, *24*, 4729.
77. Kim, D. K.; Choi, Y. S.; Chang, J. S.; Kwon, Y. S. *Thin Solid Films* **1998**, *327-329*, 612.
78. (a) Charych, D. H.; Nagy, J. O.; Sperck, W.; Bendnarski, M. D. *Science* **1993**, *261*, 585. (b) Ohnuki, H.; Saiki, T.; Kusakari, A.; Endo, H.; Ichihara, M.; Izumi, M. *Langmuir* **2007**, *23*, 4675.
79. (a) Li, C.; Huang, J.; Liang, Y. *Langmuir* **2000**, *16*, 7701. (b) Ariga, K.; Kunitake, T. *Acc. Chem. Res*. **1998**, *31*, 371.
80. Metzger, R. M. *Chem. Rev*. **2003**, *103*, 3803.

81. Xiao, K.; Liu, Y.; Huang, X.; Xu, Y.; Yu, G.; Zhu, D. *J. Phys. Chem. B* **2003**, *107*, 9226.
82. Xu, H.; Yu, G.; Xu, W.; Xu, Y.; Cui, G.; Zhang, D.; Liu, Y.; Zhu, D. *Langmuir* **2005**, *21*, 5391.
83. Matsui, J.; Yoshida, S.; Mikayama, T,; Aoki, A.; Miyashita, T. *Langmuir* **2005**, *21*, 5343.
84. Jung, G. Y.; Pearson, C.; Kilitziraki, M.; Horsburgh, L. E.; Monkman, A. P.; Samuel, D. W. I.; Petty, M. C. *J. Mater. Chem.* **2000**, *10*, 163.
85. Yoon, H. C.; Shin, H. K.; Kim, C.; Kwon, Y. S. *Synthetic Metals* **2003**, *137(1-3)*, 1427.
86. Xie, S.; Natansohn, A.; Rochon, P. *Chem. Mater.* **1993**, *5*, 403.
87. Goncalves, V. C.; Ferreira, M.; Olivati, C. A.; Cardoso, M. R.; Mendonca, C. R.; Balogh, D. T. *Colloid Polym Sci* **2008**, *286*, 1395.
88. Ricceri, R.; Abbotto, A.; Facchetti, A.; Pagani, G. A.; Gabrielli, G. *Thin Solid Films* **1999**, *340*, 218.
89. Feng, C. L.; Zhang, Y. J.; Jin, J.; Song, Y. L.; Xie, L. Y.; Qu, G. R.; Jiang, L.; Zhu, D. B. *Langmui*r **2001**, *17*, 4593.
90. Wang, J. P.; Li, J. R.; Tao, P. D.; Li, X. C.; Jiang, L. *Advanced Materials for Optics and Electronics* **2004**, *4*, 219.
91. Richardsson, T.; Petty, M. C.; Bryce, M. R.; Bloor, D. *Introduction to molecular electronics*; Oxford University Press, New York, 1995.
92. Ferreira, M.; Olivati, C. A.; Machado, A. M.; Assaka, A. M.; Giacometti, J. A.; Akcelrud, L. *Journal of Polymer Research* **2007**, *14*, 39.
93. Xu, J.; Yang, Y.; Yu, J.; Jiang, Y. *Applied surface science* **2009**, *255*, 4329.
94. Matsui, J.; Abe, K.; Mitsuishi, M.; Miyashita, T. *Mol. Cryst. Liq. Cryst*. **2004**, *424*, 187.
95. Beswick, R. B.; Pitt, C. W. *J. Colloid Interface Sci.* **1988**, *124*, 146.
96. Murakata, T.; Miyashita, T.; Matsuda, M. *Langmuir* **1986**, *2*, 786.

97. Shimomura, M.; Shinohara, E.; Kondo, S.; Tajima, N.; Nagata, Y.; Koshiishi, K. *Sensors and Mater.* **1992**, *4*, 29.
98. (a) Clays, K.; Armstrong, N. J.; Ezenyilimba, M. C.; Penner, T. L. *Chem. Mater*. **1993**, *5*, 1032. (b) Wijekoon, W. M. K. P.; Wijaya, S. K.; Bhawalkar, J. D.; Prasad, P. N.; Penner, T. L.; Armstrong, N. J.; Ezenyilimba, M. C.; Williams, D. J. *J. Am. Chem. Soc*. **1996**, *118*, 4480. (c) Nguyen, D. M.; Mayer, T. M.; Hubbard, S. F.; Singer, K. D.; Mann, J. A.; Lando, J. B. *Macromolecules* **1997**, *30*, 6150.
99. Era, M.; Kawafuji, H.; Tsutsui, T.; Saito, S.; Takehara, K.; Isomura, K.; Taniguchi, H. *Thin Solid Films* **1992**, *210/211*, 163.
100. (a) Ashwell, G. J.; Hargreaves, R. C.; Baldwin, C. E.; Bahra, G. S.; Brown, C. R. *Nature* **1992**, *357*, 393. (b) Girling, I. R.; Cade, N. A.; Kolinsky, P. V.; Jones, R. J.; Peterson, I. R.; Ahmed, M. M.; Neal, D. B.; Petty, M. C.; Roberts, G. G.; Feast, W. J. *J. Opt. Soc. Am. B* **1987**, *4*, 950.
101. (a) Chandra, M. S.; Ogata, Y.; Kawamata, J.; Radhakrishnan, T. P. *Langmuir* **2003**, *19*, 10124. (b) Chandra, M. S.; Krishna, M. G.; Mimata, H.; Kawamata, J.; Nakamura, T.; Radhakrishnan, T. P. *Adv. Mater*. **2005**, *17*, 1937.
102. (a) Cresswell, J. P.; Cross, G. H.; Bloor, D.; Feast, W. J.; Petty, M. C. *Thin solid films* **1992**, *210/211*, 216. (b) Cresswell, J. P.; Petty, M. C.; Shearman, J. E.; Allen, S.; Ryan, T. G. Ferguson, I. *Thin Solid Films* **1994**, *244*, 1067.
103. Schmid, G., Ed. *Clusters and Colloids*; VCH: Weinheim, 1994.
104. Wang, Z. L. *Adv. Mater*. **1998**, *10*, 13.
105. Colvin, V. L.; Goldstein, A. N.; Alivisatos, A. P. *J. Am. Chem. Soc*. **1992**, *114*, 522.
106. Freeman, F. G.; Grabar, K, C.; Allison, K. J.; Bright, R. M.; Davis, G. A.; Guthrrie, A. P.; Hommer, M. B.; Jackson, M. A.; Smith, P. C.; Walter, D. G.; Natan, M. J. *Science* **1995**, *267*, 1629.
107. Giersing, M.; Mulvaney, P. *J. Phys. Chem.* **1993**, *97*, 6334.

108. (a) Cassagneau, T. P. in *Colloids and Colloid Assemblies: Synthesis, Modification, Organization and Utilization of Colloid Particles*, Ed. Caruso, F.; Wiley, 2004, 398. (b) Jiang, G.; Baba, A.; Ikarashi, H.; Xu, R.; Locklin, J.; Kashif, K. R.; Shinbo, K.; Kato, K.; Kaneko, F.; Advincula, R. *J. Phys. Chem. C* **2007**, *111*, 18687.
109. Mayya, K. S.; Sastry, M. *Langmuir* **1999**, *15*, 1902.
110. Sastry, M.; Patil, V.; Mayya, K. S. *Langmuir* **1997**, *13*, 4490.
111. Tao, A.; Sinsermsuksakul, P.; Yang, P. *Nat. Nano* **2007**, *2*, 435.
112. Huang, J.; Kim, F.; Tao, A. R.; Connor, S.; Yang, P. *Nat. Mater.* **2005**, *4*, 896.
113. Mayya, K. S.; Sastry, M. *Langmuir* **1998**, *14*, 74.
114. Elliot, D. J.; Furlong, D. N.; Grieser, F. *Colloids Surf. A* **1999**, *155*, 101.
115. Meldrum, F. C.; Kotov, N. A.; Fendler, J. H. *Langmuir* **1994**, *10*, 2035.
116. Mitsuishi, M.; Ishifuji, M.; Endo, H.; Tanaka, H.; Miyashita, T. *Polymer Journal* **2007**, *39*, 411.
117. Barbee, T. W. *Proc. Soc. Photo-Opt. Instrum. Eng.* **1985**, *563*, 2.
118. Katz, H. E. *Science* **1991**, *254*, 1485.
119. Kepley, L. J.; Sackett, D. D.; Bell, C. M.; Mallouk, T. E. *Thin Solid Films* **1992**, *208*, 132.
120. Prasad, B. L. V.; Sorensen, C. M.; Klabunde, K. J. *Chem. Soc. Rev.* **2008**, *37*, 1871.
121. Ko, H; Singamaneni, S; Tsukruk, V. V. *Small* **2008**, *4*, 1576.
122. Shipway, A. N.; Willner, I. *Chem. Commun.* **2001**, 2035.
123. Tanaka, H.; Mitsuishi, M.; Miyshita, T. *Chem. Lett.* **2005**, *34*, 1246.
124. Ishifuji, M.; Mitsuishi, M.; Miyshita, T. *Chem Commun*. **2008**, 1058.
125. Valeur, B. *Molecular Fluorescence Principles and Applications*, WILEY-VCH Verlag GmbH, 2002.

126. (a) Hertz, A. In *The Theory of the Photographic Process*, 4th ed.; James, T. H., Ed.; Macmillan: New York, 1977; pp 235. (b) James, T. H. *Adv. Photochem.* **1986**, *13*, 329.

127. (a) Mishra, A.; Behera, R. K.; Behera, P. K.; Mishra, B. K.; Behera, G. B. *Chem. Rev.* **2000**, *100*, 1973. (b) Bujdák, J.; Iyi, N.; Sasai, R. *J. Phys. Chem. B* **2004**, *108*, 4470. (c) yao, H.; Domoto, K.; Isohashi, T.; Kimura, K. *Langmuir* **2005**, *21*, 1067.

128. Ferreira, L. F. V.; Lemos, M. J.; Reis, M. J.; do Rego, A. M. B. *Langmuir* **2000**, *16*, 5673.

129. Bujdák, J.; Iyi, N. *Chem. Mater.* **2006**, *18*, 2618.

130. (a) Özçelik, S.; Akins, D. L. *J. Phys. Chem. B* **1999**, *103*, 8926. (b) Deans, R.; Kim, J.; Machacek, M. R.; Swager, T. M. *J. Am. Chem. Soc.* **2000**, *122*, 8565.

131. Patra, A.; Hebalkar, N.; Sreedhar, B.; Sarkar, M.; Samanta, A.; Radhakrishnan, T. P. *Small* **2006**, *2*, 650.

132. (a) Perepichka, D. F.; Rosei, F. *Angew. Chem. Int. Ed.* **2007**, *46*, 6006, and references therein; (b) Yan, H.; Cingarapu, S.; Klabunde, K. J.; Chakrabarti, A.; Sorensen, C. M. *Phys. Rev. Lett.* **2009**, *102*, 095501.

133. Moors, A.; Guttmann, F. *New J. Chem.* **2006**, *30*, 1121. (b) Jain, P. K.; El-Sayed, I. H.; El-Sayed, M. A. *Nanotoday* **2007**, *2*, 18.

134. (a) Mulvaney, P. *Langmuir* **1996,** *12,* 788; (b) Hohenester, U.; Krenn, J. *Phys. Rev. B* **2005**, *72*, 195429.

135. Kanis, D. R.; Ratner, M. A.; Marks, T. J. *Chem. Rev.* **1994**, *94*, 195.

Scope

Optical properties of single component molecular materials can often be described in terms of modest perturbations on the responses of the molecular building blocks; with specific systems, the impact of the perturbations may be more pronounced. In all cases however, the effects are broadly independent of the form of assembly such as thin films, nanostructures and crystals, even though variations may exist at the quantitative level. In this chapter we present a very different situation encountered with an amphiphilic molecule possessing a strongly polar head group that shows similar electronic absorption spectra in the solution as well as the bulk solid state, but a dramatically different one in ultrathin LB films; the lowest energy absorption observed in the former two states is switched off completely in the latter. It is demonstrated further that a metastable form of the LB film exhibiting the normal molecular spectrum can be generated; but its lowest energy absorption decays and vanishes over a period of time. The experimental observations coupled with models constructed through computational investigations allow us to interpret the unusual optical responses, as resulting from the specific supramolecular 2-dimensional assembly in the LB film and the impact of the neighboring molecular dipoles on the intramolecular charge transfer transition. The present study illustrates that selective molecular design and directed assembly can be exploited to elicit dramatic changes in physical responses of molecular materials and realize novel effects in molecular nanostructures.

2.1. Introduction

Molecular materials fabricated through self or steered assembly of molecules, in forms such as nanostructures, thin films and crystals, are generally characterized by relatively weak, noncovalent intermolecular interactions.[1] A consequence of the weak binding forces is that the physical attributes are nearly conserved during the transition from the molecular to the assembled states. Modest modifications of the physical properties do occur as a result of perturbation of the molecular responses arising from interactions with the neighbors in the supramolecular assembly. A classic case in the field of optical materials is the formation of H- and J- aggregates with optical absorption peaks shifted due to exciton coupling.[2] In some instances the changes may be profound, for example the annihilation of fluorescence due to self-quenching[3] and the opposite effect of aggregation induced enhancement of light emission in selected molecules.[4] The impact of supramolecular interactions, weak or relatively stronger, are usually observed in all modes of assembly from the nano regime to the bulk, perhaps with some variation in the quantitative aspect of the effects.[5] A case in point is the similar pattern of electronic transitions generally observed in monolayers and bulk solids.[6] It is quite uncommon, but of considerable interest from a fundamental as well as application perspective, to find dramatic changes in the physical responses between the molecular and the assembled states, restricted to specific modes of assembly such as ultrathin films and not the bulk materials.

In this chapter we present our investigation of the unique optical properties exhibited by LB films of a diaminodicyanoquinodimethane derivative 7,7-bis(octadecylamino)-8,8-dicyanoquinodimethane (BODDQ) molecule (Fig. 2.1). This molecule with a 'push-pull' structure, is likely to be strongly zwitterionic as computations[7,8] and experiments[9] on similar molecules have revealed large ground state dipole moment. AM1 computation shows that BODDQ has a ground state dipole moment of 14.5 D. The large hyperpolarizability associated with the molecules possessing similar

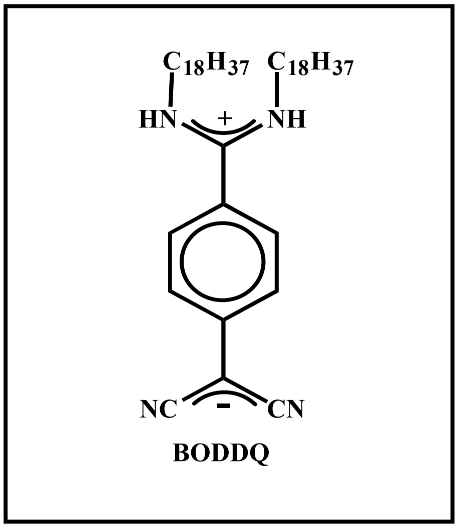

Figure 2.1. *Molecular structure of 7,7-bis(octadecylamino)-8,8-dicyanoquinodimethane*

structure has been exploited extensively in the design of materials for optical second harmonic generation investigated in our laboratory.[10] One of the interesting explorations deals with the influence of the length of substituent alkyl chains on the packing of these molecules in crystals and their nonlinear optical responses.[11] We have discovered now, a remarkable disappearance of the lowest energy optical absorption of BODDQ in its LB films.[12] The effect arising without the intervention of complexing partners, chemical or electrochemical changes or the impact of external fields appears to be a direct consequence of the packing of molecules in the LB film, as the same absorption is starkly visible in the solution as well as the bulk solid states. Most interestingly, even though a similar spectrum can be realized in a metastable form of the LB film of BODDQ, the stable form of the LB film shows no sign of the lower energy absorption, while the higher energy peak is intact. Significantly, the lower energy peak observed in the metastable film vanishes over a period of time. Following a description of the experimental investigations and characterizations of Langmuir and LB films of BODDQ through π-A isotherms, BAM and AFM, the salient spectroscopic observations are discussed. In an effort to gain insight into the unusual effects revealed by the experiments, we construct a model for the molecular assemblies in LB films and based on computational studies, develop a rationale to account for the unusual and unique switching off of the electronic absorption.

2.2. Experimental and Computational Details

2.2.1 *Langmuir and Langmuir-Blodgett Film Fabrication*

BODDQ was synthesized following the procedure reported earlier for similar molecules.[11,13] The Langmuir films were fabricated by spreading the solution of BODDQ in chloroform on the aqueous subphase maintained at constant temperature. In this study we have chosen two temperatures 20 and 30^{o}C (subphase temperature) for the film fabrications, in order to study the effect of temperature on the film behavior. The required ambient temperature was achieved by air-conditioning controlled through thermal sensors. Upon equilibration for about 30 min, the subphase temperature was found to reach a steady value (variations were within ±0.5^{o}); this value is specified as the temperature condition of the experiments. The air-conditioner was switched off during the experiment to avoid even the minimal vibrations; however it was observed that the temperature of the ambient atmosphere within the enclosure of the trough as well as that of the subphase remained constant through the complete experiment including film deposition. The general procedures used for the Langmuir and LB film preparation are given in Appendix A. π-A isotherms and BAM were used to characterize the evolution of the monolayer at the interface. The LB film was coated by vertical dipping at a speed of 5 mm/min with the monolayer held at different pressures, on hydrophilic quartz/mica substrates. The LB films were characterized using AFM in semi-contact mode and UV-visible spectroscopy.

2.2.2 *Molecular modeling and computational studies*

Computational studies were carried out at the semiempirical as well as ab initio levels. Molecular geometries were optimized using the AM1 method within the VAMP routine in Materials Studio.[14] Models for the molecular packing in the LB films were constructed using the 'Build/Surface' option in Materials Studio. Excitation energies and oscillator strengths were calculated using time-dependent density functional (TD-DFT) method; B3LYP/6-31G* level computations (Gaussian03 program)[15] were carried out on the molecular geometries optimized in the semiempirical calculations. Influence of neighboring dipoles was mimicked by placing point charges at positions dictated by the packing models; details are provided in Sec. 2.4.2.

2.3. Langmuir Films of BODDQ at the Air-Water Interface

BODDQ forms stable films at the air-water interface; these Langmuir films were investigated under different conditions of temperature, barrier compression speed and annealing effect of external vibrations. Barrier speed ranging from 2 to 8 cm/min showed little impact on the behavior of the films; hence all the studies presented in this chapter employed a speed of 5 cm/min. Temperature as well as external vibrations had significant effect, however. The π-A isotherm obtained at the ambient temperature of 20°C is shown in

Figure 2.2a; the isotherms recorded during the compression-expansion cycle (isocycle) show small hysterisis and annealing effects, but after about four cycles, are consistent and

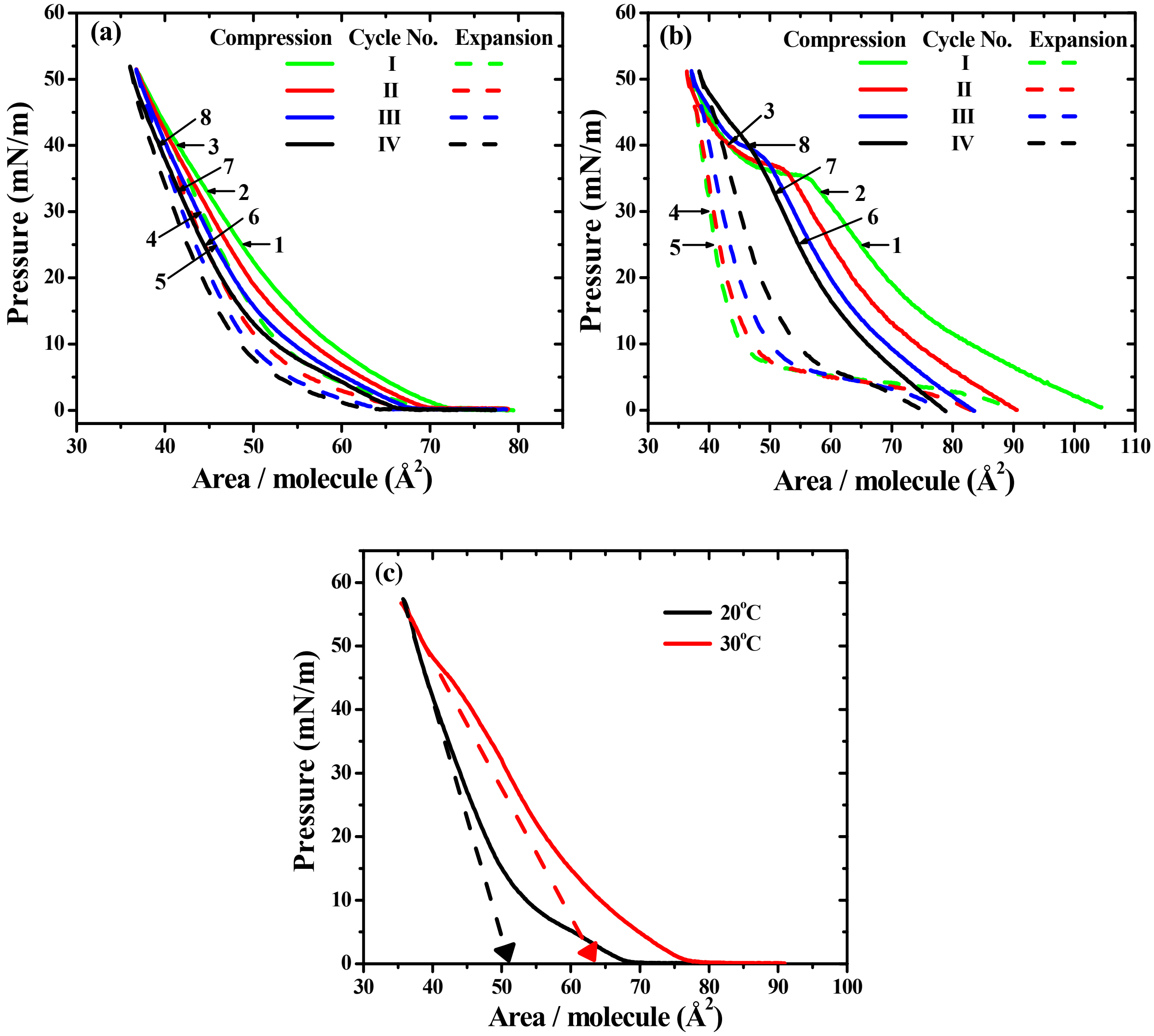

Figure 2.2. *Pressure-area isotherms of Langmuir films of BODDQ at the air-water interface, at* ***(a)*** *20°C and* ***(b)*** *30°C, showing the compression and expansion during I - IV isocycles and points where BAM images (Figure 2.3 and 2.4) are recorded (x-axis scales are different in the two figures).* ***(c)*** *Consistent isotherms obtained after four isocycles; extrapolations to estimate molecular areas are indicated.*

highly reproducible. The molecular area obtained by extrapolating the high pressure end of the steady compression isotherm is ~ 51.2 Å^2 (Fig. 2.2c). When the experiment was carried out at 30^{o}C, the behavior was entirely different. The isotherm rises at a relatively higher area and exhibits a plateau at ~ 36 mN/m (Fig. 2.2b); the expansion isotherm shows large hysterisis and subsequent isocycles show decreasing plateau regions reaching a consistent behavior after four cycles. The final isotherm with an extrapolated area of ~ 63.6 Å^2 shows no well-defined plateau (Fig. 2.2c). These π-A isotherms suggest different molecular organizations in the Langmuir films formed at the two different temperatures, the lower temperature facilitating a more compact packing. It is interesting to note further that, when the experiment was carried out at 30^{o}C, but with the air-conditioner in operation with the associated mild vibrations, the isotherm obtained was identical to the one in Figure 2.2a. This indicates that even mild annealing effects suppress the plateau formation and lead to a smooth rise of isotherm and more compact packing.

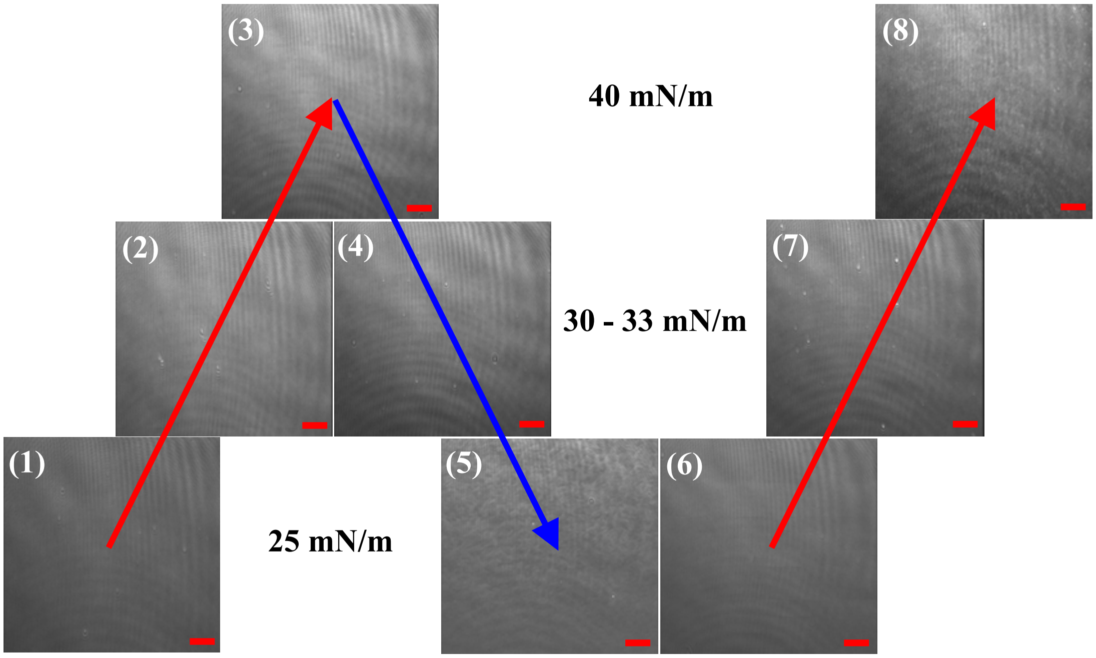

Figure 2.3. *BAM images of Langmuir films of BODDQ at the air-water interface, fabricated at 20^{o}C recorded at different surface pressures (indicated also in Figure 2.2a, along the compression isotherm in I and IV cycles (red arrow) and expansion isotherm in I cycle (blue arrow). Scale bar = 25µm in all cases*

BAM was used to monitor the evolution of the Langmuir films under various conditions of compression and expansion. Figure 2.3 shows the images of the film at different surface pressures (indicated on Fig. 2.2a) during compression followed by expansion at 20°C. The film is found to be close packed and smooth throughout. In sharp contrast, the film formed at 30°C is characterized by a domain structure even at relatively low pressures (Fig. 2.4). This gets compacted on compression, and a plateau is formed in the first isotherm possibly due to the emergence of a network structure that is clearly observed above the plateau. Upon expansion, domains of different sizes are observed and subsequent compressions lead to films with a close packing of such domains; disappearance of the plateau may be attributed to the lack of formation of the network structure. It is very likely that the molecular packing in the domains is quite different from that in the smooth uniform film obtained at 20°C. The observations noted above suggest that BODDQ behaves differently at the air-water interface when the subphase temperature is changed

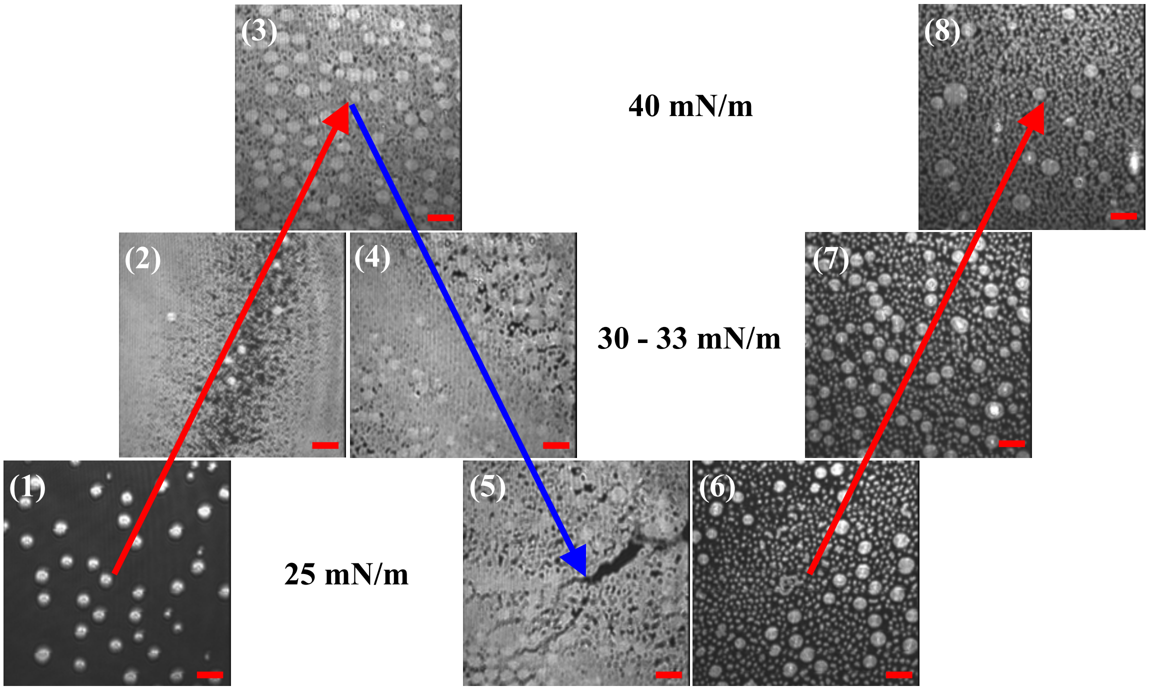

Figure 2.4. *BAM images of Langmuir films of BODDQ at the air-water interface, fabricated at 30°C recorded at different surface pressures (indicated also in Figure 2.2b, along the compression isotherm in I and IV cycles (red arrow) and expansion isotherm in I cycle (blue arrow). Scale bar = 25μm in all cases*

2.4. LB films of BODDQ Fabricated under Different Conditions

2.4.1 *AFM and Electronic Absorption Spectroscopy Studies*

The BODDQ films formed at the air-water interface were transferred to suitable substrates at different target pressures. The transfer ratios were generally > 0.90. AFM images of the films formed at the two different temperatures and deposited on mica plates at a target pressure of 45 mN/m are shown in Figure 2.5. Line profile analysis of the AFM images are shown in Figure 2.6. The film formed at 20°C shows a homogeneous and dense distribution of structures typically ~ 50 – 100 nm wide and ~ 3.0 nm high. The film fabricated at 30°C shows a very different morphology, similar to an extended structure that would result from the merger of large domains; the structure spreads over several micrometers and the thickness is ~ 2.5 nm. The film morphologies at the submicron scale are consistent with those observed at larger scales in the BAM images suggesting that the molecular assembly and organization at the air-water interface have a strong bearing on the structure of the respective LB films. The variation in the thickness of the films fabricated at the two temperatures suggests that the molecular packing is different in the two films.

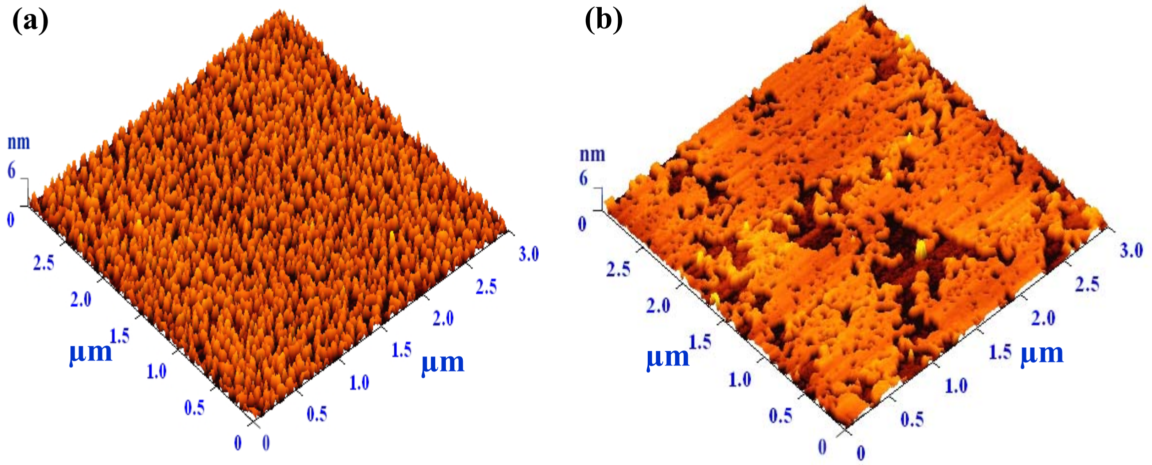

Figure 2.5. *AFM images (3-dimensional view) of monolayer LB films of BODDQ deposited at 45 mN/m surface pressure and* ***(a)*** *20°C;* ***(b)*** *30°C.*

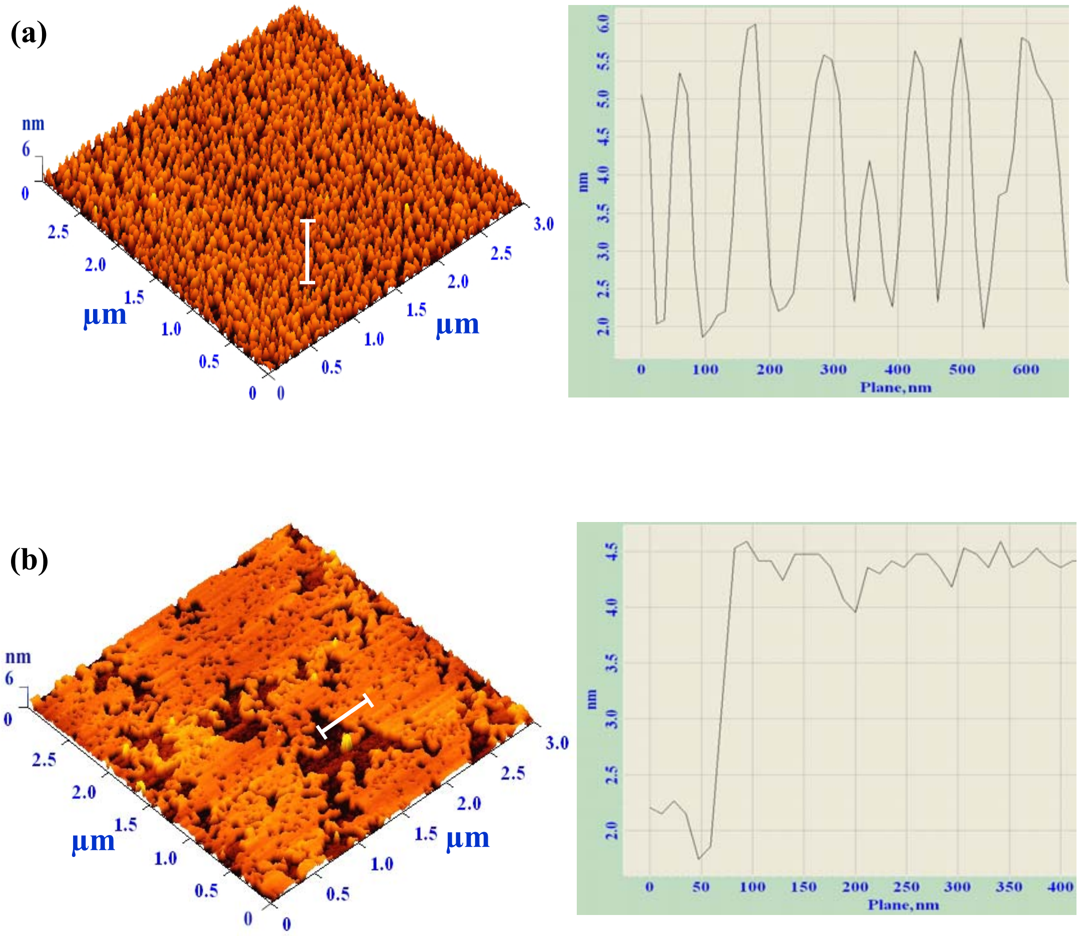

Figure 2.6. *AFM images along with line profiles of monolayer LB films of BODDQ deposited at 45 mN/m surface pressure and* ***(a)*** *20°C;* ***(b)*** *30°C.*

Electronic absorption spectra of BODDQ in chloroform and acetonitrile solutions and in the solid state are presented in Figure 2.7; two peaks are observed, one at ~ 230 nm and the other in the range 370 – 420 nm. The lowest energy peak is assignable to an intramolecular charge transfer absorption, a characteristic signature of these molecules; the pronounced negative solvatochromism is consistent with a strong reduction in dipole moment on excitation.[16] The peak position in the solid is close to that in the polar solvent, pointing to the influence of the environment of the molecule in the crystalline state.[8]

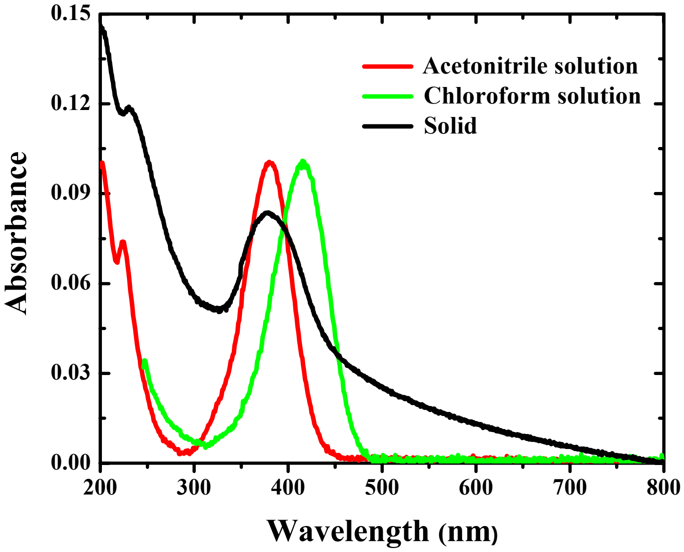

Figure 2.7. *Electronic absorption spectra of BODDQ in solutions and in the solid state.*

Spectra of the LB films fabricated at the two different temperatures and deposited at the target pressure of 45 mN/m are shown in Figure 2.8a. While the film formed at 30°C shows a spectrum similar to those in Figure 2.7, the film formed at 20°C shows a dramatically different one with no trace of the peak near 400 nm, though the higher energy peak remains intact. Most interestingly, the lower energy peak visible in the spectrum of the film formed at 30°C, decays over a period of several days and the final spectrum resembles closely that of the film formed at 20°C (Fig. 2.8b). It is notable that AFM studies reveal parallel changes in the morphology of the film with the extended structures (Fig. 2.5b) transforming to wires and small particles and the average thickness increasing marginally (Fig. 2.9). These observations clearly show that the film formed at 30°C is in a metastable state; the spontaneous transformation of the LB film in the present case is more dramatic than most of those reported in earlier studies.[17] Films fabricated at 30 mN/m at the two different temperatures display behaviors very similar to those fabricated at 45 mN/m (Fig. 2.10a). It is observed further that the lower energy absorption of the films fabricated at 30 mN/m and 30°C shows faster decay than that in the case of the film fabricated at 45 mN/m as seen in Figure 2.10b. Monitoring through microscopy and spectroscopy confirms that the film fabricated at 20^{o}C with the low energy absorption switched off, is absolutely stable over several days.

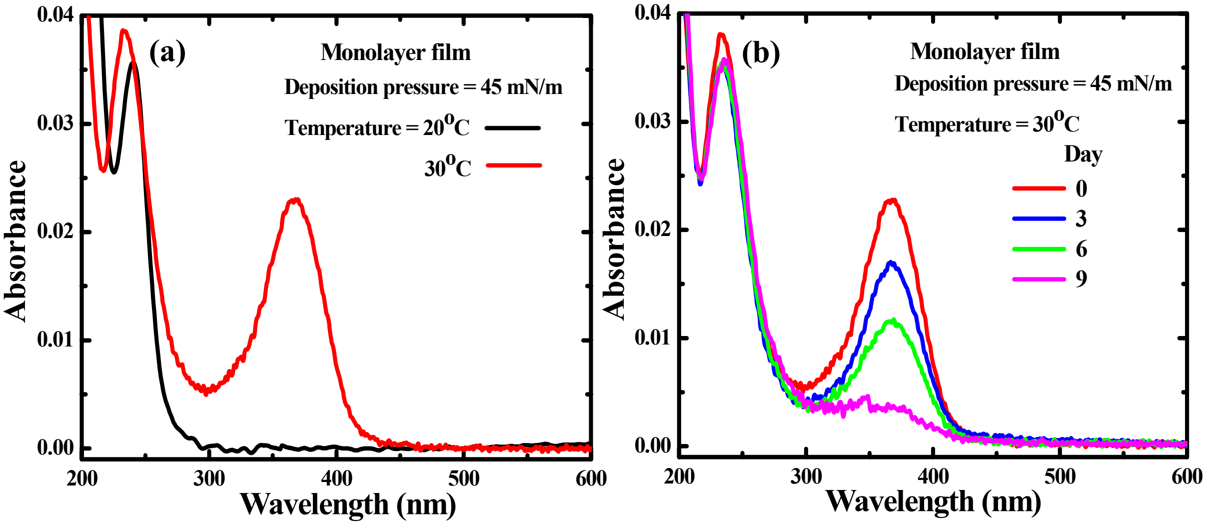

Figure 2.8. *Electronic absorption spectra of BODDQ:* ***(a)*** *Monolayer LB films fabricated at 45 mN/m and different temperatures;* ***(b)*** *Monolayer LB film fabricated at 45 mN/m and 30^{o}C over a period of 9 days.*

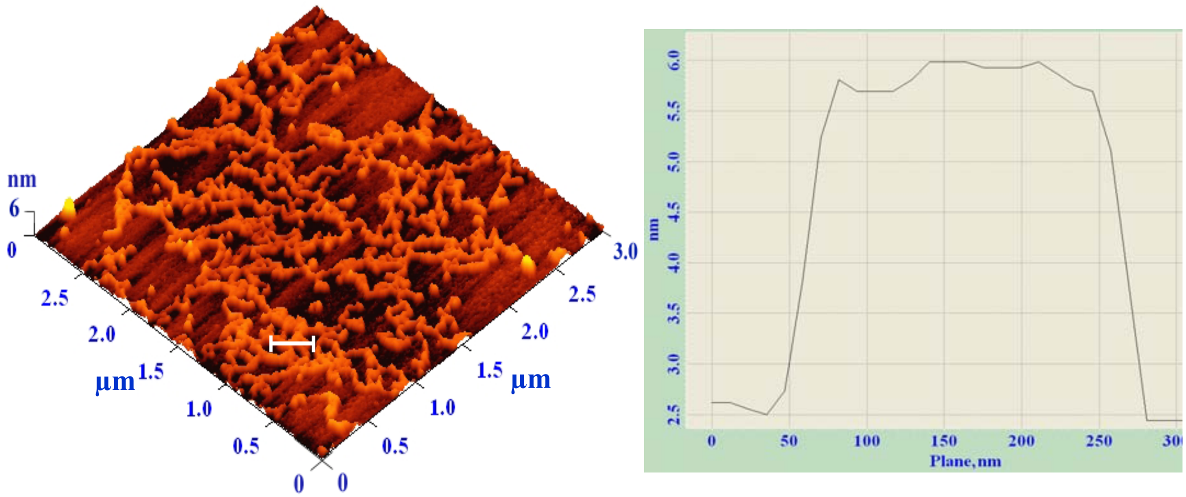

Figure 2.9. *AFM image along with line profile of monolayer LB films of BODDQ deposited at 45 mN/m surface pressure and 30^{o}C imaged after 9 days.*

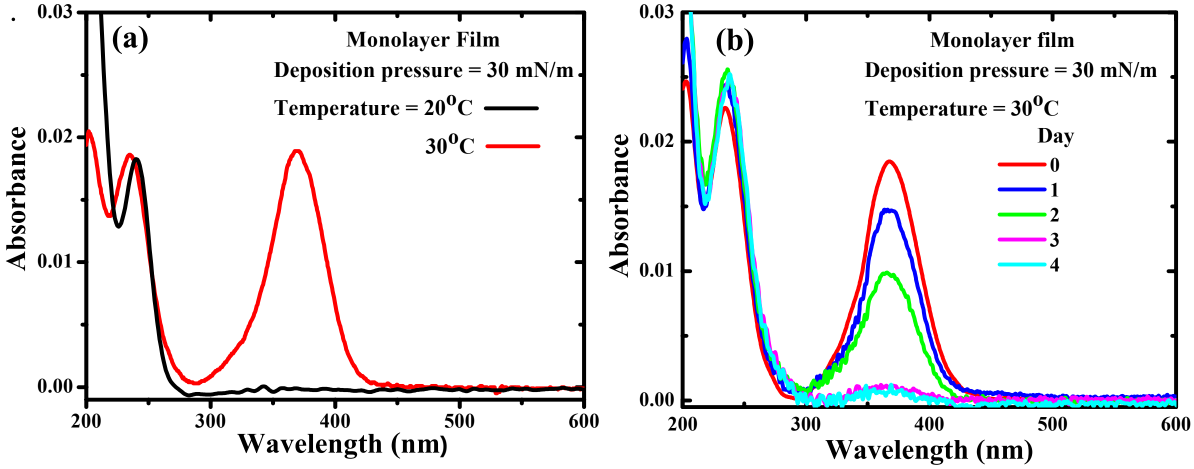

Figure 2.10. *Electronic absorption spectra of BODDQ: **(a)** Monolayer LB films fabricated at 30 mN/m and different temperatures; **(b)** Monolayer LB film fabricated at 30 mN/m and 30°C over a period of 4 days.*

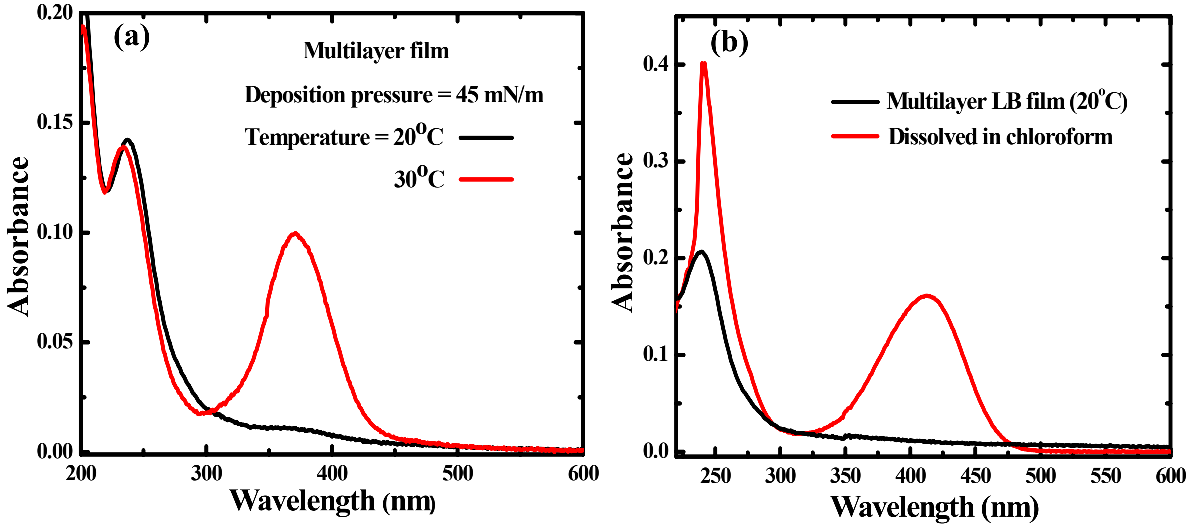

Figure 2.11. *Electronic absorption spectra of BODDQ: **(a)** Multilayer (7 strokes) LB films fabricated at 45 mN/m at different temperatures; **(b)** Multilayer LB film (25-strokes) fabricated at 20°C and the solution obtained by dissolving this film in chloroform.*

Further significant observations relate to the effect of fabrication conditions and multilayer structures. LB films fabricated at 30°C, but in presence of mild vibrations from the air-conditioner resulting in the π-A isotherm with no plateau as mentioned earlier, show no lower energy absorption peak. In the case of multilayer LB films also, the fate of the electronic absorption is completely determined by the conditions during the formation of the Langmuir film and hence the π-A isotherm observed; the lower energy absorption is present in films that exhibited the plateau in the first isotherm and absent in the films that did not (Fig. 2.11a). The remote possibility of chemical change causing the disappearance of the lower energy absorption in the films formed at 20°C can be ruled out, based on the observation of the normal spectrum of BODDQ (including the 415 nm peak) in solutions obtained by dissolving the multilayer films in chloroform (Fig. 2.11b). As the spectra of the LB films were recorded in transmission mode with normal incidence of the light beam, it is conceivable that the disappearance of the lower energy absorption in the film formed at 20°C is due to a high degree of molecular organization with the relevant transition dipole oriented normal to the substrate plane. However, this possibility can be ruled out in view of the absence of the lower energy peak in the spectra recorded with the film positioned at different angles with respect to the incident beam (Fig. 2.12a). Specular reflectance spectra with light incident at ~ 6° (Fig. 2.12b) and polarized absorption spectra (Fig. 2.13) recorded using s- and p-polarized light incident at different angles on films fabricated at 20°C showed no sign of the lower energy absorption, ruling out completely the possibility of the relevant transition dipole being oriented normal to the substrate plane.

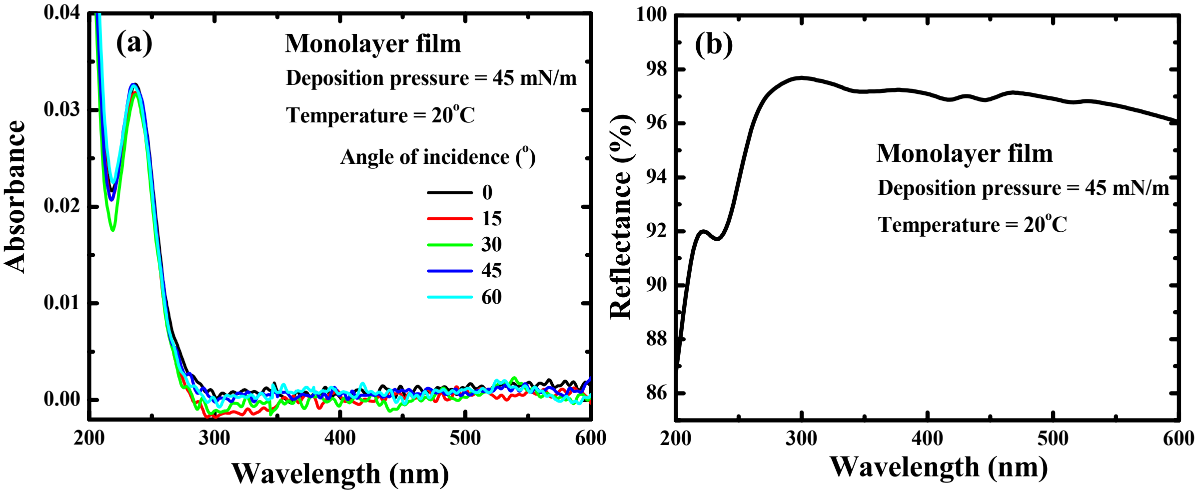

Figure 2.12. *Electronic absorption spectra of BODDQ monolayer LB film fabricated at 45 mN/m and 20°C* ***(a)*** *held at different angles with respect to the incident light beam;* ***(b)*** *specular reflectance spectrum of film fabricated at 20°C with light incident at 6°.*

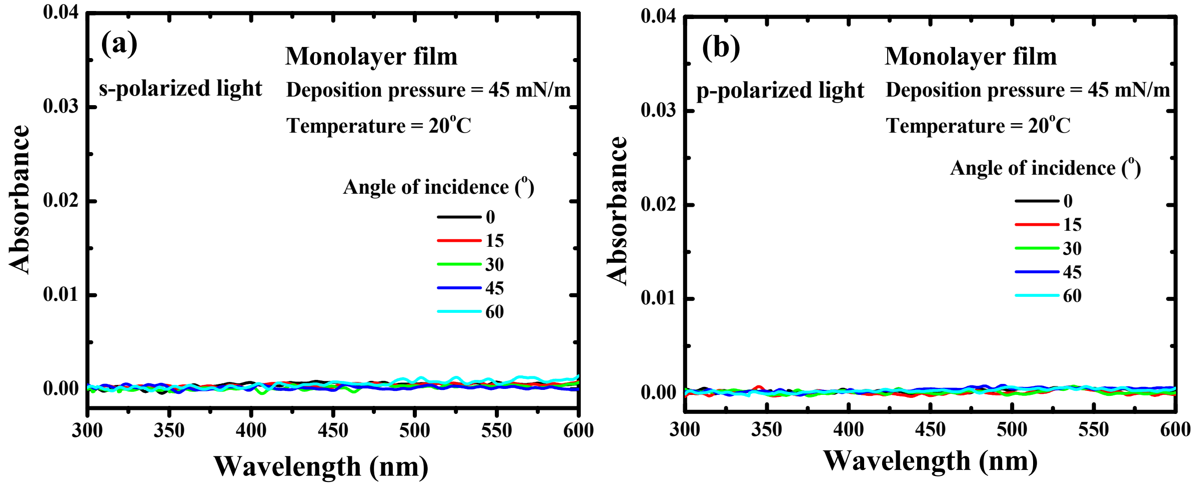

Figure 2.13. *Absorption spectra of film fabricated at 45 mN/m and 20°C with* ***(a)*** *s- and* ***(b)*** *p- polarized light incident at different angles; the wavelength range, 300 – 600 nm is dictated by the polarizer used.*

The salient experimental observations on the Langmuir and LB films of BODDQ described above may be summarized as follows. The films fabricated at 20°C are characterized by closer packing and higher stability and are devoid of the lower energy electronic absorption. The films fabricated at 30°C exhibit higher area/molecule, involve domain formation at the air-water interface and are sensitive to disturbances; the corresponding LB films show the normal electronic absorptions of BODDQ, but also signs of metastability as the lower energy absorption decays and disappears with time. The AFM images indicate that the films fabricated at the two temperatures possess different morphologies and the layer thickness is slightly higher in the stable one; the morphology of the metastable film shows slow transformation tending towards that of the stable film.

2.4.2 *Molecular Modeling and Computational Studies*

In order to construct a model to explain the unusual features of the BODDQ LB films, while reconciling the range of observations listed above, we have started with the optimization of the molecular geometry of BODDQ using semiempirical AM1 computations. The conformation chosen for the input geometry had both alkyl chains oriented in the same direction, and the major dipole axis of the head group (connecting the diaminomethylene and the dicyanomethylene carbons) approximately orthogonal to this direction. Such a chain orientation is appropriate for the asymmetric environment at the air-water interface and the head group orientation would facilitate dipole-dipole interactions between the strongly zwitterionic structures, a stabilizing effect that is likely to be dominant in the 2-dimensional assembly. The geometry obtained by full optimization of this conformer is shown in Figure 2.14a. The dipole moment of BODDQ quoted earlier refers to this structure. The hydrocarbon chains are all-*trans* and the head group shows a twist angle of ~ 28° between the diaminomethylene group and the aromatic ring plane; this feature arising due to steric effects, is characteristic of substituted diaminodicyanoquinodimethanes.[8,10] A plausible packing of these molecules into a 2-dimensional periodic lattice is shown in Figure 2.14b; the 2-dimensional space group *P*g was chosen allowing the formation of mirror image molecules and facilitating an assembly with antiparallel dipoles. The packing was tuned manually within these constraints, to achieve maximum density; the resulting unit cell parameters are $\boldsymbol{u}$ = 10.7, $\boldsymbol{v}$ = 12.1 Å. This model for the 2-dimensional assembly of BODDQ with a 'face-on' orientation of the head groups is significant, since the area/molecule predicted based on this packing, 64.7 $Å^2$ is quite close to that observed for the Langmuir film fabricated at 30°C. The thickness expected for the film from this model is ~ 21.7 Å, consistent with the monolayer thickness observed in the AFM image. It is likely that the domain and network structures seen in the BAM and AFM images of these films are constituted of BODDQ molecules with this conformation and packing.

As the film formed at 30°C is in a metastable state, we have considered different possibilities for the stable form of the BODDQ film formed at 20°C. Since AFM images indicate only a minor increase in the thickness of the film, we rule out the possibility of formation of multilayer structures. A likely scenario involves a head group structure with higher molecular twist that enables closer packing of the molecules in the 2-dimensional lattice as well as enhanced dipole-dipole interactions. The molecular geometry of BODDQ was optimized again with the twist angle between the diaminomethylene group and the aromatic ring, now constrained to 90°. The resulting structure is shown in Figure 2.14c. Packing this molecule into a 2D lattice following the same protocols as before, leads to the assembly with ‘long edge - on’ orientation of BODDQ (Fig. 2.14d); the unit cell parameters are $\boldsymbol{u}$ = 14.5, $\boldsymbol{v}$ = 7.3 Å and the area/molecule is 52.9 Å^2. This value is in good agreement with that observed in the Langmuir film formed at 20^{o}C. Again the thickness of the film expected from the model, 22.9 Å, is consistent with the slightly higher monolayer thickness observed in the AFM image.

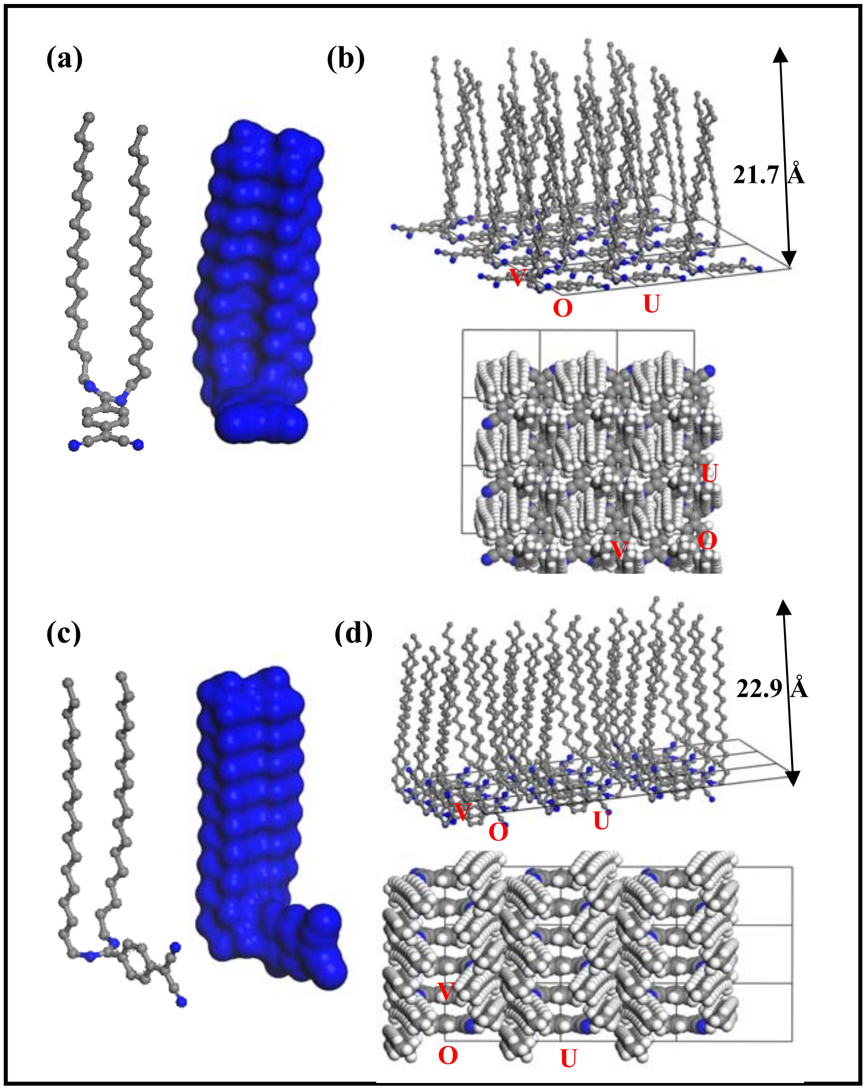

Figure 2.14. *AM1 optimized structure of BODDQ in* ***(a)*** *‘Face’ and* ***(c)*** *‘Edge’ conformations along with the Connolly surface rendering (H-atoms omitted in the structure figure for clarity). Side and top views of the packing models for the* ***(b)*** *‘Face’ and* ***(d)*** *‘Edge’ structures; the 2D axes and height of the layer are indicated (H-atoms omitted in the side view for clarity). C (grey); N (blue); H (white).*

The critical test of the molecular structures with twist angles 28° ('Face') and 90° ('Edge') and the corresponding packing models described above, is the insight they can provide into the relative stabilities of the films formed at 30 and 20°C respectively and their optical responses. In view of the strongly dipolar nature of the head groups, significant ele-

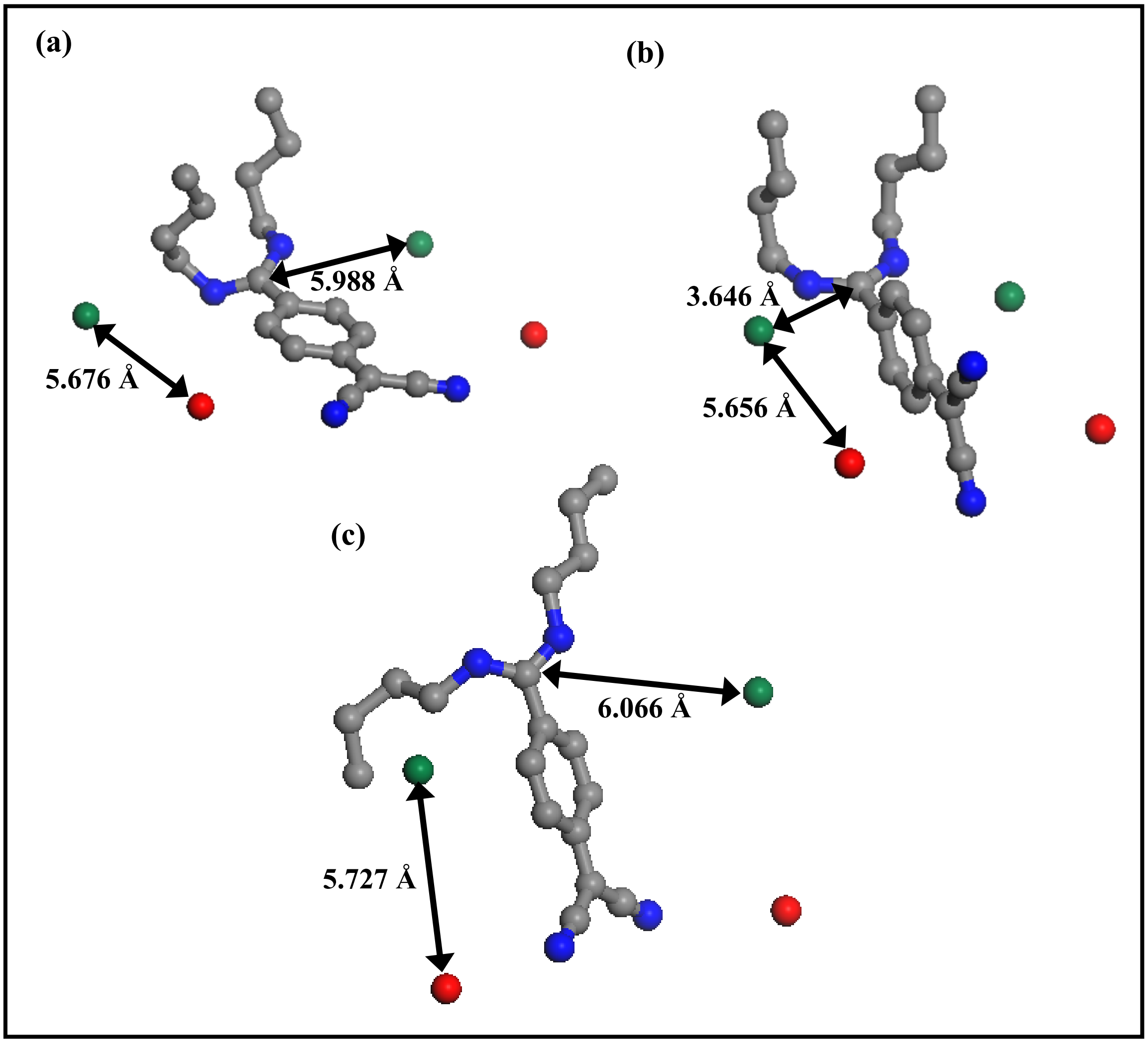

Figure 2.15. *The structures used in the computation of electronic transitions, obtained from the AM1 optimized geometries of BODDQ in* ***(a)*** *'Face' and* ***(b)*** *'Edge' conformations (Figure 2.14) and the* ***(c)*** *crystal structure of BODQ.*[11] *C (grey); N (blue). Position of positive (red) and negative (green) charges that simulate neighboring molecule dipoles in the packing models (a, b) or crystal structure (c) are shown along with significant distances.*

ctrostatic intermolecular interactions may be expected; hence every molecule would experience the field due to its neighbors. One of the simplest approaches that can be visualized to take this into account, is to introduce positive and negative point charges at the positions of the diaminomethylene and dicyanomethylene carbons respectively of the two neighboring molecules along the ***v***-axis in the 2-dimensional assembly (Fig. 2.14b and d), to mimic the effect of the adjacent antiparallel dipoles. The energies and excitation profiles of the molecules with and without such point charges were computed using TD-DFT method; the hydrocarbon chain plays no role in the optical excitations of the molecule, and therefore were truncated to butyl groups to save on computations (the terminal methyl groups alone were reoptimized). The structures employed in the computations are presented in Figure 2.15a and b. The magnitude of the charges were taken either as 1.0 or the value estimated from the computed ground state dipole moment of the free molecule and the separation between the positive and negative charges (the dipole length). The relevant results from the computations are collected in Table 2.1. Without the adjacent dipoles, the ‘Face’ structure is more stable than the ‘Edge’ structure as expected from the full geometry optimization of the former and constrained optimization of the latter. However, introduction of the adjacent dipoles stabilizes the ‘Edge’ structure over the ‘Face’ structure, a logical consequence of the stronger impact of the adjacent antiparallel dipoles at closer distances, interacting directly with the π-electrons in the latter case. Thus the ‘Edge’ structure and the corresponding packing are reasonable models for the thermodynamically stable films formed at 20^{o}C. The electronic transitions estimated from the TD-DFT calculations are even more significant. The computed lowest energy excitation of the ‘Face’ structure is at ~ 406 nm and is dominantly due to the HOMO→LUMO (80→81) transition. In the ‘Edge’ structure, this gap becomes very small and the transition probability negligible; the strongest absorption is calculated to be at ~ 317 nm due to a different transition. Introduction of the adjacent dipoles increases the excitation energies in both structures; more significantly, on going from the ‘Face’ to the ‘Edge’ structure, the strong HOMO→LUMO transition is considerably weakened, whereas the HOMO→LUMO+1 transition is enhanced. The ‘Face’ structure with $q = 0.63$ shows a strong excitation at ~ 390 nm and a weaker one at 250 – 255 nm; this is in good agreement with the absorptions of the LB film formed at 30^{o}C possessing peaks at 370 and 235 nm. A similar head group can be

Table 2.1. Results of B3LYP/6-31G* computations on the structures in Figure 2.15 (q is the value of charges placed to simulate the adjacent dipoles; the case with no value shown, represents the free structure having no adjacent dipoles): energy of the structure and absorption peak maxima (λ_{max}) with corresponding oscillator strength (f) and listing of the states contributing dominantly to the transitions. All computed transitions with λ_{max} > 200.0 nm and f > 0.05 are shown; details for the lowest two excitations {80→81}, {80→82} are provided and the strongest absorption highlighted for each structure.

Structure	**q**	**Energy (Hartrees)**	**Peak maximum (nm) [oscillator strength] {states dominating the transition}**		
			{80→81}	**{80→82}**	**{Others}**
‘Face’ (Fig. 2.15a)	-	-919.315221	**406.1 [0.982]**	324.7 [0.004]	262.5 [0.073] {78→81, 80→83}
	0.63[*]	-919.433993	**390.4 [0.941]**	312.3 [0.003]	255.6 [0.078] {79→81} 249.9 [0.086] {77→81, 80→83}
	1.00	-919.576869	**378.1 [0.921]**	305.3 [0.003]	269.4 [0.057] {79→81} 243.1 [0.091] {77→81, 80→84}
‘Edge’ (Fig. 2.15b)	-	-919.282177	1032.2 [0.001]	372.1 [0.008]	**317.4 [0.495]** {80→83} 312.4 [0.261] {80→85}
	0.88[#]	-919.560858	396.6 [0.001]	**275.7 [0.662]**	219.4 [0.061] {80→86} 206.7 [0.122] {79→82} 201.8 [0.164] {77→81}
	1.00	-919.623303	366.6 [0.001]	**270.5 [0.630]**	224.5 [0.069] {80→85} 206.0 [0.126] {79→82} 202.3 [0.177] {78→81}
‘Cryst’ (Fig. 2.15c)	-	-919.007852	**461.4 [0.521]**	369.7 [0.002]	281.6 [0.274] {80→83}
	0.81[$]	-919.199309	**393.3 [0.488]**	311.3 [0.001]	253.0 [0.235] {80→83}
	1.00	-919.280317	**375.4 [0.488]**	299.6 [0.001]	246.1 [0.217] {80→83} 220.8 [0.052] {78→81}

[*] [#] [$] Estimated using the dipole moment of the free molecule and dipole length:
[*]17.1 D, 5.676 Å; [#]24.1 D, 5.695 Å; [$]22.4 D, 5.727 Å

used to model the solution spectra of BODDQ. The ‘Edge’ structure with q = 0.88 does not show any significant absorption near 400 nm. There is a strong excitation at ~ 276 nm and a weaker one at ~ 200 – 220 nm; this conforms very well to the absorptions of the LB film formed at 20^{o}C with a strong peak at ~ 240 nm and probably some absorption below 210 nm. These computational results provide a model to explain how the low energy excitation of BODDQ near 400 nm can get switched off in the stable form of the LB film; most likely, this results from the intramolecular charge transfer transition being hampered by the field due to the adjacent antiparallel dipoles in the close packed 2-dimensional assembly. These models also suggest that the transformation of the metastable film and the concomitant decay of the low energy absorption may be attributed to the slow stabilization of the ultrathin film through concerted molecular twist enhancement and closer packing. It should be noted that a range of alternate models including simple dimer/aggregate formation that we have considered, do not provide a unified explanation of the Langmuir film behavior and electronic spectral characteristics of the LB films, as the 'Face – Edge' model does.

An important question remains: even though the low energy absorption of BODDQ molecule vanishes in the stable state of its LB film, how is it very much visible in the solid state spectrum ? The molecular packing in the 3-dimensional crystal lattice may be quite different from that in the 2-dimensional ultrathin film, resulting in different spectroscopic signature in the bulk solid state. In spite of several attempts, we could not grow good quality crystals of BODDQ with its long alkyl chains; hence its crystal structure could not be determined. However several bis(alkyl) derivatives of diaminodicyanoquinodimethane with short alkyl chains, showing absorption features very similar to BODDQ in the solution and solid states, have been investigated in our laboratory earlier,[11] and some have been characterized crystallographically. We have chosen the structure available with the longest chain, 7,7-bis(octylamino)-8,8-dicyanoquinodimethane, BODQ[11] to examine the packing in the crystal lattice and to compute the spectral features. The crystal structure shows the twist angle in the molecule to be ~ 47^o and the alkyl chains orientated in different directions, a feature unlikely to be accommodated in LB films. The aromatic rings of adjacent molecules in the crystal lattice are oriented approximately orthogonal to each other, with the major dipole axes antiparallel. We have carried out computations of the electronic structure as before; the molecular structure and the placement of the neighbor dipole charges are shown in Figure 2.15c. The computed transitions for the 'Cryst' structure (Table 2.1) parallel that of the ‘Face’ structure; the values for the case with q = 0.81 are ~ 390 and 250 nm, conforming to those observed in the solid state spectrum of BODDQ at ~ 380 and ~ 230 nm (Fig. 2.7). The insight into the solid state of BODDQ gained through the computational exploration of BODQ provides further validation of the model we have developed for the LB films of BODDQ.

2.5. Summary

We have fabricated Langmuir and LB films of the amphiphilic molecule BODDQ, possessing a strongly zwitterionic head group, and investigated their optical properties in detail. π-A isotherms and microscopy were used to characterize the films formed under different temperature conditions. Spectroscopy studies reveal stable and metastable forms of the film and most interestingly, the absence of the lower energy optical absorption of the molecule, in the stable form of the LB film; this absorption due to intramolecular charge transfer is a hallmark of these molecules and present in their solution and solid states. This observation is an unusual case of the molecular property getting modified dramatically as a result of assembly, while depending sensitively on the form of assembly. Computational explorations led to a viable model involving different conformations for the molecule and corresponding packing patterns in the 2-dimensional lattices. Computations taking into account the impact of neighboring molecular dipoles provided critical insight into the switching off of the lower energy transition in the stable LB films. Our study is an illustrative example of the realization of dramatically novel physical attributes in molecular materials through a concerted interplay of molecular structural features and packing motifs. It also demonstrates yet another unique feature that Langmuir-Blodgettry can bestow upon supramolecular assembly.

References

1. (a) Simon, J.; Bassoul P. *Design of Molecular Materials: Supramolecular Engineering*; Wiley: New York, 2000. (b) Ozin, G. A.; Arsenault, A. C. *Nanochemistry*; RSC Publishing: Cambridge, 2005.
2. (a) McRae, E. G.; Kasha, M. The Molecular Exciton Model. *PhysicalProcesses in Radiation Biology*; Academic Press: New York, 1964; pp23. (b) Kasha, M.; Rawls, H. R.; El-Bayoumi, M. A. *Pure Appl. Chem.* **1965**, *11*, 371. (c) Kasha, M. *Molecular Excitons in Small Aggregates*; Plenum Press: New York, 1976. (d) Aguilera, O. V.; Neckers, D.C. *Acc. Chem. Res.* **1989**, *22*, 171.
3. (a) David, W. E.; Solomon, B. S. *J. Phys. Chem.* **1967**, *71*, 44676. (b) Munkholm, C.; Parkinson, D. R.; Walt, D. R. *J. Am. Chem. Soc.* **1990**, *112*, 2608. (c) Yan, B.; Martin, P. C.; Lee, J. *J. Comb. Chem.* **1999**, *1*, 78. (d) Yi, P. K.; Fang, Z.; Liu, B. *Adv. Func. Mater.* **2008,** *18*, 1321.
4. (a) Özçelik, S.; Akins, D. L. *J. Phys. Chem. B* **1999**, *103*, 8926. (b) Deans, R.; Kim, J.; Machacek, M. R.; Swager, T. M. *J. Am. Chem. Soc.* **2000**, *122*, 8565. (c) Levitus, M.; Schmieder, K.; Ricks, H.; Shimizu, K. D.; Bunz, U. H. F.; Garcia-Garibay, M. A. *J. Am. Chem. Soc.* **2001**, *123*, 4259. (d) Jayanty, S.; Radhakrishnan, T. P. *Chem. Eur. J.* **2004**, *10*, 791. (e) Ren, Y.; Lam, J. W. Y.; Dong, Y.; Tang, B. Z.; Wong, K. S. *J. Phys. Chem. B* **2005**, *109*, 1135.
5. (a) Luo, .; Xie, Z.; Lam, J. W. Y.; Cheng, L.; Chen, H.; Qiu, C.; Kwok, H. S.; Zhan, X.; Liu, Y.; Zhu, D.; Tang, B. Z. *Chem. Commun.* **2001**, 1740. (b) An, B.; Kwon, S.; Jung, S.; Park, S. Y. *J. Am. Chem. Soc.* **2002**, *124*, 14410. (c) Wilson, J. N.; Smith, M. D.; Enkelmann, V.; Bunz, U. H. F. *Chem. Commun.* **2004**, 1700. (d) Patra, A.; Hebalkar, N.; Sreedhar, B.; Sarkar, M.; Samanta, A.; Radhakrishnan, T. P. *Small* **2006**, *2*, 650.
6. (a) Chou, H.; Chen, C.; Stork, K. F.; Bohn, P. W.; Suslick, K. S. *J. Phys. Chem.* **1994**, *98*, 383. (b) Terenziani, F.; Painelli, A.; Girlando, A.; Metzger, R. M. *J. Phys. Chem. B* **2004**, *108*, 10743. (c) Chandra, M. S.; Ogata, Y.; Kawamata, J.; Radhakrishnan, T. P. *J. Nonlin. Opt. Phys. Mater.* **2004**, *13*, 347. (d) Wohnrath, K.;

Constantino, C. J. L.; Antunes, P. A.; dos Santos, P. M.; Batista, A. A.; Aroca, R. F.; Oliviera, O. N. *J. Phys. Chem. B* **2005**, *109*, 4959.

7. (a) Ravi, M.; Radhakrishnan, T. P. *J. Phy. Chem.* **1995**, *99*, 17624. (b) Ravi, M.; Szablewski, M.; Hackman, N, A.; Cross, G. H.; Bloor, D.; Goeta, A. E.; Howard, J. A. K. *New J. Chem.* **1999**, *23*, 841.
8. Jayanty, S.; Radhakrishnan, T. P. *Chem. Mater.* **2004**, *13*, 2460.
9. (a) Kagawa, Y.; Szablewski, M.; Ravi, M.; Hackman, N.; Cross, G. H.; Bloor, D.; Batsanov, A. S.; Howard, J. A. K. *Nonlin. Opt.* **1999**, *22*, 235. (b) Gopalan, R. S.; Kulkarni, G. V.; Ravi, M.; Rao, C. N. R. *New. J. Chem.* **2001**, *25*, 1108. (c) Cole, J. M.; Copley, R. C. B.; McIntyre, G. J.; Howard, J. A. K.; Szablewski, M.; Cross, G. H. *Phys. Rev. B*, **2002**, *65*, 125107.
10. (a) Ravi, M.; Rao, D. N.; Cohen, S.; Agranat, I.; Radhakrishnan, T. P. *J. Mater. Chem.* **1996**, *6*, 1119. (b) Ravi, M.; Rao, D. N.; Cohen, S.; Agranat, I.; Radhakrishnan, T. P. *J. Mater. Chem.* **1996,** *6,* 1853. (c) Ravi, M.; Rao, D .N.; Cohen, S.; Agranat, I.; Radhakrishnan, T. P. *Chem. Mater.* **1997,** *9*, 830. (d) Ravi, M.; Gangopadhyay, P.; Rao, D. N.; Cohen, S.; Agranat, I.; Radhakrishnan, T. P. *Chem. Mater.* **1998**, *10*, 2317. (e) Jayanty, S.; Gangopadhyay, P.; Radhakrishnan, T. P. *J. Mater. Chem.* **2002**, *12*, 2972. (f) Jayanty, S.; Radhakrishnan, T. P. *Chem. Eur. J.* **2004**, *10*, 2661.
11. Gangopadhyay, P.; Sharma, S.; Rao, A. J.; Rao, D. N.; Cohen, S.; Agranat, I.; Radhakrishnan, T. P. *Chem. Mater.* **1999**, *11*, 466.
12. Rajesh, K.; Radhakrishnan, T. P. *Chem. Eur. J.* **2009**, *15*, 2801
13. (a) Hertler, W. R.; Hartzler, H. D.; Acker, D. S.; Benson, R. E. *J. Am. Chem. Soc.* **1962**, *84*, 3387..
14. (a) Materials Studio Version 4.1, Accelrys Software Inc. **2006**. (b) VAMP Version 8.1, Clark, T.; Alex, A.; Beck, B.; Burkhardt, F.; Chandrasekhar, J.; Gedeck, P.; Horn, A.; Hutter, M.; Martin, B.; Rauhut, G.; Sauer, W.; Schindler, T.; Steinke, T. Erlangen, Germany, **2002.**
15. Frisch, M. J.et al. *Gaussian 03*, Revision B.05; Gaussian, Inc.: Pittsburgh, PA, 2003.
16. Ravi, M.; Samanta, A.; Radhakrishnan, T. P. *J. Phys. Chem.* **1994**, *98*, 9133.

17. (a) Wang, Y.; Ozaki, Y.; Iriyama, K. *Langmuir* **1995**, *11*, 705. (b) Wang, Y.; Nichogi, K.; Iriyama, K.; Ozaki, Y. *J. Phys. Chem.* **1996**, *100*, 374. (c) Morita, S.; Iriyama, K.; Ozaki, Y. *J. Phys. Chem. B* **2000**, *104*, 1183. (d) Chandra, M. S.; Krishna, M. G.; Mimata, H.; Kawamata, J.; Nakamura, T.; Radhakrishnan, T. P. *Adv. Mater.* **2005**, 17, 1937.

Scope

Suppression of self-quenching of fluorescence emission in supramolecular systems is of fundamental interest in the design and development of novel optical materials. While a number of molecular design and assembly strategies have been formulated for the fabrication of molecular crystals with enhanced light emission, parallel explorations based on systematic approaches in the domain of molecular ultrathin films are rare. We have investigated LB films of amphiphilic molecules bearing the same hemicyanine choromophore headgroup but with different possibilities of attachment of the hydrocarbon chain, under different deposition conditions. Fluorescence spectroscopy studies indicate enhanced light emission in the derivative with a 'tail-head-tail' structure. The observed trends are attributed to the amphiphile structure, nature of deposition and the chromophore orientations revealed through polarized absorption spectra of the films. The study suggests a simple design strategy towards realization of molecular ultrathin films with enhanced light emission.

3.1. Introduction

Aggregation of molecular fluorophores is often accompanied by strong quenching of their fluorescence. As fluorescent molecular materials of interest in applications such as display devices and sensors involve supramolecular assemblies, the adverse impact of these self-quenching effects is a critical problem. Design of molecules and their assemblies aimed at circumventing the quenching effects and realizing enhanced fluorescence in molecular materials is therefore of fundamental relevance. There has been extensive efforts in this direction in the area of molecular crystals.[1] Even though LB assembly is a simple and elegant methodology that affords fine control on supramolecular assembly and hence is an efficient route to the fabrication of ultrathin films with enhanced materials attributes, no systematic approach has been developed to tune fluorescence response through tailoring the amphiphile structure and LB assembly. Fluorescent LB films with several rare-earth metal complexes as well as organic fluorophores have been investigated[2-11] and a range of phenomena including quenched or strong fluorescence[4] and electric field and radiation effects on fluorescence[7] in LB films have been reported. Fluorescence of LB films have been attributed to aggregate structures,[5,6] or excimer emission[8-10] and extensive time-resolved investigations have been carried out.[9,11] Potential applications of these materials include sensors[12] as well as probes for film structure[8] and imaging.[13]

Aminostilbazolium (hemicyanine) is a popular fluorophore finding applications as fluorescence probe[14] and laser dye.[15] Incorporated in LB films,[16-18] it has been an important candidate for molecular electronics[19] and quadratic nonlinear optical applications.[20-27] Optical second harmonic generation from LB films based on hemicyanines has been investigated extensively; utility of polyelectrolyte templating in suppressing aggregation effects and stabilizing enhanced response of the films has been demonstrated through several investigations carried out in our laboratory. [24,25,27] Fluorescence studies carried out on LB films of hemicyanines include time-resolved measurements[17,18] and investigation of the spontaneous formation of H-aggregates.[5,16]

We envisaged that the orientation and organization of the hemicyanine based amphiphiles at the air-water interface and hence in the LB film will be sensitively dependent on the molecular structure, specifically the mode of attachment of the hydrocarbon chains at the two ends. This would in turn alter the optical responses while the chromophore unit remains the same. We have focused our investigations on the three amphiphiles shown in Figure 3.1. N-*n*-alkyl-4-[2-(4-(N,N-dimethylamino)phenyl)ethenyl]-pyridinium is the hemicyanine system that has been studied extensively. [15-17,21-26] The bromide salt of the octadecyl derivative, $ODEP^+Br^-$ is shown in Figure 3.1. Second harmonic generation studies on its multilayer films will be presented in Chapter 4. N-methyl-4-[2-(4-(N,N-ethyloctadecylamino)phenyl)ethenyl]pyridinium iodide ($MEOEP^+I^-$) and N-*n*-octadecyl-4-[2-(4-(N,N-ethyloctadecylamino)phenyl)ethenyl]pyridinium bromide ($OEOEP^+Br^-$) find brief mention as members of a series of amphiphiles forming SHG active LB films;[28] SHG of some $MEOEP^+I^-$ analogues have also been reported.[29] Dibutylamino as well as alkoxy analogues of $OEOEP^+Br^-$ with ‘tail-head-tail’ structure have been shown to form predominantly noncentrosymmetric multilayer LB films capable of strong SHG.[30] Spectroscopy and epifluorescence microscopy investigations of LB films of the dihexadecylamino analogue of MEOEP$^+$I$^-$ have indicated the formation of aggregate structures.[5] Detailed investigations of Langmuir and LB films of MEOEP$^+$I$^-$ and OEOEP$^+$Br$^-$ and their fluorescence properties have however not been reported. We have followed reported procedures for the synthesis of the three amphiphiles with some modifications especially in the case of OEOEP$^+$Br$^-$. Detailed microscopy and spectroscopy investigations were carried out on the LB films deposited under different conditions. Investigation of the polarization dependence of the electronic absorption spectra provides insight into the chromophore orientations in the different LB films. Comparison of the fluorescence properties of the monolayer LB films of the three amphiphiles possessing identical fluorophore units indicates that LB films of OEOEP$^+$Br$^-$ deposited under specific conditions show 30 – 50 times enhancement over that of the weakest one based on ODEP$^+$Br$^-$! We discuss the basis for the enhancement and suggest a possible design strategy towards strongly fluorescent molecular ultrathin films.

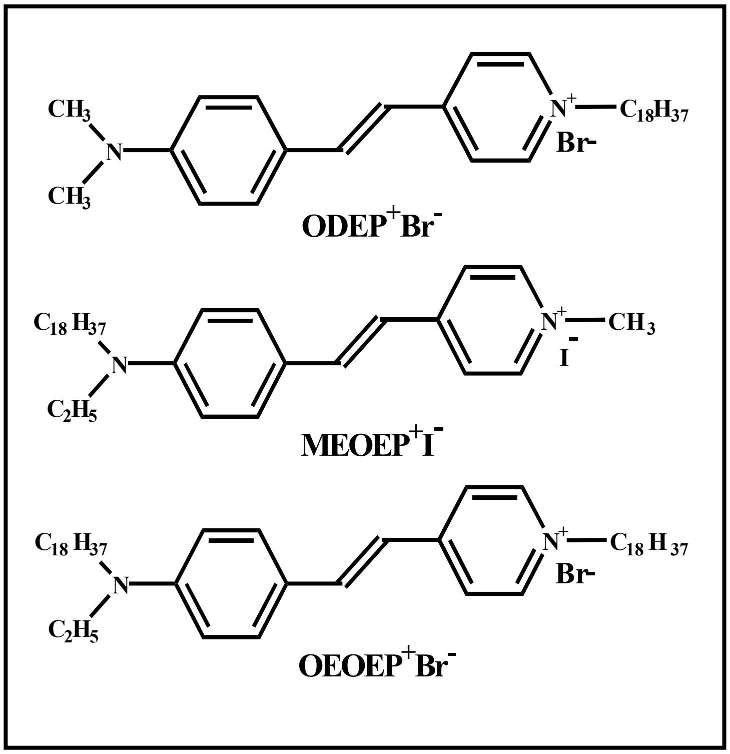

Figure 3.1. *Molecular structure of ODEP$^+$Br$^-$, MEOEP$^+$I$^-$ and OEOEP$^+$Br$^-$.*

3.2. Experimental Details

3.2.1 *Synthesis and Characterization of MEOEP$^+$I$^-$ and OEOEP$^+$Br$^-$*

ODEP$^+$Br$^-$ was synthesized following reported procedure.[24] MEOEP$^+$I$^-$ and OEOEP$^+$Br$^-$ were synthesized by the condensation of 4-(N,N-ethyloctadecylamino)benzaldehyde (EOAB) and the respective N-alkyl-4-picolinium salt. Synthesis of EOAB consists of two steps. In the first step, N-ethyl-N-*n*-octadecylaniline (EOA) was synthesized. This is followed by formylation in the second step as described below.

EOA

EOA was synthesized as shown in Scheme 3.1. Octadecyl bromide (1.00 g, 3.0 mmol) in 20 ml of toluene was added to a stirred solution of N-ethylaniline (0.36 g, 3.0 mmol) in 30% aqueous NaOH containing catalytic amount of tetrabutylammonium bromide. The reaction mixture was stirred at 70-80ºC for 7 days; the toluene phase was washed with NaCl solution and evaporated. The resultant solid, EOA was purified by several recrystallizations from hexane.

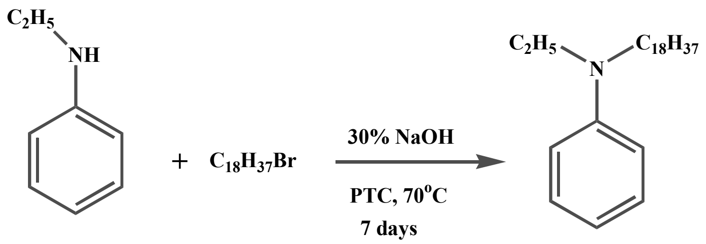

Scheme 3.1

Yield = 80%; M.P./^{o}C = 52-54; FTIR (KBr): $\bar{\upsilon}$/cm^{-1} = 2918.6, 1604.9, 1504.6, 1242.3, 850.7, 721. 4; ^{1}H-NMR ($CDCl_3$): δ/ppm = 7.22 (m, 2H), 6.69 (m, 3H), 3.38 (q, 2H), 3.36 (t, 2H), 1.28 (m, 32H), 1.12 (t, 3H), 0.89 (t, 3H).

EOAB

EOAB was prepared following the method reported earlier[31] (Scheme 3.2). EOA (1.25g, 3.35 mmol) was dissolved in 1.5 ml of DMF. Phosphorous oxychloride (2.2 ml, 23.50 mmol) was added dropwise, keeping the temperature below 10°C; a green solution was obtained. The mixture was heated at 100° C for 3 h under nitrogen atmosphere following which a brown color appeared. After cooling, the mixture was dissolved in dichloromethane and washed with dilute sodium bicarbonate solution followed by distilled water. Yellow solid of EOAB was obtained by evaporating the solvent.

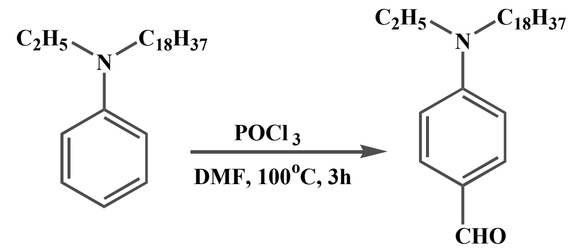

Scheme 3.2

Yield = 60%; M.P./°C = 49; FTIR (KBr): $\bar{\upsilon}$/cm^{-1} = 2916.6, 1724.5, 1664.7, 1242.2, 816.0, 721.4; ^{1}H-NMR ($CDCl_3$): δ/ppm = 9.70 (s, 1H), 7.74 (d, 2H), 6.74 (d, 2H), 3.46 (q, 2H), 3.35 (t, 2H), 1.24 (m, 35H), 0.9 (t, 3H); LC-MS: m/z = 401.

MEOEP$^+$I$^-$

N-methyl-4-picolinium iodide (0.28 g, 1.20 mmol) was added to EOAB (0.5 g, 1.25 mmol) in methanol and refluxed for 3 h in presence of 0.1 ml of piperidine (Scheme 3.3). Red precipitate of MEOEP$^+$I$^-$ was obtained on cooling the reaction mixture. The precipitate was filtered, dried and recrystallized several times from methanol. Yield = 70%; M.P./°C = 230; FTIR (KBr): $\bar{\upsilon}$/cm^{-1} = 2916.6, 2849.1, 1645.4, 1591.4, 825.6; ^{1}H-NMR (d_6-DMSO): δ/ppm = 8.63 (d, 2H, J= 6.4 Hz), 7.99 (d, 2H, J= 6.5 Hz), 7.84 (d, 1H, J=15.9 Hz), 7.52 (d, 2H, J=8.7 Hz), 7.06 (d, 1H, J=15.9 Hz), 6.69 (d, 2H, J=8.7 Hz), 4.14 (s, 3H), 3.42 (q, 2H), 3.33 (t, 2H), 1.17 (m, 32H), 1.09 (t, 3H), 0.84 (t, 3H) [where interference due to residual moisture in solvent occurs, the peak positions were determined using the spectrum recorded in $CDCl_3$]; LC-MS: m/z = 491 ($MEOEP^+$).

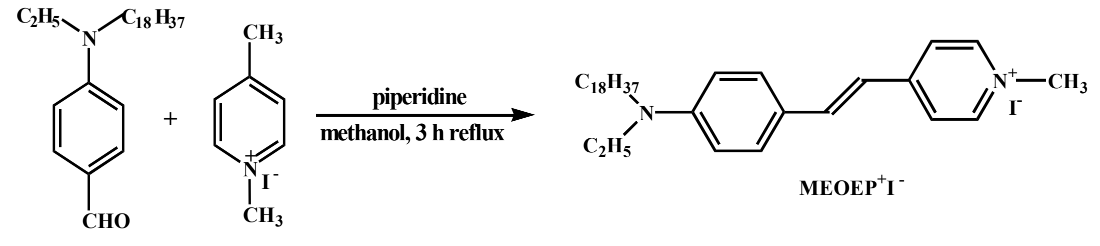

Scheme 3.3

$OEOEP^+Br^-$

$OEOEP^+Br^-$ was synthesized following Scheme 3.4 shown below. 4-methyl-N-octadecylpyridinium bromide (0.37 g, 0.87 mmol) and 0.1 ml of piperidine were added to EOAB (0.32 g, 0.80 mmol) in methanol and the mixture was refluxed for 3 h. $OEOEP^+Br^-$ precipitated out as a red crystalline solid on cooling the reaction mixture to 25°C. The precipitate was filtered, dried and recrystallized several times from methanol.

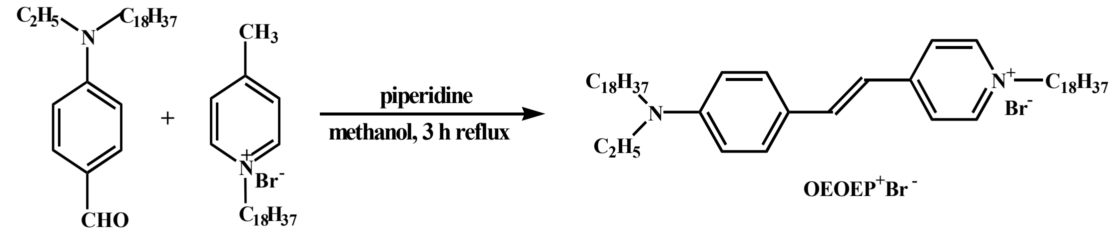

Scheme 3.4

Yield = 75%; M.P./°C = 110; FTIR (KBr): $\bar{\upsilon}/cm^{-1}$= 3044.0, 2916.6, 1572.1, 829.5; ^1H NMR (d_6-DMSO): δ/ppm = 8.75 (d, 2H, J = 6.8 Hz), 8.04 (d, 2H, J = 6.8 Hz), 7.90 (d, 1H, J = 16.0 Hz), 7.56 (d, 2H, J = 8.8 Hz), 7.12 (d, 1H, J = 16.0 Hz), 6.73 (d, 2H, J = 8.8 Hz), 4.40 (t, 2H), 3.47 (q, 2H), 3.33 (t, 2H), 1.86 (m, 2H), 1.54 (m, 2H), 1.23 (m, 60H), 1.13 (t, 3H), 0.85 (t, 6H) [where interference due to residual moisture in solvent occurs, the peak positions were determined using the spectrum recorded in $CDCl_3$]; LC-MS: m/z = 729 ($OEOEP^+$); elemental analysis (calculated for $C_{51}H_{89}N_2Br$): %C = 75.67 (75.66), %H = 10.98 (11.00), %N = 3.70 (3.46).

3.2.2 *Langmuir and LB film Studies*

Solutions of the amphiphiles were prepared in chloroform and spread on the aqueous subphase in the Langmuir trough. Earlier studies on $ODEP^+Br^-$ in our laboratory have shown that the extent of aggregation of the headgroups in the Langmuir film is sensitive to the time allowed for equilibration of the monolayer at the air-water interface.[24,26] In this study we have ensured that sufficient time (~ 60 min) was provided for the monolayer to equilibrate completely at the interface so that molecular aggregation was minimized. The monolayer was then compressed with a barrier speed of 5 cm/min. The general procedure used for the fabrication of Langmuir and LB films and more details are given in Appendix A. Morphology of the Langmuir films at the air-water interface was observed by BAM. The films were examined at different stages of compression. Hydrophilic quartz/glass substrate for the LB film deposition was prepared by immersing in piranha solution for 6 h followed by sonication and rinsing in high purity water. Freshly cleaved mica plate was also employed as the substrate for depositing LB films. Hydrophobic quartz substrate was prepared by exposing the hydrophilic plate to vapors of hexamethyldisilazane for 12 h. LB films were fabricated by vertical dipping of the substrate at a speed of 5 mm/min. The film transfer of $ODEP^+Br^-$ and $MEOEP^+I^-$ were carried out on hydrophilic substrates at a surface pressure of 30 mN/m as they collapse above 40 mN/m. $OEOEP^+Br^-$ film was deposited on hydrophilic substrates at two pressures, 30 mN/m and 45 mN/m, below and above the plateau in the π-A isotherm respectively. We have attempted the transfer of Langmuir films of the three amphiphiles on to the hydrophobic substrate. The transfer was poor for $ODEP^+Br^-$ and $MEOEP^+I^-$ as well as $OEOEP^+Br^-$ below the plateau; hence they are not considered in this study. However at 45 mN/m pressure (above the plateau), $OEOEP^+Br^-$ could be transferred efficiently; the twin alkyl chain structure and the compact packing at the higher pressure appear to facilitate this. LB films deposited on mica/quartz were imaged using AFM in semi-contact mode. All the experiments described above were repeated on at least 4 – 5 fresh samples to ascertain the reproducibility of the observations.

Electronic absorption spectra of the LB films deposited on quartz plates (with hydrophilic or hydrophobic surface) were recorded with the relevant substrate used as reference. Polarized absorption spectra were recorded using plane polarized light with the electric vector parallel and perpendicular to the plane of incidence; sheet polarizers were used for the measurements. Sample was mounted on a goniometer and rotated about the dipping direction, to obtain different angles of incidence of the light; absorption spectra were corrected for the inclined incidence of light. Orientation of the transition dipole was estimated from the observed linear dichroism following standard procedures (more details are provided in Apendix D).[32] Excitation energies and the associated transition dipole and oscillator strength for electronic transitions in the hemicyanine headgroup and its dimer structures were computed using semiempirical AM1/CI method; the PECI option with 30 orbitals were used. Calculations on the hemicyanine headgroup including solvent effects were carried out using the self-consistent reaction field method (SCRF).

Steady-state fluorescence excitation and emission spectra of the LB films were recorded in front-face detection geometry. The emission spectra of the films were recorded by exciting them at the λ_{max} of the excitation spectra. Fluorescence polarization measurements were carried out in right-angle geometry, mounting the polarizers in the excitation and emission paths.

3.3. Langmuir Films of $ODEP^+Br^-$, $MEOEP^+I^-$ and $OEOEP^+Br^-$ at the Air-Water Interface

π-A isotherms of $ODEP^+Br^-$, $MEOEP^+I^-$ and $OEOEP^+Br^-$ are shown in Figure 3.2. The former two are relatively featureless, the liquid expanded phase transforming to a condensed phase smoothly upon compression; the collapse pressure is ~ 40 - 42 mN/m. The area/molecule obtained by extrapolating the higher pressure regions of the isotherms of $ODEP^+Br^-$ and $MEOEP^+I^-$ are ~30 and ~53.3 Å^2 respectively. The larger area/molecule observed in the case of $MEOEP^+I^-$ could be due to the presence of the bigger counter ion. Detailed discussions of the π-A isotherm of $ODEP^+Br^-$ is given in Sec. 4.3.1. Unlike the other two, $OEOEP^+Br^-$ shows a clear plateau at a pressure of ~ 36 mN/m and collapse at ~ 55 mN/m. Extrapolation of the isotherm below and above the plateau indicates molecular areas of 98.6 and 35.1 Å^2 respectively. This is suggestive of a reorientation of the alkyl chains of the amphiphiles from an oblique to a more vertical disposition occurring at the plateau; small change in tilt of the headgroup and interdigitation of the chains of neighboring molecules may also occur.

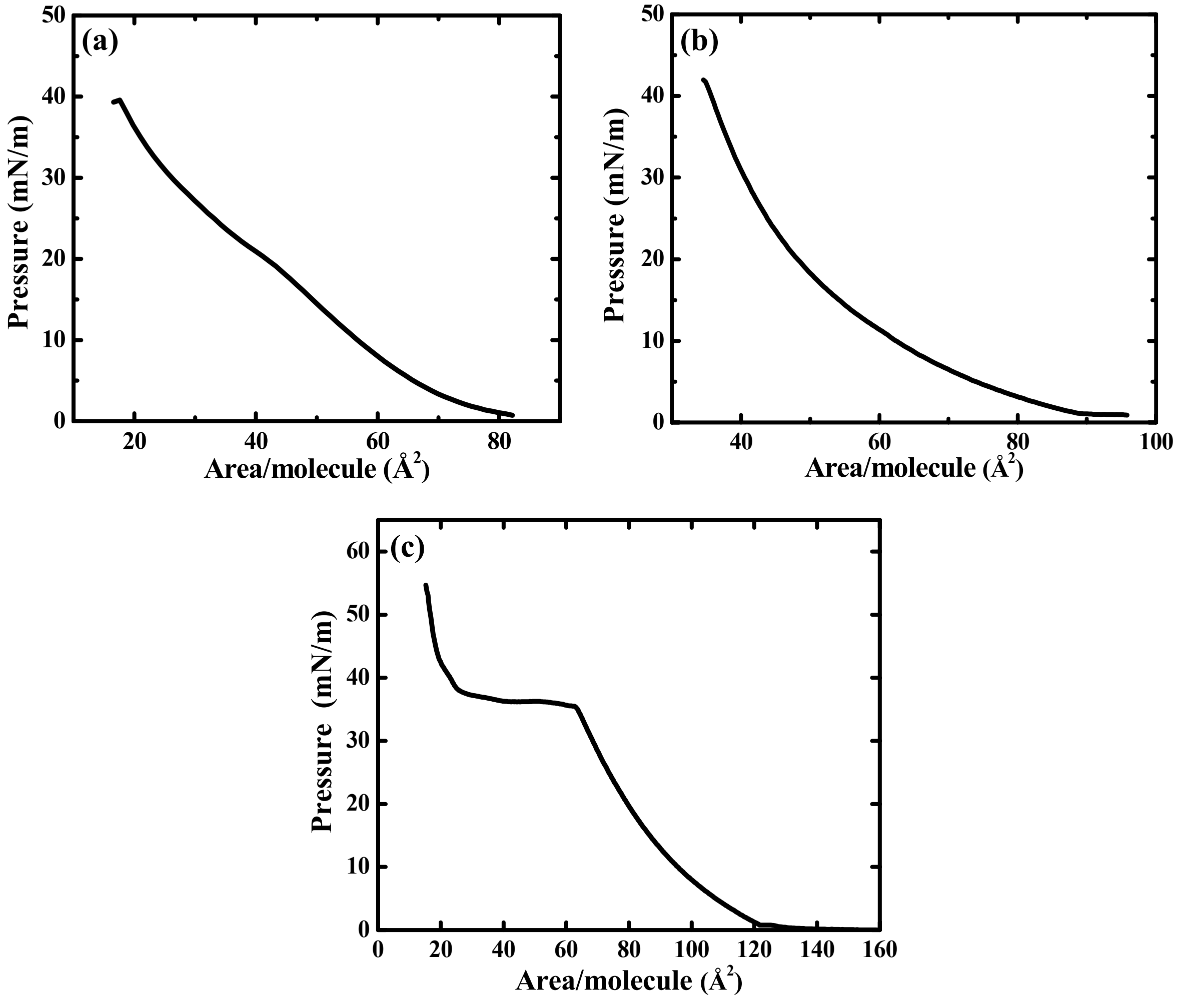

Figure 3.2. *Pressure-area isotherms of the Langmuir films of:* ***(a)*** *$ODEP^+Br^-$,* ***(b)*** *$MEOEP^+I^-$ and* ***(c)*** *$OEOEP^+Br^-$ at the air-water interface at 25°C.*

BAM imaging was used to characterize the Langmuir films at the air-water interface. $ODEP^+Br^-$ forms small aggregates at low surface pressures and a continuous film at higher pressures with gaps induced by defects resulting from the small domains formed at the lower pressures (Fig. 3.3). On the other hand smooth and continuous film formation was observed for $MEOEP^+I^-$ with no special structures at any pressure (Fig. 3.4). BAM imaging of the Langmuir film of $OEOEP^+Br^-$ shows no domain formation at lower surface pressures; the formation of nearly uniform circular domains are observed as the Langmuir film is compressed across the plateau (Fig. 3.5). Further compression above the plateau leads to the growth of these domains, their compact packing and finally coalescence into a nearly homogeneous and continuous film.

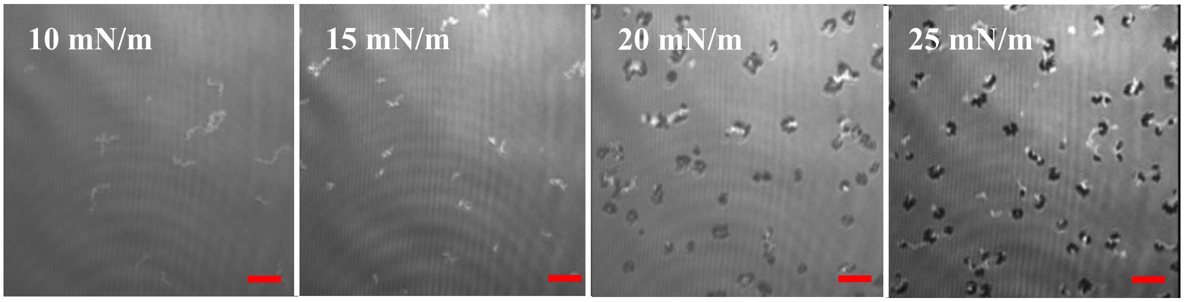

Figure 3.3. *BAM images of the Langmuir film of* $ODEP^+Br^-$ *at the air-water interface at different surface pressures (scale bar = 25 µm).*

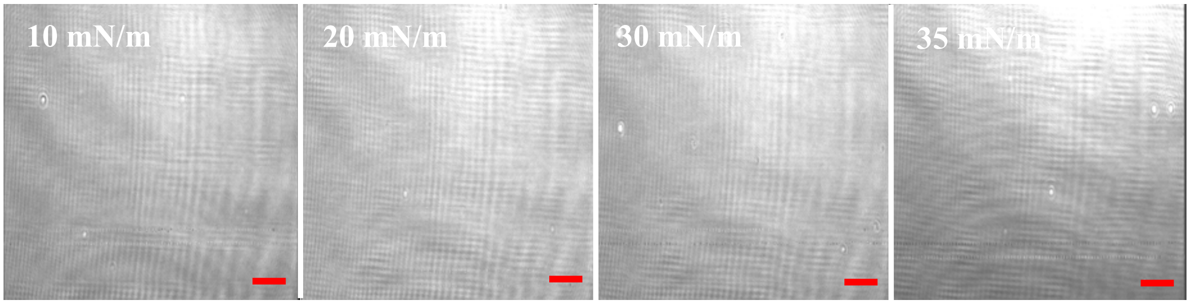

Figure 3.4. *BAM images of the Langmuir film of* $MEOEP^+I^-$ *at the air-water interface at different surface pressures (scale bar = 25 µm).*

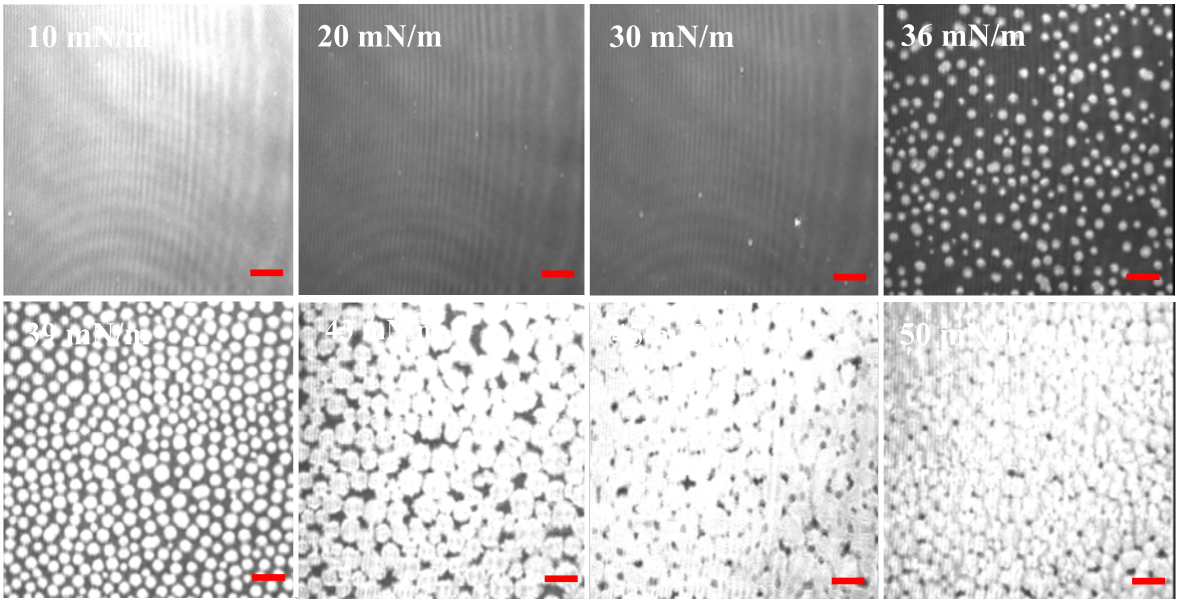

Figure 3.5. *BAM images of the Langmuir film of OEOEP$^+$Br$^-$ at the air-water interface at different surface pressures (scale bar = 25 μm).*

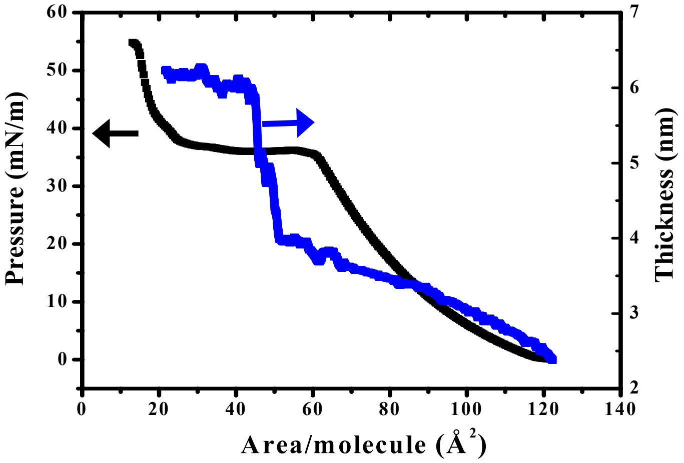

Figure 3.6. *Plot of the film thickness as a function of the area/molecule superimposed on the π-A isotherm of OEOEP$^+$Br$^-$ Langmuir film at the air-water interface at 25^{o}C*

Analysis of the reflected light intensity suggests increase in thickness of the film at the air-water interface by ~ 2 nm during the compression of OEOEP$^+$Br$^-$ monolayer across the plateau.[33] Plot of the film thickness as a function of the area/molecule shows an approximate increase of 2 nm in the film thickness across the plateau (Fig. 3.6). Details of the analysis of reflected light intensity in BAM images is provided in Appendix C.

3.4. LB Films of $ODEP^+Br^-$, $MEOEP^+I^-$ and $OEOEP^+Br^-$

Monolayer LB films were obtained by transfer of the Langmuir films on to substrates with hydrophilic as well as hydrophobic surface. Only those which showed an appreciable transfer ratio (~ 0.9 or higher) are considered in the present study. For the purpose of discussion, we designate the films using the amphiphile name, deposition pressure (in mN/m) and the nature of substrate (hydrophilic = W (water), hydrophobic = O (oil)) as shown in Table 3.1. The table lists some of the relevant characteristics of the films and their deposition. The number of molecules per unit area of the Langmuir films are estimated directly from the area/molecule read off the π-A isotherms; at 30 mN/m, it decreases in the order $ODEP^+Br^-$, $MEOEP^+I^-$, $OEOEP^+Br^-$. This is consistent with the

Table 3.1. Details of deposition of the monolayer LB films and molecular number density in the Langmuir and LB films.

LB film	**Amphiphile (Fig. 3.1)**	**Deposition pressure (mN/m)**	**Nature of substrate**	**Transfer ratio**	**Molecules per unit area (nm^{-2})**	
					Langmuir film	**LB film**
ODEPBr_30_W	$ODEP^+Br^-$	30	Hydrophilic	0.90	3.82	3.43
MEOEPI_30_W	$MEOEP^+I^-$	30	Hydrophilic	0.93	2.49	2.31
OEOEPBr_30_W	$OEOEP^+Br^-$	30	Hydrophilic	0.91	1.45	1.31
OEOEPBr_45_W	$OEOEP^+Br^-$	45	Hydrophilic	0.86	5.38	4.62
OEOEPBr_45_O	$OEOEP^+Br^-$	45	Hydrophobic	0.87	5.38	4.68

increase in molecular area from $ODEP^+Br^-$ to $MEOEP^+I^-$ due to the difference in connectivity of alkyl chains and the counterions and the impact of multiple chains and face-on orientation likely in $OEOEP^+Br^-$. The enhanced number density in the Langmuir films at the higher pressure is an obvious consequence of the reorientation of the amphiphiles and more compact packing. The number density in the LB films is estimated from the corresponding values in Langmuir films by scaling with the respective transfer ratios; the overall trend across the films remains the same.

3.4.1 *AFM Imaging*

AFM images of ODEPBr_30_W show flower-like structures[25] with ~ 2.0 – 2.5 nm in thickness, extending over several micrometers (Fig. 3.7a). In spite of repeated attempts, we found that MEOEPI_30_W as well as OEOEPBr_30_W films were not amenable to satisfactory imaging in the AFM. However, clear images of OEOEPBr_45_W and OEOEPBr_45_O could be recorded. Figure 3.7b and c show the AFM images of the former on mica (hydrophilic surface) and that of the latter on quartz (prepared with hydrophobic surface). OEOEPBr_45_W forms smooth extended films (Fig. 3.7b) with thickness in the range 2.5 – 3.5 nm. This is consistent with the likely orientation of the molecule with its headgroup contacting the substrate, perhaps at an angle, and a folded structure with both chains extending outwards. OEOEPBr_45_O forms films with a more holey surface (Fig. 3.7c); the thickness is found to be 5.0 – 6.0 nm. This is suggestive of an extended conformation of $OEOEP^+$ with one chain contacting the hydrophobic substrate, consistent with the report of Ashwell *et al.*.[28] Due to the 'tail-head-tail' structure of $OEOEP^+Br^-$, interaction of the headgroup with the substrate in OEOEPBr_45_W is facilitated by the folded structure, whereas interaction of the tail in OEOEPBr_45_O, allows an extended conformation that improves packing and promotes hydrophobic interactions. The differences in the molecular conformations and packing as well as the nature of substrates lead to the observed morphologies of the two films. The conclusions above regarding the orientations of the chains in the two films are supported by the observation of water drops placed on the OEOEPBr_45_W and OEOEPBr_45_O films that indicate the surface of both films to be hydrophobic.

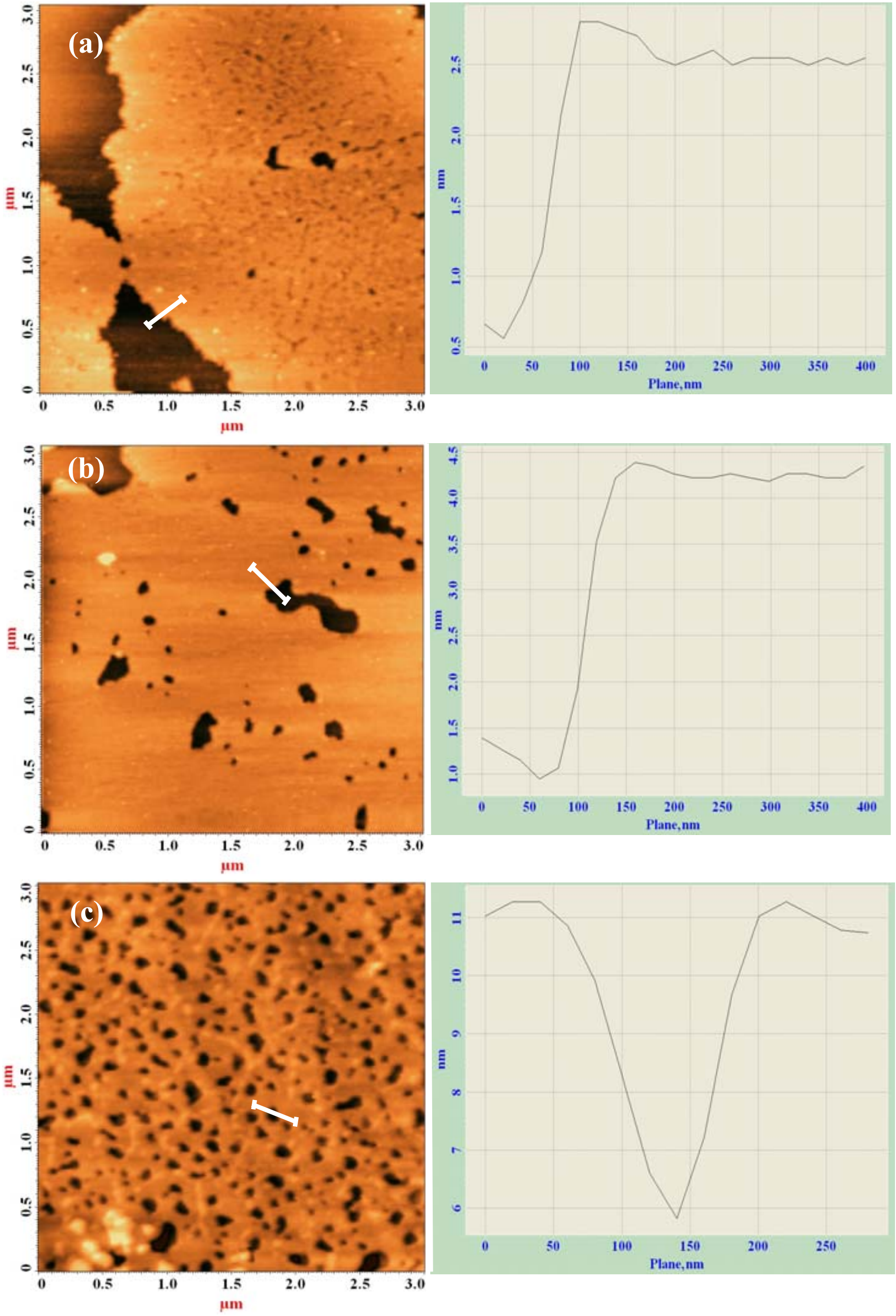

Figure 3.7. *AFM images of the monolayer LB films of:* ***(a)*** *ODEPBr_30_W on mica* ***(b)*** *OEOEPBr_45_W on mica and* ***(c)*** *OEOEPBr_45_O on quartz (with hydrophobic surface); the line profile analysis for each image is shown on the right.*

3.4.2 *Electronic Absorption Spectroscopy Studies*

Electronic absorption spectra of the monolayer LB films are collected in Figure 3.8. All the films show absorption with λ_{max} in the visible range at 460 – 480 nm. This is the characteristic absorption of the hemicyanine headgroup common to all of them. The relatively larger absorbance of the two films deposited above the plateau compared to the other three reflect the higher number density of molecules. Solution spectra of the three compounds show λ_{max} in the range 475 – 510 nm (Fig. 3.9); in each case the absorption shifts to the blue with increasing polarity of the solvent, for example, the peaks of ODEP$^+$Br$^-$ appear at 495 nm and 476 nm respectively in chloroform and acetonitrile. These observations suggest that the local environment of the chromophores in the LB films is fairly polar. AM1/CI computation on the basic chromophore system, N-methyl-4-[2-(4-dimethylaminophenyl)ethenyl]pyridinium cation, indicates a single strong absorption with λ_{max} at 478.7 nm (Table 3.2). When solvation effect due to a polar medium is included in the computation, the absorption maximum is found to shift to the blue; for example, in acetonitrile and dimethylsulfoxide, the λ_{max} is computed to be at ~ 417 nm. The trends in the computed absorption characteristics are consistent with the experimental observations

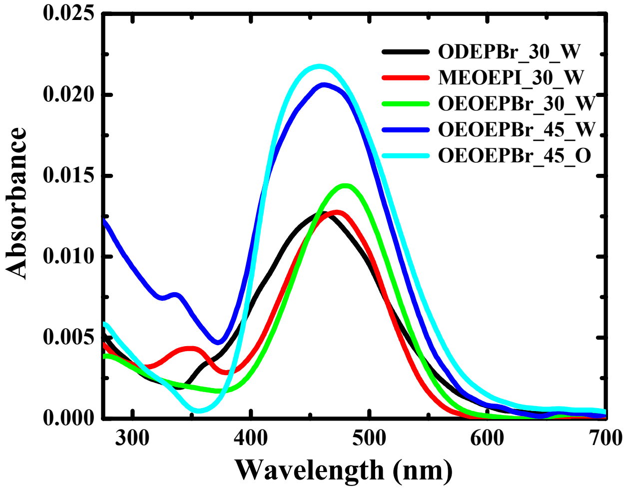

Figure 3.8. *Absorption spectra of monolayer LB films of the hemicyanine based amphiphiles fabricated under different experimental conditions (see Table 3.1 for the nomenclature used for the films).*

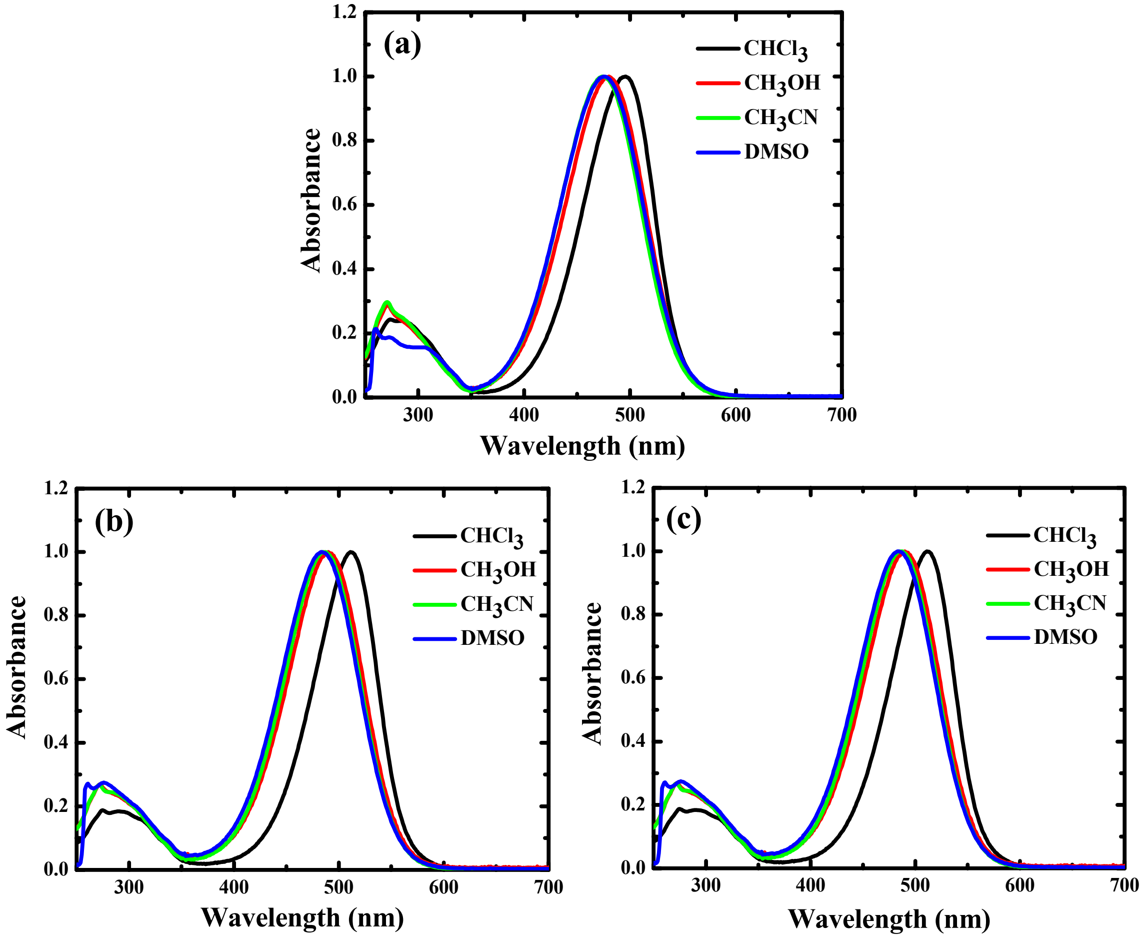

Figure 3.9. *Electronic absorption spectra of* ***(a)*** *ODEP$^+$Br$^-$,* ***(b)*** *MEOEP$^+$I$^-$ and* ***(c)*** *OEOEP$^+$Br$^-$ in different solvents.*

and arise due to the large ground state dipole moment of the chromophore. The computation also confirms that the transition dipole coincides with the donor-acceptor dipole axis connecting the N atoms of the dialkylamino and pyridinium groups as expected for an intramolecular charge transfer system. The spectra of ODEP$^+$Br$^-$ films and OEOEP$^+$Br$^-$ films deposited above the plateau are slightly broader compared to the other two with a weak shoulder emerging at lower wavelengths; origin of this will be clear from the discussions below.

Table 3.2. Results of AM1/CI computations without and with solvent effects on N-methyl-4-[2-(4-dimethylaminophenyl)ethenyl]pyridinium cation. λ_{max} for the lowest energy transition is shown in each case

Structure		**λ_{max} (nm)**	**Oscillator strength**
Monomer	No Solvent	478.7	1.228
	H_2O	416.7	1.124
	CH_3CN	417.8	1.126
	DMSO	417.5	1.126
Dimer (No solvent)	Parallel Dipoles	414.7	2.773
	Antiparallel Dipoles	417.5	2.524

We have investigated the polarization dependence of the absorption spectra in order to gain an understanding of the molecular orientations in the various films; spectra were recorded by rotating the film about the dipping direction so that light is incident at different angles, α in both p- and s-polarizations (Fig. 3.10). In all the films, when light is incident normal to the sample plane ($\alpha = 0^o$), the absorption shows negligible polarization dependence, whereas linear dichroism is observed when light is incident at an angle ($\alpha \neq 0^o$). These observations indicate that the transition dipoles of the chromophores are oriented at some

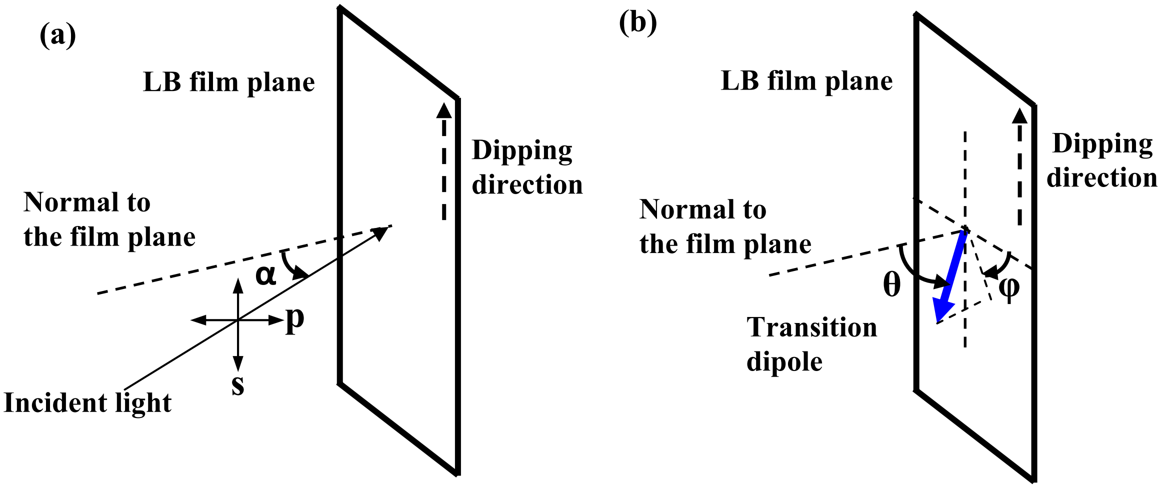

Figure 3.10. *Schematic diagram of the sample geometry used in polarized absorption measurements: **(a)** orientation of incident of light, **(b)** orientation of the transition dipole (blue arrow) of the chromophore.*

angle (θ) with respect to the normal to the film, but their azimuths (φ) in the film plane have a random distribution. MEOEPI_30_W and OEOEPBr_30_W films showed decreasing intensity for the p-polarized absorption compared to s-polarized absorption, with increasing α angle as shown in Figure 3.11 and 3.12 respectively. On the other hand ODEPBr_30_W, OEOEPBr_45_W and OEOEPBr_45_O showed broadening and emergence of a blue-shifted second peak in the absorption spectrum, as α was increased from 0° to 60° (Fig. 3.13, Fig. 3.14 and Fig. 3.15 respectively); similar observations on ODEP$^+$Br$^-$ film have been reported earlier.[18] Deconvolution of these spectra indicated λ_{max} at ~ 410 and 470 nm. The peak at 470 nm is due to the hemicyanine headgroup as noted above. The blue-shifted peak is ascribable to H-dimer or aggregate structures in the film;[18] this is supported by our AM1/CI computations which yielded λ_{max} value of ~ 414.7 nm for the parallel dimer of the hemicyanine head group (Table 3.2).

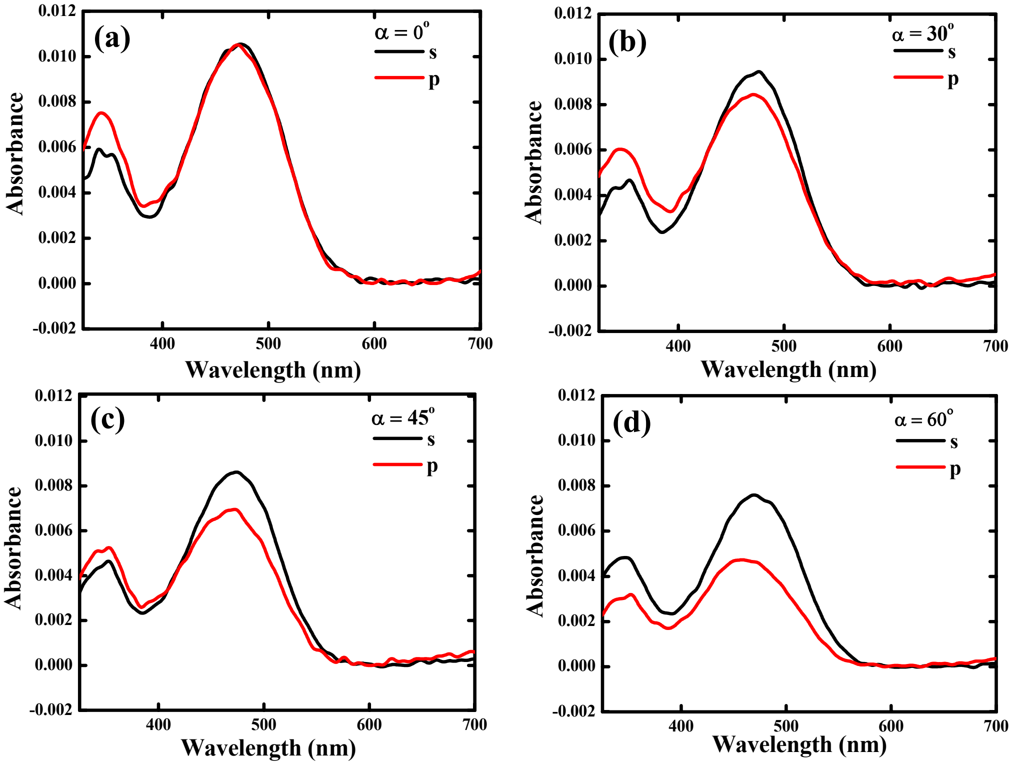

Figure 3.11. *Polarized absorption spectra of the monolayer LB film of MEOEPI_30_W recorded at different angles of incidence, α,* ***(a)*** *0°,* ***(b)*** *30°,* ***(c)*** *45° and* ***(d)*** *60°.*

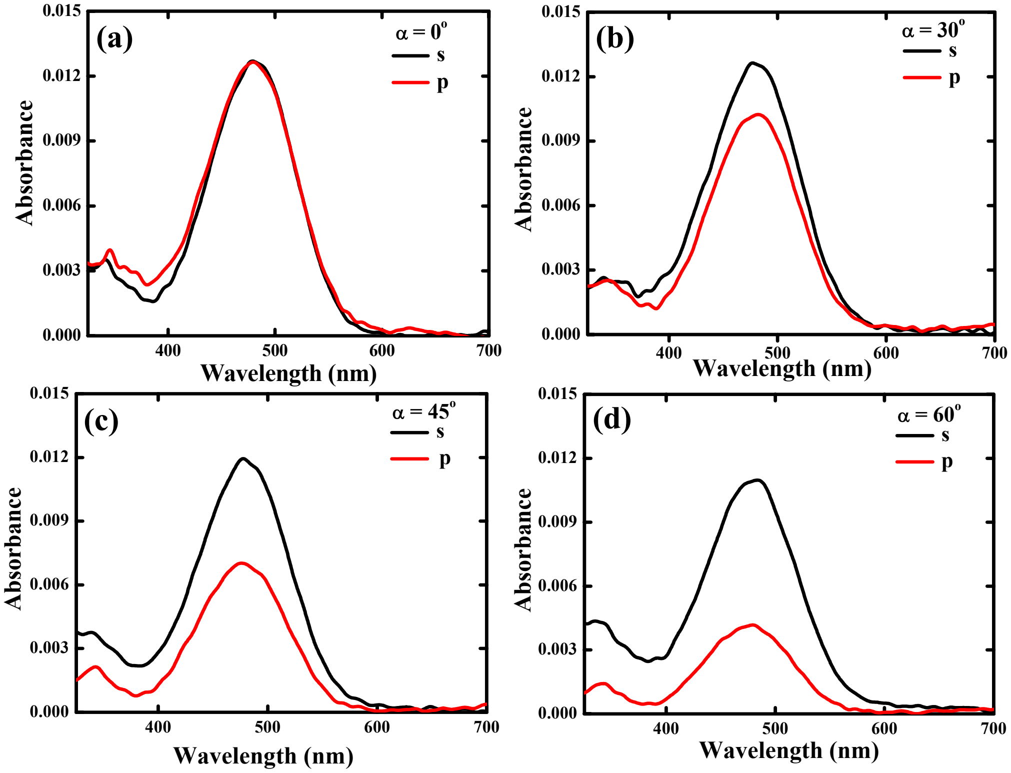

Figure 3.12. *Polarized absorption spectra of the monolayer LB film of OEOEPBr_30_W recorded at different angles of incidence, α,* **(a)** *0°,* **(b)** *30°,* **(c)** *45° and* **(d)** *60°.*

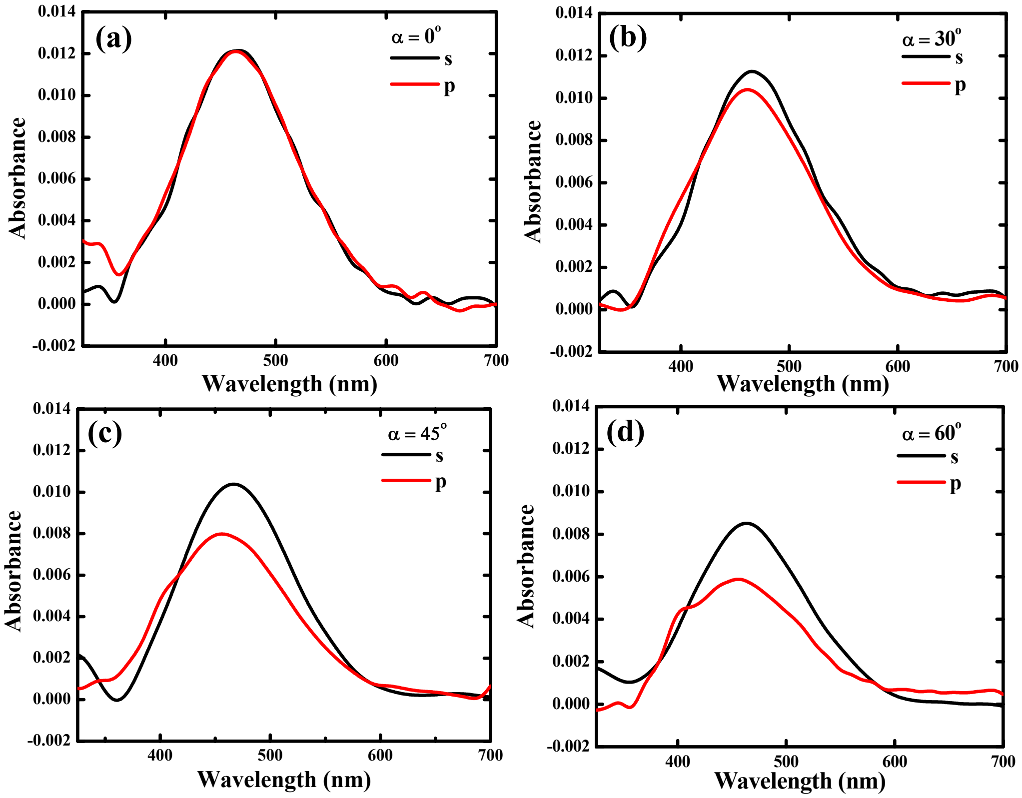

Figure 3.13. *Polarized absorption spectra of the monolayer LB film of ODEPBr_30_W recorded at different angles of incidence, α,* **(a)** *0°,* **(b)** *30°,* **(c)** *45° and* **(d)** *60°.*

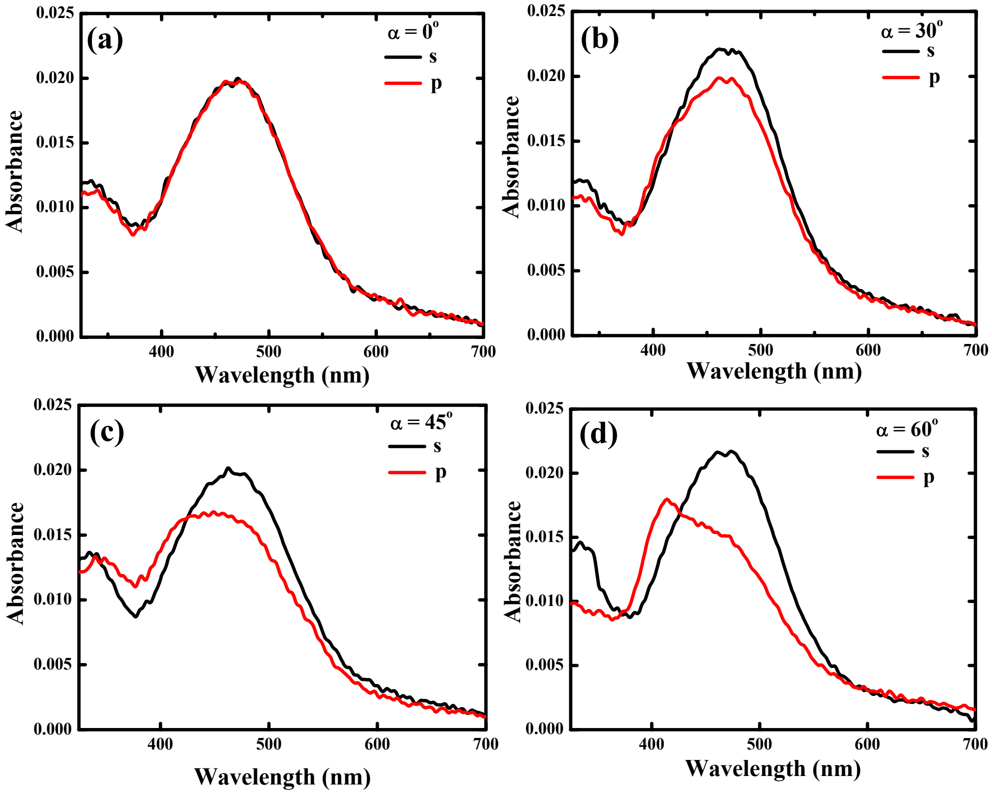

Figure 3.14. *Polarized absorption spectra of the monolayer LB film of OEOEPBr_45_W recorded at different angles of incidence, α,* ***(a)*** *0°,* ***(b)*** *30°,* ***(c)*** *45° and* ***(d)*** *60°.*

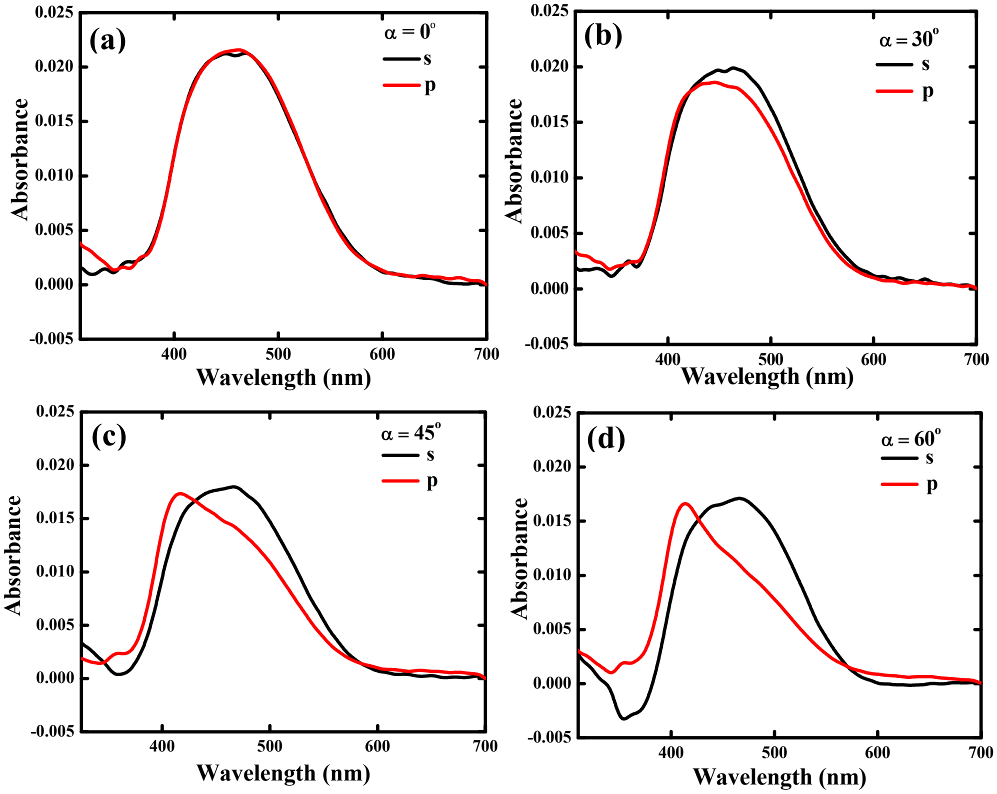

Figure 3.15. *Polarized absorption spectra of the monolayer LB film of OEOEPBr_45_O recorded at different angles of incidence α,* ***(a)*** *0°,* ***(b)*** *30°,* ***(c)*** *45° and* ***(d)*** *60°.*

Table 3.3. Absorbance at λ_{max} of the monolayer LB films measured using unpolarized light and orientation of the transition dipole of the headgroup with respect to the normal (θ) in the monolayer LB films inferred from the polarized absorption spectra with light incident at different angles, α.

LB film	Absorbance at λ_{max}	α (deg.)	θ (deg.)	
			λ_{max} ~ 410 nm	λ_{max} ~ 470 nm
ODEPBr_30_W	0.012	30	45.0	60.5
		45	49.1	61.6
		60	49.6	61.5
MEOEPI_30_W	0.012	30	-	62.2
		45	-	63.4
		60	-	65.1
OEOEPBr_30_W	0.014	30	-	70.1
		45	-	73.9
		60	-	73.1
OEOEPBr_45_W	0.020	30	53.2	61.9
		45	51.5	60.0
		60	52.8	61.0
OEOEPBr_45_O	0.021	30	52.5	60.2
		45	48.9	60.8
		60	49.9	62.1

Orientation of the transition dipole was estimated from the observed linear dichroism.[32] The angle of orientation of the transition dipole, θ extracted from the spectra of the monolayer LB films are collected in Table 3.3 (procedure used for the calculation is given in Appendix D). In the case of ODEPBr_30_W, OEOEPBr_45_W and OEOEPBr_45_O, the value corresponding to both the wavelengths are listed. The angles estimated suggest that the headgroups of the monomers in ODEPBr_30_W have an average tilt of 61.2^o and the aggregates a tilt of 47.9^o with respect to the film normal. The orientation and characteristics, slightly different from that reported[18] in the earlier study on the dodecyl analog of ODEP$^+$Br$^-$, may be attributed to the changes in the hydrocarbon chain length, temperature and pH of the subphase and the equilibration of the Langmuir film at the air-water interface.[26] The headgroups in the MEOEPI_30_W film show very similar orientation as monomers in ODEPBr_30_W film with an average tilt of 63.6^o. The case of

$OEOEP^+Br^-$ films is most interesting. The molecular organizations in OEOEPBr_45_W and OEOEPBr_45_O are similar to that in ODEPBr_30_W with the average tilt of monomers being 61.0° and that of the aggregates 52.5° in the former and 61.0° and 50.4° respectively in the latter. However, OEOEPBr_30_W is unique in the whole set, with the tilt angle of the headgroups showing the largest value of 72.4°; there is no sign of aggregation either. This orientation of the headgroups tending towards parallel to the substrate is consistent with the low number density of molecules in the Langmuir as well as LB films of $OEOEP^+Br^-$ (Table 3.1).

3.4.3 *Fluorescence Emission Responses of the Films*

The hemicyanine chromophore is known to show strong fluorescence in solution.[14,15] We have investigated the fluorescence response of the monolayer LB films of the three amphiphiles deposited at 30 mN/m on hydrophilic substrate and that of $OEOEP^+Br^-$ deposited at higher pressure and on hydrophobic substrate. Fluorescence excitation and emission spectra of the five films are collected in Figure 3.16; the emission λ_{max} of all the films appear in the range 600 – 630 nm. The spectra shown are those normalized by the absorbance at λ_{max} for each LB film so that samples with similar optical density are compared. Intensities are shown relative to that of ODEPBr_30_W which shows the weakest fluorescence in the series; the values at the emission maximum are collected in Table 3.4. It is well known that the fluorescence of $ODEP^+Br^-$ film is quenched strongly by aggregation effects.[18] The emission intensity of MEOEPI_30_W is found to be approximately 6 times that of ODEPBr_30_W. The significant difference between $ODEP^+Br^-$ and $MEOEP^+I^-$ is the change in the point of attachment of the hydrocarbon chain with respect to the ionic part of the headgroup. This facilitates better solvation of the headgroup in the Langmuir film of $MEOEP^+I^-$ leading to the reduced aggregation reflected in the absorption spectrum of MEOEPI_30_W and the moderate enhancement in the fluorescence emission. The emission from OEOEPBr_45_W and OEOEPBr_30_W are approximately 11 and 17 times higher than that of ODEPBr_30_W respectively. In the former, the fluorescence is strong in spite of some aggregation; this possibly arises due to partial modification of the interaction between the fluorophores by the double hydrocarbon chains. The much stronger emission from the film deposited below the plateau appears to be related to the effective reduction of the interaction of the hemicyanine headgroups by the nearly face-on orientation on the substrate coupled with the separation provided by the hydrocarbon chains attached at both ends. The emission is found to be strongest in OEOEPBr_45_O, about 30 times that of ODEPBr_30_W. In OEOEPBr_45_O, in addition to the conducive molecular packing facilitated by the extended conformation, the attachment of the chains to the hydrophobic substrate and the positioning of the hemicyanine fluorophores away from it, possibly suppresses any quenching effects due to the substrate; such phenomena have been discussed earlier in the context of dye molecules adsorbed on glass.[34]

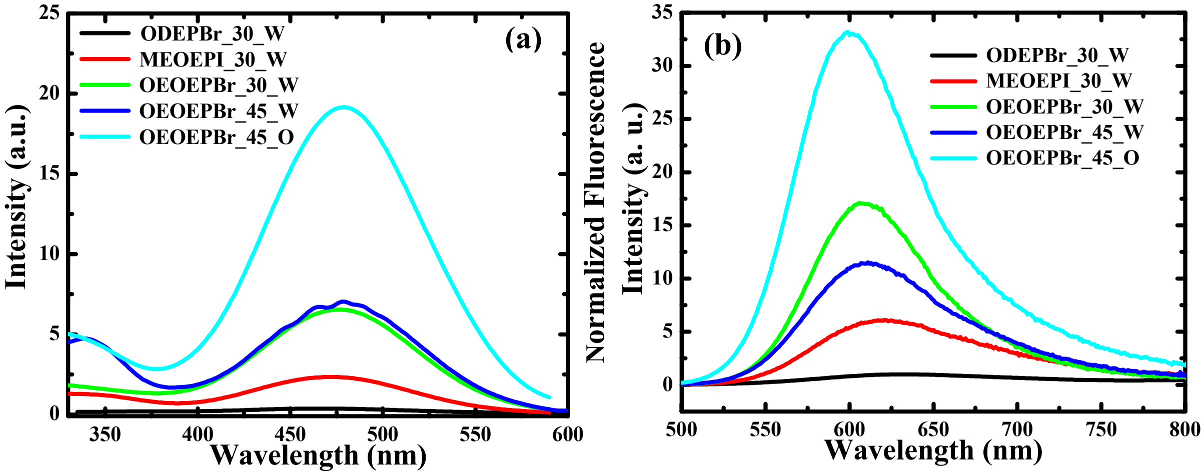

Figure 3.16. *Fluorescence **(a)** excitation and **(b)** emission spectra of monolayer LB films of the hemicyanine based amphiphiles (fluorescence intensities are normalized by the absorbance at λ_{max} of the respective film and relative values are shown).*

Fluorescence intensity normalized with respect to the optical density is meaningful in a photophysical sense as emission related to comparable input of photons is assessed. However, normalization with respect to the number of molecules (i.e. fluorophore units) provides a better comparison from a materials perspective. Table 3.4 lists also the fluorescence intensity of the different LB films, normalized with respect to the number den-

Table 3.4. Intensities of fluorescence from the monolayer LB films: intensity at λ_{max} of the emission spectrum (in arbitrary units), intensity normalized with the absorbance as well as the number density of molecules in the films and the fluorescence anisotropy estimated from fluorescence polarization measurements.

LB film	Fluorescence intensity (arb. units)	Relative fluorescence intensity normalized by		Fluorescence anisotropy
		absorbance at λ_{max}	number density of molecules	
ODEPBr_30_W	2.6	1.0	1.0	0.13
MEOEPI_30_W	15.8	6.0	8.9	0.12
OEOEPBr_30_W	52.1	17.0	51.9	0.12
OEOEPBr_45_W	45.9	11.0	13.0	0.08
OEOEPBr_45_O	144.9	32.9	40.4	0.09

sity of molecules in the LB films. In terms of this number as well, OEOEPBr_30_W and OEOEPBr_45_O show the strongest responses; however, due to the relatively smaller density of molecules, the efficiency of the former emerges as the highest. This is indirectly related to the more efficient light absorption per molecule exhibited by OEOEPBr_30_W. Measurements of fluorescence polarization reveal moderate anisotropy[35] in all the monolayer LB films (Table 3.4); this may be attributed to the organized structure of the fluorophores in these ultrathin films (see Appendix E for details).

The study presented in this chapter reveals the significance of the structural design of amphiphiles as well as deposition conditions in determining the fluorescence response of monolayer LB films. In the case of $ODEP^+Br^-$ and $MEOEP^+I^-$ having a single long hydrocarbon chain, the supramolecular organization and intermolecular interactions are ineffective in suppressing self-quenching effects. In $OEOEP^+Br^-$ on the other hand, the long hydrocarbon chains at both ends of the headgroup bestow a 'tail-head-tail' structure that guides the packing of the fluorophore units and controls the intermolecular interactions, leading to minimization of self-quenching effects and enhancement of fluorescence emission. The multiple chains also facilitate efficient assembly of the amphiphiles on a hydrophobic surface which appears to be a simple but effective strategy to elicit maximum fluorescence response from these ultrathin films.

3.5. Summary

We have characterized the Langmuir films of a novel hemicyanine based cationic amphiphiles with ‘tail-head-tail’ structure displaying an organized domain structure at the air-water interface. The impact of this amphiphile structure in terms of the attachment of the hydrocarbon chains, on the headgroup orientation and fluorescence properties of the monolayer LB film was revealed through comparison with other amphiphiles bearing the same headgroup. Significance of the conditions and mode of deposition in realizing strongly fluorescent monolayer LB films were also demonstrated. Our observations suggest a simple molecular design strategy and preferred deposition parameters to realize enhanced optical responses in ultrathin films of fluorescent molecules. Implications of the current findings for other materials attributes such as nonlinear optical responses remain to be explored.

References

1. (a) Wilson, J. N.; Smith, M. D.; Enkelmann, V.; Bunz, U. H. F. *Chem. Commun.* **2004**, 1700; (b) Jayanty, S.; Radhakrishnan, T. P. *Chem. Eur. J.* **2004**, *10*, 791; (c) Ren, Y.; Lam, J. W. Y.; Dong, Y.; Tang, B. Z.; Wong, K. S. *J. Phys. Chem. B* **2005**, *109*, 1135; (d) Davis, R.; Kumar, N. S. S.; Abraham, S.; Suresh, C. H.; Rath, N. P.; Tamaoki, N.; Das, S. *J. Phys. Chem. C* **2008**, *112*, 2137; (e) Hong, Y. N.; Lam, J. W. Y.; Tang, B. Z. *Chem. Commun.* **2009**, 4332.
2. (a) Huang, C. H.; Wang, K. Z.; Zhu, X. Y.; Wu, N. Z.; Xu, G. X.; Xu, Y.; Liu, Y. Q.; Zhu, D. B.; Liu, Y. W.; Xue, Z. Q. *Solid State Commun.* **1994**, *90*, 151; (b) Huang, H.; Liu, H.; Xue, Q.; Qian, D. *Colloids Surfaces A* **1999**, *154*, 327; (c) Wang, J.; Wang, H.; Fu, L.; Liu, F.; Zhang, H. *Mater. Sci. Engg. B* **2003**, *B97*, 83.
3. (a) Dutta, A. K.; Vanoppen, P.; Jeuris, K.; Grim, P. C. M.; Pevenage, D.; Salesse, C.; De Schryver, F. C. *Langmuir* **1999**, *15*, 607; (b) Liu, Y.; Liu, M. *Thin Solid Films* **2002**, *415*, 248.
4. (a) Van der Auweraer, M.; Verschuere, B.; De Schryver, F. C. *Langmuir* **1988**, *4*, 583; (b) Nagamura, T.; Toyozawa, K.; Kamata, S. *Colloids Surfaces A* **1995**, *102*, 31; (c) Liu, L.; Liu, Z.; Xu, W.; Xu, H.; Zhang, D.; Zhu, D. *Thin Solid Films* **2006**, *515*, 2596.
5. (a) Lusk, A. L.; Bohn, P. W. *Langmuir* **2000**, *16*, 9131; (b) Lusk, A. L.; Bohn, P. W. *J. Phys. Chem. B* **2001**, *105*, 462.
6. (a) Dutta, A. K. *Langmuir* **1996**, *12*, 5909; (b) Parichha, T. K.; Talapatra, G. B. *Opt. Mater.* **1998**, *11*, 9; (c) Parichha, T. K.; Talapatra, G. B. *J. Phys. Chem. Solids* **1999**, *60*, 111.
7. (a) Itaya, A.; Masuhara, H.; Taniguchi, Y.; Imazeki, S. *Langmuir* **1989**, *5*, 1407; (b) Ohta, N.; Ito, T.; Yamazaki, I. *Mol. Cryst. Liq. Cryst. A* **1998**, *314*, 119.
8. Murakata, T.; Miyashita, T.; Matsuda, M. *Langmuir* **1986**, *2*, 786.
9. Yamazaki, I.; Tamai, N.; Yamazaki, T. *J. Phys. Chem.* **1987**, *91*, 3572.
10. Ito, S.; Okubo, H.; Ohmori, S.; Yamamoto, M. *Thin Solid Films* **1989**, *179*, 445.
11. (a) Biesmans, G.; Verbeek, G.; Verschuere, B.; Van der Auweraer, M.; De Schryver, F. C. *Thin Solid Films* **1989**, *169*, 127; (b) Tamai, N.; Yamazaki, T.;

Yamazaki, I. *Thin Solid Films* **1989**, *179*, 451; (c) Tamai, N.; Yamazaki, T.; Yamazaki, I. *Can. J. Phys.* **1990**, *68*, 1013; (d) Sluch, M. I.; Vitukhnovsky, A. G.; Warren, J. G.; Petty, M. C. *Thin Solid Films* **1992**, *210-211*, 211; (e) Ichinose, N.; Nishimura, Y.; Yamazaki, I. *Chem. Phys. Lett.* **1992**, *197*, 364; (f) Verma, A. L.; Zhang, Z.; Tamai, N.; Nakashima, K.; Yoneyama, M.; Iriyama, K.; Ozaki, Y. *Langmuir* **1998**, *14*, 4638; (g) Zhanga, Z.-J.; Verma, A. L.; Tamai, N.; Nakashima, K.; Yoneyama, M.; Iriyama, K.; Ozakia, Y. *Thin Solid Films* **1998**, *333*, 1.

12. Beswick, R. B.; Pitt, C. W. *J. Colloid Interface Sci.* **1988**, *124*, 146.
13. Shimomura, M.; Shinohara, E.; Kondo, S.; Tajima, N.; Nagata, Y.; Koshiishi, K. *Sensors Mater.* **1992**, *4*, 29.
14. Jones, M. A.; Bohn, P. W. *Anal. Chem.* **2000**, *72*, 3776.
15. Zhao, C. F.; Gvishi, R.; Narang, U.; Ruland, G.; Prasad, P. N. *J. Phys. Chem.* **1996**, *100*, 4526.
16. Song, Q.; Evans, C. E.; Bohn, P. W. *J. Phys. Chem.* **1993**, *97*, 13736.
17. Huang, Y.; Cheng, T.; Li, F.; Luo, C.; Huang, C.; Cai, Z.; Zeng, X.; Zhou, J. *J. Phys. Chem. B* **2002**, *106*, 10031.
18. Abraham, E.; Grauby-Heywang, C.; Selector, S.; Jonusauskas, G. *J. Photochem. Photobio. B* **2008**, *93*, 44.
19. Ulman, A. *An Introduction to Ultrathin Organic Films: From Langmuir-Blodgett to Self-Assembly*; Academic Press: Boston, 1991.
20. Song, Q.; Xu, Z.; Lu, W.; Bohn, P. W. *Colloids Surfaces A* **1994**, *93*, 73.
21. Ashwell, G. J.; Hargreaves, R. C.; Baldwin, C. E.; Bahra, G. S.; Brown, C. R. *Nature* **1992**, *357*, 393.
22. (a) Girling, I. R.; Cade, N. A.; Kolinsky, P. V.; Jones, R. J.; Peterson, I. R.; Ahmed, M. M.; Neal, D. B.; Petty, M. C.; Roberts, G. G.; Feast, W. J. *J. Opt. Soc. Am. B* **1987**, *4*, 950. (b) Scildkraut, J. S.; Penner, T. L.; Willand, C. S.; Ulman. A. *Opt. Lett*. **1988**, *13*, 134. (c) Sato, O.; Baba, R.; Hashimoto, K.; Fujishima, A. *J. Phys. Chem.* **1991**, *95*, 9636. (d) Carpenter, M. A.; Willand, C. S.; Penner, T. L.; Williams, D. J.; Mukamel, S. *J. Phys*. *Chem*. **1992**, *96*, 2801.
23. (a) Cross, G. H.; Girling, I. R.; Peterson, I. R.; Cade, N. A.; Earls, N. A. *J. Opt. Soc. Am. B* **1987**, *4*, 962. (b) Hayden, L. M.; Kowel, S. T.; Srinivasan, M. P. *Opt.*

Commun. **1987**, *61*, 351. (c) Li, F.; Jin, L.; Huang, C.; Zheng, J.; Guo, J.; Zhao, X.; Liu, T. *Chem. Mater.* **2001**, *13*, 192.

24. Chandra, M. S.; Ogata, Y.; Kawamata, J.; Radhakrishnan, T. P. *Langmuir* **2003**, *19*, 10124.
25. Chandra, M. S.; Krishna, M. G.; Mimata, H.; Kawamata, J.; Nakamura, T.; Radhakrishnan, T. P. *Adv. Mater*. **2005**, *17*, 1937.
26. (a) Chandra, M. S.; Radhakrishnan, T. P. *Mol. Cryst. Liq. Cryst.* **2003**, *403*, 77. (b) Chandra, M. S.; Ogata, Y.; Kawamata, J.; Radhakrishnan, T. P. *J. Nonlin. Opt. Phys. Mater*. **2004**, *13*, 347.
27. Rajesh, K.; Chandra, M. S.; Hirakawa, S.; Kawamata, J.; Radhakrishnan, T. P. *Langmuir* **2007**, *23*, 8560.
28. Ashwell, G. J.; Dyer, A. N.; Lochun, D. *Mol. Cryst. Liq. Cryst.* **1999**, *337*, 421.
29. Cross, G. H.; Peterson, I. R.; Girling, I. R.; Cade, N. A.; Goodwin, M. J.; Carr, N.; Sethi, R. S.; Marsden, R.; Gray, G. W.; Lacey, D.; McRoberts, A. M.; Scrowston, R. M.; Toyne, K. J. *Thin Solid Films* **1988**, *156*, 39.
30. Ashwell, G. J.; Jackson, P. D.; Crossland, W. A. *Nature* **1994**, *368*, 438.
31. Plater, M. J.; Jackson, T. *Tetrahedron* **2003**, *59*, 4673.
32. N'soukapoé-Kossi, C. N.; Sielewiesiuk, J.; Leblanc, R. M.; Bone, R. A.; Landrum, J. T. *Biochim. Biophys. Acta* **1988**, *940*, 255.
33. (a) Patino, J. M. R.; Sanchez, C. C.; Nino, N. M. R. *Langmuir* **1999**, *15,* 2484; (b) Winsel, K.; Honing, D.; Lunkenheimer, K.; Geggel, K.; Witt, C. *Eur. Biophys. J.* **2003**, *32*, 544.
34. Lee, M.; Kim, J.; Tang, J.; Hochstrasser, R. M. *Chem. Phys. Lett.* **2002**, *359*, 412.
35. Togashi, D. M.; Romã, R. I. S.; Gonçalves da Silva, A. M.; Sobral, A. J. F. N.; Costa, S. M. B. *Phys. Chem. Chem. Phys.* **2005**, *7*, 3874.

Scope

Aggregation of hemicyanine dye molecules is a problem of fundamental relevance to their linear and nonlinear optical properties. This is an important issue in the fabrication of LB films based on the hemicyanine dye and their optical second harmonic generation capability, and has been studied extensively by several research groups. Polyelectrolyte templating technique developed in our laboratory effectively suppresses the aggregation of cationic hemicyanine based amphiphiles in monolayer LB films leading to enhanced and stable SHG. Polyelectrolyte can influence considerably, the formation and structure of multilayer LB films and hence their optical responses. This interesting possibility has not been explored so far. In this chapter we present our investigations on the impact of different polyelectrolytes (salts of poly(4-styrenesulfonic acid), deoxyribonucleic acid and carboxymethylcellulose) on the mode of formation of multilayer LB films of $ODEP^+Br^-$ *and their SHG response.* π-A *isotherms and BAM reveal the impact of the polyelectrolyte complexation on the Langmuir films. Transfer ratios observed during film deposition, supported by electronic absorption spectra and AFM images of the multilayer LB films, suggest that the polyanions influence the deposition sequence leading to significant variations in the SHG. Carboxymethylcellulose is identified as an optimal template that induces favorable z-type deposition, leading to the formation of stable multilayer films. These films exhibit the expected quadratic increase of SHG with the extent of deposition; significantly the film response is very stable under extended laser irradiation. It is proposed that structural adjustments of the sandwiched polymer layer leads to the observed deposition sequence and film stability. Polyelectrolyte templating is demonstrated to be a simple and effective strategy for the fabrication of multilayer LB films to elicit efficient quadratic nonlinear optical response. Studies with other hemicyanine based amphiphiles (*$MEOEP^+I^-$ *and* $OEOEP^+Br^-$*) are also presented and the efficiency of this approach in those cases is discussed.*

4.1. Introduction

Molecules possessing a conjugated π-electron system are prime candidates for the development of novel electronic, optical and nonlinear optical (NLO) materials because of their fast and efficient responses. Attributes of molecular materials can be fine-tuned through the control of molecular structure by chemical synthesis and the design of the supramolecular organization using a range of chemical and physical approaches. Several strategies have been developed that lead to molecular materials exhibiting strong second order NLO responses such as SHG.[1-3] Even order effects such as SHG, necessarily require a noncentrosymmetric organization of the molecules in the material (Sec. 1.4.2), and efficient SHG results from an optimal orientation of the molecules that effectively exploits the hyperpolarizability tensor (β) components.[4] Incorporation of features such as chirality,[5] sterically bulky groups,[6] optimally long alkyl chains[7] and H-bond functionalities[8] in the molecular design have led to crystals exhibiting strong SHG. Other chemical approaches include salt formation,[9] cocrystallization[10] and assembly of helical superstructures.[11] The dominant tendency of molecular crystals to form centrosymmetric lattices has led to the development of several physical approaches to the fabrication of molecular materials for SHG applications. These include electric field poling in polymers,[12] intercalation in host lattices,[13] PVD[14] and ultrathin film assembly through methods such as the LbL[15] and LB techniques.[16-18] Formation of x- or z-type LB films is one of the most elegant and direct approaches to the noncentrosymmetric assembly of molecules and should therefore be an ideal choice for the fabrication of molecular materials for SHG. However, the LB technique is limited by difficulties such as the instability of the amphiphiles of interest at the air-water interface,[19] inefficient or inappropriate (y-type and centrosymmetric) transfer during multilayer deposition[20] and molecular reorganization in the deposited metastable films.[18,21] Earlier studies from our laboratory have shown that the SHG of LB films can decay as a result of the laser irradiation associated with the SHG experiment itself.[22] The traditional approach of addressing some of these problems by mixing the desired amphiphiles with molecules like fatty acids,[23] has the deleterious effect of diluting the active groups in the 2-dimensional lattice and possibly phase separation,[17] often leading to undesirable consequences including diminished SHG. Techniques like alternate dipping[24] call for specialized instrumentation and fabrication protocols and the stability of the films still depends on the choice of the partner amphiphiles employed.

A simple and convenient approach developed in our laboratory, based on polyelectrolyte templating[19] tackles a number of these problems efficiently. Molecular aggregation of the hemicyanine based amphiphile, $ODEP^+Br^-$ was suppressed and the SHG of the monolayer LB film (ODEP_Br) enhanced by the templating effect of polyelectrolytes.[25] It was also shown that the laser-induced decay of the SHG is arrested by polyelectrolyte complexation.[22] Since efficient systems for SHG based on LB films would necessarily require multilayer structures with appropriate molecular orientations across the layers, we decided to investigate the potential of the polyelectrolyte templating approach in addressing this critical issue. $ODEP^+Br^-$ is chosen for the investigation, because hemicyanine based amphiphiles are well-known for molecular aggregation/reorganization in Langmuir and LB films leading to the decay of SHG efficiency,[17,23,25-27] and thus serve as a stringent test case. Experiments were carried out with different polyanions introduced in the aqueous subphase. The Langmuir films were examined using BAM and the LB films investigated by optical absorption, AFM and SHG measurements. It is demonstrated that polyelectrolyte templating has profound impact on the construction of multilayers of the NLO-phore based amphiphilic molecule and that an optimal choice of the polyelectrolyte leads to LB films with high stability and enhanced SHG response. A model is presented that describes the potential role of polyelectrolyte complexation. Preliminary studies of the impact of polyelectrolyte templating on other hemicyanine based amphiphiles $MEOEP^+I^-$ and $OEOEP^+Br^-$ are also carried out.

4.2. Experimental Details

The polyelectrolytes used in the present study are sodium salts of poly(4-styrenesulfonic acid) ($(Na^+)_nPSS^{n-}$; MW = 70,000), deoxyribonucleic acid ($(Na^+)_nDNA^{n-}$; highly polymerized CT DNA) and carboxymethylcellulose ($(Na^+)_nCMC^{n-}$; MW = 90,000) (Fig. 4.1). High purity water without or with dissolved polyelectrolytes (~ 1.8 μM based on monomer molecular weight) was used as the subphase. Solutions of the amphiphiles in chloroform were spread on the subphase keeping the mole ratio of amphiphile to the polyanions in the subphase ~ 1:8; this is found to be the optimal ratio to achieve efficient complexation with the polyelectrolytes.[25] After equilibration (~60 min without and ~120 min with polyelectrolytes), the π-A isotherms were recorded using a barrier speed of 5 cm/min. Isocycling experiments show that the isotherms are highly reproducible with negligible hysterisis; the films held at pressures below the collapse are stable for several hours. The general procedures used for the Langmuir and LB film preparation are given in Appendix A. Hydrophilic glass and quartz plates for the LB film deposition were prepared by immersing in aqueous sodium hydroxide for 12 h followed by sonication and rinsing in high purity water. The LB film was coated by vertical dipping at a speed of 5 mm/min with the monolayer held at a pressure of 30 mN/m for ODEP$^+$Br$^-$ and MEOEP$^+$I$^-$ and 45 mN/m for OEOEP$^+$Br$^-$. A close examination of the isotherms and analysis of the area/molecule using modeling studies suggest that at this pressure, the amphiphiles are close packed with nearly vertical orientation of their headgroups. Electronic absorption spectra of the LB films were recorded for monolayer and multilayer films deposited on glass. Spectra of monolayer films on quartz were also recorded.

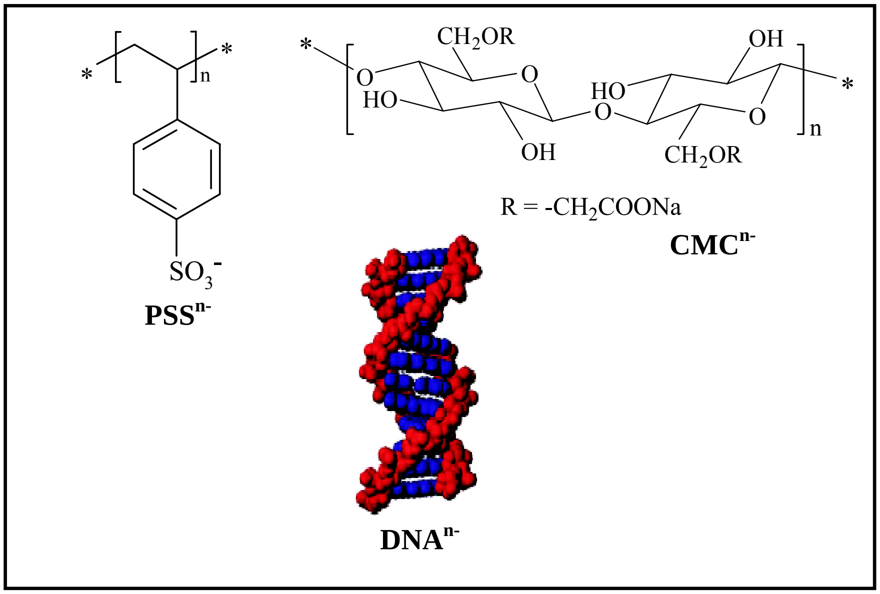

Figure 4.1. *Molecular structure of the various polyelectrolytes used in the studies presented in this chapter.*

Incident angle dependence of the SHG intensity of the films deposited on glass substrates was measured using a pulsed beam from a repetitively Q-switched Nd-YAG laser at a wavelength of 1064 nm with a pulse duration of 140 ns (average laser power = 450 mW). Details of the equipment and the experimental procedure are presented in Appendix F. The Maker fringe recorded for quartz was fitted to standard equations;[28] the envelope of the fitted fringe was drawn and its value at 0^{o} was taken as a measure of the reference SHG signal. SHG fringes of the LB films were treated similarly; the value of the envelope of the fitted fringes at a fixed angle (chosen as 45^{o} for convenience) was taken as the SHG intensity and normalized using the value of quartz measured under identical conditions. Details of the theoretical fitting of the fringes are given in Appendix F. Stability of the films and their SHG were assessed by subjecting a given sample to measurements involving laser irradiation with average power of 950 mW for ~ 10 min followed by electronic absorption measurement, the cycle repeated 8 times. This was followed by SHG measurements alone on the same sample under similar conditions as above, repeated another 7 times. The sample was effectively subjected to nearly 150 min of laser irradiation at 950 mW.

4.3. Polyelectrolyte Assisted Deaggregation and SHG Enhancement in Multilayer LB Films of $ODEP^{+}Br^{-}$

4.3.1 *Langmuir films*

$ODEP^{+}Br^{-}$ forms a stable monolayer at the air-water interface. Earlier studies[25,29] from our laboratory showed that the chromophore head groups of $ODEP^{+}Br^{-}$ amphiphiles remain monomeric or undergo aggregation in the Langmuir film (ODEP_Br), depending on the time taken for equilibration of the monolayer after spreading the chloroform solution on the water surface (mentioned in Sec. 3.2.2). In this study, we have ensured that the equilibration in all cases was slow enough so that molecular aggregation was absent in the resulting Langmuir film; this is confirmed by the electronic absorption spectra of the LB films as shown later. The π-A isotherms of $ODEP^{+}$ monolayer with only Br^{-}, and with the different polyelectrolytes introduced in the subphase are shown in Figure 4.2. The isotherms show an inflection or plateau in the region of 10 - 20 mN/m pressure; the extrapolated molecular areas suggest that these result from reorientation of the headgroup of the amphiphile. The well-defined plateau in the case of ODEP_CMC indicates the strong affinity of the headgroup – polyelectrolyte combination to the aqueous subphase and the consequent barrier to headgroup reorientation upon compression. The plateau in the case of ODEP_PSS occurs at a lower pressure and is less pronounced indicating a relatively easier reorientation. The molecular areas obtained by extrapolation of the isotherm below the plateau/inflection are ~ 69, 104, 99 and 103 Å^2 for ODEP_Br, ODEP_PSS, ODEP_DNA and ODEP_CMC respectively. The complexation of the cationic amphiphile with the polyanions is reflected in the shift of the areas to higher values; the complexation could be driven by electrostatic, H-bonding and π-π interactions depending on the polyelectrolyte. Extrapolation of the isotherms above the plateau/inflection gives areas in the range 45 – 60 Å^2/molecule, indicating a change towards edge-on (vertical) orientation of the headgroups, the variations arising due to the impact of the counterions as well as possible tilts in the orientation. The slopes of the isotherms even at low areas are not very steep suggesting that the monolayers are still compressible; the areas reduce to ~ 27 – 35 Å^2/molecule at 30 mN/m, the pressure at which we have carried out the LB deposition. This is consistent with

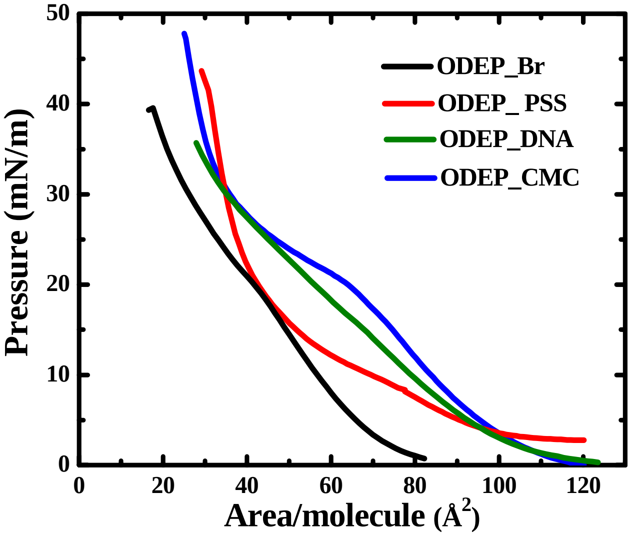

Figure 4.2. *Pressure-area isotherms of ODEP$^+$ monolayer at the air-water interface with only Br$^-$ and additionally, PSS^{n-}, DNA^{n-} and CMC^{n-} in the aqueous subphase.*

the area of ~ 30 Å^2/molecule for vertical orientation of the ODEP$^+$ headgroup, inferred from molecular modeling. Examination of the collapse pressures across the series suggests that CMC^{n-} and PSS^{n-} impart enhanced stability to the monolayer.

BAM imaging of the Langmuir films at different stages of compression are shown in Figure 4.3. In the absence of polyelectrolytes the Langmuir film shows several gaps that

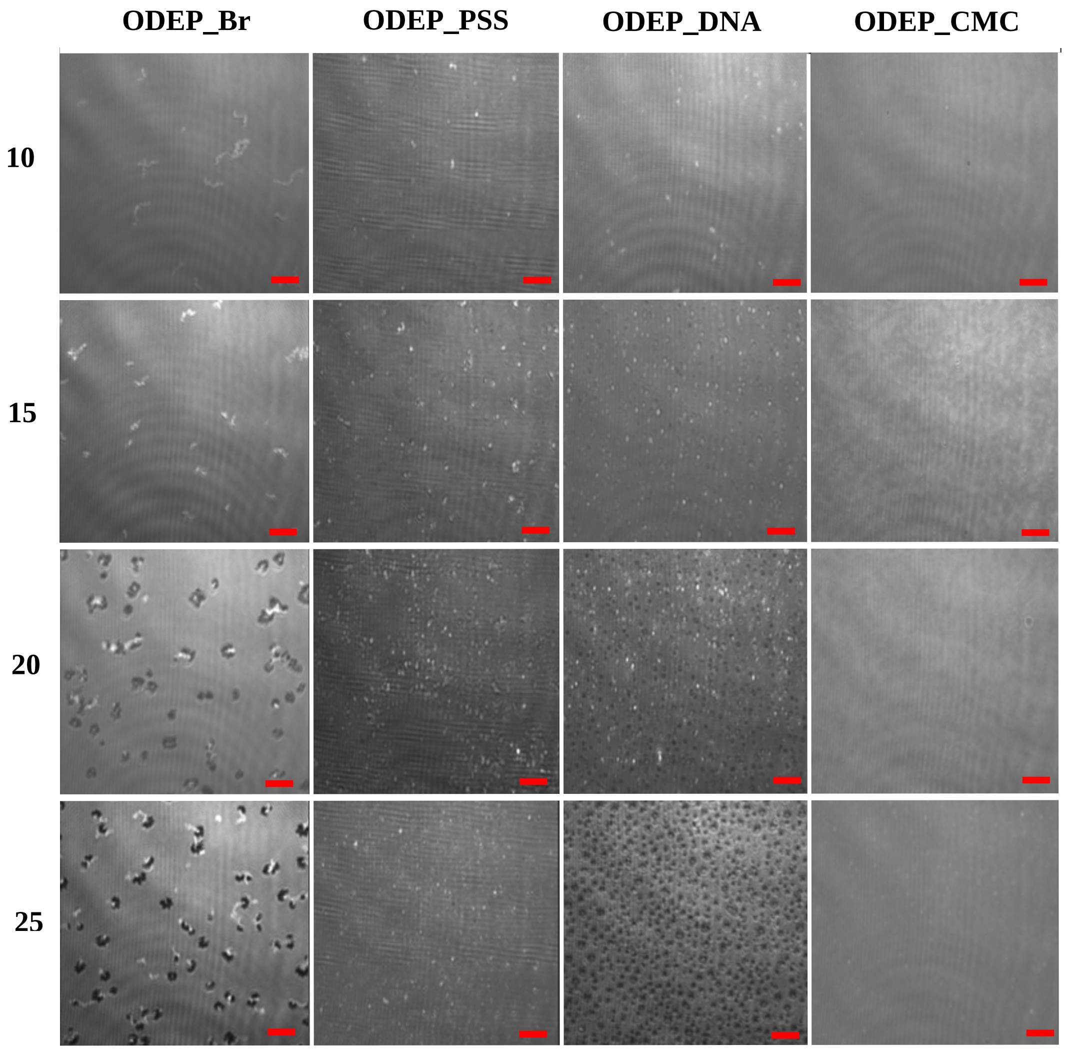

Figure 4.3. *BAM images of ODEP$^+$ monolayer at the air-water interface with only Br$^-$ and additionally, PSS^{n-}, DNA^{n-} and CMC^{n-} in the aqueous subphase recorded at different surface pressures (mN/m). Scale bar = 25 μm.*

appear to be induced by defects in the film resulting from small domains formed at lower pressures (discussed in Sec 3.3). The polyelectrolytes play a beneficial role by creating continuous and smooth films at the air-water interface; the images show that CMC^{n-} is the most effective in this respect. PSS^{n-}, DNA^{n-} and CMC^{n-} possess sulfonic, phosphoric and carboxylic acid sites respectively. The aqueous subphase has a pH of ~ 5.5 (due to the dissolution of atmospheric carbon dioxide). It is likely that CMC^{n-} is partly protonated under these conditions and hence subject to different modes of interaction with the ODEP$^+$ head group.

4.3.2 *Film deposition and Electronic Absorption Spectroscopy of LB films*

Mono and multilayer LB films of ODEP$^+$ were deposited on hydrophilic glass/quartz substrates by vertical dipping. As observed earlier,[22] monolayer deposition is

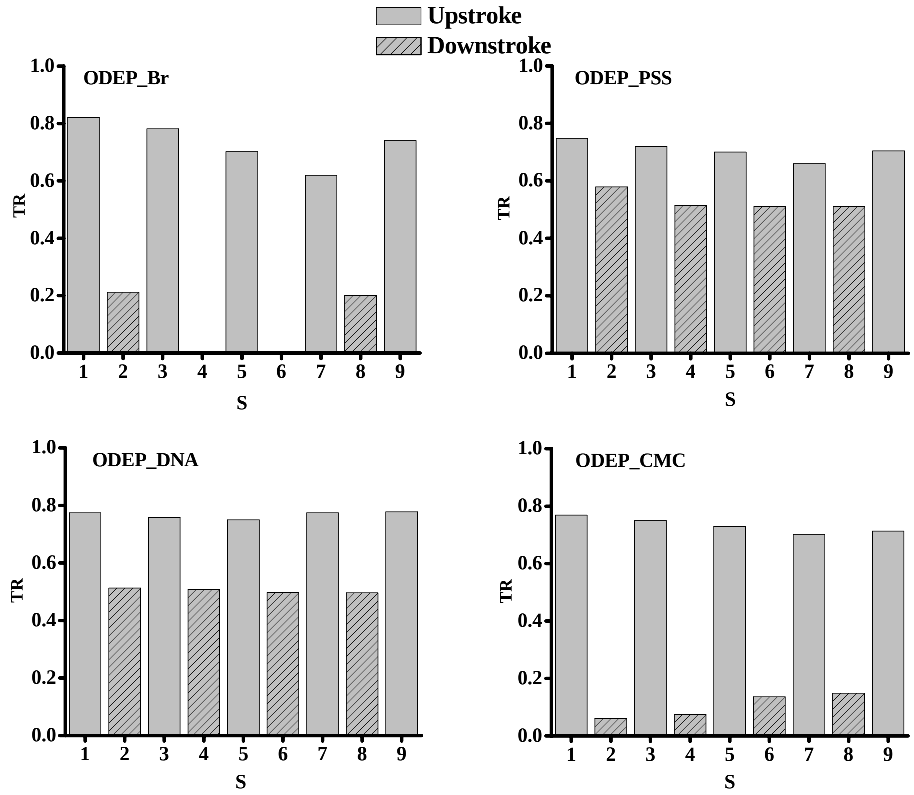

Figure 4.4. *Transfer ratios for the deposition of LB films of ODEP_Br, ODEP_PSS, ODEP_DNA and ODEP_CMC during strokes (S) 1 to 9; odd and even strokes correspond to up and downstrokes respectively.*

not influenced very much by the variations in the subphase composition, however multilayer depositions show strong differences. Transfer ratios (TR) for up to 9 vertical strokes/depositions (5 up, 4 down) in each of the four cases are shown in Figure 4.4. It is observed that appreciable transfer occurs during the upstrokes in all cases. Downstrokes lead to little or no deposition in the case of ODEP_Br and ODEP_CMC, the case with the former being quite random; the LB film transfers in these systems tend towards z-type. ODEP_PSS and ODEP_DNA on the other hand exhibit ~ 0.5 transfer during downstrokes; even though they are not exactly y-type, the tendency is towards such a deposition sequence. Thus it is seen that the polyelectrolytes exert strong influence on the multilayer formation, the effect varying with the specific type employed.

In order to have an appraisal of the deposited films in quantitative terms that can be used while exploring their electronic absorption and SHG responses, we define two types of cumulative transfer ratios (CTR) for the multilayer structures. For the case of n strokes with transfer ratios, TR_i in the i^{th} stroke,

$$CTR_{\ddagger} = \sum_{i=1}^{n} TR_i$$

$$CTR_{\pm} = \sum_{i=1}^{n} (-1)^{i-1} TR_i$$

$CTR_{\ddagger}$ reflects the total population of amphiphiles deposited on the substrate during the multilayer LB film transfer. In general, the chromophores are likely to deposit with opposite orientation during the up and down strokes; the net population of oriented molecules deposited in such a case is indicated by $CTR_{\pm}$, obtained by adding the TR for upstrokes and subtracting the value for the downstrokes (it is implicitly assumed that the TR for upstrokes are larger than that during downstrokes, otherwise the modulus of the algebraic sum may be taken). For the purpose of discussion we designate the multilayer LB films of $ODEP^+$ by the total number of up and down strokes (S) involved in the deposition sequence; for each of the four systems, we have fabricated and investigated the films, 1S, 3S, 5S, 7S and 9S (only odd numbers appear because the final stroke in each case is upward). It may be noted that this is a convenient nomenclature, but does not reflect the actual number of layers deposited. The values of CTR obtained for the different multilayer films are collected in Table 4.1.

Table 4.1. Cumulative transfer ratios (CTR$_{\ddagger}$ and CTR$_{\pm}$) for the deposition of multilayer LB films of ODEP^{+} with only Br^{-} and additionally different polyelectrolytes in the aqueous subphase.

Multilayer film	ODEP_Br		ODEP_PSS		ODEP_DNA		ODEP_CMC	
	CTR$_{\ddagger}$	CTR$_{\pm}$	CTR$_{\ddagger}$	CTR$_{\pm}$	CTR$_{\ddagger}$	CTR$_{\pm}$	CTR$_{\ddagger}$	CTR$_{\pm}$
1S	0.85	0.85	0.76	0.76	0.76	0.76	0.80	0.80
3S	1.78	1.40	1.96	0.91	2.06	1.04	1.63	1.41
5S	2.50	2.00	3.16	1.11	3.36	1.36	2.67	1.79
7S	3.00	2.66	4.33	1.29	4.6	1.55	3.53	2.64
9S	4.07	3.25	5.62	1.39	5.85	1.81	4.08	3.24

Optical absorption spectra of the 1S films are shown in Figure 4.5. The strongest absorption occurs at 448 nm in ODEP_Br and in the range 475 - 485 nm in ODEP_PSS, ODEP_DNA and ODEP_CMC. This peak corresponds to unaggregated ODEP^{+} (the

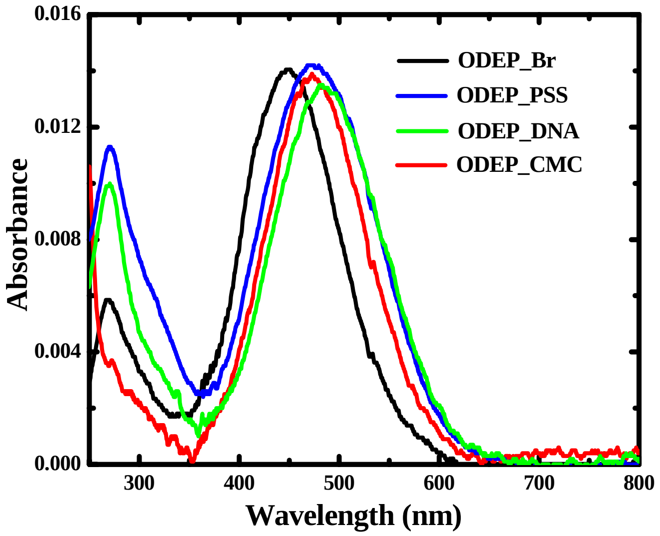

Figure 4.5. *Electronic absorption spectra of: 1S films of ODEP_Br, ODEP_PSS, ODEP_DNA and ODEP_CMC (spectra of ODEP_Br and ODEP_CMC are scaled slightly to make the absorbances at ~ 470 nm similar for all the systems so that the absorbances in the UV region can be compared).*

aggregates typically show λ_{max} ~ 355 nm[22,25,29]). The small red shift in the case of the templated films could be attributed to the effect of the polyelectrolyte environment. It may be stressed that the deaggregation in ODEP_Br is a result of the slow equilibration of the Langmuir film and that in the case of the other films, polyelectrolytes effectively suppress the aggregation.[25] The peak observed at ~ 268 nm in ODEP_Br is also characteristic of ODEP$^+$. The peak is notably stronger and associated with a weak shoulder in the case of ODEP_PSS and ODEP_DNA; these result from the absorptions of the corresponding polyelectrolytes in the UV region (Fig. 4.5).[19,22] A polyelectrolyte absorption occurring deeper into the UV regime leads to the observed spectrum of ODEP_CMC. These spectra provide evidence for the complexation of the polyelectrolytes with ODEP$^+$ and their presence in the corresponding LB films. Spectra of the multilayer films fabricated without and with polyelectrolytes are presented in Figure 4.6. Figure 4.7 provides the plots of absorbance (at λ_{max}) of the different multilayer LB films (1S to 9S) as a function of the respective $\text{CTR}_{\ddagger}$. The linearity observed (regression coefficient for fit to straight line is close to 1 and the y-intercept negligible in all cases) proves the validity of the measure we have employed for the material transfer.

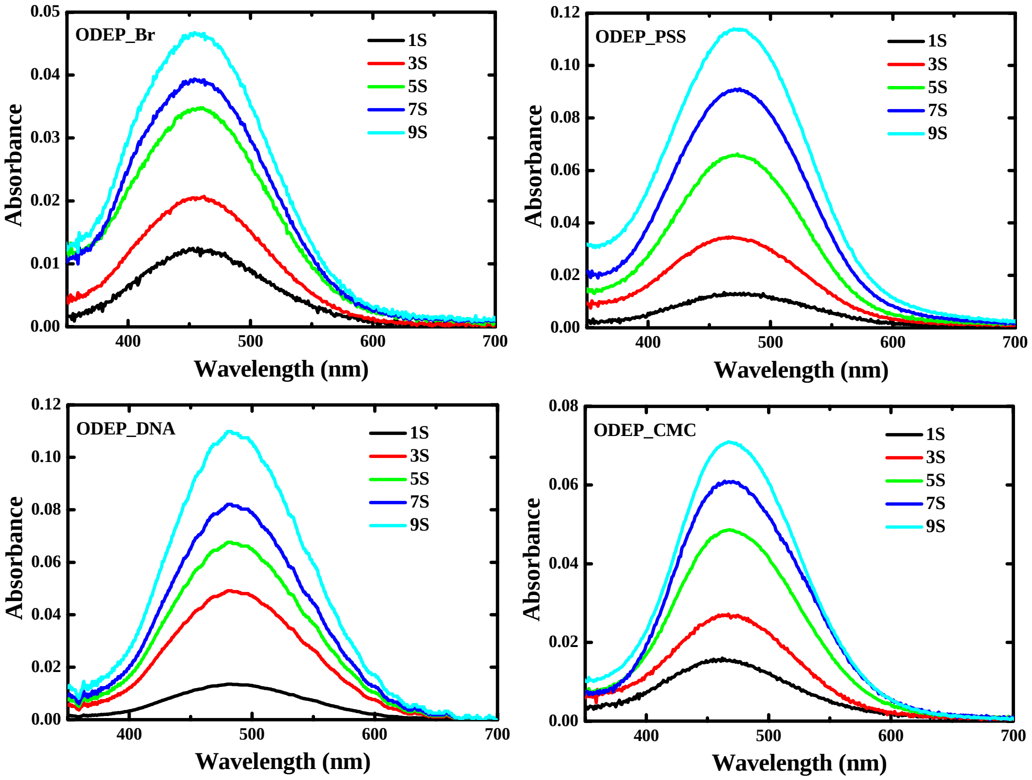

Figure 4.6. *Electronic absorption spectra of multilayer LB films of ODEP$^+$fabrictaed without and with polyelectrolytes in the subphase.*

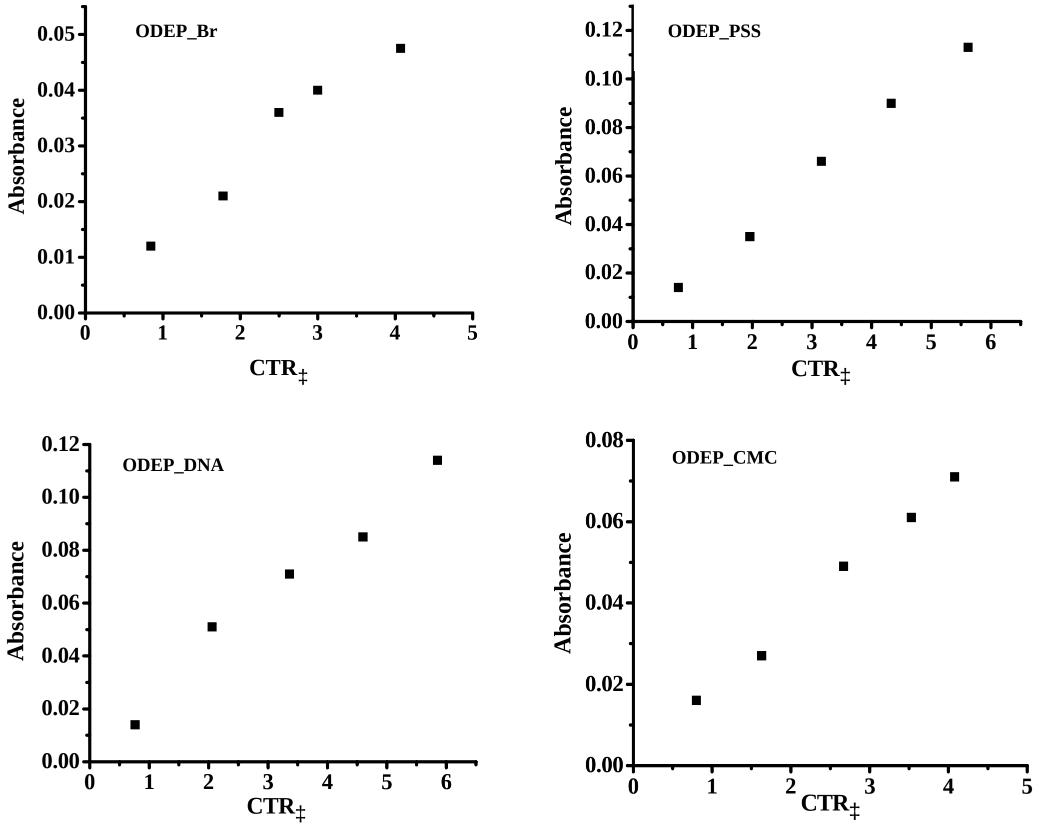

Figure 4.7. *Absorbance at peak maximum against the cumulative transfer ratio,* $CTR_{\ddagger}$ *for multilayer LB films of ODEP_Br, ODEP_PSS, ODEP_DNA and ODEP_CMC. Correlation coefficient and y-intercept from least square fit of the four data sets to straight lines are respectively: (0.97, 0.003), (0.99, -0.003), (0.99, 0.006), (0.99, 0.001).*

4.3.3 *AFM Imaging of LB films*

Morphology of the LB films was investigated by AFM. Earlier studies from our laboratory[22] demonstrated the dramatic change in morphology of monolayer LB films of $ODEP^{+}$ as a result of templating by PSS^{n-}, DNA^{n-} and CMC^{n-}. In the case of multilayer formation, ODEP_Br and ODEP_CMC showed nearly uniform z-type deposition and hence were more amenable to imaging; ODEP_PSS and ODEP_DNA films did not yield good images. To be consistent with the samples employed in the SHG studies, LB films deposited on glass substrate were imaged. Figure 4.8 reveals the significant differences in

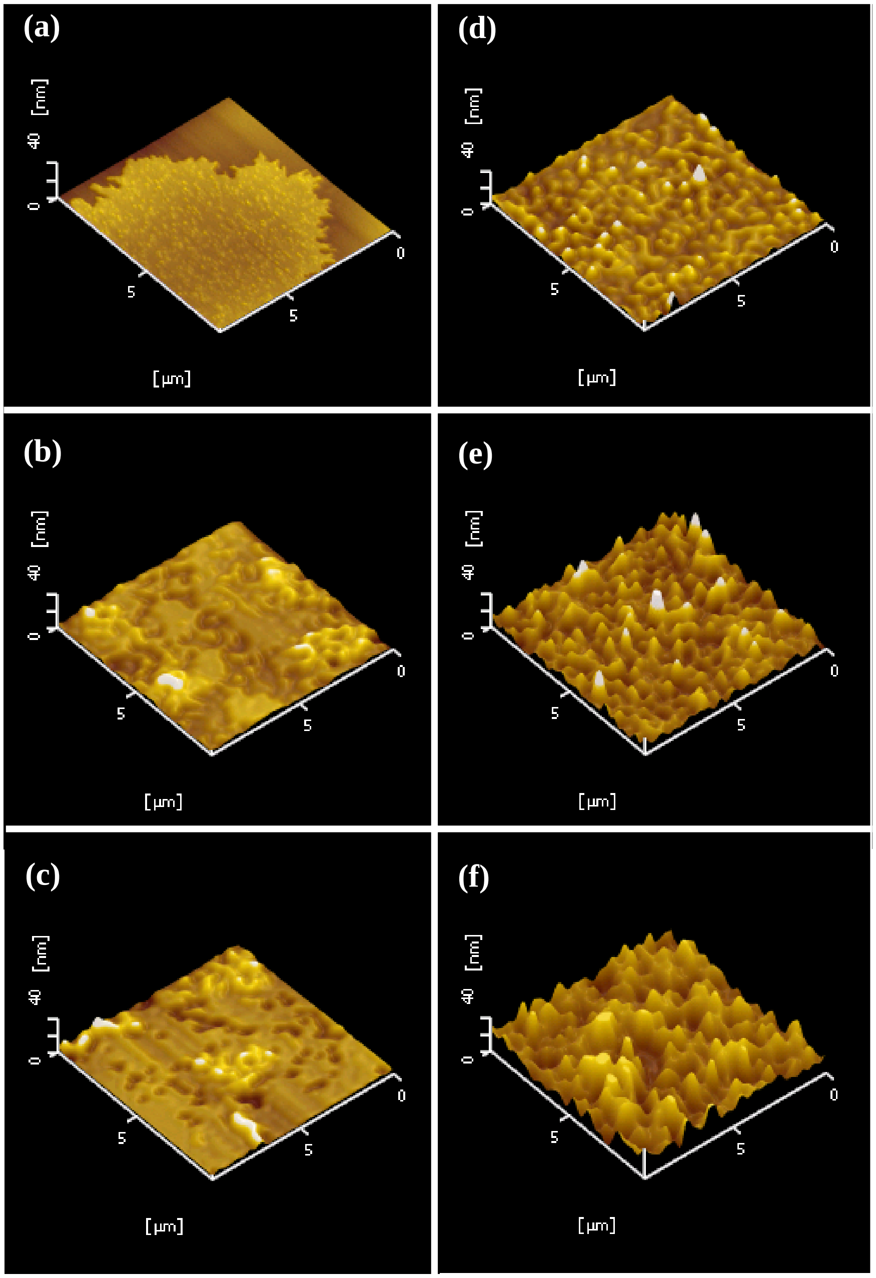

Figure 4.8. *AFM images of ODEP_Br* ***(a)*** *1S,* ***(b)*** *5S,* ***(c)*** *7S and ODEP_CMC* ***(d)*** *1S,* ***(e)*** *5S,* ***(f)*** *7S LB films.*

the morphology of the films of ODEP_Br and ODEP_CMC. The differences are most clearly manifested in the 1S films; while ODEP_Br shows flower-like structures typically ~2.5 nm thick and several microns in diameter, ODEP_CMC shows more fragmented but extended structures with an average thickness of ~ 4.3 – 4.5 nm. The increased thickness of ODEP_CMC is consistent with the presence of polyelectrolyte. Thickness of the 5S and 7S LB films are respectively 6.6 – 7.0 nm and 9.0 – 10.0 nm for ODEP_Br and 13.0 – 14.5 nm and 17.0 – 19.0 nm for ODEP_CMC (Fig. 4.9); estimation of the thickness using surface analysis is described in Appendix B. The increases in the thickness compared to the 1S films are by factors of approximately three and four respectively. This is consistent with the $CTR_‡$ values and the model of multilayer deposition presented in Sec. 4.3.5.

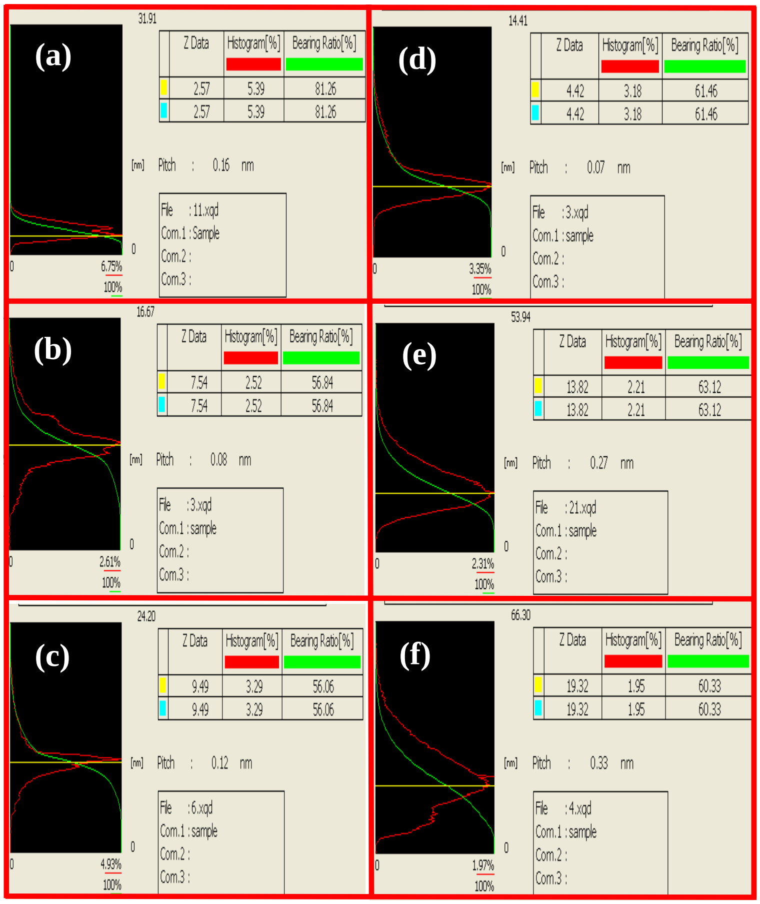

(a)

	Z Data	Histogram[%]	Bearing Ratio[%]
		🟥	🟩
🟨	2.57	5.39	81.26
🟦	2.57	5.39	81.26

Pitch : 0.16 nm

File : 11.xqd
Com.1 : Sample
Com.2 :
Com.3 :

(d)

	Z Data	Histogram[%]	Bearing Ratio[%]
		🟥	🟩
🟨	4.42	3.18	61.46
🟦	4.42	3.18	61.46

Pitch : 0.07 nm

File : 3.xqd
Com.1 : sample
Com.2 :
Com.3 :

(b)

	Z Data	Histogram[%]	Bearing Ratio[%]
		🟥	🟩
🟨	7.54	2.52	56.84
🟦	7.54	2.52	56.84

Pitch : 0.08 nm

File : 3.xqd
Com.1 : sample
Com.2 :
Com.3 :

(e)

	Z Data	Histogram[%]	Bearing Ratio[%]
		🟥	🟩
🟨	13.82	2.21	63.12
🟦	13.82	2.21	63.12

Pitch : 0.27 nm

File : 21.xqd
Com.1 : sample
Com.2 :
Com.3 :

(c)

	Z Data	Histogram[%]	Bearing Ratio[%]
		🟥	🟩
🟨	9.49	3.29	56.06
🟦	9.49	3.29	56.06

Pitch : 0.12 nm

File : 6.xqd
Com.1 : sample
Com.2 :
Com.3 :

(f)

	Z Data	Histogram[%]	Bearing Ratio[%]
		🟥	🟩
🟨	19.32	1.95	60.33
🟦	19.32	1.95	60.33

Pitch : 0.33 nm

File : 4.xqd
Com.1 : sample
Com.2 :
Com.3 :

Figure 4.9. *Surface profile analysis of the images of ODEP_Br* **(a)** *1S,* **(b)** *5S,* **(c)** *7S and ODEP_CMC* **(d)** *1S,* **(e)** *5S,* **(f)** *7S films shown in Figure 4.8.*

4.3.4 *Second harmonic generation Studies of LB films*

As noted in Section 4.3.2, due to the effective deaggregation of the NLO-phore units, the LB films of ODEP$^+$ show optical spectra with peak near 470 nm and non-negligible absorption at 532 nm. The latter facilitates resonance enhancement of the SHG when 1064 nm wavelength laser is used as the fundamental. SHG fringe patterns were obtained for the LB films deposited on the two surfaces of the glass substrate. Theoretical fitting of the SHG fringe patterns[28] obtained for the LB films of ODEP$^+$ without and with the polyelectrolytes are shown in Figure 4.10 to 4.13. Square root of the SHG intensities extracted from such fittings for the different multilayer LB films are plotted in Figure 4.14, against the respective CTR$_\pm$ values. Justification for the use of CTR$_\pm$ is as follows.

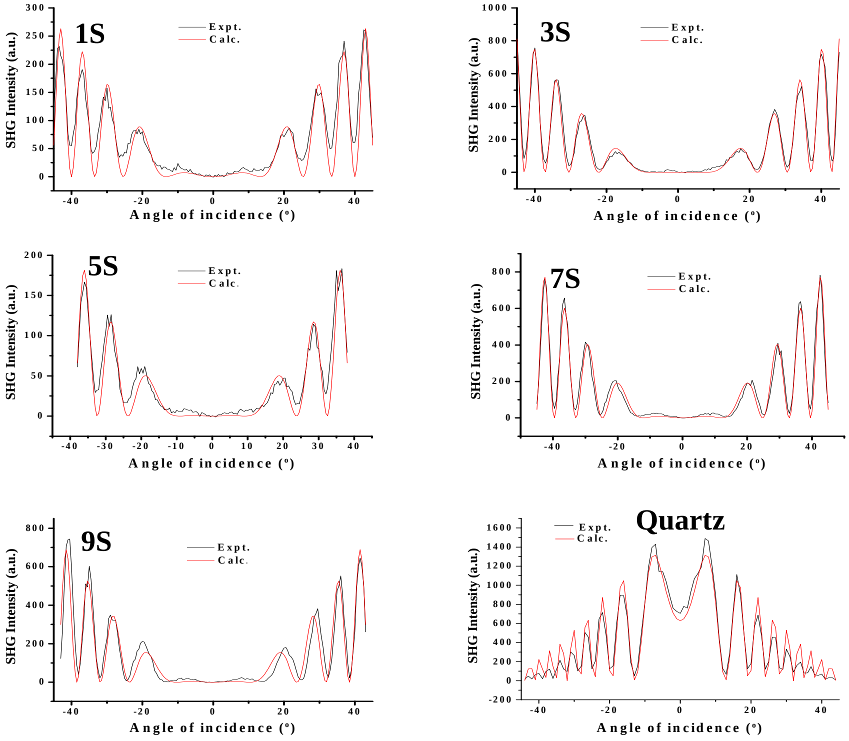

Figure 4.10. *Fitting of the SHG fringe patterns of the LB films of ODEP_Br and Y-cut quartz used as reference. See Appendix F for details of the fitting procedure.*

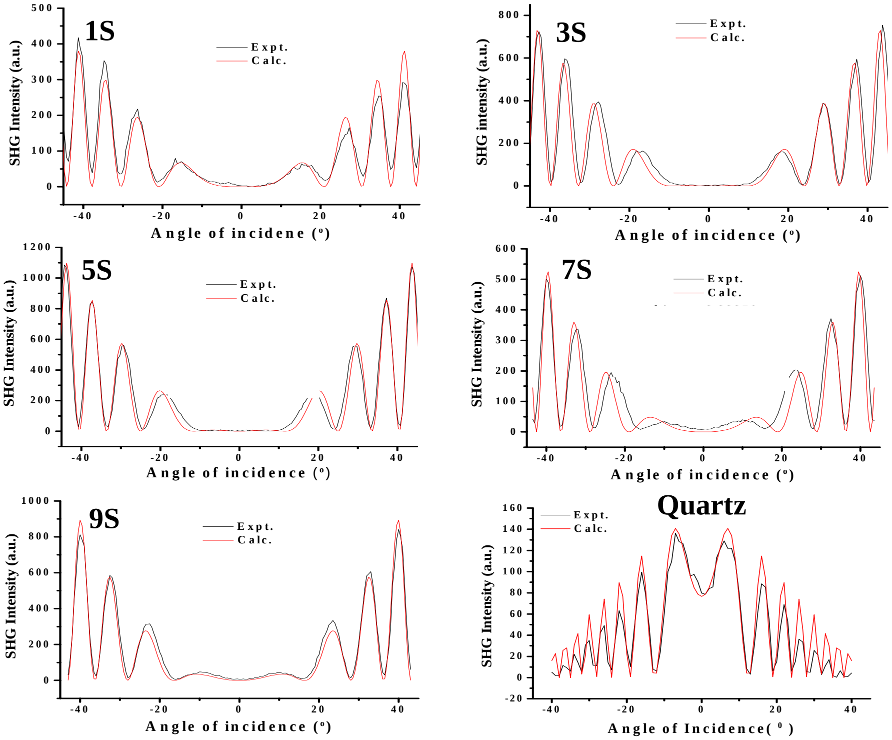

Figure 4.11. *Fitting of the SHG fringe patterns of the LB films of ODEP_PSS and Y-cut quartz used as reference. See Appendix F for details of the fitting procedure.*

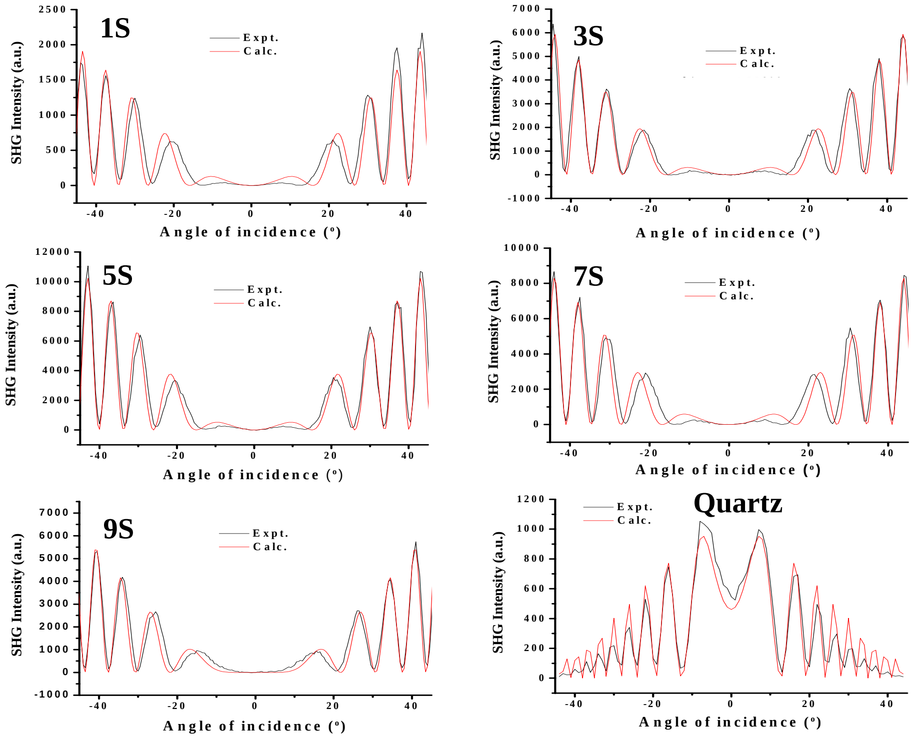

Figure 4.12. *Fitting of the SHG fringe patterns of the LB films of ODEP_DNA and Y-cut quartz used as reference. See Appendix F for details of the fitting procedure.*

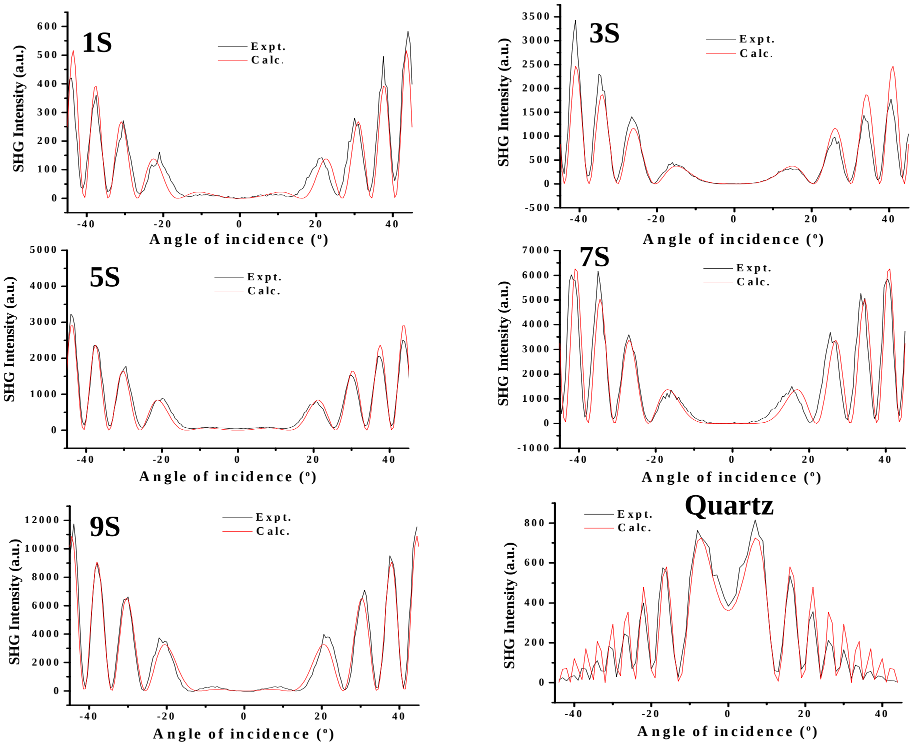

Figure 4.13. *Fitting of the SHG fringe patterns of the LB films of ODEP_CMC and Y-cut quartz used as reference. See Appendix F for details of the fitting procedure.*

In ideal y-type LB film deposition, 100% transfer occurs during up and downstrokes, and in ideal z- or x-type depositions, such transfer occurs during up or downstrokes respectively. However, in practice the transfers during a specific stroke may not be the ideal 100% or 0%. When deposition occurs during both up and down strokes to different extents as observed with our samples, the molecules deposited in alternate strokes, may in principle be oriented in the same or opposite directions. Since the latter is the more likely event, $CTR_{\pm}$ provides the appropriate measure of the population of $ODEP^{+}$ that will effectively contribute to the SHG response. Therefore, irrespective of the type of LB film deposition, $SHG^{1/2}$ is expected to show linear increase with the experimentally observed $CTR_{\pm}$. Deviations from such a trend would be indicative of post-deposition rearrangements or instabilities in the multilayer structures.

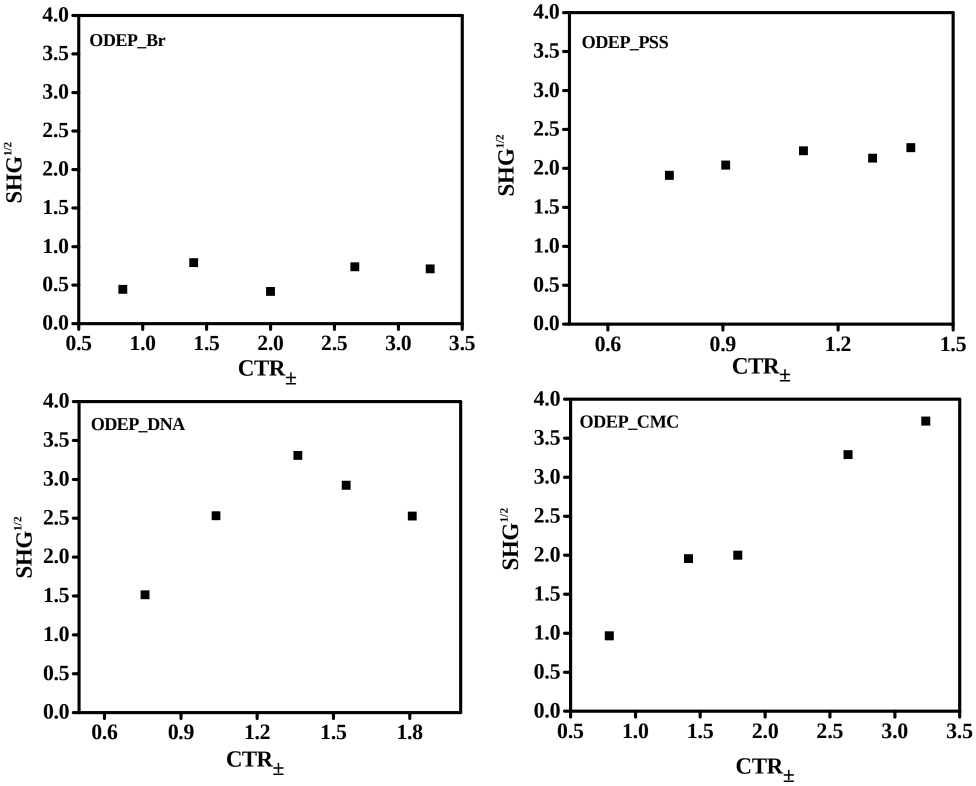

Figure 4.14. *Plot of the square root of normalized SHG intensity* ($SHG^{1/2}$) *versus the cumulative transfer ratio,* $CTR_{\pm}$, *for multilayer LB films of ODEP_Br, ODEP_PSS, ODEP_DNA and ODEP_CMC; note that the* y-*scales are same in all the plots but the* x-*scales are chosen differently because of the varying deposition sequences.*

Figure 4.14 shows that the SHG of ODEP_Br remains nearly constant and weak in the different multilayer films. This behavior consistent with earlier observations,[30] suggests that even though the depositions are nearly z-type, the amphiphilic molecules undergo post deposition reorganization leading to effective reduction of the SHG response. The origin of these effects may be traced to the instabilities in monolayer films of ODEP_Br.[22,25,26] Even though the monolayer film of ODEP_PSS shows a considerably higher SHG, it does not show any significant increase with multilayer depositions. The polyelectrolyte efficiently deaggregates the NLO-phore headgroups within a layer, but fails to maintain the integrity between the levels in the multilayer sequence. ODEP_DNA shows the expected increase of SHG with the multilayer transfers but once again succumbs to instabilities in structures higher than 5S. ODEP_CMC is found to be the most successful multilayer structure in the present study; the z-type deposition leads to steady increase of the stable SHG response. The plot of $SHG^{1/2}$ versus $CTR_{\pm}$ is nearly linear as expected from homogeneous layer growth and subsequent stability; the correlation coefficient for fit to a straight line is 0.99 and the slope 1.13. The non-negligible y-intercept of 0.15 is typical of multilayer LB films and suggests subtle variations between the first layer attached to the substrate and subsequent ones deposited on previous amphiphile layers.[18] The response from the 9S film of ODEP_CMC is nearly equal to the strong SHG demonstrated in hemicyanine dye included in silica zeolite films.[31] Stability tests showed that the multilayer ODEP_CMC films (9S) retain to a large extent, their electronic absorption spectrum as well as SHG response, when subjected to periodic high intensity laser irradiations as well as continuous irradiation for extended period of time. Figure 4.15 shows that the long-term decrease in electronic absorption intensity of the 9S film is < 5% and that in SHG < 20%; the fluctuations in the SHG values are within the error limits of the measurement. These experiments demonstrate the high stability of the molecular assembly in the multilayer ODEP_CMC films. Stability of ODEP_Br and the other templated multilayer films was checked on 5S films and showed slightly poorer stability compared to ODEP_CMC (Fig. 4.16).

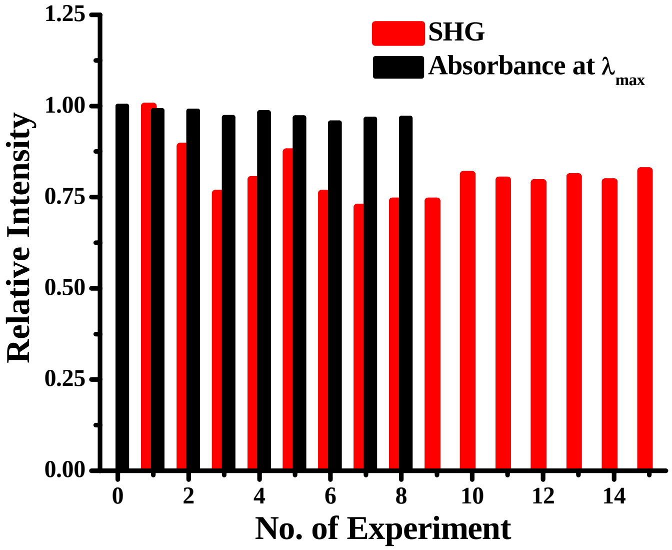

Figure 4.15. *Relative intensities of SHG and electronic absorption at λ_{max} of 9S film of ODEP_CMC observed in repeated experiments involving high power laser irradiation. The first 8 involved alternating SHG and electronic absorption measurements whereas the last 7 involved only SHG measurement. The values are normalized with respect to the initial value in each case.*

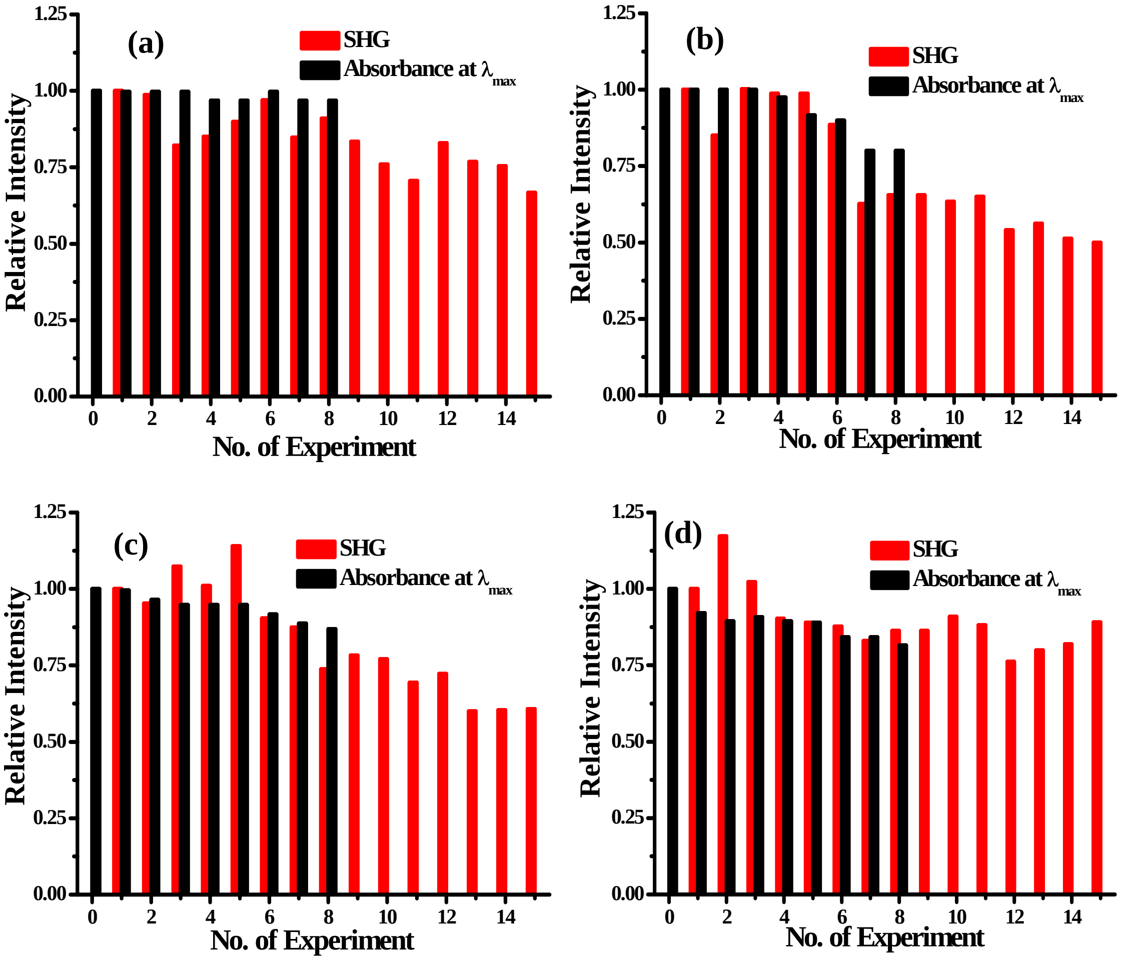

Figure 4.16. *Relative intensities of SHG and electronic absorption at λ_{max} of 5S films of* ***(a)*** *ODEP_Br,* ***(b)*** *ODEP_PSS,* ***(c)*** *ODEP_DNA and* ***(d)*** *ODEP_CMC observed in repeated experiments involving high power laser irradiation.*

4.3.5 *Model for the multilayer LB films*

A model for the formation of multilayer LB films of ODEP$^+$ with and without polyelectrolytes has to take into account, the experimentally observed transfer ratios corroborated by the electronic absorption intensities and the trends exhibited in the SHG responses of the different films. It also has to be consistent with the growth of the film thickness demonstrated in the AFM images. Schematic representation of a model that can be conceived based on all these considerations is shown in Figure 4.17. The contrasting deposition sequences suggested illustrate the critical role played by the polyelectrolytes in the multilayer formation. Sequence A is relevant to ODEP_Br. Appreciable (~ 80%) transfer to the hydrophilic substrate occurs during the first upstroke. The poor transfer in the subsequent downstroke is likely to be the consequence of the strong affinity of the headgroup for water resulting from the ionic nature of the complex consisting of the cationic pyridinium moiety and bromide ion. The less than quantitative transfer and the gaps present in the first layer can facilitate the interdigitation of amphiphiles shown in the figure. Due to the complex surface structure resulting from the second stroke and the possibility of molecular reorganization known in ODEP_Br LB film, the appreciable transfer during the third stroke does not lead to any net increase in SHG. A possible structure satisfying local pockets of hydrophilic and hydrophobic interactions, leading to little net molecular orientation within the second layer is shown to result from the third stroke. The partially hydrophilic nature of the surface precludes any effective transfer during the fourth stroke. The structure formed following the fifth stroke shows net cancellation of molecular orientations within and between the second and third layers transferred. The cycle continues as in the fourth and fifth strokes building up higher multilayer films with no net increase of SHG response. Sequence B models the multilayer formation in ODEP_PSS and ODEP_DNA. Following the appreciable transfer in the first upstroke, a partial transfer occurs during downstroke in an interdigitated fashion; binding of the amphiphile with the polyelectrolyte is likely to hamper a more efficient transfer from the aqueous surface. Electrostatic interactions between the polyelectrolyte decorated surface of the deposited layers and the amphiphile-polyelectrolyte complex on the aqueous surface facilitate efficient transfer during the third stroke and the cycle continues. Due to the lower transfer ratios during downstrokes, the SHG is expected to increase with the number of depositions. The absence of such an increase in the observed SHG can result only from post-deposition reorganizations of the NLO-phore headgroups. Sequence B shows that the polyelectrolyte segments will be quite extensive in the corresponding films; this may promote reorganization of the amphiphile headgroups and also make the more pliable films less amenable to imaging as noted earlier.

Sequence C represents the multilayer formation of ODEP_CMC. The first upstroke leads to efficient transfer, but unlike the case of ODEP_PSS and ODEP_DNA, the second stroke fails to transfer a layer in tail-to-tail fashion. This can be attributed to the more hydrophilic nature of CMC^{n-} compared to PSS^{n-} and DNA^{n-} owing to the large number of hydrogen bonding groups in addition to the acid functionality and the resulting strong affinity of the headgroup – polyelectrolyte complex for the aqueous subphase. Earlier studies suggest that PSS^{n-} with its aromatic groups has a relatively more hydrophobic

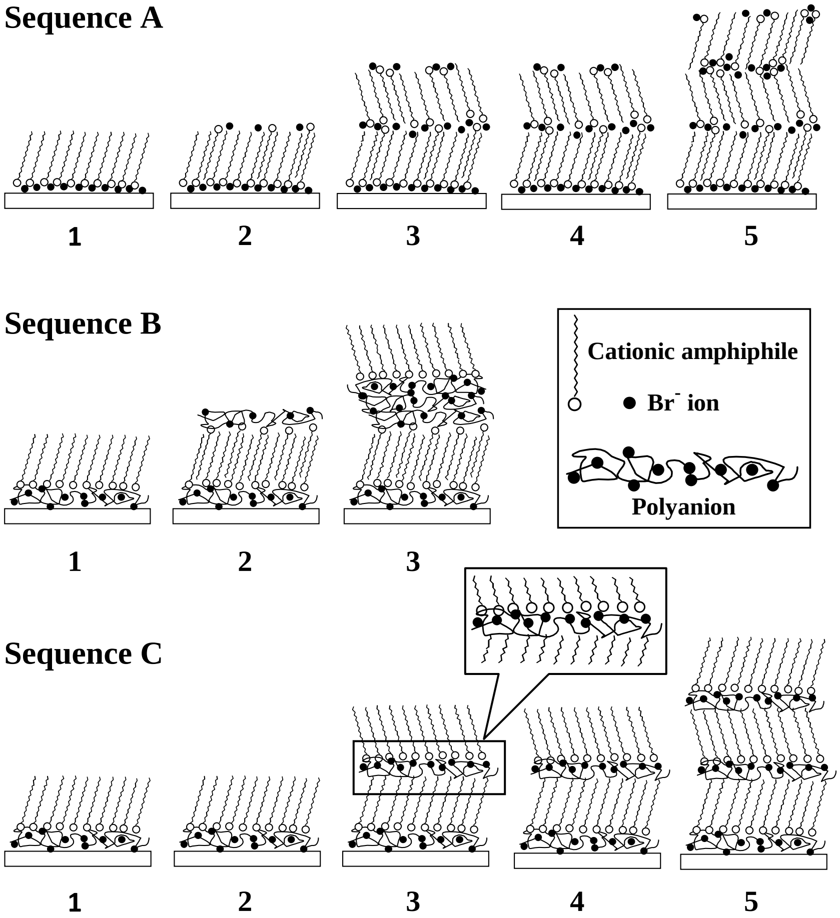

Figure 4.17. *Deposition sequences proposed for the formation of multilayer LB films of* $ODEP^+$ *in the absence (Sequence A) and presence (Sequences B and C) of polyelectrolyte templates. Expanded view of the sandwiched polyelectrolyte during Sequence C is shown. Numbers refer to the deposition strokes and the schematic representations are clarified in the legend; open and filled circles indicate cationic and anionic groups respectively.*

backbone[32] and the observed trends in binding of ammonium based surfactants by CMC^{n-} can be interpreted in terms of a more hydrophilic character.[33] It is notable that CMC^{n-} has facilitated multilayer transfer of azobenzene NLO-phore based amphiphiles;[34] the current observations reaffirm its suitability for stabilizing multilayers of cationic surfactants. Efficient transfer during the third stroke is enabled by possible structural adjustments of the CMC^{n-} chains (second polyelectrolyte layer in **3**) wherein the ionic groups are oriented away from the hydrocarbon tails of the amphiphiles in the first layer, leading to effective head-to-tail organization between the amphiphile layers; the conformational flexibility of the monomeric units in CMC^{n-} might play a significant role in this. This results in the steady growth of the SHG response. Events in the second and third strokes are repeated and the cycle continued.

The relatively more hydrophobic nature of PSS^{n-} and the inability of PSS^{n-} and DNA^{n-} to adjust to the demands of $ODEP^{+}$ layers are limiting factors in the ODEP_PSS and ODEP_DNA multilayer structures. The compact organization of the $ODEP^{+}$ layers with similar molecular orientations across the layers, achieved through appropriate tuning of the CMC^{n-} chains sandwiched in between, is likely to be the key to the attainment of stable and efficient SHG response of ODEP_CMC multilayer films. The surface roughness of the films observed in the AFM may arise from the variation of the penetration of the amphiphiles into the adjacent polyelectrolyte layer.

4.4. Langmuir and Monolayer LB films of $MEOEP^{+}I^{-}$ and $OEOEP^{+}Br^{-}$: Effect of Polyelectrolyte Templating

In this section we present our preliminary explorations of the impact of polyelectrolyte templating on the fabrication of Langmuir and monolayer LB films of $MEOEP^{+}I^{-}$ and $OEOEP^{+}Br^{-}$ and the SHG responses from LB films. The polyelectrolyte CMC^{n-} was employed in these studies since CMC^{n-} was found to be the optimal one that leads to favorable deposition sequences and enhanced and stable SHG responses from multilayer LB films of $ODEP^{+}$.

4.4.1 *Langmuir and LB Film of MEOEP$^+$*

The π-A isotherms of MEOEP$^+$ monolayer with only I$^-$ as well as with CMC^{n-} introduced in the subphase are shown in Figure 4.18. In contrast to the observations with ODEP_Br, the polyelectrolyte introduced in the subphase had no significant impact on the π-A isotherms (Fig. 4.18a). The limiting area is ~ 50 Å^2 irrespective of the counter ion present in the subphase. This may be due to the fact that the iodide counter ion is relatively large and its replacement with the polyelectrolyte may not cause any significant shift in the isotherms as observed in the case of ODEP_Br. It is also possible that the mode of attachment of the hydrocarbon tail in MEOEP$^+$ facilitates deeper penetration of the methyl pyridinium end into the aqueous subphase and better salvation so that the interaction with the polyelectrolyte does not lead to reorganization of the amphiphile and shifts in the isotherms. Presence of CMC^{n-} however does enhance the stability of the Langmuir film as seen in the increase of the collapse pressures. Collapse pressure of MEOEP_I and MEOEP_CMC, are 44 and 50 mN/m respectively. The effect of polyelectrolyte in stabilizing the Langmuir film is further established by recording the change in area of the film as a function of time (creep plot) at different surface pressures. The creep plots show

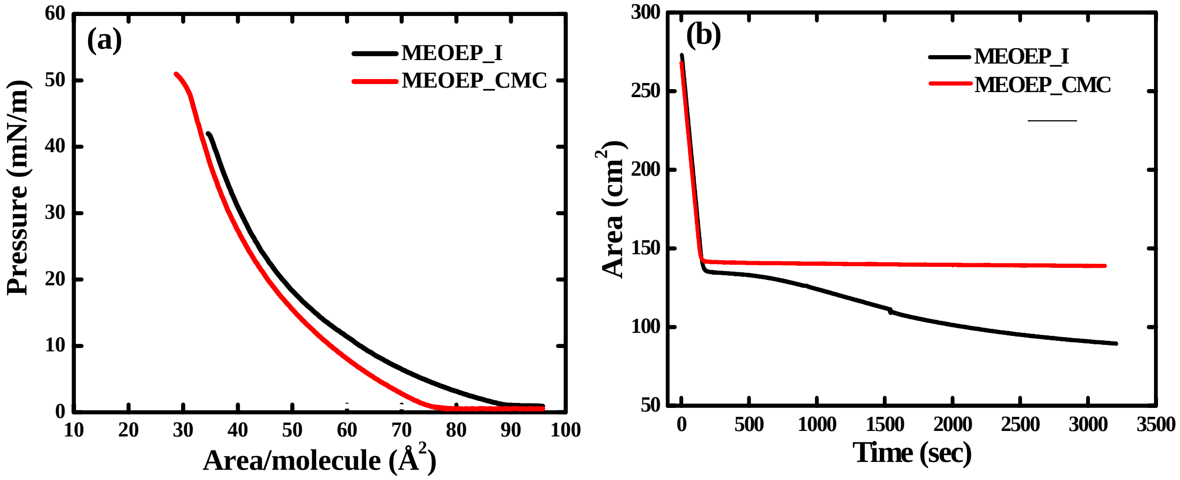

Figure 4.18. ***(a)*** *Pressure-area isotherms and* ***(b)*** *area-time plots of MEOEP$^+$ monolayer with only I$^-$ and additionally CMC^{n-} in the aqueous subphase at 25^{o}C.*

that the film undergoes steady collapse at higher surface pressures when iodide is the counter ion present in the subphase, whereas with CMC^{n-} added in the subphase, even at higher pressure such as 40 mN/m, the area remains constant for an extended period of time (Fig. 4.18b). The stability observed is indicative of level of complexation of MEOEP^{+} with the polyelectrolyte in the Langmuir film at the air-water interface.

Solution of MEOEP^{+} in chloroform absorbs strongly at ~ 513 nm (sec. 3.4.2). Absorption spectra of monolayer LB films of MEOEP^{+} fabricated without and with CMC^{n-} in the subphase are shown in Figure 4.19. The LB films show a strong absorption at ~ 470 nm irrespective of the counter ions present in the subphase. This indicates that the electronic environment of MEOEP^{+} is similar in both the LB films. The weak absorption at ~ 345 nm present in the case of MEOEP_I may be due to small aggregation in the film. The spectrum of the film fabricated with CMC^{n-} in the subphase suggests that CMC^{n-} does not transfer along with the MEOEP^{+} amphiphiles on to the LB film. This is understandable in view of the likelihood that in spite of some interaction, CMC^{n-} does not reorganize the MEOEP^{+} Langmuir film and bind to it strongly.

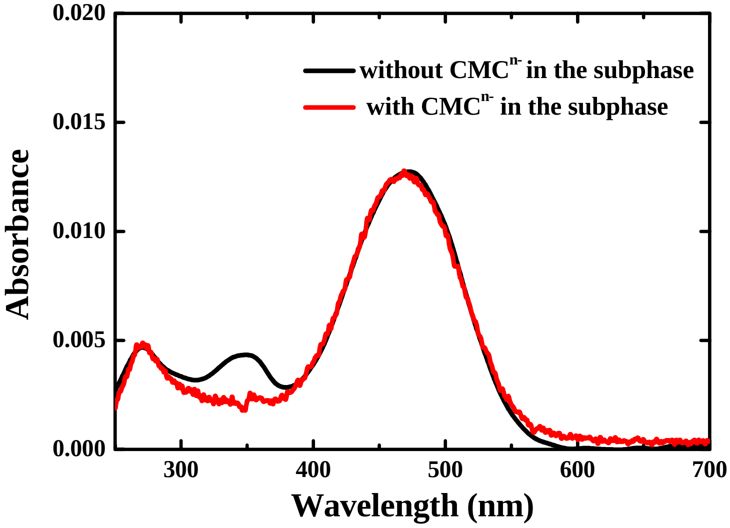

Figure 4.19. *Electronic absorption spectra of monolayer LB films of MEOEP^{+} without and with polyelectrolyte.*

We have carried out SHG studies of the monolayer LB films of MEOEP_I and MEOEP_CMC. The LB films were fabricated at a target pressure of 30 mN/m. MEOEP_I shows strong and stable SHG response as reported by Cross et al. earlier.[35] As expected, the film fabricated with CMC^{n-} in the subphase shows very similar SHG response. SHG fringe patterns and their fitting obtained for MEOEP^{+} monolayer fabricated without and with CMC^{n-} in the subphase are shown in Figure 4.20. The normalized SHG intensities with respect to Y-cut quartz estimated from the fringe fitting for the two films are 3.4 and 3.2 respectively. This study shows that CMC^{n-} exerts a stabilizing influence on MEOEP^{+} Langmuir films, but does not transfer into the LB film and hence has no impact on its SHG response. Interestingly we find that, even though MEOEP^{+}I^{-} is not amenable to multilayer LB film deposition, presence of CMC^{n-} in the subphase facilitates this.

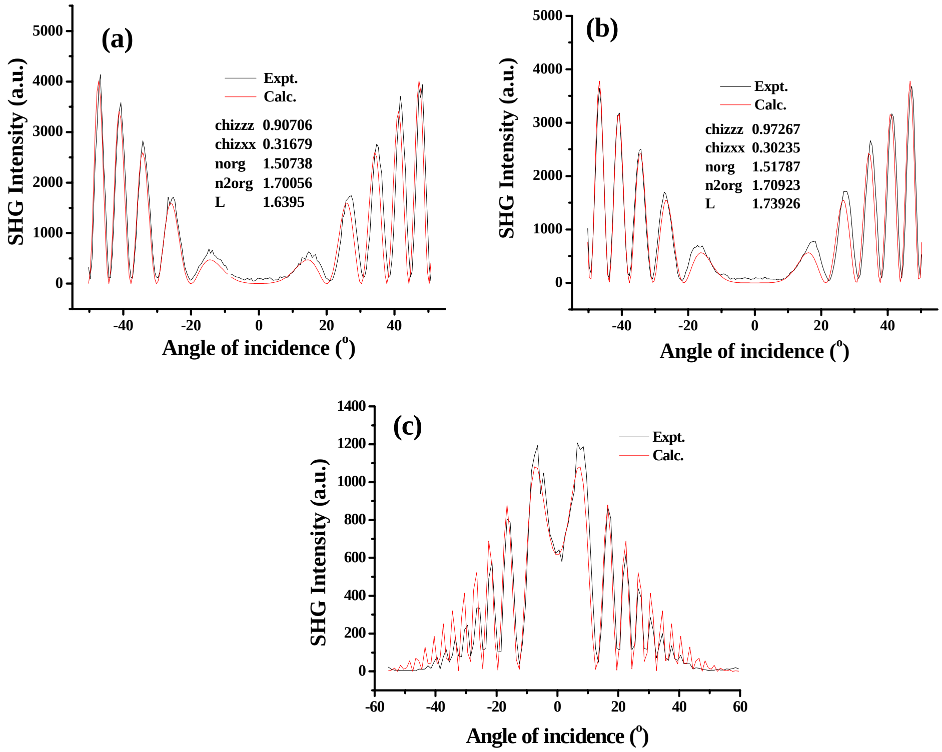

Figure 4.20. *SHG fringe patterns and their theoretical fitting obtained for monolayer LB films of MEOEP^{+}fabricated* ***(a)*** *without and* ***(b)*** *with CMC^{n-}in the subphase and* ***(c)*** *for Y-cut quartz used as reference. See Appendix F for details of the fitting procedure.*

4.4.2 *Langmuir and LB films of OEOEP$^+$*

The π-A isotherm of OEOEP$^+$Br$^-$ at the air-water interface with pure water as the subphase and with CMC^{n-} introduced in the water are shown in Figure 4.21. Shift of the isotherm towards higher molecular area and the higher pressure at which the plateau forms when CMC^{n-} is present in the subphase suggest effective complexation of OEOEP$^+$ with the polyelectrolyte at the interface.

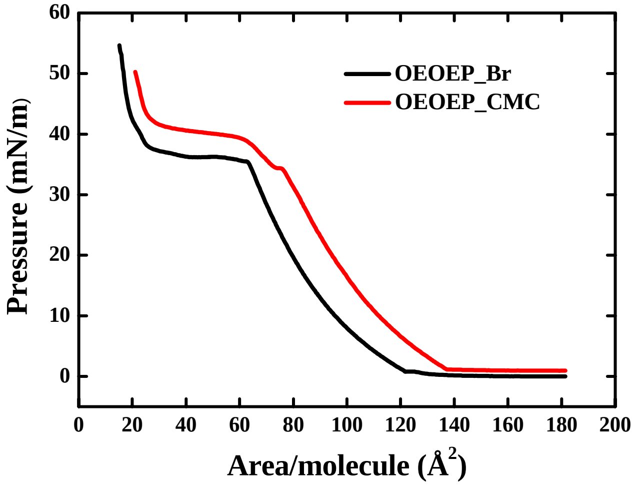

Figure 4.21. *Pressure-area isotherm of OEOEP$^+$monolayer at the air-water interface without and with CMC^{n-} in the subphase, at 25^{o}C*

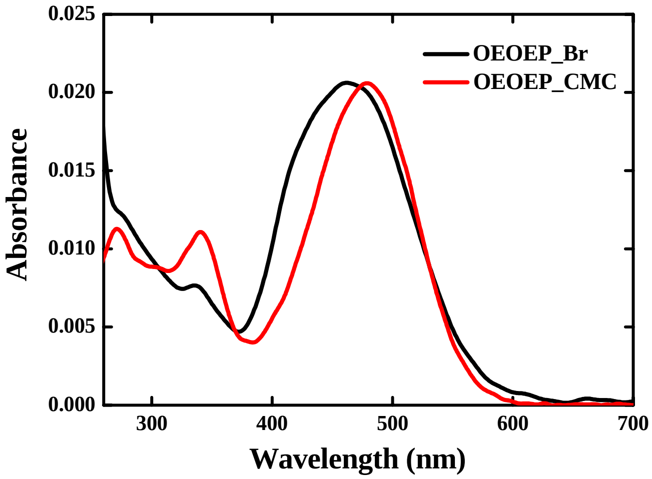

Figure 4.22. *Electronic absorption spectra of monolayer LB films of OEOEP$^+$ fabricated without and with CMC^{n-} in the subphase.*

Electronic absorption spectrum of OEOEP$^+$Br$^-$ in chloroform solution shows a peak at ~ 515 nm. Spectra of the monolayer LB films of OEOEP$^+$ are shown in Figure 4.22. OEOEP_Br monolayer LB film shows a broad absorption with λ_{max} at ~ 465 nm and a shoulder at ~ 420 nm (discussed in detail in Sec. 3.4.2). The peak at ~ 420 nm is ascribable to H-dimer or aggregate structures in the film. The film fabricated by templating with CMC^{n-} shows a narrow absorption with λ_{max} at ~ 480 nm; there is no sign of aggregate formation. This suggests the effective deaggregation of OEOEP$^+$ chromophore in the film by complexing with CMC^{n-} introduced in the subphase and hence in the LB film. The observed red shift in the spectrum of the templated film points to a different local environment in the LB films.

SHG responses from the monolayer LB films of OEOEP$^+$ fabricated at 45 mN/m without and with CMC^{n-} in the subphase are shown in Figure 4.23. Theoretical fitting of the fringes are also shown. The normalized SHG intensities with respect to Y-cut quartz refer-

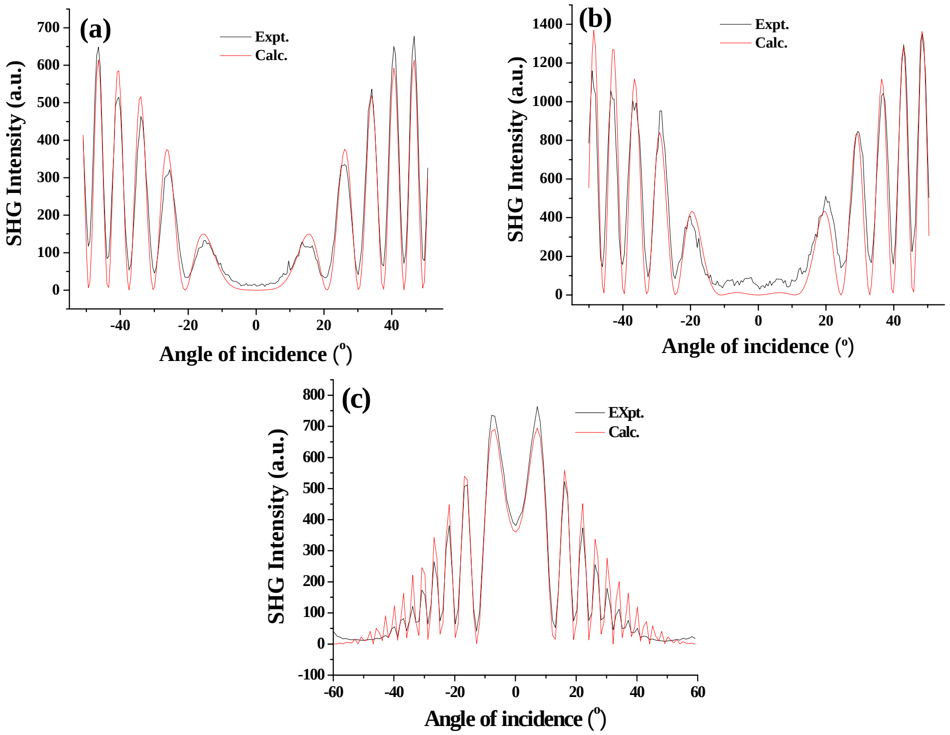

Figure 4.23. *SHG fringe patterns and their theoretical fitting obtained for monolayer LB films* ***(a)*** *OEOEP_Br* ***(b)*** *OEOEP_CMC and* ***(c)*** *for Y-cut quartz used as reference. See Appendix F for details of the fitting procedure.*

ence are 0.74 and 1. 81 for OEOEP_Br and OEOEP_CMC respectively. The ~ 2.5 fold enhancement of the SHG can be attributed to the suppression of the aggregate formation in the film by the polyelectrolyte templating.

4.5. Summary

ODEP_Br is a classic NLO-phore based amphiphile prone to molecular aggregation and diminished SHG efficiency in LB films. We have constructed multilayer LB films of $ODEP^+$ without and with the support of polyelectrolyte templates. Marked variations were observed in the deposition sequences depending on the polyelectrolyte employed. With only Br^- as the counterion, it was z-type with some deviations, whereas in presence of the polyelectrolytes, PSS^{n-} and DNA^{n-}, the deposition tends towards y-type. Templating by CMC^{n-} forces the deposition closest to z-type. SHG studies showed that the response was weak and constant when no polyelectrolytes were present. Even though the SHG was considerably enhanced when templated with PSS^{n-}, no steady increase with multilayer deposition was observed. The situation was better with DNA^{n-} templating, but the most efficient and steady increase of SHG response was observed when templated by CMC^{n-}. The latter also showed remarkable stability to laser irradiation. A viable model was presented to discuss the impact of different polyelectrolytes on multilayer LB film formation; the success of CMC^{n-} may be attributed to the strongly hydrophilic nature of this polymer facilitating z-type deposition of the multilayers and its capability to reorganize appropriately and bind the $ODEP^+$ layers enforcing similar orientation. Preliminary explorations of the impact of polyelectrolyte templating on $MEOEP^+I^-$ and $OEOEP^+Br^-$ films are presented. Studies with CMC^{n-} indicate little impact in the case of the former, but beneficial outcome in the latter.

The study presented in this chapter demonstrates a convenient chemical approach based on polyelectrolyte templating that can be exploited for the fabrication of mono and multilayer LB films of NLO-phore based amphiphiles to achieve ultrathin films exhibiting enhanced and stable SHG response. The methodology is superior to the traditional approach of admixing fatty acids since it does not reduce the number density of the active molecules in the 2-dimensional lattice. Compared to the alternate dipping protocol used to build multilayer structures with preferentially oriented amphiphile layers, the present method is much simpler to implement and more general and wider in scope.

References

1. (a) Williams, D. J. *Angew. Chem. Int. Ed. Engl.* **1984**, *23*, 690. (b) Chemla, D. S.; Zyss, J., Eds. *Nonlinear Optical Properties of Organic Molecules and Crystals*; Academic Press: New York, 1987; Vol.1.

2. (a) Zyss, J.; Ledoux, I. *Chem. Rev*. **1994**, *94*, 77. (b) Verbiest, T.; Clays, K.; Samyn, C.; Wolff, J.; Reinhoudt, D.; Persoons, A. *J. Am. Chem. Soc*. **1994**, *116*, 9320. (c) Ray, P. C.; Das, P. K. *Chem. Phys. Lett*. **1995**, *244*, 153. (d) Maury, O.; Viau, L.; Sénéchal, K.; Corre, B.; Guégan, J.-P.; Renouard, T.; Ledoux, I.; Zyss, J.; Le Bozec, H. *Chem. Eur. J.* **2004**, *10*, 4454.

3. (a) Bahl, A.; Grahn, W.; Stadler, S.; Feiner, F.; Bourhill, G.; Brauchle, C.; Reisner, A.; Jones, P. G. *Angew. Chem. Int. Ed. Engl*. **1995**, *34*, 1485. (b) Sitha, S.; Rao, J. L.; Bhanuprakash, K.; Choudhary, B. M. *J. Phys. Chem. A* **2001**, *105*, 8727.

4. (a) Nie, W. *Adv.Mater*.**1993**, *5*, 520. (b) Kanis, D. R.; Ratner, M. A.; Marks, T. J. *Chem. Rev*. **1994**, *94*, 195. (c) Marks, T. J.; Ratner, M. A. *Angew. Chem., Int. Ed. Engl*. **1995**, *34*, 155. (d) Zyss, J.; Nicoud, J. F. *Curr. Opin. Solid State Mater. Sci*. **1996**, *1*, 533.

5. (a) Rieckhoff, K.; Peticolas, W. F. *Science* **1965**, *147*, 610. (b) Eaton, D. F. *Science* **1991**, *253*, 281. (c) Gangopadhyay, P.; Rao, D. N.; Agranat, I.; Radhakrishnan, T. P. *Enantiomer* **2002**, *7*, 119.

6. (a) Levine, B. F.; Bethea, C. G.; Thurmond, C. D.; Lynch, R. T.; Bernstein, J. L. *J. Appl. Phys*. **1979**, *50*, 2523. (b) Lipscomb, G. F.; Garito, A. F.; Narang, R. S. *J. Chem. Phys*. **1981**, *75*, 1509. (c) Zyss, J. *J. Phys*. *D* **1993**, *26*, B198.

7. (a) Gangopadhyay, P.; Sharma, S.; Rao, A. J.; Rao, D. N.; Cohen, S.; Agranat, I.; Radhakrishnan, T. P. *Chem. Mater*. **1999**, *11*, 466. (b) Gangopadhyay, P.; Rao, S. V.; Rao, D. N.; Radhakrishnan, T. P. *J. Mater. Chem*. **1999**, *9*, 1699. (c) Gangopadhyay, P.; Radhakrishnan, T. P. *Chem. Mater*. **2000**, *12*, 3362. (d) Gangopadhyay, P.; Srinivas, N. K. M. N.; Rao, D. N.; Radhakrishnan, T. P. *Opt. Mater*.**2002**,*21*,55.

8. (a) Serbutovicz, C.; Nicoud, J. F.; Fischer, J.; Ledoux, I.; Zyss, J. *Chem. Mater.* **1994**, *6*, 1358; (b) Huang, K.; Britton, D.; Etter, M. C.; Byrn, S. R. *J. Mater. Chem.* **1995**, *5*, 379.

9. (a) Marder, S. R.; Perry, J. W.; Schaefer, W. P. *Science* **1989**, *245*, 626. (b) Marder, S. R.; Perry, J. W.; Yakymyshyn, C. P. *Chem. Mater*. **1994**, *6*, 1137. (c) Jayanty, S.; Gangopadhyay, P.; Radhakrishnan, T. P. *J. Mater. Chem.* **2002**, *12*, 2792. (d) Prakash, M. J.; Radhakrishnan, T. P. *Chem. Mater.* **2006**, *18*, 2943.

10. (a) Jagadish, B.; Williams, L. J.; Carducci, M. D.; Bosshard, C.; Mash, E. A. *Tet. Lett*. **2000**, *49*, 9483. (b) Koshima, H.; Hamada, M.; Yagi, I.; Uosaki, K. *Cryst. Growth. Des*. **2001**, *6*, 467. (c) Koshima, H.; Miyamoto, H.; Yagi, I.; Uosaki, K. *Cryst. Growth. Des*. **2004**, *4*, 807. (d) Prakash, M. J.; Radhakrishnan, T. P. *Cryst. Growth. Des*. **2005**, *5*, 721.

11. (a) Kauranen, M.; Verbiest, T.; Boutton, C.; Teerenstra, M. N.; Clays, K.; Schouten, A. J.; Nolte, R. J. M.; Persoons, A. *Science* **1995**, *270*, 966. (b) Deussen, H. -J.; Hendrickx, E.; Boutton, C.; Korg, D.; Clays, K.; Bechgaard, K.; Persoons, A.; Bjurnholm, T. *J. Am. Chem. Soc*. **1996**, *118*, 6841. (c) Verbiest, T.; Elshocht, S. V.; Kauranen, M.; Hellemans, L.; Snauwaert, J.; Nuckolls, C.; Katz, T. J.; Persoons, A. *Science* **1998**, *282*, 913. (d) Gangopadhyay, P.; Radhakrishnan, T. P. *Angew. Chem. Int. Ed*. **2001**, *40*, 2451.

12. (a) Mohajerani, E.; Gilbert, A.; Mitchell, G. R. *J. Phys. D.* **1992**, *25*, 1304. (b) *Poled Polymers and their Applications to SHG and EO Devices*; Miyata, S.; Sasabe, H., Eds.; Gordon and Breach: Amsterdam, 1997.

13. (a) Weissbuch, I.; Lahav, M.; Leiserowitz, L.; Meredith, G. R.; Vanherzeele, H. *Chem. Mater*. **1989**, *1*, 114. (b) Ramamurthy, V.; Eaton, D. F. *Chem. Mater*. **1994**, *6*, 1128. (c) Hoss, R.; Konig, O.; Kramer-Hoss, V.; Berger, U.; Rogin, P.; Hulliger, J. *Angew. Chem., Int. Ed*. Engl. **1996**, *35*, 1664.

14. (a) Cai, C.; Bösch, M. M.; Tao, Y.; Müller, B.; Gan, Z.; Kündig, A.; Bosshard, C.; Liakatas, I.; Jäger, M.; Günter, P. *J. Am. Chem. Soc.* **1998**, *120***,** 8563. (b) Cai, C.; Bösch, m. M.; Müller, B.; Tao, Y.; Kündig, A.; Bosshard, C.; Gan, Z.; Biaggio, I.; Liakatas, I.; Jäger, M.; Schwer, H.; Günter, P. *Adv. Mater.* **1999**, *11*, 745. (c) Rashid, A. N.; Erny, C.; Günter, P. *Adv. Mater.* **2003**, *15*, 2024. (d) Anthony, S. P.; Srinivas, N. K. M. N.; Rao, D. N.; Radhakrishnan, T. P. *J. Mater. Chem.* **2005**, *15*, 739.

15. Laschewsky, A.; Mayer, B.; Wischerhoff, E.; Arys, X.; Bertrand, P.; Delcorte, A.; Jona, A. *Thin Solid Films* **1996**, *284-285*, 334.

16. (a) Scheelen, A.; Winant, P.; Parsoons, A. In *Organic Molecules for Nonlinear Optics and Photonics* Eds. Messier, J.; Kajazar, F.; Prasad, P. N.; Kluwer: Dordrecht; 1991, p 497. (b) Ashwell, G. J. *J. Mater. Chem.* **1999**, *9*, 1991.

17. Ashwell, G. J.; Hargreaves, R. C.; Baldwin, C. E.; Bahra, G. S.; Brown, C. R. *Nature* **1992**, *357*, 393.

18. Petty, M. C. *Langmuir-Blodgett Films*, University Press, Cambridge **1996**.

19. Sharma, S.; Chandra, M. S.; Radhakrishnan, T. P. *Langmuir* **2001**, *17*, 8118.

20. (a) Inoue, T.; Yase, K.; Okada, M.; Okada, S.; Matsuda, H.; Nakanishi, H.; Kato, M. *Jpn. J. Appl. Phys.* **1988**, *27*, 1635. (b) Miyamoto, Y.; Kaifu, K.; Saito, M.; Kato, M.; Kawamura, K. *Thin Solid Films* **1989**, *178*, 493. (c) Shin, D.; Park, M.; Lim, S. *Thin Solid Films* **1998**, *327-329*, 607. (d) Munn, R. W.; Szczur, O. *Mol. Cryst. Liq. Cryst.* **2001**, *355*, 305. (e) Sharma, S.; Radhakrishnan, T. P. *J. Phys. Chem. B* **2003**, *107*, 147.

21. (a) Schönhoff, M.; Chi, L. F.; Fuchs, H.; Lösche, M. *Langmuir* **1995**, *11*, 163. (b) Wang, Y.; Nichogi, K.; Terashita, S.; Iriyama, K.; Ozaki, Y. *J. Phys. Chem.* **1996**, *100*, 368. (c) Xu, J.; Lu, X.; Han, K.; Zhou, G.; Zhang, Z. *Langmuir* **1997**, *13*, 3187.

22. Chandra, M. S.; Krishna, M. G.; Mimata, H.; Kawamata, J.; Nakamura, T.; Radhakrishnan, T. P. *Adv. Mater.* **2005**, *17*, 1937.

23. (a) Girling, I. R.; Cade, N. A.; Kolinsky, P. V.; Jones, R. J.; Peterson, I. R.; Ahmed, M. M.; Neal, D. B.; Petty, M. C.; Roberts, G. G.; Feast, W. J. *J. Opt. Soc. Am. B* **1987**, *4*, 950. (b) Scildkraut, J. S.; Penner, T. L.; Willand, C. S.; Ulman. A. *Opt. Lett*. **1988**, *13*, 134. (c) Sato, O.; Baba, R.; Hashimoto, K.; Fujishima, A. *J. Phys. Chem.* **1991**, *95*, 9636. (d) Carpenter, M. A.; Willand, C. S.; Penner, T. L.; Williams, D. J.; Mukamel, S. *J. Phys. Chem.* **1992**, *96*, 2801.

24. (a) Ma, S.; Han, K.; Lu, X.; Wang, W.; Zhang, Z.; Yao, Z. *Optics Commun.* **1994**, *111*, 513. (b) Ma, S.; Lu, X.; Xu, J.; Wang, W.; Zhang, Z. *J. Phy. D.* **1997**, *30*, 2651. (c) Ashwell, G. J.; Ranjan, R.; Whittam, A. J.; Gandolfo, D. S. *J. Mate*r**.** *Chem***.** **2000**, *10*, 63.

25. Chandra, M. S.; Ogata, Y.; Kawamata, J.; Radhakrishnan, T. P. *Langmuir* **2003**, *19*, 10124.

26. (a) Cross, G. H.; Girling, I. R.; Peterson, I. R.; Cade, N. A.; Earls, N. A. *J. Opt. Soc. Am. B* **1987**, *4*, 962. (b) Hayden, L. M.; Kowel, S. T.; Srinivasan, M. P. *Opt. Commun.* **1987**, *61*, 351. (c) Marowsky, G.; Chi, L. F.; Möbius, D.; Steinhoff, R.; Shen, Y. R.; Dorsch, D.; Rieger, D. *Chem. Phys. Lett.* **1988**, *147*, 420. (d) Kajikawa, K.; Kigata, K.; Takezoa, H.; Fukuda, A. *Mol. Cryst. Liq. Cryst.* **1990**, *182A*, 91. (e) Li, F.; Jin, L.; Huang, C.; Zheng, J.; Guo, J.; Zhao, X.; Liu, T. *Chem. Mater.* **2001**, *13*, 192.

27. Girling, I. R.; Cade, N. A.; Kolinsky, P. V.; Earls, J. D.; Cross, G. H.; Peterson, I. R. *Thin Solid Films* **1985**, *132*, 101.

28. (a) Jerphagnon, J.; Kurtz, S. K. *J. Appl. Phys.* **1970,** *41,* 1667. (b) Mizrahi, V.; Sipe, J. E. *J. Opt. Soc. Am. B* **1988,** *5,* 660. (c) Kuzyk, M. G.; Singer, K. D.; Zahn, H. E.; King, L. A. *J. Opt. Soc. Am. B* **1989,** *6,* 742.

29. (a) Chandra, M. S.; Radhakrishnan, T. P. *Mol. Cryst. Liq. Cryst.* **2003**, *403*, 77. (b) Chandra, M. S.; Ogata, Y.; Kawamata, J.; Radhakrishnan, T. P. *J. Nonlin. Opt. Phys. Mater*. **2004**, *13*, 347.

30. Stroeve, P.; Saperstein, D. D.; Rabolt, J. F. *J. Chem. Phys.* **1990**, *92*, 6958.

31. (a) Kim, H. S.; Lee, S. M.; Ha, K.; Jung, C.; Lee, Y.; Chun, Y. S.; Kim, D.; Rhee, B. K.; Yoon, K. B. *J. Am. Chem. Soc.* **2004**, *126*, 673. (b) Kim, H. S.; Sohn, K. W.; Jeon, Y.; Min, H.; Kim, D.; Yoon, K. B. *Adv. Mater.* **2007**, *19*, 260.

32. Hayakawa, K.; Kwak, J. C. T. *J. Phys. Chem.* **1982**, *86*, 3866.

33. Hayakawa, K.; Santerre, J. P.; Kwak, J. C. T. *Macromolecules* **1983**, *16*, 1642.

34. Panambur, G.; Zhang, Y.; Yesayan, A.; Galstian, T.; Bazuin, C. G.; Ritcey, A. M. *Langmuir* **2004**, *20*, 3606.

35. Cross, G. H.; Peterson, I. R.; Girling, I. R.; Cade, N. A.; Goodwin, M. J.; Carr, N.; Sethi, R. S.; Marsden, R.; Gray, G. W.; Lacey, D.; McRoberts, A. M.; Scrowston, R. M.; Toyne, K. J. *Thin Solid Films* **1988**, *156*, 39.

Scope

A number of methodologies for immobilizing metal nanoparticles in 2-dimensional aggregate structures on various substrates, some with concomitant tuning of the surface plasmon resonance (SPR), have been reported. Many of them involve special functionalization of the nanoparticles, multiple fabrication steps or lengthy procedures. The study presented in this chapter demonstrates that monolayer LB film of a hemicyanine-based amphiphile with cationic headgroup is an easily fabricated platform for harnessing citrate-stabilized gold nanoparticles. It is shown that a single immersion step can be used to immobilize the nanoparticles uniformly on large area films and that systematic variation of the immersion time from 10 min to 6 h leads to controlled assembly of the particles and tuning of the SPR band over ~ 100 nm. A model for the structural reorganization in the LB film that facilitates the assembly of nanoparticles is presented and the advantages of the current methodology over earlier protocols are pointed out. The versatility of LB films in terms of the molecular level control of fabrication it enables and the variety of film structures that can be realized, point to the wide scope for future explorations, expanding upon the present observations.

5.1. Introduction

Electronic and optical properties of metal and semiconductor nanoparticles are sensitively dependent on their size, shape and assembly. Metal nanoparticles can manifest the characteristics of molecules[1] and their organized assembly is reminiscent of the formation of supramolecular architectures, both accompanied by perturbation of the electronic structure and hence the optical responses. Interaction of metal nanoparticles modifies the SPR[2,3] leading to significant changes in the optical extinction; this is of interest in a wide range of applications including surface enhanced Raman scattering (SERS)[4] and sensors.[5] Several methods for the controlled aggregation of metal nanoparticles have been reported. A widely used approach is that based on the functionalization of nanoparticles, the assembly triggered by the interaction of the functional groups.[1,3,6] Special techniques such as ac dielectrophoresis have been used to assemble nanoparticles inside electrical nanogaps.[7] Electrostatic interactions between capped nanoparticles and linking groups have been exploited to achieve controlled aggregation of nanoparticles and tuning of the SPR.[8] Perhaps the most common approach to the assembly of metal nanoparticles is that based on the templating effect of macromolecules and substrates. Some of the templates used to organize metal nanoparticles into assemblies of various dimensions are DNA,[9] proteins such as chaperonin[10] and tobacco mosaic virus.[11]

Assembly in solution is generally monitored through spectroscopy or light scattering measurements; sample preparation for microscopy usually involves drop-casting these solutions on appropriate substrates, hence the possibility of introducing artifacts during the drying process cannot be ruled out. Immobilization and assembly of metal nanoparticles on solid substrate surfaces not only allows direct imaging in microscopes but also facilitates various device applications. LbL[12] as well as LB[13] deposition techniques have been used to fabricate metal nanoparticle aggregates in the form of ultrathin films on suitable substrates. Substrates treated to form surface charges, patterned or modified with self-assembled monolayers (SAM), can be immersed in solutions of the nanoparticles effecting the immobilization of the nanoparticles, often through electrostatic interactions;[14,15] further aggregation of the nanoparticles into 2-dimensional assemblies have been induced by ligand replacement or through solvent evaporation. Deposition of mono or multilayer LB films of ionic amphiphiles would be a convenient method to produce substrates with charged surface capable of gathering capped metal nanoparticles from solution and assembling them through electrostatic interactions. This would be particularly fruitful if the extent of immobilization and 2-dimensional assembly of the nanoparticles can be varied smoothly to tune responses such as the SPR absorption.[16] Since LB films with areas of several square centimeters can be fabricated easily, such procedures will yield large area nanoparticle assemblies. Even though experiments along these general lines have been reported,[17,18] lengthy fabrication times were involved and multilayer films with varying number of spacer layers had to be employed to achieve SPR tuning.[18] It is desirable to develop a simple LB film based approach that facilitates a single step, efficient immobilization of nanoparticles in 2-dimensional assemblies with controlled variation of particle density allowing direct characterization by microscopy and realizing SPR absorption tuning over a wide wavelength range.

We envisaged that ODEP$^+$Br$^-$ (discussed in Chapter 3 and 4) could serve as an efficient platform to assemble metal nanoparticles bearing negatively charged capping layer. Electron microscopy and spectroscopy studies show that a single step process involving immersion of monolayer LB films of ODEP$^+$Br$^-$ in aqueous solutions of citrate-stabilized gold nanoparticles for times as short as 10 min initiates adsorption of the nanoparticles on the LB film and that systematic variation of the immersion time up to ~ 6 h can be used to achieve controlled 2-dimensional aggregation of the nanoparticles and smooth tuning of the SPR absorption peak over a wide wavelength range. We analyze the gradual aggregation of nanoparticles on the ultrathin film and present control experiments that establish the relevance of the LB film in the present protocol. AFM imaging is used to construct a model that describes reorganization of the monolayer LB film into multilayer structures facilitating the immobilization of the nanoparticles. Finally the present protocol is compared with procedures developed in earlier studies.

5.2. Fabrication of Ultrathin Film - Nanoparticle Composite

Monolayer LB film of ODEP$^+$Br$^-$ was fabricated by following procedures discussed in Chapter 3 and 4. A chloroform solution of ODEP$^+$Br$^-$ was spread on aqueous subphase and compressed to a pressure of 30 mN/m followed by transfer to substrates by vertical dipping with a dipping speed of 5 mm/min. The characteristics of Langmuir and LB films of ODEP$^+$Br$^-$ and the impact of polyelectrolyte templating have been investigated extensively during earlier studies in our laboratory, and as discussed in the last chapter.[19-21] Monolayer LB film of ODEP$^+$Br$^-$ was deposited on carbon-supported copper grids (for transmission electron microscope (TEM) imaging; used also for field emission scanning electron microscope (FESEM) imaging), mica (for AFM imaging) or quartz with hydrophilic surface (for electronic absorption spectroscopy). All substrates have hydrophilic surface (as shown by the water meniscus) and deposition was carried out in a single upstroke from inside the subphase; the transfer ratio was generally ≥ 0.9.

Gold nanoparticles were prepared following the citrate reduction procedure[22] with slight modifications. Aqueous solutions of citrate-stabilized gold nanoparticles prepared from 0.005 wt% of $HAuCl_4$ were used in the studies presented in this chapter. Briefly, an aqueous solution of sodium citrate (10 mg/mL, 10mL) was added to a boiling aqueous solution of $HAuCl_4$ (0.05 mg/mL, 500mL) under vigorous stirring. The solution turned blue within 1 min and wine-red ~ 2 min later. Boiling was continued for another 20 min. The solution was stirred for 10 min after removing the heat source. Gold nanoparticles synthesized using 0.01 wt% of $HAuCl_4$ solution were also used in some of the control experiments. The substrate with the monolayer LB film was immersed in the aqueous solution of citrate-stabilized gold nanoparticles at 25°C for periods ranging from 10 min to 10 h. On taking out of the solution, the films were washed repeatedly with high purity water to remove any material physically adhering on the film. The stability of the film was verified by keeping it in pure water for several hours and observing that the SPR spectrum remained unaffected; the film is found to be stable even against ultrasonication in water for ~ 2 h. These observations indicate that the gold nanoparticles are bound electrostatically on the $ODEP^+Br^-$ film and that there is no material precipitated via heterogeneous nucleation on the film.

5.3. Electron Microscopy

FESEM and TEM images of the gold nanoparticles immobilized on the LB film by immersion for different times are collected in Figures 5.1 and 5.2 respectively. The FESEM images clearly show the nanoparticles immobilized on the surface of the substrate. These and the TEM images reveal that the particles are mostly spherical (with diameter in the range 12 – 18 nm) with occasional triangular ones; crystalline nature of the gold nanoparticles is demonstrated by observation of the electron diffraction pattern (Fig. 5.3). Films immersed for 10 and 30 min show several isolated nanoparticles, but also a few chain

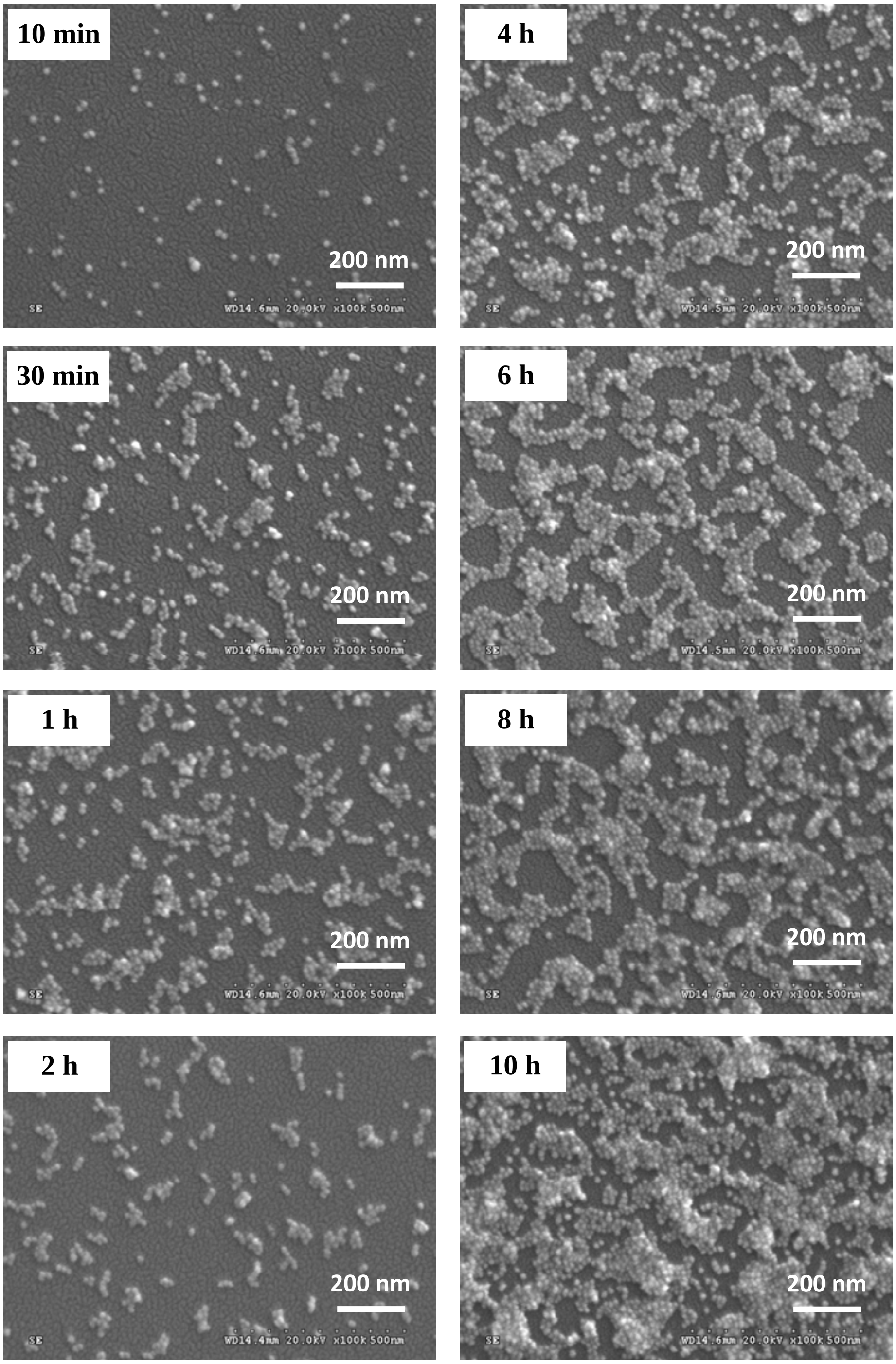

Figure 5.1. *FESEM images of gold nanoparticles immobilized on LB film of* ODEP$^+$Br$^-$*; the time of immersion of the LB film in the gold nanoparticle solution is indicated. Scale bar = 200 nm.*

and 2-dimensional aggregates. With increasing immersion time, the total number of immobilized nanoparticles as well as the extent of aggregation increase. There are hardly any isolated nanoparticles in samples immersed for more than 2 h. Extended aggregates

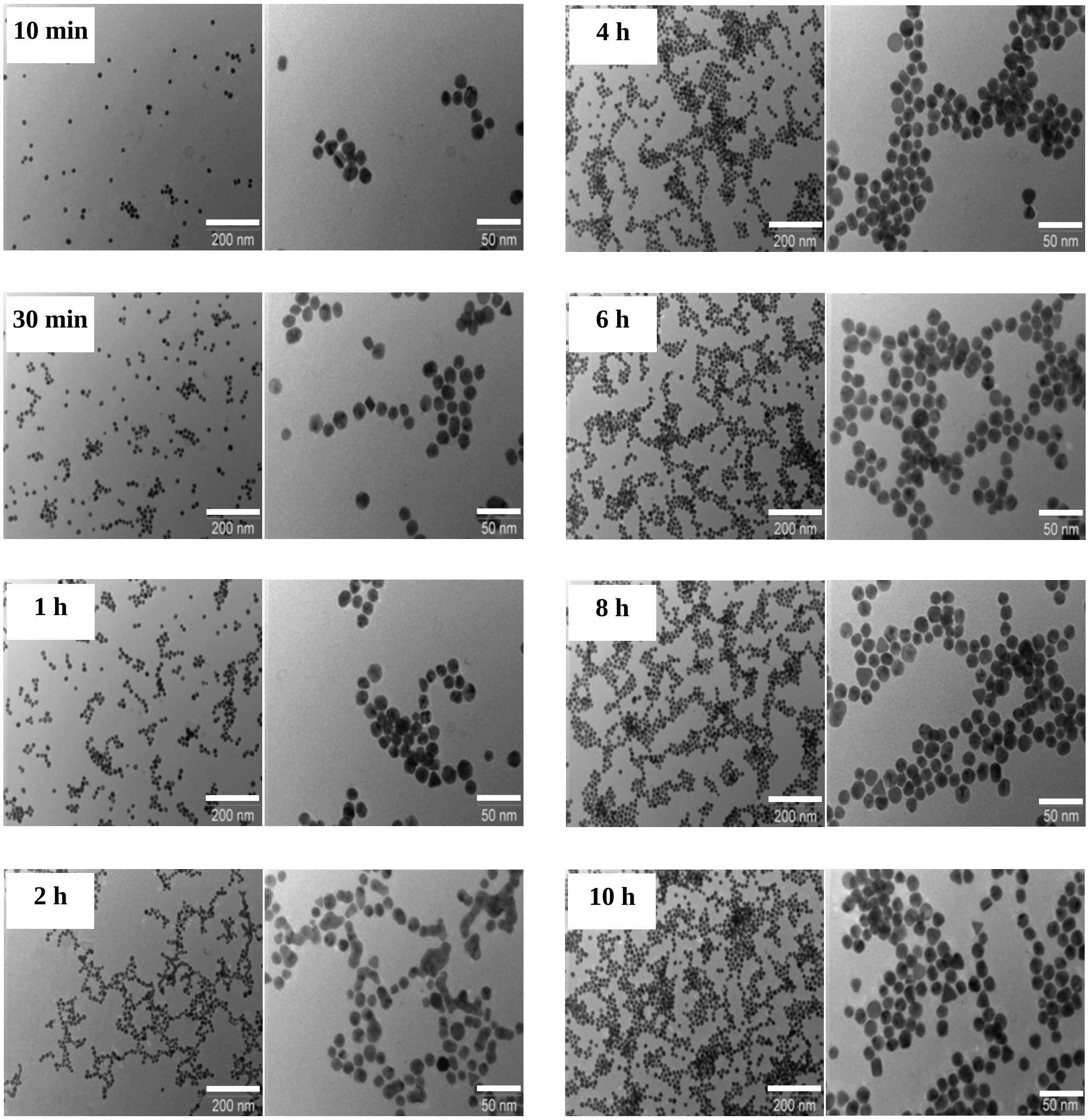

Figure 5.2. *TEM images of gold nanoparticles immobilized on LB film of ODEP$^+$Br$^-$; the time of immersion of the LB film in the gold nanoparticle solution is indicated. Images with two magnifications (scale bar = 200 nm, 50 nm) are shown in each case.*

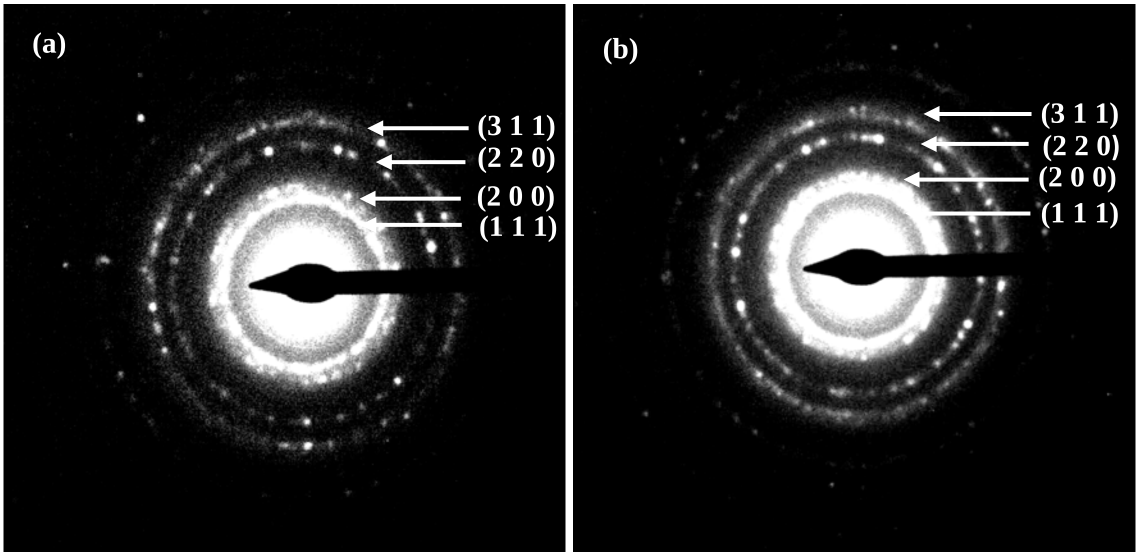

Figure 5.3. *Electron diffraction pattern of gold nanoparticles immobilized on ODEP$^+$Br$^-$ LB film by immersion for **(a)** 2h and **(b)** 4h.*

which still maintain a 2-dimensional assembly are found upto an immersion time of 8 h. Beyond this immersion time, occasional formation of multilayers of nanoparticles is observed. The count of nanoparticles immobilized on the LB film estimated from the TEM images are plotted as a function of the immersion time in Figure 5.4a. The plot of the count of particles against the square root of time shows a linear region up to ~ 4h and leveling off beyond (Fig. 5.4b). Examination of the interparticle distances suggests that the centre-to-centre distance between neighboring particles in the aggregate structures is typically < 20 nm. Assuming this cut-off distance, the number of neighbors of each particle observed in the images of films immersed for 10 min – 6 h was estimated. Particles in the image area (950 x 700nm^2, Fig. 5.2) were counted by marking each one individually; simultaneously their coordinates were saved.[23] Using these coordinates and the scaling between pixels and actual distances in the image, all interparticle distances were evaluated using a home-made computer program. The percentages of particles with no neighbors (isolated particles) and with neighbors ranging from 1 – 6 are plotted in Figure 5.5. It is seen that the percentage of isolated particles decreases steadily and becomes negligible with increasing immersion time; similar is the case with particles having one neighbor. The percentages of particles with two and three neighbors increase initially but then decline gradually, whereas the percentages of particles with four to six neighbors increase with the immersion time. This analysis describes clearly, the gradual build up of the aggregated structures with increasing time of immersion of the films. We have observed that nanoparticle solutions prepared from 0.01 wt% of $HAuCl_4$ lead to similar effects but show higher density of nanoparticles in the film (Fig. 5.6). Multilayer formation was observed to occur quicker than in the case of the nanoparticle solution prepared from 0.005 wt% of $HAuCl_4$

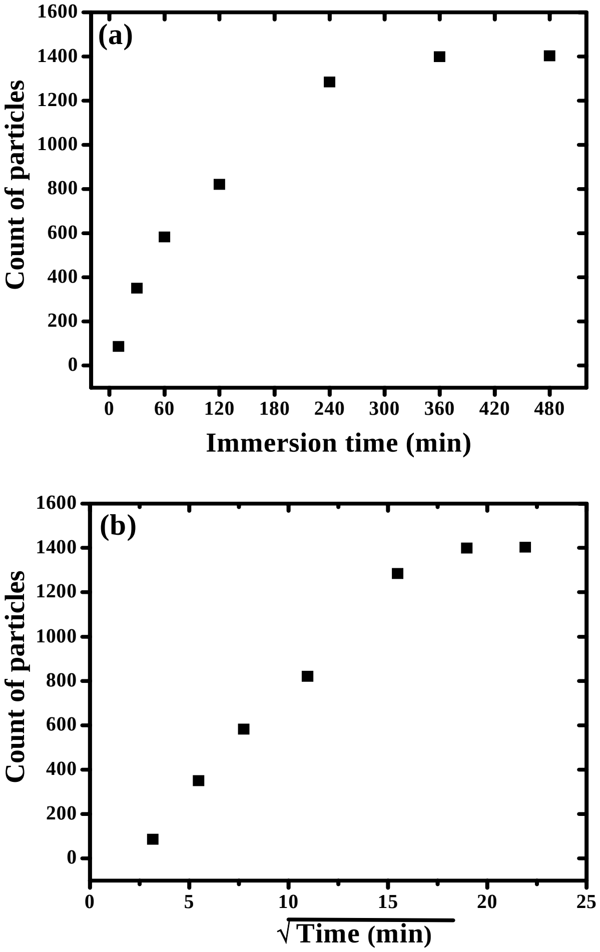

Figure 5.4. *Count of gold nanoparticles (count made on TEM images shown in Figure 5.2 (scale = 200 nm; coverage area ~ 950* x *700* nm^2*) immobilized on the* $ODEP^+Br^-$ *LB film as a function of* ***(a)*** *immersion time and* ***(b)*** *square root of immersion time.*

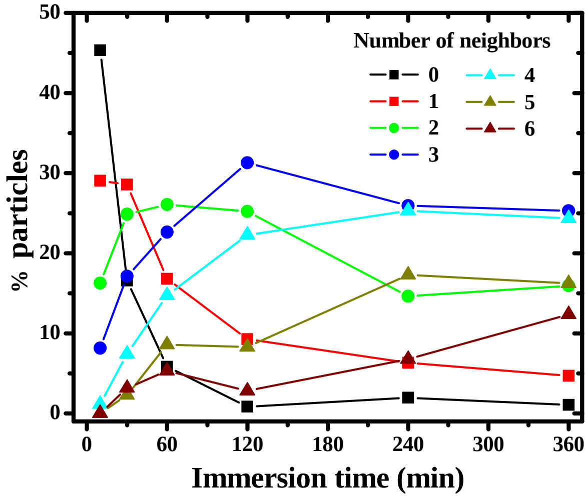

Figure 5.5. *Percentage of particles with different number (0 – 6) of neighboring particles (defined as those with a centre-to-centre distance < 20 nm) as a function of immersion time; the line is only a guide to the eye.*

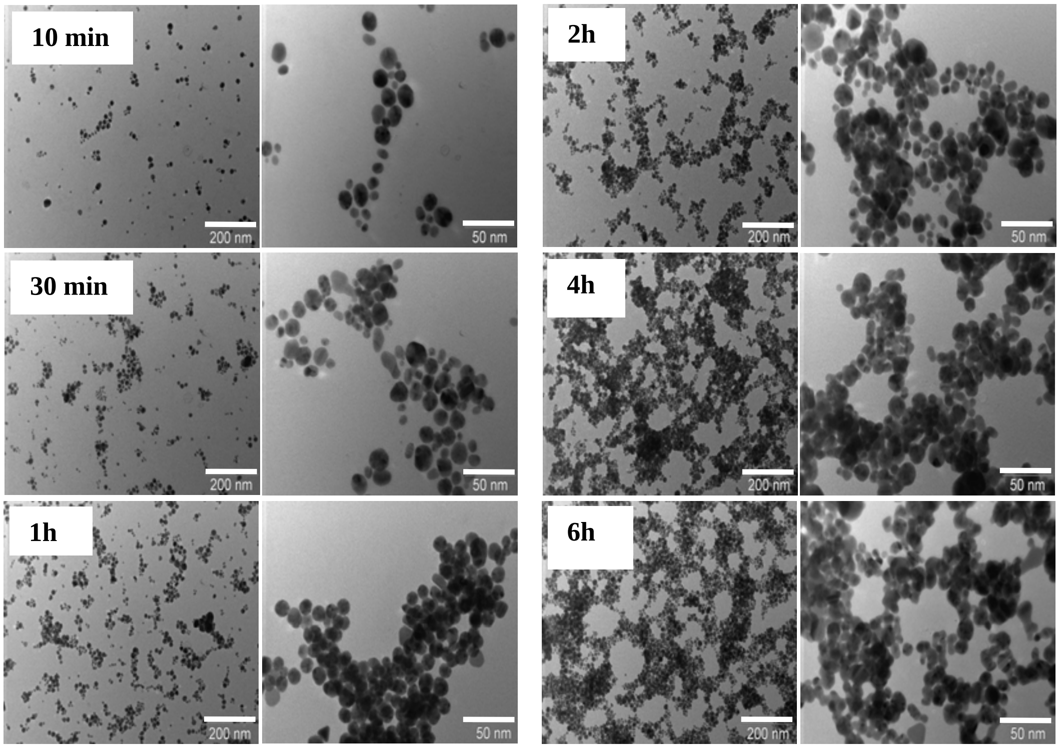

Figure 5.6. *TEM images of gold nanoparticles immobilized on LB film of ODEP$^+$Br$^-$ using gold nanoparticles solution prepared by the reduction of 0.01wt% of HAuCl$_4$; the time of immersion of the LB film in the gold nanoparticle solution is indicated. Images with two magnifications (scale bar = 200 nm, 50 nm) are shown in each case.*

5.4. Surface Plasmon Resonance Tuning

The increasing population and aggregation of the nanoparticles are expected to strongly influence the SPR extinction of these films. Figures 5.7a and b show the progression of the extinction spectra of films immersed for different periods of time; spectra of the gold nanoparticle solution and ODEP$^+$Br$^-$ monolayer LB film are also included in Figure 5.7b for comparison. Immobilization of gold nanoparticles on the LB film is evident from the SPR absorption observed even in the film immersed for as short a time as 10 min. Deconvolution of the spectrum clearly reveals the presence of ODEP$^+$Br$^-$ film with its characteristic absorption at ~ 460 nm and the gold nanoparticle peak at ~ 540 nm. The latter is red-shifted with respect to that of the aqueous solution of citrate-stabilized gold nanoparticles (~ 520 nm); this may be attributed to the impact of the local dielectric environment created by the ionic head groups of the LB film. Films immersed for 30 min show enhanced intensity and deconvolution of the spectrum indicates a new peak emerging at ~ 590 nm. The latter appears to result from the delocalized plasmon resonance of nanoparticle assemblies observed in the microscopy images. The spectrum is similar for films immersed for 1 h, but the long wavelength peak registers a small red shift. With longer immersion periods, the spectrum shows steady increase in intensity; spectral deconvolution reveals that the intensity of the peak at 540 nm remains low throughout, perhaps going through a mild maximum near 3 h, whereas the higher wavelength peak shows steady increase in intensity and red shift. The position and intensity of the latter two peaks are depicted in the plots in Figure 5.7c. Evolution of the SPR spectra cease when the immersion time reaches about 8 h (Fig. 5.7a, b); films immersed for 10 h show negligible difference indicating that the 2-dimensional assemblies are saturated at this point. It should be mentioned that, in order to account for the full spectrum, the deconvolution included two more peaks in addition to the ones noted above – one in the UV region at ~ 210 – 230 nm and the other at ~ 800 - 900 nm. Both become appreciable only in spectra of samples immersed for more than 2 h and increase with time thereafter. The former accounts for the absorption into the conduction band of gold nanoparticles; the latter possibly includes contributions from scattering as well as the plasmon absorption of the extended nanostructures. The peak positions obtained from the deconvolution of the spectra are

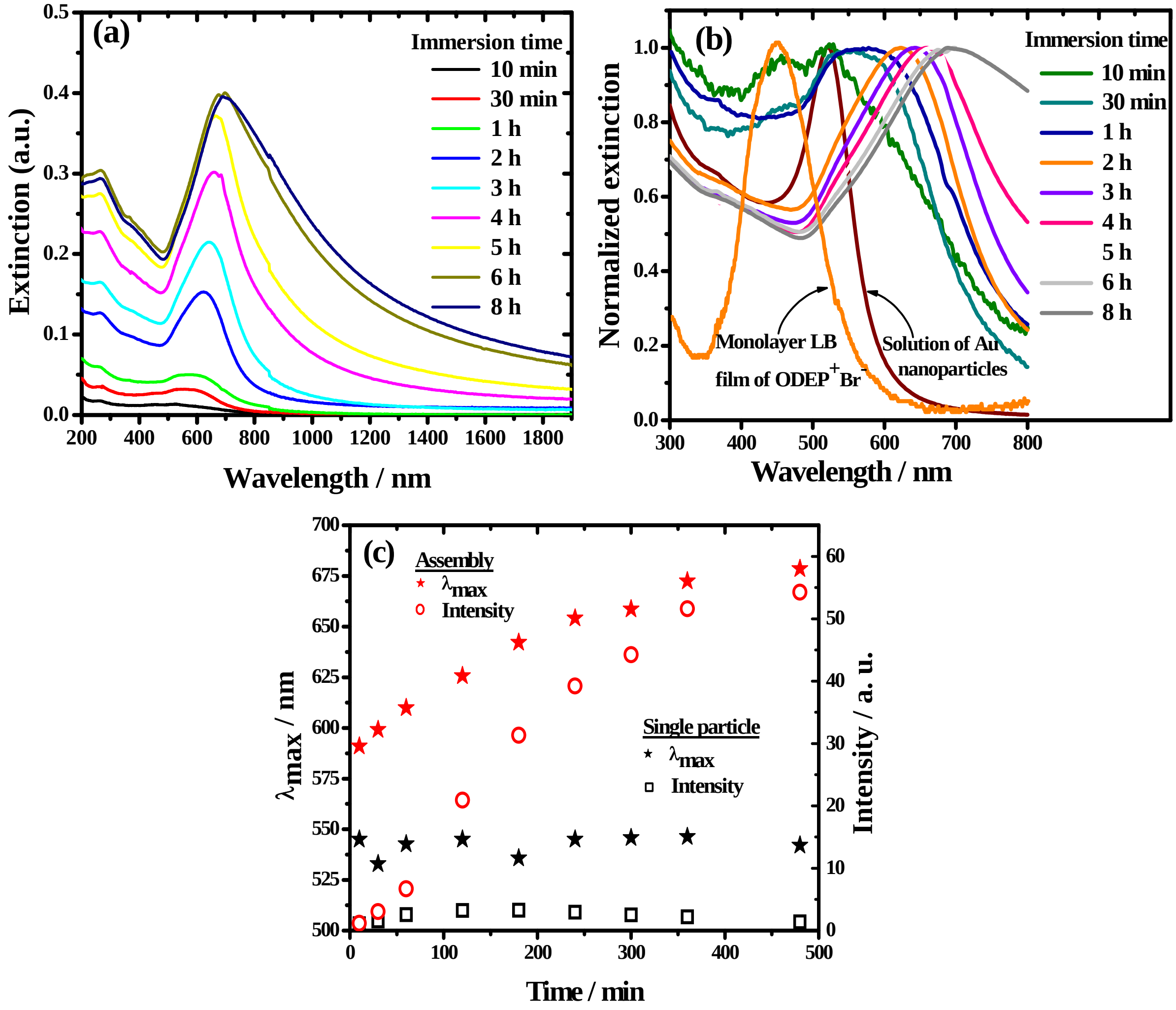

Figure 5.7. ***(a)*** *Extinction spectra of gold nanoparticles immobilized on LB film of ODEP*$^+$*Br*$^-$ *on quartz by immersion of the film in gold nanoparticle solution prepared from 0.005 wt% HAuCl*$_4$ *for different time periods;* ***(b)*** *Normalized (intensity at* λ_{max} *= 1.0) spectra of ODEP*$^+$*Br*$^-$ *monolayer LB film, gold nanoparticle solution and those shown in (a);* ***(c)*** *Variation of the* λ_{max} *and intensities of the SPR absorption peaks due to the isolated gold nanoparticles and their assemblies (obtained by deconvolution of the spectra;), with the time of immersion of the LB film in the gold nanoparticle solution.*

collected in Table 5.1. A typical deconvolution of the spectrum using multiple Gaussians is shown in Figure 5.8; the correlation coefficient for the deconvolution was typically > 0.996 in all cases.

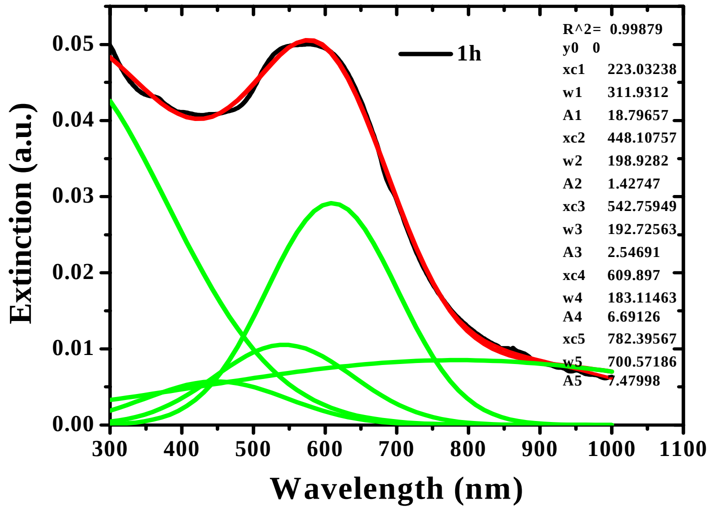

Figure 5.8. *Deconvolution of the electronic absorption spectrum of the ODEP$^+$Br$^-$ LB film immersed in gold nanoparticle solution for 1h, using five Gaussians.*

Table 5.1. The peak maxima obtained from the deconvolution of the spectra of films dipped in gold nanoparticle solution for different periods of time.

Immersion time (min)	**Peak 1**		**Peak 2**		**Peak 3**		**Peak 4**		**Peak 5**	
	λ_{max} (nm)	Area	λ_{max} (nm)	Area	λ_{max} (nm)	Area	λ_{max} (nm)	Area	λ_{max} (nm)	Area
10	235.5	4.19	464.2	0.61	545.0	1.08	591.0	1.18	654.6	1.07
30	218.5	13.97	464.0	0.62	532.9	1.52	599.2	3.04	705.5	1.09
60	223.0	18.79	448.1	1.42	542.8	2.54	609.9	6.69	782.4	7.47
120	239.7	55.04	466.0	1.07	545.0	3.22	625.7	20.93	803.9	11.79
180	240.0	78.63	461.2	1.01	535.7	3.27	642.1	31.33	827.8	19.64
240	221.2	89.35	451.1	1.63	545.0	2.93	654.1	39.23	828.5	24.66
300	214.8	91.36	459.0	1.29	545.8	2.52	658.6	44.25	834.1	28.32
360	213.8	66.18	462.2	1.39	546.3	2.20	672.5	51.60	868.0	38.35
480	228.2	70.70	460.0	1.46	542.0	1.37	678.5	54.27	887.2	55.86

The SPR absorption due to the isolated nanoparticles increases slightly with increasing immersion time in the beginning but then shows a decrease. This implies that nearly all the nanoparticles are incorporated into the assemblies when immersion times extend beyond ~ 3 h; this is borne out by the microscopy images as well. Simple variation of the immersion time from 10 min to 8 h tunes the absorption peak due to the nanoparticle assemblies from ~ 590 – 680 nm, accounting for an overall tuning of 160 nm with respect to the peak for the nanoparticle solution at 520 nm. The red shift of the SPR bands arises due to the influence of the LB film and the assembly of the gold nanoparticles into short chain segments followed by extended 2-dimensional lattices as seen in the electron microscopy images (Figs. 5.1, 5.2). The latter is consistent with the well-known behavior of the longitudinal mode of the plasmon resonance in a chain of nanoparticles evolving steadily with the number of particles in the chain and the extent of aggregation.[24] As in the case of the isolated gold nanoparticles, it is possible that the SPR absorption of their assemblies is also influenced by the local dielectric environment due to the ionic headgroup of ODEP$^+$Br$^-$. We have not observed any strong impact of the gold nanoparticles on the linear or nonlinear optical responses of ODEP$^+$Br$^-$; such effects may be anticipated in variants of the system.

5.5. Role of Monolayer ODEP$^+$Br$^-$ LB film on the Assembly of Nanoparticles

The earlier mentioned observation (Sec. 5.2) that washing and even ultrasonication does not dislodge the nanoparticles from the LB film is suggestive of strong binding. In order to assess the role of the LB film of the cationic amphiphile in harnessing the gold nanoparticle from solution and assembling them in 2-dimensional aggregate structures, we have carried out several control experiments. Electronic absorption spectrum shows that plain quartz substrate with hydrophilic surface prepared as for the deposition of LB films, when immersed in citrate-stabilized gold nanoparticle solution even for 12 h does not immobilize any appreciable amount of nanoparticles on its surface. When a monolayer LB film of arachidic acid is immersed in the gold nanoparticle solution even for several hours, hardly any nanoparticle is immobilized on the film, indicating that the non - ionic nature of the molecules forming the LB film does not attract the citrate - stabilized gold nanoparticles. In this context, it may also be noted that immersion for 40 – 120 h was required for evaporated thin films of octadecylamine to uptake gold nanoparticles from solution; no SPR tuning was reported in that study.[25] We have experimented also with seve-

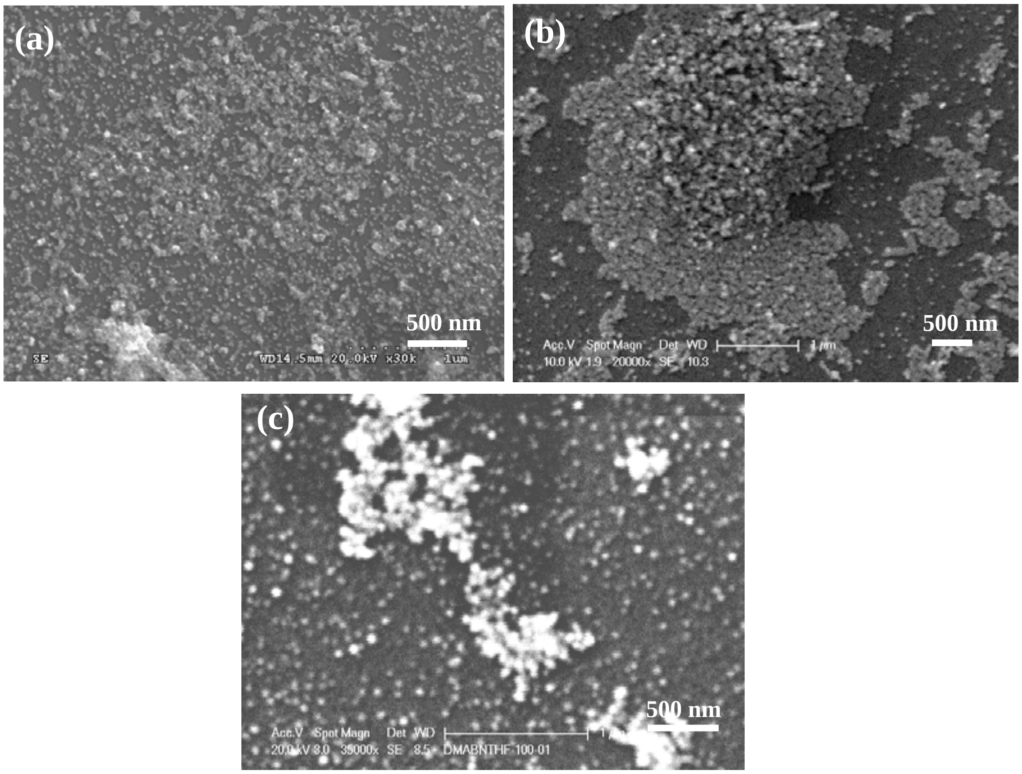

Figure 5.9. *SEM images of immobilized gold nanoparticles on* ***(a)*** *drop-casted film of ODEP$^+$Br$^-$,* ***(b)*** *spin-coated film of ODEP$^+$Br$^-$ and* ***(c)*** *dip-coated film of poly(diallyldimethylammonium chloride).*

ral positively charged surfaces prepared by drop-casting as well as spin-coating chloroform solution of ODEP$^+$Br$^-$ on different substrates as well as dip-coating glass substrate with the polycation, poly(diallyldimethylammonium chloride). These were subsequently immersed in gold nanoparticle solution. Multilayer aggregated structures of nanoparticles often formed randomly, observed in all these cases (Fig. 5.9) point to the fact that a uniform LB film provides easy access to a clean 2-dimensional nanoparticle assembly. Thus the cationic amphiphile based LB film appears to be ideally suited for efficient gathering of nanoparticles from solution. It is likely that the positively charged ODEP$^+$ molecules screen the repulsive interaction between the negative surface charges of the gold nanoparticles which keep them apart in solution and lead to their 2-dimensional assembly.

5.6. AFM Imaging and a Model for the Nanocomposite Film

AFM provides useful insight into the structure of the LB film - nanoparticle composite. Figure 5.10a shows an image of the monolayer LB film of ODEP$^+$Br$^-$ on mica; the characteristic flower-like structures ~ 2 nm thick (Fig. 5.11) and extending over several microns, are similar to those discussed in Sec. 3.4.1 and 4.3.3. The significant features observed in the image of the film immersed in the gold nanoparticle solution for 10 min (Fig. 5.10b) may be attributed to the LB film and gold nanoparticle aggregates. The extended structures are mostly ~ 8 – 9 nm thick; structures having thicknesses of ~ 4 nm as well as ~ 2 nm can also be found in a few places (Fig. 5.12a). While the first two appear to be formed through the reorganization of the monolayer LB film into 4-layer and 2-layer structures, the last ones are remnants of the monolayer. Another common feature observed is the particle-like entities on top of these films. The lateral dimensions (~ 100 – 120 nm)

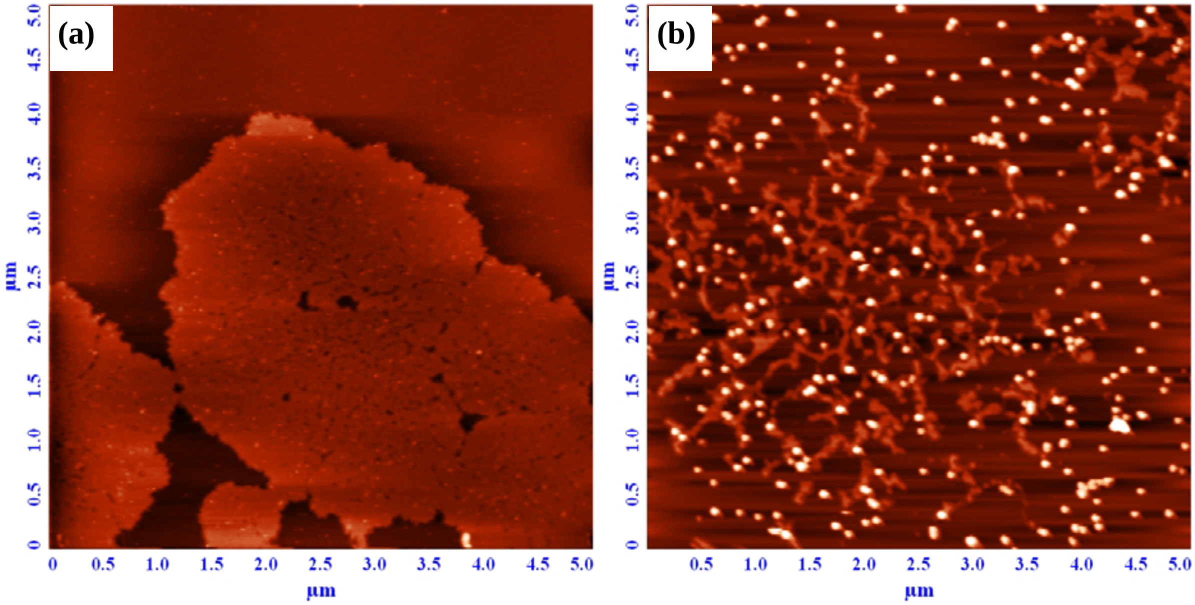

Figure 5.10. *AFM images of* ***(a)*** *ODEP$^+$Br$^-$ monolayer LB film,* ***(b)*** *ODEP$^+$Br$^-$ LB film immersed in citrate-stabilized gold nanoparticle solution for 10 min.*

and total height (~ 22 – 24 nm or 18 – 20 nm) of these features suggest that they are the 2-dimensional gold nanoparticle aggregates immobilized on the 4-layer and 2-layer LB films; the X-Y resolution of the AFM is insufficient to resolve the individual nanoparticles in the aggregates. The step-like features in the line profile analysis (Fig. 5.12b) shows the contribution of the LB film to the total height of these features. The isolated particle-like structures observed in the image also have similar dimensions (Fig. 5.12c), suggesting that these are again gold nanoparticle aggregates immobilized on small fragments of the multilayer film.

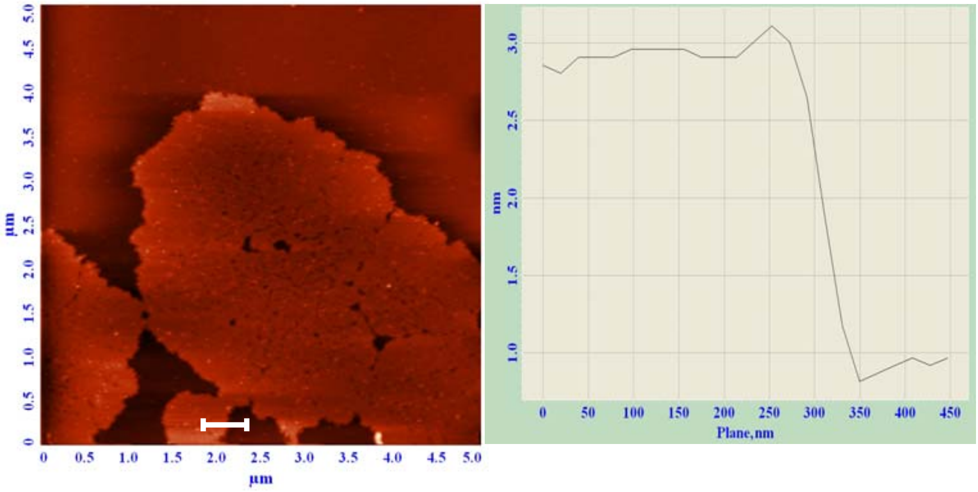

Figure 5.11. *AFM image along with a line profile of ODEP$^+$Br$^-$ monolayer LB film.*

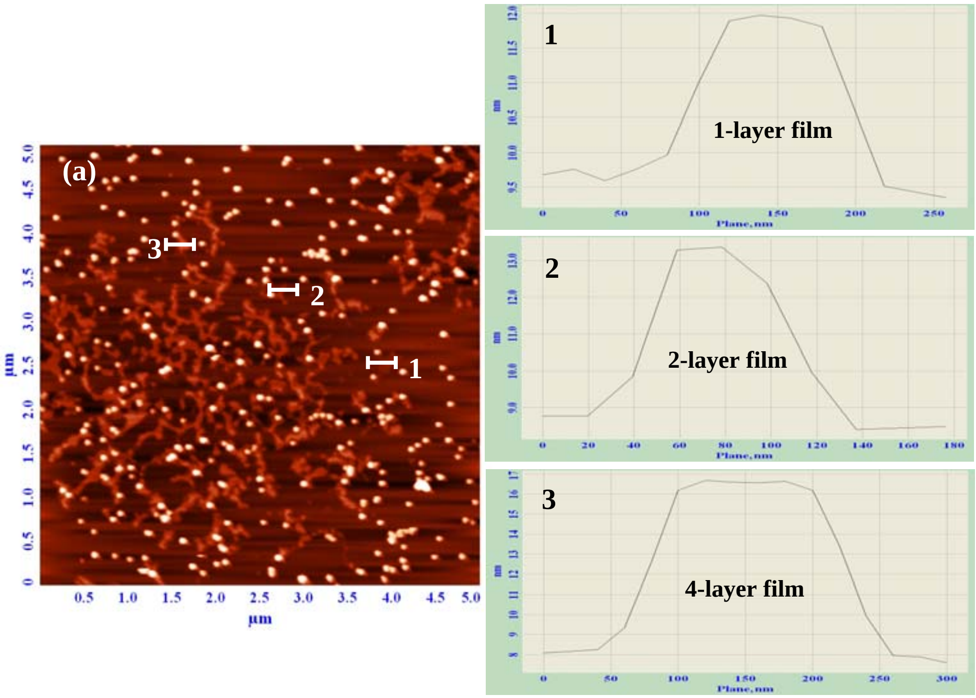

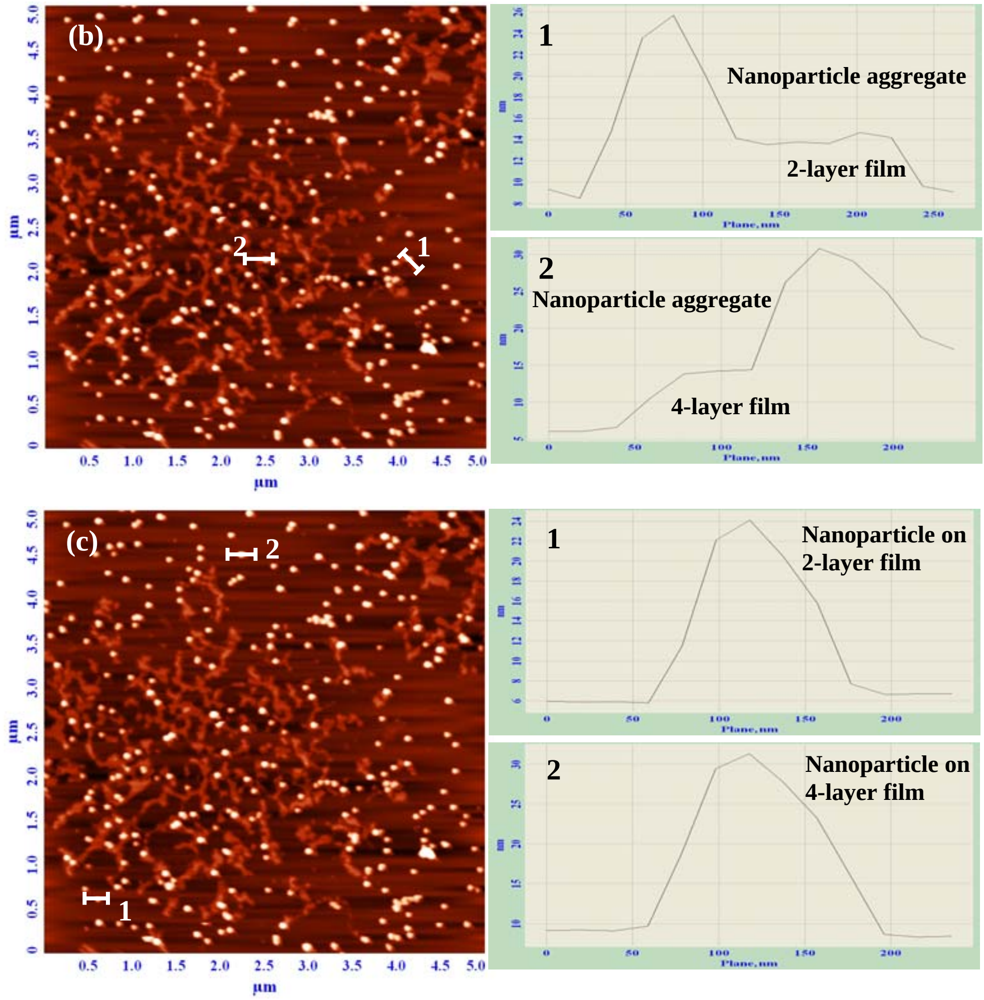

Figure 5.12. *AFM image along with line profiles of LB film of ODEP$^+$Br$^-$ immersed in citrate-stabilized gold nanoparticle for 10 min. Line profiles for three different kinds of features observed* ***(a)*** *on extended film,* ***(b)*** *on particles found on the extended film and* ***(c)*** *on isolated particles are shown.*

A control experiment was carried out wherein the monolayer LB film was immersed in an aqueous solution of sodium citrate with pH adjusted to ~ 6 (comparable to that of the gold nanoparticle solution) by addition of dilute hydrochloric acid. Multilayer islands similar to those in Figure 5.10b are observed in this case as well, and as expected there are no features corresponding to gold nanoparticles aggregates (Fig. 5.13). This demonstrates that when immersed in an appropriate medium, the monolayer reorganizes to expose a hydrophilic surface that is capable of accepting the gold nanoparticles. The various features observed in the AFM images suggest that when the monolayer LB film is immersed in the nanoparticle solution, it reorganizes into 2- and 4-layer structures and then the gold nanoparticles attach on them. This would indeed be a natural process by which the LB film of ODEP$^+$Br$^-$ deposited on the hydrophilic substrate with the headgroup attached to the substrate and hydrocarbon chains extending outward (Z-type), is transformed to produce a hydrophilic surface that is capable of accepting the citrate-stabilized gold nanoparticles. A schematic representation of this model is shown in Figure 5.14. It is relevant to note here that ODEP$^+$Br$^-$ Langmuir film transfers appreciably only during upstrokes and hence forms Z-type films.[21] Similar mechanism is likely to operate in the films formed on quartz and carbon-supported copper grid with hydrophilic surfaces.

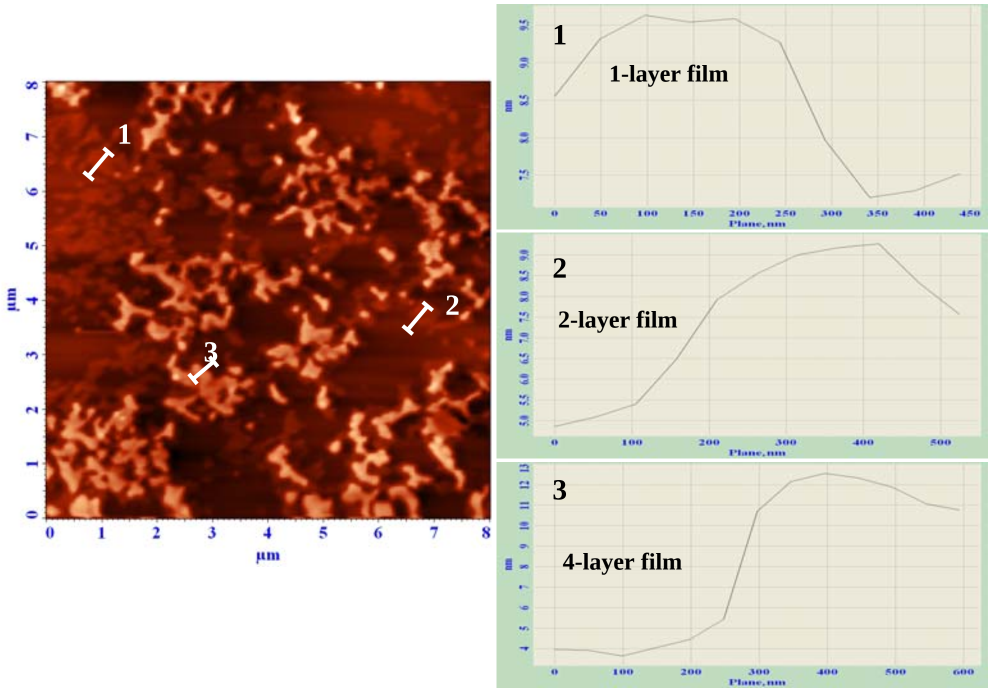

Figure 5.13. *AFM image and line profiles of LB film of ODEP$^+$Br$^-$ immersed for 10 min in an aqueous solution of sodium citrate.*

The features of the ODEP$^+$Br$^-$ LB film with the gold nanoparticles deposited on it and the control experiments allow us to describe the assembly process involved. When dipped in the nanoparticle solution, the monolayer reorganizes to form the multilayer islands. The gold nanoparticles diffuse from bulk solution and get attached to the ionic surface of the molecular ultrathin film; as noted earlier, the initial time dependence of the particle coverage is found to be proportional to the square root of time as expected for a process dominated by bulk diffusion.[26] This sequence of events acts as a fine control on the assembly process and its kinetics. The concentration of the gold nanoparticle solution provides a facile handle to tune the whole process.

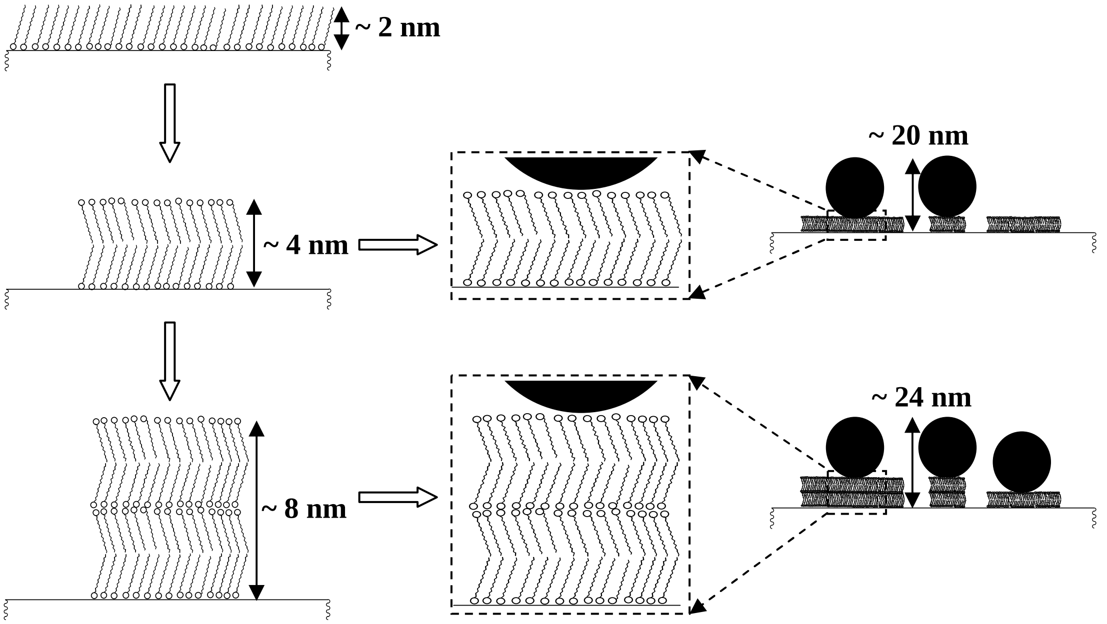

Figure 5.14. *Schematic representation of the monolayer, 2-layer and 4-layer LB film and the gold nanoparticles immobilized on the hydrophilic surface of the multilayer structures. Approximate representative heights of different features are indicated.*

5.7. Comparison with Earlier Methodologies

It is instructive to compare the fabrication of the nanoparticle assemblies in the present study with previous reports of related investigations. Positively charged substrates formed by covalent attachment of end group functionalized silanes or polycation adsorption have been used to immobilize colloidal gold to form 2-dimensional assemblies.[26] Several more studies have employed SAM and LbL assembled thin films.[27] Another approach involved LB deposition of amphiphiles along with metal nanoparticles spread either on the interface or adsorbed from the aqueous subphase.[28] SPR tuning over a wide range of wavelenghts was not demonstrated in most of these cases. Sub-monolayer deposition of gold nanoparticles on silica substrates having a thermally-grown silica layer and coated with bifunctional aminosilane followed by treatment with alkanethiol has been shown to lead to the formation of ordered 2-dimensional array of the nanoparticles.[29] The procedure requires ~ 36 h and each further cycling ~ 24 h; controlled aggregation and tuning of the SPR absorption was demonstrated using this rather time-consuming protocol.[16] As noted in Sec. 5.1, tuning of the SPR absorption of gold nanoparticles in multilayer structures was achieved by depositing them on LB films fabricated with increasing number of spacer layers of poly(N-dodecylacrylamide);[18] immersion in gold nanoparticle solutions was carried out typically for 6 – 12 h in each cycle. A still different approach involves self-assembly of citrate-stabilized gold nanoparticles induced by addition of different amounts of cetyltrimethylammonium bromide (CTAB).[30] The 'glueing' with CTAB involves ~ 12 h long substrate preparation followed by another 12 h for assembling the gold nanoparticle monolayers. Comparison with the various studies noted above shows that, the protocol we have developed involving a one-step immersion process requiring anywhere from a few minutes to a few hours leading to smooth variation in the particle density and effective tuning of the SPR absorption, is very simple to implement and efficient.

5.8. Summary

The study presented in this chapter demonstrated a simple and facile procedure to immobilize large area 2-dimensional assemblies of metal nanoparticles through electrostatic interaction with a monolayer LB film of an ionic amphiphile. Smooth variation in the extent of aggregation was realized through variation of the immersion time from 10 min – 6 h; the procedure is particularly advantageous to enforce fine control of the nanoparticle immobilization and assembly. The accompanying shifts in the surface plasmon resonance spectra indicated efficient tuning of the optical response in these composite ultrathin films. This can be exploited in various applications involving effects such as fluorescence enhancement and SERS. Another aspect to be explored is the potential utility of the present fabrication methodology in developing nanocomposite materials with enhanced nonlinear optical responses.

References

1. (a) Perepichka, D. F.; Rosei, F. *Angew. Chem. Int. Ed.* **2007**, *46*, 6006, and references therein; (b) Yan, H.; Cingarapu, S.; Klabunde, K. J.; Chakrabarti, A.; Sorensen, C. M. *Phys. Rev. Lett.* **2009**, *102*, 095501.
2. (a) Liz-Marzan, L. M. *Langmuir* **2006**, *22*, 32; (b) Moores, A.; Goettmann, F. *New J. Chem.* **2006**, *30*, 1121.
3. Prasad, B. L. V.; Sorensen, C. M.; Klabunde, Kenneth J. *Chem. Soc. Rev.* **2008**, *37*, 1871.
4. Ko, H; Singamaneni, S; Tsukruk, V. V. *Small* **2008**, *4*, 1576.
5. Shipway, A. N.; Willner, I. *Chem. Commun.* **2001**, 2035.
6. (a) Rao, C. N. R.; Kulkarni, G. U.; Thomas, P. J.; Edwards, P. P. *Chem. Soc. Rev.* **2000**, *29*, 27; (b) Feldheim, D. *Electrochem. Soc. Interface* **2001**, *10*, 22; (c) Murugadoss, A.; Pasricha, R.; Chattopadhyay, A. *J. Colloid Interface Sci.* **2007**, *311*, 303; (d) Lim, I. S.; Zhong, C. *Gold Bull.* **2007**, *40*, 59.
7. Barsotti, R. J.; Vahey, M. D.; Wartena, R.; Chiang, Y.; Voldman, J.; Stellacci, F. *Small* **2007**, *3*, 488.
8. Shipway, A. N.; Lahav, M.; Gabai, R.; Willner, I. *Langmuir* **2000**, *16*, 8789.
9. (a) Warner, M. G.; Hutchison, J. E. *Nature Mater.* **2003**, *2*, 272; (b) Niemeyer, C. M.; Simon, U. *Eur. J. Inorg. Chem.* **2005**, *18*, 3641; (c) Bidault, S.; Garcia de Abajo, F. J.; Polman, A. *J. Am. Chem. Soc.* **2008**, *130*, 2750.
10. McMillan, R. A.; Howard, J.; Zaluzec, N. J.; Kagawa, H. K.; Mogul, R.; Li, Y.; Paavola, C. D.; Trent, J. D. *J. Am. Chem. Soc.* **2005**, *127*, 2800.
11. Dujardin, E.; Peet, C.; Stubbs, G.; Culver, J. N.; Mann, S. *Nano Lett.* **2003**, *3*, 413.
12. (a) Cassagneau, T. P. in *Colloids and Colloid Assemblies : Synthesis, Modification, Organization and Utilization of Colloid Particles*, Ed. Caruso, F., Wiley, **2004**, 398; (b) Jiang, G.; Baba, A.; Ikarashi, H.; Xu, R.; Locklin, J.; Kashif, K. R.; Shinbo, K.; Kato, K.; Kaneko, F.; Advincula, R. *J. Phys. Chem. C* **2007**, *111*, 18687.
13. (a) Sastry, M. in *Colloids and Colloid Assemblies : Synthesis, Modification, Organization and Utilization of Colloid Particles*, Ed. Caruso, F., Wiley, **2004**, 369;

(b) Ujihara, M.; Mitamura, K.; Torikai, N.; Imae, T. *Langmuir* **2006**, *22*, 3656; (c) Tao, A. R.; Huang, J.; Yang, P. *Acc. Chem. Res.* **2008**, *41*, 1662.

14. (a) Kumar, A.; Mandale, A. B.; Sastry, M. *Langmuir* **2000**, *16*, 6921; (b) Shipway, A. N.; Willner, I. *Chem. Commun.* **2001**, 2035; (c) Hoeppener, S.; Maoz, R.; Cohen, S. R.; Chi, L.; Fuchs, H.; Sagiv, J. *Adv. Mater.* **2002**, *14*, 1036; (d) Katz, E.; Shipway, A. N.; Willner, I. in *Nanoscale Materials* Ed. Liz-Marzan, L. M.; Kamat, P. V.; Springer, **2003**, 5; (e) Yin, D.; Horiuchi, S.; Masuoka, T. *Chem. Mater.* **2005**, *17*, 463; (f) Bansmann, J.; Kielbassa, S.; Hoster, H.; Weigl, F.; Boyen, H. G.; Wiedwald, U.; Ziemann, P.; Behm, R. J. *Langmuir* **2007**, *23*, 10150; (g) Ko, S. H.; Park, I.; Pan, H.; Grigoropoulos, C. P.; Pisano, A. P.; Luscombe, C. K.; Fréchet, J. M. J. *Nano Lett.* **2007**, *7*, 1869.
15. (a) Liu, S.; Zhu, T.; Hu, R.; Liu, Z. *Phys. Chem. Chem. Phys.* **2002**, *4*, 6059; (b) Cant, N. E.; Critchley, K.; Zhang, H.; Evans, S. D. *Thin Solid Films* **2003**, *426*, 31. (c) Liu, S.; Maoz, R.; Sagiv, J. *Nano Lett.* **2004**, *4*, 845; (d) George, C.; Ricci, D.; Di Zitti, E. *Superlatt. Microstr.* **2008**, *44*, 608.
16. Khatri, O. P.; Murase, K.; Sugimura, H. *Langmuir* **2008**, *24*, 3787.
17. (a) Kondo, Y.; Fukuoka, H.; Nakano, S.; Hayashi, K.; Tsukagoshi, T.; Matsumoto, M.; Yoshino, N. *Langmuir* **2007**, *23*, 5857; (b) Tsunashima, R.; Noro, S.; Akutagawa, T.; Nakamura, T.; Karasawa, T.; Kawakami, H.; Toma, K. *J. Phys. Chem. C* **2007**, *111*, 901.
18. (a) Mitsuishi, M.; Ishifuji, M.; Endo, H.; Tanaka, H.; Miyashita, T. *Polymer J.* **2007**, *39*, 411; (b) Ishifuji, M.; Mitsuishi, M.; Miyashita, T. *Chem. Commun.* **2008**, 1058; (c) Ishifuji, M.; Mitsuishi, M.; Miyashita, T. *J. Am. Chem. Soc.* **2009**, *131*, 4418.
19. Chandra, M. S.; Ogata, Y.; Kawamata, J.; Radhakrishnan, T. P. *Langmuir* **2003**, *19*, 10124.
20. Chandra, M. S.; Krishna, M. G.; Mimata, H.; Kawamata, J.; Nakamura, T.; Radhakrishnan, T. P. *Adv. Mater*. **2005**, *17*, 1937.
21. Rajesh, K.; Chandra, M. S.; Hirakawa, S.; Kawamata, J.; Radhakrishnan, T. P. *Langmuir* **2007**, *23*, 8560.

22. Graber, K. C.; Freeman, R. G.; Hommer, M. B.; Natan, M. J. *Anal.Chem.* **1995**, *67*, 735.
23. The Software ImageJ (Ver. 1.41o (Wayne Rasband, National Institute of Health, USA; Java 1.6.0_10) was used.
24. (a) Maier, S. A.; Kik, P. G.; Atwater, H. A. *Appl. Phys. Lett.* **2002**, *81*, 1714; (b) Wei, Q. -H.; Su, K. -H.; Durant, S.; Zhang, X. *Nano Lett.* **2004**, *4*, 1067; (c) Khlebtsov, N. G.; Melnikov, A. G.; Bogatyrev, V. A.; Dykman, L. A. In *Photopolarimetry in Remote Sensing (NATO Science Series II.) Mathematics, Physics, and Chemistry*; Vidden, G.; Yatskiv, Y. S.; Mishchenko, M. I. Dordrecht, Eds.; Kluwer: The Netherlands, **2004**; p 265; (d) Harris, N.; Arnold, M. D.; Blaber, M. G.; Ford, M. J. *J. Phys. Chem. C* **2009**, *113*, 2784.
25. Sastry, M.; Rao, M. K.; Ganesh, N. *Acc. Chem. Res.* **2002**, *35*, 847.
26. Schmitt, J.; Mächtle, P.; Eck, D.; Möhwald, H.; Helm, C. A. *Langmuir* **1999**, *15*, 3256.
27. (a) Chumanov, G.; Sokolov, K.; Cotton, T. M.; *J. Phys. Chem.* **1996**, *100*, 5166; (b) Malikova, N.; Pastoriza-Santos, I.; Schierhorn, M.; Kotov, N. A.; Liz-Marzn, L. M. *Langmuir* **2002**, *18*, 3694; (c) Yang, Y.; Shi, J.; Tanaka, T.; Nogami, M.; *Langmuir* **2007**, *23*, 12042; (d) Kim, J.; Lee, S. W.; Hammond, P. T.; Shao-Horn, Y.; *Chem. Mater.* **2009**, *21*, 2993.
28. (a) Hassenkam, T.; Nørgaard, K.; Iversen, L.; Kiely, C. J.; Brust, M.; Bjørnholm, T. *Adv. Mater.* **2002**, *14*, 1126; (b) Mayya, K. M.; Gole, A.; Jain, N.; Phadtare, S.; Langevin, D.; Sastry, M. *Langmuir* **2003**, *19*, 9147; (c) Chen, L.; Dudek, A.; Lee, Y.; Chang, C. *Langmuir* **2007**, *23*, 3123; (d) Zhong, L.; Jiao, T.; Liu, M. *Langmuir* **2008**, *24*, 11677.
29. Sato, T.; Brown, D.; Johnson, B. F. G. *Chem. Commun.* **1997**, 1007.
30. Yang, Y.; Matsubara, S.; Nogami, M.; Shi, J.; Huang, W. *Nanotechnology* **2006**, *17*, 2821.

6.1. Overview of the Present Work

Assembly of molecules into materials, and effective exploitation of the molecular responses to achieve desired materials properties and functions requires careful control and optimization through the utilization of a range of noncovalent intermolecular interactions. Organization of molecules of interest into molecular materials displaying interesting and useful materials responses can be realized by a variety of techniques. Among these Langmuir-Blodgett (LB) deposition is a simple, elegant and efficient technique for the fabrication of materials in the form of ultrathin films. The main objective of the thesis was to fabricate ultrathin films of organic functional molecules using the LB method and to explore the critical role of molecular design, and fabrication conditions in achieving novel materials attributes. We have fabricated monolayer LB films of a novel zwitterionic amphiphile BODDQ and a series of hemicyanine based amphiphiles $ODEP^+Br^-$, $MEOEP^+I^-$ and $OEOEP^+Br^-$ as well as polyelectrolyte templated multilayer LB films of $ODEP^+Br^-$ and explored their optical and nonlinear optical responses, characterizing unusual phenomena and enhanced effects in specific cases. Utility of the monolayer LB film of $ODEP^+Br^-$ in the controlled aggregation of citrate-stabilized gold nanoparticles in 2-dimensional assemblies was also addressed. We summarize below, the new findings presented in this thesis, in terms of the molecules developed, their assemblies explored and materials responses elicited.

Several derivatives of diaminodicyanoquinodimethane have been investigated in our laboratory earlier, in order to probe their strong quadratic nonlinear optical response as well as enhanced fluorescence emission in the crystalline state. As part of this thesis work, we have synthesized the amphiphilic derivative BODDQ and explored its unusual behavior in monolayers formed at the air-water interface and in LB films. We have also developed the different amphiphilic derivatives of the well-known hemicyanine system, by different modes of attachment of the hydrocarbon chain. Polyelectrolyte complexation of these molecules at the air-water interface is also studied. A new class of composite materials is developed by assembling metal nanoparticles on monolayer LB films, exploiting electrostatic interactions.

Molecular organization in the LB films can be controlled through design of the amphiphile structure and by tuning the film fabrication parameters. We have probed in great detail, the fabrication of ultrathin films of the different amphiphiles under different film preparation conditions. Temperature is found to exert an unusual influence in the organization of monolayer LB films of BODDQ. An interesting metastable state of the film was obtained at the higher temperature and its evolution monitored by spectroscopy and microscopy. Detailed computational studies allowed us to construct a model to understand the molecular assembly in the film fabricated under different conditions. The molecules adopte 'edge' and 'face' conformations in the films, fabricated at 20 and 30^{o}C respectively, the former providing a more compact and stable organization. Our study with the three hemicyanine based amphiphiles demonstrates the potential of the LB technique coupled with molecular design in controlling the molecular orientation in the ultrathin films. Polarized electronic absorption spectra revealed that the hemicyanine chromophore in the single chain systems (ODEP^{+}Br^{-} and MEOEP^{+}I^{-}) show similar orientation whereas that in OEOEP^{+}Br^{-} with a tail-head-tail structure is oriented very differently in LB films fabricated at the same deposition pressure. OEOEP^{+}Br^{-} adopts different conformations in the LB films when the nature of the substrate is changed, an extended one on hydrophobic substrate and a folded one on hydrophilic substrate. The polyelectrolyte templating methodology developed in our laboratory was found to be a simple and efficient way to control the molecular dipole orientation across the layers in multilayer films. This is achieved through the complexation with the polyelectrolytes introduced in the subphase that affect the deposition sequence during the film fabrication. Among the polyelectrolytes employed CMC^{n-} was found to facilitate the favorable z- type deposition. In our experiments on the assembly of citrate stabilized gold nanoparticles on monolayer LB film of ODEP^{+}Br^{-}, we have explored the molecular reorganization in the LB film. Our microscopy studies suggest that the islands of multilayers are formed in order to facilitate the assembly of the nanoparticles.

Molecular materials are generally characterized by weak noncovalent interactions between their building blocks. As a result of this, the characteristics of the molecules are nearly unaffected during the transition from the isolated to the assembled state.

Observations of significant changes in the physical responses due to intermolecular interactions in the supramolecular assembly therefore attract special attention. Our detailed investigation of LB films of BODDQ provided useful insight into the impact of the organization adopted by the molecules in the films fabricated under different experimental conditions, on the electronic absorption of the films. The film fabricated at 30^{o}C showed an electronic absorption spectrum similar to that of the isolated molecules as well as the bulk solid state, whereas the lower energy absorption is completely switched off in the film fabricated at 20^{o}C; the film formed at 30^{o}C is found to be metastable, evolving towards the stable one formed at 20^{o}C. The combination of π-A isotherms, microscopy, spectroscopy and computational modeling was used to construct a unified picture that explains this unusual phenomenon. The local electric field offered by the neighboring zwitterionic molecules is proposed to be responsible for suppressing the low energy charge transfer absorption. Our studies on the fluorescence emission of LB films of the three different amphiphiles based on the same hemicyanine headgroup suggested that the orientation and organization of the amphiphiles controlled by the mode of attachment of the hydrocarbon chain alters the optical responses while the fluorophore unit remains the same. Maximum emission achieved in the monolayer LB film of OEOEP^{+}Br^{-} owes its origin to the 'tail-head-tail' structure that guides the packing of the fluorophores and minimizes of self-quenching effects. Structural adjustments and hydrophilicity of the polyelectrolytes are shown to be the key factors that determine the molecular dipole orientation in the multilayer LB films and give rises to the SHG response. Earlier studies in our laboratory have demonstrated the utility of polyelectrolyte templating in achieving stable and enhanced optical SHG in monolayer LB films. Our present studies unravel the critical role of polyelectrolytes in directing the formation of suitable multilayer LB films that exhibit stable and strong optical SHG response. Organized assembly of nanoparticles is of current interest in various fields as they exhibit optical properties different from that of the individual particles. We demonstrated this in our study where tuning of the surface plasmon resonance absorption of the gold nanoparticles in the composite films over a wide wavelength range was achieved by controlling the formation of the 2-dimensional aggregate structures on LB film of a cationic amphiphile, through a simple and fast protocol.

We have presented in this thesis, the design and fabrication of several novel molecular materials with interesting optical properties. We believe that our studies on the fabrication, characterization and optical and nonlinear optical responses of the new materials in the form of ultrathin films provide new directions for explorations in these areas. The findings presented in the thesis cover new chemistry, molecules, materials, phenomena and models.

6.2. Future Prospects

A series of further investigations can be envisaged based on the work presented in this thesis. The novel optical attributes observed in the materials based on molecular ultrathin films that we have demonstrated can be used in several applications. The unusual ‘switching off’ of the electronic absorption in the BODDQ film can possibly be exploited in mechanical sensors or switching devices. The enhanced fluorescence emission obtained in the LB films through the optimal choice of amphiphile structure and conditions of deposition can be effectively utilized in applications such as light emitting diodes and sensors. Incorporation of lanthanide ions in the LB films of the neutral pyridine analogue of $ODEP^+Br^-$ can open up a new class of fluorescent LB films.

The polyelectrolyte templating methodology we have demonstrated for the construction of multilayer LB films with strong and stable SHG responses affords sufficient flexibility to fabricate ultrathin films of any ionic amphiphile with headgroups designed for electronic, magnetic or optical applications. The methodology would be very versatile if other kinds of intermolecular interactions besides the strong electrostatic ones can be exploited. It would also be of great interest to explore the use of the polyelectrolyte templated LB films in waveguiding applications. Organized assembly of carbon nanotubes (CNT) in 2-dimensional lattice structures is of current interest in the field of electronics and sensors. Incorporation of CNT in LB films can be achieved by following similar protocol as that used in the polyelectrolyte templating method. CNT possessing appropriate functional groups can interact with amphiphiles of opposite charge at the interface and thus be transferred on to the substrate. This idea is currently being investigated in our laboratory.

The methodology we have developed for the fabrication of ultrathin film-nanoparticle composite materials can be extended to achieve enhanced nonlinear optical responses and surface enhanced Raman scattering. The utility of LB technique in fabricating laterally patterned films with controlled wetting properties on the nanometre scale without any lithographic processes is of interest in various fields. Fabrication of patterned LB films of BODDQ and $OEOEP^+Br^-$ by varying the film fabrication parameters would open up new avenues to be explored. Such patterned LB films can be used in the organized assembly of metal nanoparticles and hence in the development of nanoscale electronic/photonic devices. The materials, methodologies and phenomena developed and investigated in this thesis open up several new frontiers for exploration in future.

APPENDIX A

Langmuir and Langmuir-Blodgett Film Fabrication

π-A isotherms were investigated on a Nima Model 611M LB trough using a Wilhelmy plate for pressure sensing (Fig. A1). The components of the trough were described in Sec. 1.3.3. Dimensions of the trough we have used are 30 x 10 x 0.35 cm^3. Millipore MilliQ water (resistivity > 18 MΩ.cm) was used for the subphase in all experiments; typically ~ 220 ml of water was taken in the trough. Solution of amphiphiles in chloroform (Uvasol grade, EMerck) was spread on the subphase. Experiments were generally carried out at 25°C unless specified otherwise, as in Chapter 2, with the trough placed in a clean environment (air filtered through HEPA filters). After spreading the amphiphile solution, a minimum wait period of 30 min to a maximum of 120 min was allowed depending on the amphiphile used. The π-A isotherms were recorded using a barrier speed of 5 cm/min. All π-A experiments were repeated on fresh subphases typically 3 - 5 times to confirm reproducibility. In most cases, the monolayer was subjected to a few isocycles and the reproducible isotherm obtained was recorded.

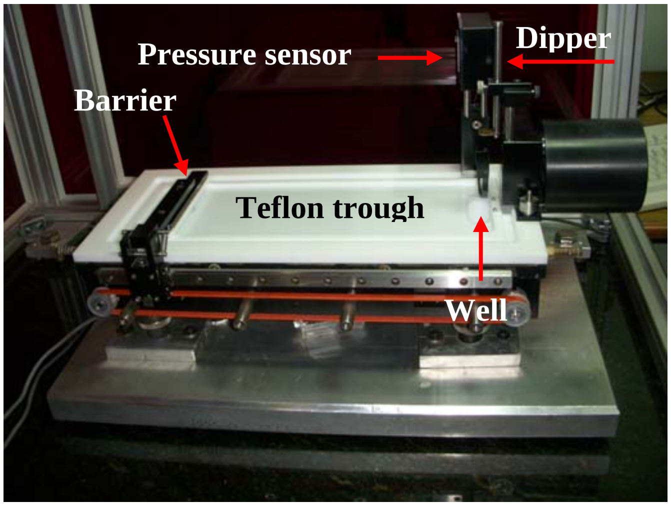

Figure A1. *Langmuir-Blodgett trough used in our laboratory.*

LB films were deposited either on glass or quartz substrates. Hydrophilic surface for the monolayer deposition was prepared using the following protocol employing high purity water in all operations. The substrate was cleaned with detergent followed by several rinsings in water; it was sonicated in fresh water three times for 15 - 20 min each. The surface was made hydrophilic by immersing in aqueous solution of sodium hydroxide for 12 h or treating with pirhana solution (H_2O_2: H_2SO_4 = 1 : 3) for 6 h followed by sonication and rinsing in water. Hydrophobic surface was prepared by exposing the substrate to vapors of hexamethyldisilazane for 12 h. The LB films were deposited on the substrate by the vertical dipping procedure employing a dipping speed of 5 mm/min with the monolayer held at the desired pressure. Freshly cleaved mica plates were also used to fabricate samples for AFM imaging. LB films deposited on carbon supported copper grids were used for electron microscopy studies; the grid was placed on a glass substrate by careful insertion into a teflon tape wound on the substrate.

APPENDIX B

Microscopy Techniques

(a) *Brewster Angle Microscope*

Brewster angle microscopy allows the *in situ* study of thin films at the gas/liquid or gas/solid interface. The principle of the method is illustrated in Figure B1. When a beam of p-polarized light is incident on the surface at a specific angle, θ (Brewster angle), such that

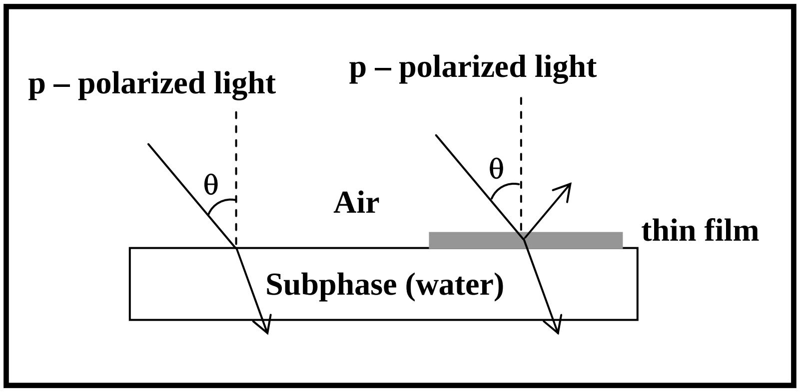

Figure B1. *Principle of Brewster angle microscopy.*

$$\tan\theta = \frac{n_{\text{subphase}}}{n_{\text{air}}}$$

where n's are the refractive indices, it is completely transmitted; no reflection occurs and the view from the top of the surface looks dark. Introduction of a thin film at the interface between the two phases alters its optical characteristics and a small amount of the incident light is reflected. This provides a sensitive way to image the monolayer on the water surface.

The equipment used in our experiments, Nanofilm Model BAM 2Plus is shown in Figure B2. The wavelength and power of the laser used are 532 nm and 20 mW respectively. Using the 20x objective lens, a maximum resolution of ~ 1 μm can be achieved in the images.

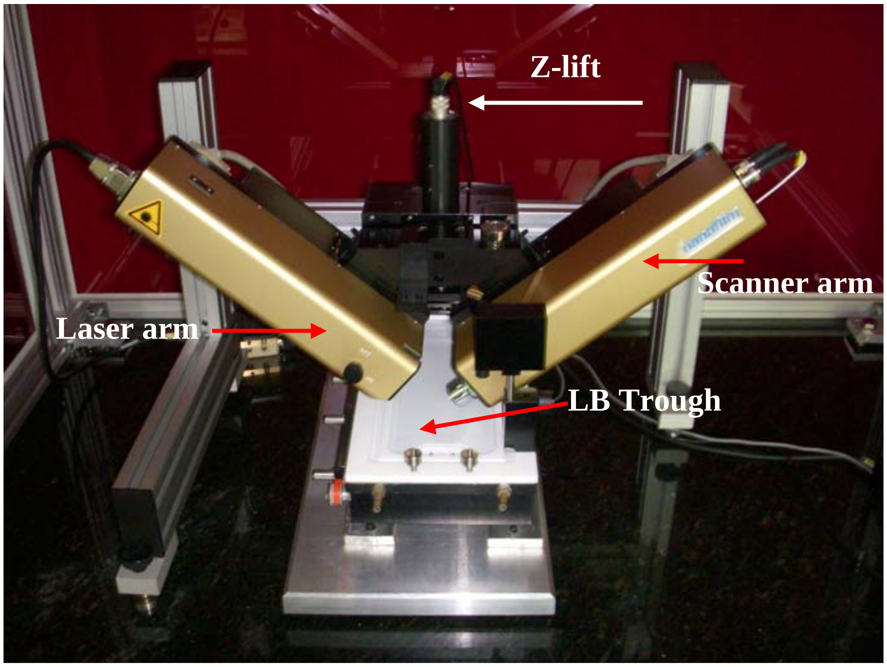

Figure B2. *Brewster angle microscope used in our laboratory, the picture shows also the LB trough positioned under the BAM.*

(b) *Atomic Force Microscope*

AFM images of LB films deposited on quartz, glass and mica substrates were recorded on NT-MDT Model Solver Pro M and SEIKO Model SPA 400 atomic force microscopes. All images presented were recorded in the non-contact mode using tips having force constant of 10 – 20 N/m. The images presented in Chapter 2, Chapter 3 and Chapter 5 were obtained using Solver Pro M and those in Chapter 4 using SPA 400. Line profiles and surface analysis options available in the software provided by the AFM manufacturers were used to analyze the thickness and morphology of the nanostructures in the LB films. The bearing ratios used in Chapter 4 determined from surface analysis signify the percentage of data points at or above any specified height level in the image and ranges from 0 at the highest point in the image to 100 at the substrate level.

(c) *Scanning and Transmission Electron Microscopes*

Scanning electron microscopy imaging of the ultrathin film-nanoparticle composite presented in Chapter 5 were carried out using a HITACHI S-4300SE/N FESEM and Philips XL30 ESEM with a beam voltage of 20 kV. Transmission electron microscopy images were obtained on a TECNAI G^2 FEI F12 TEM at an accelerating voltage of 120kV.

APPENDIX C

Estimation of Monolayer Thickness by Brewster Angle Microscopy

As noted in Appendix B, BAM is a very useful tool to characterize the morphology of ultrathin films at the air-water interface. Intensity of the reflected light will be nearly zero when p-polarized light is incident at the Brewster angle of water (53.1 degrees) on a clean aqueous subphase. The intensity of the reflected light from a film covered surface depends on the thickness of the film and the type of material used. The thickness of the film increases during the compression of the film which in turn increases the intensity of the reflected light. Thus the signal at Brewster angle contains the information about the optical thickness of the film.

In the study presented in Chapter 3, we have analyzed the variation in the thickness of the $OEOEP^+Br^-$ monolayer during the compression of the film. BAM was calibrated using the software supplied by the manufacturer, prior to spreading the chloroform solution of $OEOEP^+Br^-$. After the calibration of the instrument the optical configuration was kept unchanged throughout the experiment. Anisotropy of the film was checked before starting the thickness measurement and found to be isotropic. After equilibration for about 1 h the monolayer was compressed with a barrier speed of 5 cm/min. The film thickness was monitored simultaneously using the Kinetics and Thin Film Model options in the Utility palette of the software. Refractive index of the film was taken as 1.5; inferences about the film thickness were found to vary very little depending on the choice of refractive index in the range 1.3 to 1.7. The thickness measurement was carried out by following reported procedure earlier.[1]

1. (a) Patino, J. M. R.; Sanchez, C. C.; Nino, N. M. R. *Langmuir* **1999**, *15,* 2484; (b) Winsel, K.; Honing, D.; Lunkenheimer, K.; Geggel, K.; Witt, C. *Eur. Biophys. J.* **2003**, *32*, 544.

APPENDIX D

Estimation of Molecular Orientation from Polarized Absorption Measurements

Absorbances at λ_{max} when the light is polarized parallel (p) and perpendiculars (s) to the plane of incidence (Fig. 3.10) are denoted respectively as $A_{\parallel}$ and $A_{\perp}$, the linear dichroism is defined using Eq.1.

$$D = \frac{(A_{\parallel} - A_{\perp})}{(A_{\parallel} + A_{\perp})} \qquad \text{...... 1}$$

The linear dichroism for different angles of incidence, α can be calculated using Eq.2

$$D_{\alpha} = \frac{(2 - \tan^2 \theta)}{\tan^2 \theta \left(\dfrac{1 + \cos^2 \alpha}{\sin^2 \alpha} \right) + 2} \qquad \text{...... 2}$$

where θ is the orientation of the transition dipole of the molecule as shown in Figure 3.10. Using Eq.2 and D_{α} measured at different α, θ can be estimated.[1]

In the case of absorption spectra overlapping with multiple peaks, deconvolution can be carried out to estimate the absorbances of individual peaks and hence the corresponding linear dichroism. Such exercises were carried out for the films ODEPBr_30_W, OEOEPBr_W_45 and OEOEPBr_O_45 in Chapter 3, and the orientation of transition dipoles responsible for the absorption with peaks at 410 nm and 470 nm, estimated.

1. N'soukapoé-Kossi, C. N.; Sielewiesiuk, J.; Leblanc, R. M.; Bone, R. A.; Landrum, J. T. *Biochim. Biophys. Acta* **1988**, *940*, 255.

APPENDIX E

Analysis of Fluorescence Anisotropy

In Chapter 3, we have estimated the anisotropy of the LB films by polarized fluorescence measurements using linearly polarized light produced by placing polarizers in the excitation and emission paths. The samples were excited using horizontally and vertically polarized light. The films were kept at ~ 30^o to the excitation beam and the emission light was collected in right-angle geometry.

Anisotropy (r) of LB films is calculated using Eq.1.[1]

$$r = \frac{(I_{VV} - GI_{VH})}{(I_{VV} + 2GI_{VH})} \qquad \text{......1}$$

where I_{VV} and I_{VH} correspond respectively to the intensities of vertically and horizontally polarized emission obtained with vertically polarized excitation light. The factor G in Eq.1 is the ratio of the sensitivities of the detection system for vertically and horizontally polarized light, estimated using Eq.2.

$$G = \frac{I_{HV}}{I_{HH}} \qquad \text{......2}$$

where I_{HV} and I_{HH} correspond respectively to the intensities of vertically and horizontally polarized emission obtained with horizontally polarized excitation light.

1. Togashi, D. M.; Romã, R. I. S.; Gonçalves da Silva, A. M.; Sobral, A. J. F. N.; Costa, S. M. B. *Phys. Chem. Chem. Phys.* **2005**, *7*, 3874.

APPENDIX F

Measurement and Analysis of Second Harmonic Generation (SHG) from LB Films

Incident angle dependence of the SHG intensities of the films was measured using a pulsed beam from a repetitively Q-switched Nd-YAG laser (Lee, Model 818TQ, 1.0 kHz) at a wavelength of 1064 nm with a pulse duration of 140 ns (average laser power = 450 mW) and a peak power of 5.1 kW. Top view of the setup is shown in Figure F1. Since the dynamic range of the boxcar system is not very wide, neutral density filters were used to control the light intensity. The samples were mounted on a motor-controlled rotational stage. The angle of incidence of the laser beam on the film, θ was varied from -60 to 60°. In the p-p polarization measurements (Fig. F2) p-polarized fundamental laser beam was used and the p-polarized second harmonic light was detected by a photomultiplier tube (Hamamatsu, Model R212). The signal from the photomultiplier tube was sent to a boxcar averager (Stanford Research, Model SR250). All the instruments were controlled by a personal computer.

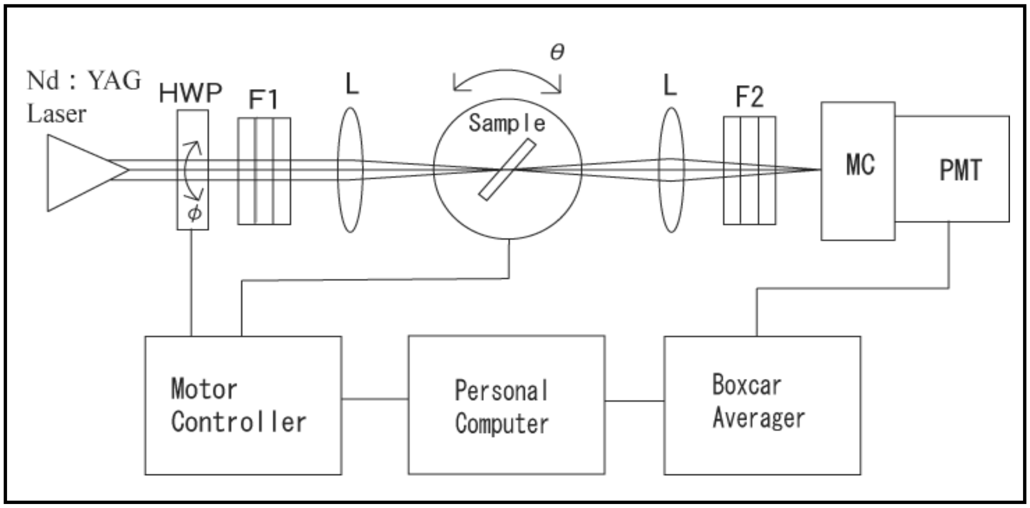

HWP: Half wave plate, F1, F2: Filters, L: Lens, MC: Monochromator, PMT: Photomultiplier tube

Figure F1. *Setup used for the measurement of SHG from LB films.*

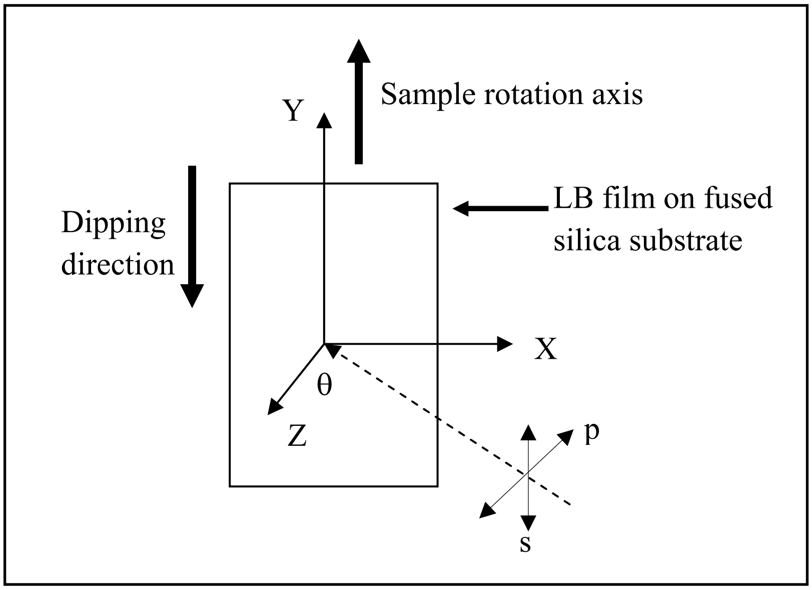

Figure F2. *Geometry of the LB film placement and fundamental laser beam polarization.*

Analysis of the SHG fringe pattern

The laser beam intensity (I_ω) was estimated from the fitting of the data for quartz used as the reference, recorded before and after each LB film experiment. Standard expressions reported for the fringe intensity pattern were used[1-2] and the χ_{XXX} value of quartz was taken from literature[2]. The fringes recorded for the LB films are fitted subsequently. The value of the substrate thickness, the refractive indices n_ω and $n_{2\omega}$ of the LB film at frequencies ω and 2ω respectively and the susceptibility tensor components, χ_{ZZZ} and χ_{ZXX} of the LB film are the fitting parameters for the p-p polarization data studied. The nonlinear least square fitting was programmed using MicroCal Origin 7.0.

1. (a) Kuzyk, M. G.; Singer, K. D.; Zahn, H. E.; King, L. A. *J. Opt. Soc. Am. B* **1989,** *6,* 742; (b) Mizrahi, V.; Sipe, J. E. *J. Opt. Soc. Am. B* **1988,** *5,* 660; (c) Herman, W. N.; Hayden, L. M. *J. Opt. Soc. Am. B* **1995**, 12, 416.
2. Jerphagnon, J.; Kurtz, S. K. *J. Appl. Phys.* **1970,** *41,* 1667.

PUBLICATIONS

1. **Rajesh, K**.; Chandra, M. S.; Hirakawa, S.; Kawamata, J.; Radhakrishnan, T. P. *Langmuir* **2007**, *23*, 8560.
   Polyelectrolyte Templating Strategy for the Fabrication of Multilayer hemicyanine Langmuir-Blodgett Films Showing Enhanced and Stable Second Harmonic Generation

2. Patra, A.; **Rajesh, K**.; Radhakrishnan, T. P. *Bull. Mater. Sci.* **2008**, *31*, 421.
   Optical Materials Based on Molecular Nano/microcrystals and Ultrathin Films

3. **Rajesh, K**.; Radhakrishnan, T. P. *Chem. Eur. J.* **2009**, *15*, 2801.
   Optical Response Sensitive to the Assembly in a Molecular Material: Ultrathin Film with a Vanishing Electronic Absorption

4. **Rajesh, K**.; Rajendra, K.; Radhakrishnan, T. P. *J. Phys. Chem. B* **2010**, *114,* 849.
   Fluorescence Enhancement in Langmuir-Blodgett Films: Role of Amphiphile Structure, Orientation and Assembly

5. **Rajesh, K**.; Sreedhar, B.; Radhakrishnan, T. P. *ChemPhysChem* (in press)
   Assembly of Gold Nanoparticles on a Molecular Ultrathin Film: Tuning the Surface Plasmon

PRESENTATIONS

1. **Rajesh, K**.; Chandra, M. S; Radhakrishanan, T. P.
   Poster presented in the JNC Research Conference on Chemistry of Materials held at Kollam October 01-03, 2005.
   Instability in Langmuir-Blodgett Films of a Zwitterionic NLO-Phore: Spectroscopic and Microscopic Studies

2. **Rajesh, K**.; Radhakrishnan, T. P.
   Poster presented in the annual national review coordination meeting on Nano Science and Nano Technology (NSNT), ARCI, Hyderabad, February 21-23 2007.
   Polyelectrolyte Templating in Langmuir-Blodgett films: Fabrication of Multilayer Hemicyanine LB films Showing Enhanced and Stable SHG

3. **Rajesh, K**.; Radhakrishnan, T. P.
   Poster presented in the International Conference on Nano Science and Technology (ICONSAT-2008), Chennai, India, February 27-29, 2008.
   Instability in Langmuir-Blodgett Films of NLO-Phore molecules.

4. **Rajesh, K.**
   Oral presentation at the 6th Annual in-house Symposium of School of Chemistry, University of Hyderabad (Chemfest-2008), Hyderabad, India, March 8-9, 2009.
   Molecular Optical Materials based on Ultrathin Films

5. **Rajesh, K.**
   Oral presentation at Dr. K. V. Rao 9th Annual Research Award Program, Hyderabad, India, on March 21, 2009.
   Molecular Optical and Nonlinear Optical Materials Based on Ultrathin Films

6. **Rajesh, K**.; Radhakrishnan, T. P.
   Poster presented in the International Conference on Nanostructured Materials (ICNM), Kottayam, Kerala, India, April 6-8, 2009.
   Molecular Optical Materials based on Ultrathin Films
   (**Received ʻ2nd’ Prize for Poster presentation**)